

Flyleaf—a blank page

AN ABSTRACT OF THE THESIS OF

Humberto Eduardo Nation for the degree of Master of Science in Applied Anthropology presented on December 20, 2018.

Title: Analysis of Culturally Derived Speleothems by INAA and ICP-MS, A Multi-Analytical Approach

Abstract approved: _____

Leah D. Minc

Over the last two decades, archaeologists have documented the widespread ancient Maya practice of collecting cave formations (speleothems) from ritually important caves and transporting them to their settlements. Little is known about their specific uses within settlements, but it is hypothesized that these objects convey a degree of sanctity from the caves to the surface settlements. This phenomenon has raised several questions such as the spatial and temporal extent of these interactions, and specifically what the speleothems can tell us about the relationship between Maya polities and proximal or distant caves. This study contributes to the study of Maya cave ritual by assessing whether the provenance or origin of speleothems can be determined from their geochemical composition. Few studies have attempted with limited success the chemical characterization and sourcing of speleothems from geologically diverse regions with INAA and with ICP-MS. This study attempts to determine the applicability of INAA in sourcing a larger sample set from a more homogenous geological setting with samples obtained by the Belize Valley Speleothem Project

(BVSP) of central Belize. A total of 104 speleothems from 46 caves were characterized via INAA, and the results utilized to evaluate the Provenance Postulate, i.e., that the between-source differences must exceed within-source variation for sourcing determination to be possible. We compared the chemical variability at three spatial scales: within caves, among caves, and between drainage systems. Analytical results are compared with those from samples procured by the Xibun Archaeological Research Project (XARP) collected along the Sibun River Valley in southeast Cayo and south Belize districts, Central Belize and one samples origination from the Poptun area in northeast Petén, Guatemala. While the BVSP samples derived from multiple caves within the Cayo District in Central Belize, only 15 caves had three or more replicates, making it difficult to adequately assess within-cave variability and explore the provenance postulate meaningfully. However, the combined BSVP and XARP data sets allowed us to explore the variability among four identified drainage systems. Our results indicate that speleothem samples from the Sibun River Basin and Petén are significantly depleted in some trace (i.e.: Mg, Cr, Zn, Sr) and rare earth elements (, Yb, Lu, Eu, Th and U), with concentrations near the limits of detection of INAA. Nonetheless, the extremely low concentrations of certain chemical species are also useful in differentiating homogeneous lithic materials. While it is clear that INAA is an appropriate method to chemically characterized and possibly source speleothems to individual caves, our results indicate that complementary analytical methods such as ICP-MS and INAA would yield far more complete chemical characterization. Our results also emphasize the necessity of learning the complex geological and geochemical constraints of the study area and sample material. Lastly, concise recommendations are put forward in hope of guiding future speleothem of ceramic provenance studies.

© Copyright by Humberto E. Nation
December 20, 2018
All Rights Reserved

Analysis of Culturally Derived Speleothems by INAA and ICP-MS,
A Multi-Analytical Approach

by
Humberto Eduardo Nation

A THESIS

submitted to

Oregon State University

in partial fulfillment of
the requirements for the
degree of

Master of Science

Presented December 20, 2018

Commencement June 2019

Master of Science thesis of Humberto Eduardo Nation
presented on December 20, 2018.

APPROVED:

Major Professor, representing Applied Anthropology

Director of the School of Language, Culture and Society

Dean of the Graduate School

I understand that my thesis will become part of the permanent collection of Oregon State University libraries. My signature below authorizes release of my thesis to any reader upon request.

Humberto Eduardo Nation, Author

ACKNOWLEDGEMENTS

This thesis was only possible with the help and assistance of my advisors Dr. Leah D. Minc, whose patience, guidance on and comments help me focused my writing and move forward with my research; and Dr. James E. Brady who initiated me into the field of archaeology and provided relentless guidance and support, to you two, I'm thankful and forever grateful. I would also like to thank Dr. Holley Moyes, Dr. Patricia McAnany and Dr. Polly Peterson for providing the samples for this study as well as Dr. Jaime Awe for facilitating the exportation of the samples and Dr. Hector Neff for facilitating access to ICP-MS instrumentation as well and his guidance and insight. My daughter Sofia C. Nation also deserves my acknowledgement and appreciation for helping me process and label the samples and format the thesis to OSU specifications.

Lastly, I would also like to thank my family, wife Juana, daughter Sofia, sister Elizabeth Nation, my nephew Adrian Vicente for all their support, encouragement and my parents Maria Elena Granados Sanchez and Otis G. Nation. They instilled in me the tenacity and convictions that had guided my academic journey.

This master thesis is dedicated to all of you, to those who have been part of my life one way or another and hope this will inspire someone to pursue their academic curiosity... no thought is to simple, no idea to small.

TABLE OF CONTENTS

	Page
Chapter 1. Introduction.....	2
Chapter 2. The Maya	5
2.1 Maya Geography	5
2.2 Overview of Maya Prehistory.....	6
2.2.1 The Archaic Period (8000 BCE – 2000 BCE)	7
2.2.2 The Maya Preclassic Period (2000 BCE – 250 CE).....	8
2.2.3 The Maya Classic Period (250 – 950 CE).....	9
2.2.4 The Maya Post Classic Period (950 – 1539).....	11
2.2.5 Contact Period and Aftermath.....	12
2.3 Maya Creation Myths and Sacred Landscapes	13
2.4 Maya Ritual Cave Use.....	15
2.5 Why Study Speleothems?	18
2.5.1. Breakage, Transport and Usage of Speleothems by the Maya..	18
2.5.2 Sourcing of Culturally Derived Speleothems.....	19
2.5.3 Study Objectives	20
Chapter 3. Geology, Geochemistry of Speleothems, and Provenance.....	21
3.1 Speleothems.....	21
3.1.1 Parent Materials.....	22
3.1.2. Ontogeny of Speleothems	24
3.1.3 Implications for Provenance Determination	25
3.2 Belize Geology and Karstic Landscapes	27
3. 2.1 Stratigraphy and Paleogeography of the Corozal Basin in Northern Belize	30

TABLE OF CONTENTS (Continued)

	Page
3.2.2 Karst Landscapes and Morphology in Belize	32
3.3. Study Area Geology and Karst Landscape	35
3.4 Expectations and Implications	35
Chapter 4. Materials and Methods.....	38
4.1 Sample Materials.....	38
4.2 INAA	39
4.2.1 Speleothem Analysis by INAA	40
4.2.2 Sample Preparation for INAA.....	41
4.2.3 Analysis Protocol	42
4.3 Analysis by LA- TOF- ICP-MS	43
Chapter 5. Results for the Cayo District	46
5.1 Analytical Approaches	46
5.2. Variability among Speleothems within a Cave.....	46
5.3 Variability among Caves.....	55
Chapter 6. Results for Inter-Regional Comparisons	64
6.1. Drainage Systems	64
6.2 Geochemistry of Drainage Systems	66
Chapter 7. Discussion and Conclusions	72
7.1 Analytical Considerations	72
7.2 Conclusions.....	73
7.3 Recommendations for Future Work.....	75
Referenced Cited	77

TABLE OF CONTENTS (Continued)

	Page
Appendix A Figures.....	90
Appendix B Tables.....	199

LIST OF FIGURES

<u>Figure</u>		<u>Page</u>
1.	Maximum Extent of the Maya Civilization.....	5
2.	Geological Map of Belize.....	28
3.	Stratigraphic Columns for the Corozal and Belize Basins.....	29
4.	Karst Regions of Belize.....	34
5.	Cayo District Group Samples	39
6.	Magnesium Concentrations by Cave	48
7.	Bromine Concentrations by Cave	49
8.	Scandium Concentrations by Cave	50
9.	Cobalt Concentrations by Cave	51
10.	Strontium Concentrations.....	52
11.	Europium Concentrations.....	53
12.	Uranium Concentrations.....	54
13.	Average Absolute Elemental Concentrations.....	56
14.	Average Absolute Elemental Concentrations for REE	57
15.	Concentrations in log base 10 of Aluminum vs Iron.....	58

LIST OF FIGURES (Continued)

<u>Figure</u>	<u>Page</u>
16. Bivariate Plot of Sr vs. Cs	59
17. Concentrations in log base 10 of Lanthanum vs Samarium.....	60
18. Concentrations in log base 10 of Lutetium vs Uranium.....	61
19. Concentrations in log base 10 of Thorium vs Uranium.....	62
20. Magnesium Concentrations by Drainage Systems	67
21. Thorium Concentrations by Drainage Systems	68
22. Ternary Plots of Rare Earth Elements	70

LIST OF TABLES

<u>Table</u>	<u>Page</u>
1. Maya Chronology.....	7
2a. Sample Inventory for BVSP; Barton Creek and Cave's Branch.....	28
2b. Sample Inventory for BVSP; Macal and Pine Ridge.....	202
2c. Sample Inventory for BVSP; Roaring Creek and San Antonio.....	203
3a. Major and Trace Element Raw Data; BC and CB.....	204
3b. Major and Trace Element Raw Data; M and PR.....	205
3c. Major and Trace Element Raw Data; RC and SA.....	206
4a. Rare Earth Elements Raw Data; BC and CB	207
4b. Rare Earth Elements Raw Data; M and PR	208
4c. Rare Earth Elements Raw Data, RC and SA	209
5a. Absolute Values for Major and Trace Elements; BC and CB	210
5b. Absolute Values for Major and Trace Elements; M and PR	211
5c. Absolute Values for Major and Trace Elements; RC and SA	212
6a. Absolute Values for Rare Earth Elements; BC and CB	213

LIST OF TABLES (Continued)

<u>Table</u>	<u>Page</u>
6b. Absolute Values for Rare Earth Elements; M and PR	214
6c. Absolute Values for Rare Earth Elements; RC and SA	215
7a. Major and Trace Elements Log Base 10; BC and CB	216
7b. Major and Trace Elements Log Base 10; M and PR	217
7c. Major and Trace Elements Log Base 10; RC and SA	218
8a. Rare Earth Element Log Base 10; BC and CB	219
8b. Rare Earth Element Log Base 10, M and PR	220
8c. Rare Earth Element Log Base 10, RC and SA	221
9a. Major, Trace and Rare Earth Elements in ppm; (XARP)	222
9b Major, Trace and Rare Earth Elements in Log Base 10; (XARP)	222
10. Caves Sites Composition by Group	65
11. Standard Reference Materials for INAA	224

**Analysis of Culturally Derived Speleothems by INAA
and LA-ICP-MS
A Multi-Analytical Approach**

Humberto Eduardo Nation Granados

Chapter 1. Introduction

Cave visitation by Mesoamerican prehispanic cultures is well documented and goes back to the early Olmec civilization ca. 1200 BCE (Grove, 1973). This practice heavily influenced later civilizations such as the Zapotec, Aztec, and Maya cultures. Perhaps because of the karstic terrains they inhabited, especially in the Yucatan plateau, the ancient Maya continued and expanded their use of caves for ritual use. Today, most if not all explored caves and grottoes, from the southern lowlands of Honduras, Guatemala, and Southern Belize to the northern lowlands of Quintana Roo, Yucatan, Campeche, Tabasco, and Chiapas have yielded vast archaeological materials. However, these cultural remnants are not indicative of occupation but of ritual use as evident from the studies of caves like Naj Tunich (Brady and Stone, 1986), Loltun (Seler, 1901), Quen Santo (Thompson, 1975), Actun Tunichil Muknal (ATM) (Helmke *et al.*, 1999), Balankanche (Thompson, 1975; Andrews, 1971), Jolja (Bassie, 2002), Actun Chanona (McAnany *et al.*, 2005; Sandra-Varela and Dore, 2005), and Mid Night Terror (Kieffer, 2015; Wrobel *et al.*, 2012). This long-term use and re-use of caves underlies the importance of caves to the ancient Maya and our obligation to explore and study the complex and dynamic relationship between landscape and cultural use by the Maya.

In a little more than two decades, archaeologists have documented the widespread occurrence of “foreign” ceramic materials in caves, as well as the breakage and transport of cave mineral formations such as stalactites, stalagmites, and cave pearls (hereafter speleothems) by the ancient Maya to their settlements. This practice has raised several questions such as the spatial and temporal extent of these practices, their meaning, and specifically what all these tell us about the relationship between Maya polities and proximal or distant caves. Many have speculated that the movement of speleothems could have been associated with ritual practices or beliefs (Grove, 1973; Pohl and Pohl,

1983; Peterson, 2006). Others (Brady *et al.*, 2005) have proposed that the materials removed might in fact indicate an act of desecration by a rival polity. In either case, without knowing with reasonable certainty the origin or provenance of these lithic artifacts, any attempts at describing the significance or relevance of speleothems found at a given archaeological site are just suppositions and interpretations based on lithic debitage within the cultural association.

While there are numerous studies on the provenance of marble and limestone statues that link these cultural materials to specific rock quarries, there have been few studies that have attempted the same for speleothems. In a seminal article on speleothem utilization, Brady *et al.* (1997:741–744) provide evidence that Instrumental Neutron Activation Analysis (INAA) of speleothems from caves in the region of Copan, Honduras, can produce chemical signatures that are discrete to individual caves. However, it was uncertain whether the method would be applicable to caves in the Maya lowlands of Belize and the Petén of Guatemala where the geology is far more homogeneous than in highland Honduras. Two pilot studies, by Peterson *et al.* (2006) and replicated by Nation *et al.* (2012), utilizing Inductively Coupled Plasma – Emission Spectrometry (ICP-ES) and Laser Ablation Time of Flight Inductively Coupled Plasma – Mass Spectrometry (La- TOF-ICP-MS) respectively, indicated that such techniques could be used to chemically differentiate between a small set of samples, suggesting that speleothems from different drainages and caves could be distinguished.

The present work is a formal pilot study to determine the applicability of INAA in sourcing a larger sample set from a more homogenous geological setting and replicating, if possible, the results of the 1997 INAA analysis mentioned above. Additionally, we compared our INAA results with the data set from the 2012 ICP-MS analysis in order to understand the limitations of each instrumental method and if and how they complement each other.

To better distill the information that our samples may hold we first conducted an extensive literature review on four areas as follows: 1) Maya history and cosmology, 2) geology and geography of Belize and the study area, 3) geochemistry and formation of speleothems, and 4) analytical techniques and methodology of Instrumental Neutron Activation Analysis and ICP-MS. The first area of study, as presented in Chapter 2, provides a brief overview of Maya civilization, history, geography, and a discussion of the creation myths and cosmological view of the ancient Maya in order provide perspective as to the cultural significance of our analysis. Chapter 3 provides background information on the complex geology of Belize, the processes of speleothem formation and geochemistry. Chapter 4 discusses the materials and methods, including sample preparation and protocols for both the INAA analysis of the BVSP samples and those samples from the Xibun Archaeological Research Project (XARP) analyzed by LA-TOF-ICP-MS. Chapter 5 presents a brief explanation of the NAA results and data analysis, with a discussion of the variability within and between caves. In Chapter 6 we discuss interregional comparison and drainage systems as discerned from their geochemical signatures. Finally, in Chapter 7, we present a summary of our findings and observations, present the conclusions from this study, and provide recommendations for future similar studies.

It is our hope that this thesis serves to further advance our understanding of the Maya and future provenance studies in archaeology.

This area comprises multiple ecological and climate settings from the highland hardwood and conifer forests of Guatemala and Chiapas, to tropical rain forest of Soconusco, El Petén, Belize, Tabasco, and Campeche, to seasonal and dryer semitropical forests of the northern Yucatan.

Culturally, the Maya areas are geographically divided, from south to north as follows: 1) The coastal and piedmont of the Soconusco Area along the Pacific Coast; 2) the Highlands or Southern Maya Highlands comprising the Sierra Madre de Chiapas, the Central Highlands of Chiapas (Los Altos de Chiapas) in Mexico and in Guatemala proper, the Guatemalan Highlands and the Sierra de los Cuchumantes; 3) the Southern Maya Lowlands comprised of all tropical and subtropical lowlands or “bajos” between the Motagua River basin, into the Petén region, most of southern and western Belize, and along the Usumacinta and La Pasión Rivers towards the tropical jungles and marshlands of Tabasco and Campeche; and 4) the Northern Maya Lowlands, comprised of northern Belize and the Mexican states of Yucatan and Quintana Roo. While ecologically and politically diverse, all these share a unique cultural heritage and history.

2.2 Overview of Maya Prehistory

A more recent historical chronology of the Maya civilization as published by Estrada-Belli (2011) will be utilized and referenced for the historical discussion. This chronology is shown in Table 1.

Table 1. Maya Chronology, (Estrada-Belli, 2011).

PERIOD	DIVISION		DATES
Archaic			8000 - 2000 BCE
Preclassic	Early Preclassic		2000 - 1000 BCE
	Middle Preclassic	Early Middle Preclassic	1000-600 BCE
		Late Middle Preclassic	600 – 350 BCE
	Late Preclassic	Early Late Preclassic	350 – 1BCE
		Late Preclassic	1 BCE – 159 CE
		Terminal Preclassic	159 – 250 CE
Classic	Early Classic		250 – 550 CE
	Late Classic		550 – 830 CE
	Terminal Classic		830 – 950 CE
Postclassic	Early Postclassic		950 BC – 1200 CE
	Late Postclassic		1200 – 1539 CE
Contact			1511 – 1697 CE

2.2.1 The Archaic Period (8000 BCE – 2000 BCE)

The chronology given by Estrada-Belli (2011) delimits the historical range of the ancient Maya civilization to about 3697 years, between 2000 BCE to around 1697 CE, with the preceding Archaic period still a great unknown. However, recent discoveries (Gonzalez *et al.*, 2008; Chatters *et al.*, 2014; Stinnesbeck *et al.*, 2017) from separate flooded cave passages in the Yucatan Peninsula put initial human occupation in the area between 11,000 to 13,000 years BCE during the late Pleistocene. These, while significant, do not represent

Maya culture, which would not appear for thousands of years later. Much debate as to the first appearance of the Maya was generated by a study Hammond *et al.* (1976), that indicated a radiocarbon date of occupation at the site of Cuello in modern day Belize, around 2600 BCE. Years later, a reassessment of the same site by Andrews and Hammond (1990), yielded radiocarbon dates of occupation for Cuello between 1100 and 400 BCE, during the Preclassic Period and well within the accepted timeframes of Maya cultural expansion northward from the Pacific Coast, to the highlands, the southern lowlands and ultimately the northern lowlands of the Belize and Yucatan proper.

2.2.2 The Maya Preclassic Period (2000 BCE – 250 CE)

It is during the Early Preclassic period (ca. 2000 BCE to 250 CE) that settlements with distinct Maya cultural indicators (pottery, figurines and architecture) begin to appear first in the Soconusco region and the Piedmont of the Pacific Coast and central highlands of Guatemala (Estrada-Belli, 2011). By the Middle Preclassic (600 to 250 BCE), the Maya had extended from the lowlands of Petén and Belize to the northern lowlands of the Yucatan. By the Middle Preclassic to Late Preclassic, some villages had developed into large city states such as Nakbé, Tikal, Uaxactun, Seibal, and El Mirador. During this period, competition for hegemony between the major centers intensified, leading to alliances between city-states such as between El Mirador, Nakbé and El Tintal (Miller, 1999; Webster, 2002). Recent evidence suggests that trade, commerce, and migration were established between the Maya centers in the Petén area and the highlands sites of Izapa and Kaminaljuyu (Wright *et al.*, 2010; Wright, 2012), the declining Olmec cities along the Gulf Coast, and the emerging political centers of Teotihuacan in the Valley of Mexico (Price *et al.*, 2000) and San José Mogote and Monte Albán in the Valley of Oaxaca (Hodell *et al.*, 2004; Price *et al.*, 2000).

There is ample evidence of ritual cave utilization during the Late Preclassic throughout the ancient Maya world (Prufer and Brady, 2004). The types of materials associated with these rituals is limited to fragmented pottery sherds and remains of sacrificial victims with some caves also showing light cave modifications such as at Naj Tunich (Brady, 1989), Balam Na (Garza *et al.*, 2002), and Cobanerita (Brady *et al.*, 1997). While usage of caves for ritual during the Late Preclassic was relatively minimal, it established an important precedent for use that would increase over time, especially in the Classic and Late Classic (Stone, 1995).

2.2.3 The Maya Classic Period (250 – 950 CE)

Between the Terminal Preclassic and into the Early Classic (*ca.* 150 to 250 CE) some city-states in the Petén consolidated their power at the expense of others. With the decline of El Mirador and its allies, Tikal became one of the preeminent powers in the region (Webster, 2002), and engaged in periodic conflict with the nearby cities of Uaxactun and El Naranjo in the Petén region, Calakmul in present day Campeche, and Caracol in present day Belize (Kelly, 1996; Demarest, 2004).

It is during the Classic period that the Maya as a culturally distinct Mesoamerican group attained and extended its hegemony over the region. However, in Mesoamerica, power was not as defined as the territorial empires of ancient Rome or Persia, with ever expanding geographical holdings, but rather as a localized control over resources and trade and dominance over other Maya polities (Estrada-Belli, 2011). Trade and political alliances developed with Teotihuacan and Monte Alban in central Mexico with embassies and representations in each other polities (Hansen, 2014). External intervention by Teotihuacan in Petén politics resulted in the deposition of the Tikal king (*ca.* 378 CE) and the introduction of another lineage partial to Teotihuacan supremacy (Coe, 1999; Stuart, 2000). Over time, Tikal regained its dominance over the

Petén region and expanded to the southeast through alliances with Copan and Quiriguá (Coe, 1999; Estrada-Belli, 2011). With the eclipse of Teotihuacan hegemony towards the middle of the Classic period, ca. 562 CE, the alliance forces of Caracol and Calakmul were finally able to defeat Tikal, becoming the preeminent powers in the southern lowlands in the east and west, respectively.

Ritual cave use became more common and elaborate during the Classic and Post Classic periods. In Naj Tunich, extensive architectural modifications, interments, writing, and petroglyphs (Brady 1989). Similarly, construction of altars and expansion of chambers for ritual use during this period are observed in Balankanche (Andrews 1971) and Barton Cave (Wrobel 2012).

Over the next 300 years, other centers in the periphery began to rise in importance. Palenque and Yaxchilan began to compete for hegemony against Calakmul and influence other nearby polities such as Bonampak (Estrada-Belli, 2011; Sharer and Loa, 2006). In the northern lowlands, old cities such as Cobá, Uxmal, Mayapan, and Chichen Itza, began to grow in influence and size. This shift in hegemony from the southern lowlands to the northern lowlands is what is referred to as the Classic Maya Collapse (Martin and Grube, 2000), marked by the abandonment of cities in the southern lowlands, attributed to endemic warfare, environmental degradation, and drought (Coe, 1999).

Coincident with increased warfare among settlements (including evidence of their destruction or abandonment), is the evidence of an intensification in the use of caves for ritual practice during this period, manifested by extensive cave modifications, increase in offerings, and human sacrifice in deeper and harder to reach areas, and at times destruction of modified spaces within the caves. Of particular interest are those caves associated with surface sites that similarly exhibit signs of destruction or abandonment. While numerous studies point to

various plausible causes for the “collapse”, one thing was certain: the underground landscape did not escape the event.

2.2.4 The Maya Post Classic Period (950 – 1539)

Following the collapse of the Classic Period, the political, economic, and religious activity of Maya culture shifted towards the northern lowlands of the Yucatan and the Maya highlands (Sharer and Loa, 2006; Estrada-Belli, 2011), with the trade bypassing the Petén region altogether (Foster, 2002). During the Early Post Classic, the northern centers of Chichen Itza and Uxmal saw increased activity and growth, while sites along the Pacific coast and piedmont were abandoned or relocated (Sharer and Loa, 2006). With the rise of the city of Mayapan towards the 12th century CE, the northern Maya established and controlled the trade routes along the Caribbean and Gulf coasts, thus stabilizing the decline for a couple of centuries (Masson, 2012; Sharer and Traxler, 2006). However, important major highland centers like Kaminaljuyu were abandoned and the political landscape fragmented into various Mayan ethnicities and warlords (Sharer and Loa, 2006).

Mayapan was abandoned around 1448 CE, followed by prolonged warfare reminiscent of the southern lowland Maya collapse (Masson and Peraza-Lope, 2014). By the time of European contact, the Maya world was a fragmented amalgamation of independent provinces in the Yucatan and more powerful Maya kingdoms in the Maya highlands, all with one common culture but varied sociopolitical structures (Andrew, 1984).

During the Post Classic, ritual cave utilization continued but decreased significantly throughout all the Maya realm. In the northern Maya lowlands, ritual cave use focused around flooded sink holes or “cenotes” such as those in Chichen Itza, Coba, and Bolonch’en, as described by Thompson (1975), or any cave or significant size (Andrews, 1971). Surveys have recovered little, or no

Post Classic materials associated with cave ritual with the exception of a few selected caves. These materials are composed mostly of offerings of crude ceramic fragments and shell ornaments, with very few sacrificial remains and minimal cave modification (Helmke, 1999; Kieffer, 2010).

2.2.5 Contact Period and Aftermath

First contact with Spanish explorers occurred in 1511 CE along the Yucatan coast (Masson and Peraza-Lope, 2014), followed by three more expeditions between 1517 and 1519 (Sharer and Traxler, 2006). In 1524, the K'iche capital of Utatlán was taken by the Spaniards and this conquest was followed by the Kaqchikel capital city of Iximche and the Mam capital of Zaculeu in 1525, bringing the Suconusco and highland Maya kingdoms under Spanish control (del Aguila Flores, 2007). In 1527, Francisco de Montejo began several campaigns in the northern Yucatan peninsula finally subduing it in 1546 (Sharer and Traxler, 2006); however, the Maya kingdoms in the Petén basin remained independent until Martín de Ursúa conquered the Itza capital of Tayasal in 1697, thus bringing the Maya cultural areas into the viceroyalty of New Spain.

Over the Colonial period and into the 19th century, there were numerous uprisings from various Maya ethnic groups, all put down by either the colonial power or the republican states that followed. These ethnicities were numerous and represented a significant percentage of the populations in Guatemala, the Mexican states of Chiapas, Yucatán, Campeche, Tabasco and Quintana Roo, the northwestern districts of Belize and in the most western departments of El Salvador and Honduras (Ochoa and Martel, 2002).

In the centuries after the conquest by the Spaniards, the catholic church attempted to stamp out any remnants of ancient Maya religion. However, as it occurred in most of Latin America and Mexico specifically, ancient practices

blended with the doctrines of evangelization to produce a local Christianity that informed the new Maya identity and became embedded into the local tradition and folklore. Ritual cave used was delegated to local shamans with their practice consider witchcraft. Nonetheless, ritual cave uses by present day Maya continue and is a commonly accepted occurrence (Holland, 1961).

With this geohistorical perspective, and despite 500 years of forced Christianization, westernization, and globalism, cultural elements persist through oral tradition and ritual that tie the present-day Maya to their ancestors.

2.3 Maya Creation Myths and Sacred Landscapes

Throughout Mesoamerican cultures, there are strong commonalities and associations between the natural landscape and the spirit world and immortals (Leeming and Page, 2000). These spirit worlds are usually primordial and uninhabited, some with water, an empty sky and deities with various anthropomorphic and/or zoomorphic appearance (Vivéros de Castro, 1998; Leeming and Page, 2000; Lopez Austin, 1997). The Maya creation myth is one example of how their cosmology imparts an aura of sanctity and divinity to their surrounding landscapes. By analyzing this and distilling key aspects of the narrative, we can gain insight into ancient Maya thought.

As described in the Popol Vuh genesis, from Recinos (1950) and subsequent translations, the story goes as follows: "In the beginning there was only stillness, silence and water, with no light, no land, plants, people or animals". The story continues, narrating that lying in the primordial waters were six gods: the Framer, the Shaper, Xpiyacóc, Xmucané, Tepew and the Quetzal Serpent - who helped the god of the sky and wind Hurakán create the Earth. Here we must note that stillness, silence, and water were present before the creation of Earth, and thus are essential elements in Maya religious thought.

The story continues, stating that to separate the newly created Earth from the sky, the deities “planted a tall ceiba tree” thereby creating the “space for life.” This “space for life” is the description of landscape, the living space inhabited by all surface dwelling creatures. The roots of the ceiba tree penetrated deep into the nine levels of the underworld (Xibalbá), while the branches reached into the thirteen levels of the upper-world. The plants and animal were created, and the gods attempted to create humans, first from mud and secondly from wood; but these were defective and destroyed, with the surviving wooden humans becoming monkeys. This passage illustrates why the Maya attributed a supernatural essence to everything in their surroundings, as everything, plants, animals and landscape was created by the gods, and thus godly.

Again, the story continues, recounting that despite all the creations, there was no sun or moon, and no humans. Herein, the story of the Hero Twins Hunajpu and Xbalanqué begins, and with it, the genesis of man. The twins were conceived by their mother Ixkik’ after speaking to the head of their father Hun Hunahpu who spat on her hand as he hung from a cacao tree, after being killed by the Lords of Xibalbá. The twins had become great ball players and challenged the Lords of the underworld to a ball game in Xibalbá to bring their father back to life. However, they were permitted to play only after surviving numerous trials in the underworld. With great skill and cunning, they won the ball game and their father came back to life as the Maize God. The Hero Twins ascended from the underworld to the surface and continued to the sky becoming the sun and the moon. With these celestial bodies in place, the gods created the final human form from dough made from corn (Recinos, 1950). It is from this last passage that the final deities are created and the supernatural relation between humans and the physical world are firmly affixed.

This underworld was known as Metnal to the Yucatec Maya and as Xibalbá in the holy book of Popol Vuh (MacLeod and Puleston, 1978). This was a

place of dread and the realm of the dead (Recinos, 1950). However, it is also associated with life giving water, and as noted by MacLeod and Puleston (1978), the place where the sun retreats during the night in its daily cycle of death and rebirth, fitting to the mythological Hero Twins of Maya genesis (Recinos, 1950; Stone, 1995).

Notwithstanding the diversity of Mayan dialects, present day oral traditions and rituals relate every Maya ethnicity to a commonly shared mythology, practice, and discourse (Ochoa and Martel, 2002; Thompson, 1970). As noted above, the cosmological narrative of the Maya imbued every aspect of their surroundings with supernatural significance, from the water, to the sun, to the silence, to the darkness. Therefore, it stands to reason that such cosmological thought will inform their behavior and in turn be projected into the landscape. An examination of such behavior and projection will be contextualized and validate our study.

2.4 Maya Ritual Cave Use

Early documentation of ritual cave utilization by the Maya dates to the late 19th and early 20th centuries with the explorations of Loltun Cave by Edward Thompson in 1897, followed by reports on a series of caves near Copán by George Gordon in 1898, and findings on a cave in Quen Santo published by Edward Seler in 1901; numerous offerings, modifications, and ossuaries were reported in every instance (Thompson, 1975).

Throughout most of the 20th century, more caves and grottos were discovered and explored throughout the region, yielding a vast cache of archaeological material and remains. For example, Eduardo Quiroz Cave near Benque Viejo, Belize, explored by Gann in the 1920's had numerous modifications (walls, altars, and passageways) connecting several clearly ceremonial chambers as evident by large amounts of broken sherds scattered in

their floors (Thompson, 1975). However, the significance of these findings was diluted by the eco-evolutionary and materialistic lenses of archaeology theory at the time, which favored a more utilitarian and scientific investigative framework and interpretation. With the advent of post-processual theory, the investigative framework allowed for a more subjective interpretation of the entire landscape (e.g., mountains, rivers, caves, clouds.), and any associated cultural materials (Prufer and Brady, 2004). Towards the later part of the 20th century continues cave discoveries and explorations produced more findings.

For example, Chamber C of Actun Balam, Jaguar Cave, produced large numbers of sherds, in excess of 22,000, mixed with other objects of bone, shell, flint, and obsidian (Pendergast, 1969). Similarly, Rio Frio Cave (also in Belize) had large amounts of sherds suggestive of ceremonial breakage and an apparent area of worship to a stalagmitic idol (Prendergast, 1970). Last, Naj Tunich has various paintings and glyph texts scattered throughout the cave. These paintings depict local iconographic fauna such as deer, the figures of ballplayers, ballcourts and musicians, figures engaged in sexual intercourse and ritual bloodletting, as well as significant cave modifications, ornate ceramics, stingray needles, petroglyphs, and a small number of tombs associated with elite individuals (Brady and Stone, 1986). Moreover, the importance of this particular cave is discerned not only from the amount of material within, but also for its length of use, from Preclassic (100 BCE to 200 CE) ceramics and pottery, to large cave modifications such as altars and platforms of Classic period (250 to 500 CE), to the Late Classic (550 to 830 CE) paintings and inscriptions.

The quantity and quality of archaeological remains found within caves demanded the recognition of other than a utilitarian use of caves by the Maya. Earlier publications (MacLeod and Puleston, 1978) attempted to interpret Maya mythology and cosmology from the cultural modifications found within various caves from combined perspectives of ethnohistorians, iconographers,

epigraphers, linguists, archaeoastronomers, and archaeologists. Specifically, they argued that only with the combined perspectives of these disciplines can we arrive at an accurate interpretation of ritual cave use and of the cosmological and religious significance that caves had for the ancient Maya.

Understanding the relationship of the Maya to the earth and the earth gods is an important one as it informs us on the visualization of the natural landscape through the lenses of the ancient Maya. For example, more recent work by Brady (2003) rejects the associations of caves to the underworlds, characterizing them as misinterpretations of actual associations with the earth (Brady, 2003; Wölfel, 2006). As evidence, he cites the veneration and mention of the Q'eqchi earth lord Tzuultaq'a. As discussed in Wölfel (2006), a link between caves and rich earth gods is made by the ethnographic study of Tzeltal and Tzotzil beliefs conducted by Vogt and Stuart (2005). Therein, they report the Tzotzil earth lord to be a "large fat Ladino" who also "owns all water holes and controls the lighting and the clouds." To further support the idea of localized cave-person relationship with the Maya, Wölfel (2006) mentions a concept that dates to prehispanic times, one in which "every mountain has its own mountain God" as emphasized by Köhler, (2006) and in contradiction to a single earth god as formulated by Vogt (1981).

This dual interdependence between one god and one landscape feature is also translated to a dual relationship between one site and one cave (Brady, 1997a and 1997b). Additionally, as reported in Prufer and Brady (2004), 90% of the caves surveyed in the region with archaeological content do not show evidence of sedentary occupation, but of ritual use. This is significant as indicates the religious use of landscape by the Maya, namely in caves, and contextualizes the archaeological material and modifications within a ritualistic framework (Prufer and Brady, 2004; Brady, 1989, 1997b; Brady and Prufer, 2002).

This ritualistic use suggests that the cave and anything within it was viewed by the ancient Maya as hallowed, imputed with the supernatural, and not unlike Christian relic traditions (Prufer and Brady, 2004). From this, it is not unreasonable to envision the deposition of cultural materials within the caves (e.g., vases, pots, figurines, human sacrifices) as offerings, and the removal of cave materials (stalactites, stalagmites, speleothems, cave pearls, etc.) from the caves as a holy relic, imbued with “desired supernatural attributes”, (i.e., amulets) to the surface (settlement) sites.

2.5 Why Study Speleothems?

2.5.1. Breakage, Transport and Usage of Speleothems by the Maya

The breakage and transport of speleothems during ancient Maya cave visitation has become an increasingly well-documented phenomenon since the practice was first noted over two decades ago (Brady *et al.*, 1997). This phenomenon has raised several questions such as the spatial and temporal extent of these interactions, practices, and specifically the relationship between Maya polities and proximal or distant caves. Recent studies have substantially increased our understanding of the scale of breakage and redeposition of detached material in surface sites. Brady *et al.* (2005) conducted a speleothem inventory in Cave 1 at Balam Na in Guatemala and documented that nearly 60% of the stalactites had been broken. The 1,660 broken stalactites indicate that an impressive amount of material had been removed from this small (40 m long) cave since few stalactites littered the floor of the cave. The study by Peterson *et al.* (2005) is significant in providing actual physical evidence for the close relationship between caves and settlements. In it, Peterson recorded that thousands of speleothems had been incorporated into public and residential architecture at settlements investigated by the Xibun Archaeological Research Project (XARP) in central Belize (McAnany *et al.*, 2004; McAnany and Thomas, 2003; McAnany, 2002, 1998). This practice of incorporating speleothems into

the built environment of Maya settlements probably accounts for a large percentage of the speleothems removed from caves and reflects a fundamental religious motive.

Other studies have also documented the incorporation of speleothems into the built architecture at surface and underground sites. As reported by Maureen Carpenter (Phillips *et al.*, 2014), excavations of Structure 1 at the site of Las Cuevas, Belize, uncovered various cut speleothems in the fill of the plaza area stairs along the structure. In the same report, Marieka Arksey reports the speleothem fragments in the fill of Level 4 and the fill of unit 22, suggesting these may have been placed there intentionally in part due to their association with the cave (Phillips *et al.*, 2014)

2.5.2 Sourcing of Culturally Derived Speleothems

In a seminal article on speleothem utilization, Brady *et al.* (1997) provided evidence that Instrumental Neutron Activation Analysis (INAA) of speleothems from caves in the region of Copan, Honduras, can produce chemical signatures that are discrete to individual caves. It was uncertain, however, whether the method would be applicable to caves in the southern Maya lowlands where the geology was thought to be far more homogeneous than in highland Honduras. Until now, no subsequent research in the Maya lowlands via INAA was attempted to test the implications of the first study.

However, attempts at sourcing speleothems by other methods and instrumentation have been conducted. For example, Peterson *et al.* (2005) utilized ICP-Emission Spectroscopy on speleothems samples from the Sibun River Basin to provide physical evidence for the close relationship between caves and settlements. After noting the vast amounts of speleothem samples at the surface site of Hershey and its proximity to the cave of Actun Chanona, she reasoned that obtaining a chemical characterization or “finger-printing” of intact

speleothems found *in situ*, and those found within cultural context (surface sites), would allow us to trace the source to individual cave or caves, and give us an opportunity to map very specific settlement/cave relationships, and thereby elucidating the religious importance of their cave of origin.

Moreover, Nation *et al.* (2006, 2012) reproduced Peterson's analysis utilizing the same samples but using an instrumentation and protocol variant, laser ablation - ionized coupled plasma - time of flight - mass spectrometry (LA-ICP-TOF-MS) at the Institute for Integrative Research in Materials, Environments, and Societies at California State University, Long Beach. Lastly, Brennan *et al.* (2013) also used ICP-MS, ICP-AES in his characterization of limestone monuments from northern Belize. This last study is significant in that it utilizes a combination of petrographic analysis and element/cation ratios to further differentiate between samples.

2.5.3 Study Objectives

In summary, caves and materials derived from them (i.e.: speleothems), had a significant relevance to the ancient Maya, based both on ritual remains found in caves and on the occurrence and ubiquity of speleothems in Maya surface sites and architecture. The preceding literature review contextualizes the importance of understanding these relationships and the necessity of continued research in the area. Prior studies demonstrate the use of INAA as a viable method of sourcing these lithic materials, differentiating samples within the same cave and between different caves for the one sub-region of the Maya world. However, the broader feasibility of speleothem provenance determination is untested. To better understand the challenges of this task, we will explore the geology of our area of study and the process of speleothem formation, with an eye to identifying those factors that potentially contribute to the creation of distinctive chemical signatures.

Chapter 3. Geology, Geochemistry of Speleothems, and Provenance

3.1 Speleothems

The term “speleothem” was first defined by Moore (1952) as simply “a secondary mineral deposit formed from water in caves.” More recently (Hill and Forti, 1997), the phrase “from water” was eliminated as “secondary mineral deposit” already implies a chemogenic deposition (Self, 2004). We must note that while the word speleothem is readily applied to a variety of mineral deposit formations, only those formed within caves are true speleothems. This serves to distinguish them from those secondary and tertiary mineral deposits found in other geographies and landscapes such as waterfalls or lava tubes (Self, 2004).

Typically, speleothems occur in the interior of crevices, caves, grottos, and rock shelters that dot karst landscapes throughout the world and in areas where significant limestone sequences are present in the stratigraphy. Speleothems include stalactites, stalagmites, frostwork, flowstone, gourds, helictites, soda straws, curtains, and cave pearls. These types are defined by their morphology and not by their location, thus some speleothem types can be found in non-cave settings such as mineral springs (Self, 2004; Self and Hill, 2003). This study analyzed a variety of speleothem fragments of different types (stalactite, stalagmite, flowstone, curtains, soda straws and cave pearls) all found in different areas within caves and some as noted in surface sites, indicating extraction from a cave. All these samples derived from a karst landscape and are thus primarily composed of diagenetic calcium carbonate varieties, with small aggregates of various origins. As discussed below, their geochemistry is expected to reflect both limestone and karst geology, and speleothem ontogenesis.

3.1.1 Parent Materials

Speleothems are carbonate rocks, composed of calcium carbonate deposited via a chemogenic process over thousands or millions of years (Tucker *et al.*, 1990; Park, 1983). These formations are secondary or tertiary remineralizations of one or more overlaying substrates, usually marine limestone facies (Sholle *et al.*, 1983). To better understand the geochemistry associated with speleothems, we must follow the process from the initial deposition of the parent material (limestone), through its dissolution, and redeposition. Note that throughout these processes, minute amounts of contaminants, nutrients, and trace elements are incorporated into the matrix of the mineral (Fernandez-Cortez *et al.*, 2011).

Limestone is classified as a sedimentary rock and is composed primarily from the skeletal remains of shallow marine organisms such as corals, mollusks and forams, and depending on their proximity to the coast, these deposits may also contain various forms of terrigenous detrital materials such as clays, silts, and sands (Tucker *et al.*, 1990; Sholle *et al.*, 1983; Seibold and Berger, 1993 and 2013). While these additions are minute, they can be spatially and/or temporally unique enough to identify certain stratigraphic horizons and/or events such as the K/T boundary (Sholle *et al.*, 1983) and potentially enable provenance distinctions of limestone materials.

Once the limestone sequence has been lithified, buried, and become part of the earth's crust, it is subject to other geological forces. The vast majority of limestone deposits are subjected to uplift and erosion, with outcroppings exposed to the elements while the bulk remains buried but relatively near or at the surface. These last are the ones that provide us with karst topography and geomorphology in many parts of the world and in Belize proper (Miller, 1996).

It is in these near surface limestone deposits that most caves and grottos are found, and within them, speleothems. The tectonic forces that have brought the limestones to the surface have also fractured them creating conduits for water to infiltrate deep underground (Miller, 1996). However, cave and speleothem formation are not dependent on rock fracturing and water infiltration alone. Overlaying terrains covered in vegetation are necessary for active dissolution of the underlying limestone sequences, as plant decay produces a variety of soluble polymeric compounds known as fluvic and humic acids (Drever, 1994). As the soil profile develops, the concentrations of these acids are found in the top organic layer. In humid tropical regions such as in the Yucatan, these tend to be washed down the soil profile to the bedrock where the acidity lowers the pH of the runoff and groundwaters, thereby weakening and dissolving the bedrock, especially along fractures (Reeder *et al.*, 1996; Miller, 1996). An early study (Drever and Vance, 1994) found that these organic acids greatly affect the mineralogy of the soils due to their affinity to complex and transport iron and aluminum to the point that it is reflected in the geochemistry of the underlying speleothems.

The dissolution of the rock means that the matrix of calcium carbonate solid is ionized and enters into solution, increasing the acidity of filtrate by forming carbonic acid. This creates a positive feedback in relation to the dissolution of the limestone substrate. As the limestone dissolves, the carbonate ion $[\text{CO}_3]^{2-}$ combines with free H^+ creating the carbonic acid, which further dissolves the CaCO_3 matrix (Wolfgang, 2004). These dissolution processes and the complexing nature of the organic acids represent a second opportunity to incorporate other elements into the mineral matrix of the carbonate speleothem by chemical instead of biological processes. Herein, dissolution kinetics and equilibrium mechanisms drive the incorporation of metals, trace elements, and rare earth elements. Given that the potential sources of these aggregates include all the overlying strata, and barring long range horizontal

hydrogeologic movements, they can be spatially and/or temporally constrained to particular watersheds thus localizing chemical signatures in the speleothems.

3.1.2. Ontogeny of Speleothems

Speleothems are primarily composed of three species of minerals: calcite, aragonite and gypsum (Hill and Forti, 1997), while some other deposits also include dolomite (Dunham, 1962). Thus, the ontogeny of these minerals determines the ontogeny of speleothems. While the dissolution of these minerals is dependent on multiple factors such as soil and water acidity, hydrology and hydrogeology of the area, evaporation and presence or absence of certain elements (e.g., sulfur for gypsum and manganese for aragonite), their deposition and growth on a given substrate is governed by more constraining variables found within the cave proper.

A seminal article by Allison (1923), high-lighted the multivariate factors affecting the deposition and growth of speleothems, even under near static conditions. He established several factors affecting the deposition, growth, and morphology of speleothems, including drip, air circulation, relative humidity, temperature, and solute concentration. He further argued that these microenvironmental parameters also affect the morphology of speleothems, in that symmetry in ground columns (stalagmites) is indicative of constant growth conditions, while extremely unsymmetrical stalactites and stalagmites must be classified and examined by sections as these are evidence of non-static deposition rates.

Later studies (Moore, 1962; Sletov, 1985 and 1999; Stepanov, 1971) verified the relationship of these parameters as determinants in the deposition of calcite minerals and the growth of speleothems (Maltsev, 1997a, 1997b, 1997c; Stepanov, 1997). Moreover, the hydrodynamics within speleothems change over time resulting in different types of morphologies not evident at first glance. As

exemplified, a seemingly robust stalactite when cut may reveal a “soda straw” core, indicating a fundamental change in the internal hydrology of the speleothem, and thus morphology and deposition rates (Maltsev, 1998). Similarly, flowstones can occur along ceiling cracks forming “curtains” over pools or along the walls of a cave by seepage. While all the determinant factors discussed above are the same, “free hanging” formations are more susceptible to air currents within the cave, resulting in twisted and bended straws, curtains, and flowstones (Maltsev, 1998). Considering the ontogenesis of speleothems and the near absence of steady state conditions over geologic time spans, we must realize that a flowstone, straw, cave pearl, stalactite, or stalagmite is a composite creation of multiple depositional facets, that taken over a specific geographical area may reflect past regional climatic changes.

3.1.3 Implications for Provenance Determination

In summary, multiple factors may affect the formation and thus the geochemistry of speleothems must be considered as follows:

- External climatic variables – such as temperature and precipitation, affecting rates of erosion, dissolution and deposition.
- Parent material – subtle differences in elemental composition of limestone substrate.
- Surficial soils – with subtle terrigenous inputs that percolate through the limestone.
- Vegetation – humic and fluvic acids which affect rates of rock dissolution.
- Hydrogeologic drainage – subsurface water flow through karstic system.
- Internal cave climatic variables – such as temperature, humidity, and ventilation which affect rate of deposition.

Thus, to assess the scale of variability, it is necessary to consider the spatial distribution of these factors across the study area.

3.2 Belize Geology and Karstic Landscapes

The cave areas sampled in this study are located in central Belize, in the Cayo and Belize Districts, respectively. The country of Belize is in present day central America and towards the southeast of the Mesoamerica cultural region. Geographically, is located between latitudes 15.90 and 18.48 N, and between longitudes -87.47 and – 98.19 W. Belize is bordered to the North and Northwest by Mexico, to the West and South by Guatemala and to the East by the Caribbean Sea. The general climate of these region is tropical with pronounced wet and dry seasons, with local topographical influence variations (Walker, 1973). Topographically, the country can be divided into two physiographic regions, one dominated by the Maya Mountains with an elevation around 1100 m and surrounded by younger hills and plains of calcareous rocks (Miller, 1996), and a second region comprising the northern lowlands, and along with the southern coastal plain. These low-lying areas, especially in the northern part are characteristically flat and often swampy, with many lagoons. The coastal lowlands themselves turn into mangrove swamp toward the south and to tropical pine savanna towards the northwest areas of Corozal District (Hartshorn *et al.*, 1984).

The recent geological development of Belize is the result of complex continental drifting of the North America and South America plates, and the associated faulting and rifting between contact zones (Flores, 1952). The southwest motion of the North America plate towards the Yucatan platform coupled with the Eastward movement of the Caribbean Plate and a series of sea transgressions and regression events during the last 80 million years have given rise to the present day structurally dominant features of the Maya Mountains to the southwest (Anderson *et al.*, 1971, Bateson *et al.*, 1977), the off-shore atolls and coral reefs, and the relatively gentle topography in most of the inland and coastal plains (see Figure 2). Belize is divided into three main geological provinces: Northern Belize, Southern Belize, and South-Central Belize (Aitken

and Steward, 2002). The Southern Belize province contains the Belize basin, while the South-Central Belize province encompasses the Maya Mountains. The Northern Belize Province is comprised of the Corozal basin, itself an extension of the Yucatan platform and stratigraphically part of the North Petén Basin of Guatemala. (Reeder *et al.*, 1996; Weber *et al.*, 2006). Our sample areas are in the Northern Belize Province within the Corozal Basin and thus we will cover the geology of this province in greater depth.

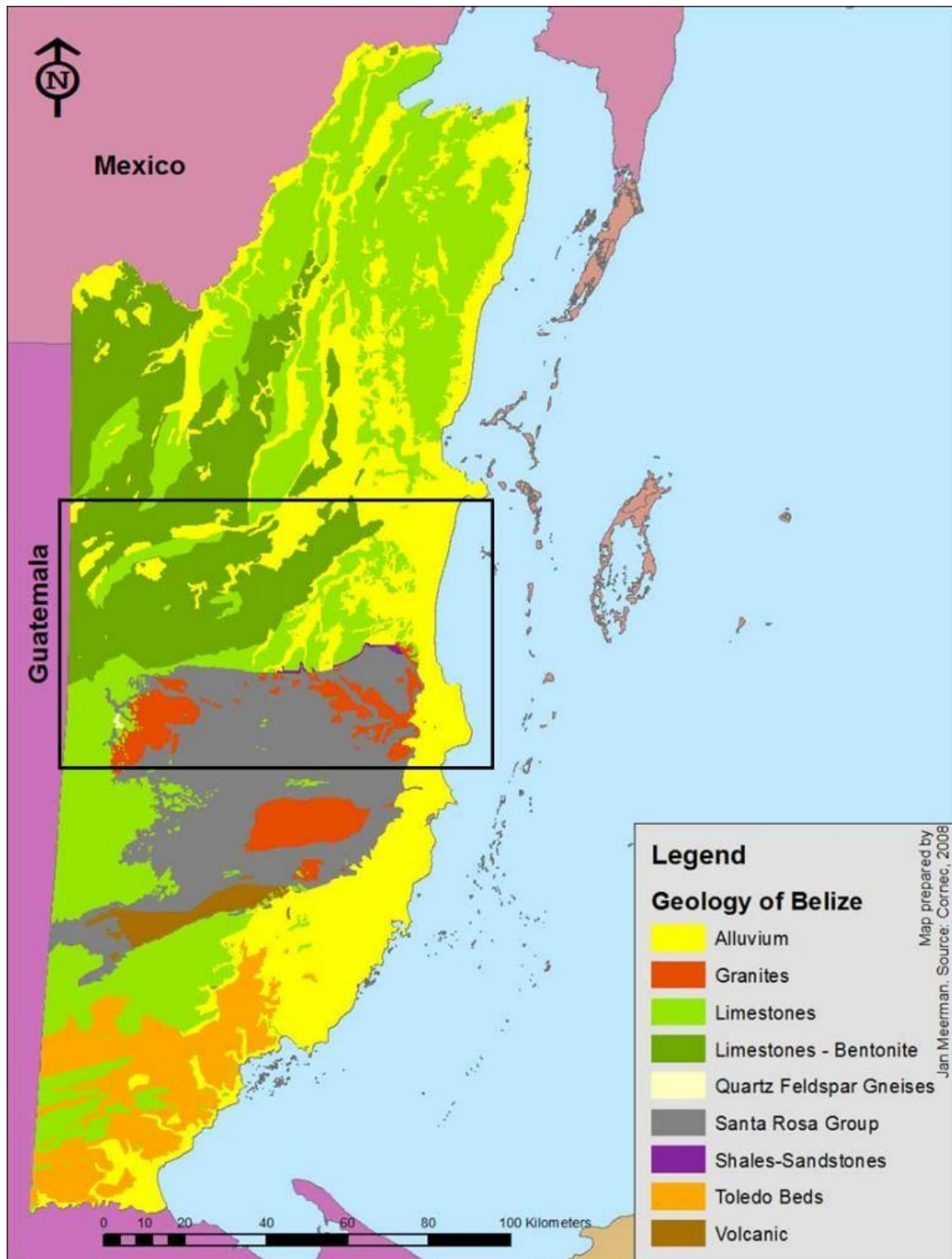


Figure 2. Geological Map of Belize. As adapted from Jan Meeman (2008) and showing the study area (inset).

3.2.1 Stratigraphy and Paleogeography of the Corozal Basin in Northern Belize

There are four distinct stratigraphic sequences (Aitken and Steward, 2002; Petersen *et al.*, 2012) that comprise and underlie most of southeast Mexico, the Yucatan platform and the Northern Belize Province in particular. From the oldest (bottom) to youngest (top) these are: The Santa Rosa Group, overlain by the Hillbank Formation, topped by the Yalbac Formation, and finally the Barton Creek Formation with its related tertiary and quaternary deposits depending on location (Reeder *et al.*, 1996) (Figure 3).

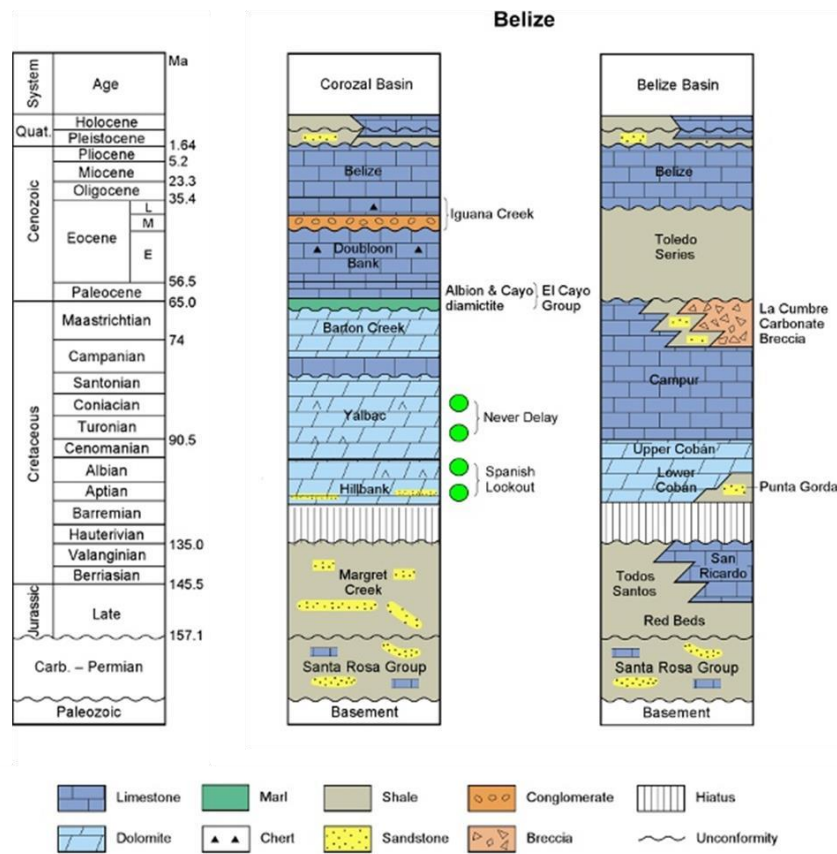


Figure 3. Stratigraphic columns for the Corozal and Belize Basins in correspondence to chronostratigraphic column. Most of the calcareous horizons are unconformably deposited and date to the middle Cretaceous. (from Petersen *et al.*, 2012).

The properties of these stratigraphic units are as follows:

The Santa Rosa Group. The Santa Rosa Group comprises the basement rocks for most of the region that encompass the southeast of Mexico, Guatemala, the Yucatan Platform (Reeder *et al.*, 1993; Weber *et al.*, 2006), and by extension the Belize and the Corozal Basin (Day, 1986). In Belize, the Santa Rosa Group is characterized by middle to late Paleozoic aged (350 to 250 MA) metasedimentary rocks, shales, schists and phyllites with intercalated horizons of metaquartzites, with clastic sedimentary rocks and interbedded limestones that form the largest part of the Maya Mountains in central Belize (Weber *et al.*, 2006; Reeder *et al.*, 1996). Outcrops of the Santa Rosa Group occur in the Mountain Pine Ridge portion of the Maya Mountain Block (Reeder *et al.*, 1996). The Maya Mountains are themselves intruded by granites which provide a unique geological and geochemical character to the rocks of the immediate vicinity and down gradient along drainage systems.

Hillbank Formation. The Hillbank Formation is a 75 to 700-meter-thick unconformable deposit following tectonic episodes of faulting and uplift, resulting in erosion and major sea transgressions during the late Jurassic to early Cretaceous (Gill *et al.*, 2016). These transgressions flooded the entire Northern Belize province and the Corozal Basin in particular. Continued tectonic activity during the Cretaceous uplifted the Belmopan-Shipstern subsurface ridge, thus splitting what is now central northern Belize into two distinct depositional environments: one characterized by a hypersaline lagoonal basin to the North and West, and a shallow sea to the East (Aitken and Steward, 2002). Thus, the Hillbank Formation is comprised of two alternating, yet genetically related facies consisting of (1) a dark tan clayey, microcrystalline calcareous dolostone and (2) fluvial clastic deposits or coarse sandstone. This is significant to note as it affects the clastic and elemental composition of these sequences. The Hillstone Formation can be further subdivided vertically into three sequences: The Lower Hillbank Dolostone/Sandstone indicative of a shallow marine environment with

alluvial and fluvial interfacies; the Middle Hillbank Dolostone or MHBD, representative of sabkha and shallow marine environment, and lastly the Upper Hillbank Sandstone or UHBS, with its clastic sediment indicative of alluvial and fluvial depositional environments (Gill *et al.*, 2016).

Yalbac Formation. The Yalbac Formation is a 200 to 2741 m-thick conformably deposited sequence over the Hillbank and represents a continuance of shallow marine sedimentation (King and Petruny, 2014). The Yalbac Formation is subdivided into three members (Y1-Y3) of genetically related facies. The basal or lower member (Y3) is composed of mixed transitional siliclastic and dolomitic deposits grading into calcareous dolostone indicative of shallow marine, sabkha, and hypersaline environments. The middle member (Y2) consists of thick-bedded dolomitic facies with sporadic anhydrite-rich layers consistent with shallow subtidal, near-reefal deposits to shallow restricted lagoon and tidal flat environments. The upper member (Y1) mainly consists of dolomitic and anhydritic facies, indicative of sabkha, supratidal, intertidal, shallow subtidal environments associated with a terminal shallowing phase.

Barton Creek Formation. The Barton Creek Formation with a thickness between 488 and 791 m represents all deposits above the Yalbac formation (Aitken and Steward, 2002). These encompass the late Cretaceous Barton Creek proper, with its tan to grey limestone and dolostone, and all tertiary and quaternary deposits (King and Petruny, 2003; Gill *et al.*, 2016; and Miller, 1996). In the Corozal Basin these Cenozoic deposits include the unconformably deposited KT boundary interval of the Albion Island Formation with its characteristic impactoclastic beds, the Paleogene El Cayo group composed mainly of limestone, itself overlain by the limestones of the Doubloon Bank group of Eocene age, and clastic and carbonates of Miocene-Pliocene of the Orange Walk group (King *et al.*, 2004). The uppermost cover consists of Pleistocene and Holocene detrital deposits forming in a relatively thin layer of clastic soils from

parent carbonates, marls, bentonitic clays, and poorly consolidated sands (Miller, 1996). The area of northern and central Belize has experienced little tectonic activity during the Cenozoic, with low subsidence in the Corozal basin and uplift in the Maya Mountain region resulting in the rise of Oligocene age carbonates near their basement (Miller, 1984). These events and the karstic nature of the underlying Barton Creek carbonates have resulted in numerous river terraces, cave levels, and outcrops from different sequences that, for this study can affect the availability and types of lithic material, and most importantly, the geochemical signature of those samples.

3.2.2 Karst Landscapes and Morphology in Belize

Prior to the mid 1990's, information regarding the karst landscapes in Belize were few and sporadic, limited to field notes from speleological explorations, personal communications, abstracts from caving-oriented publications, government reports, unrelated geological studies and unpublished monographs (Miller, 1996). In 1996, an overview of Belize's karst landscapes, geology, and hydrology was published by Thomas Miller. Therein, a comprehensive outline of Belize's karst features was established and to which we will reference in this study.

A karst environment is characterized by poorly to medium lithified and highly soluble subsurface rocks. In the case of Belize, these are comprised mostly of cretaceous carbonates (limestones and dolostones), with some tertiary and quaternary poorly lithified carbonate deposits as it occurs in the Corozal basin (Miller, 1996, Reeder *et al.*, 1993.). Eight karst regions have been identified in Belize based on differences in parent material/surficial geology, see Figure 4 as adapted from Miller (1986). These are: 1) Boundary Fault, 2) Vaca Plateau, 3) Sibun-Manatee, 4) Little Quartz Ridge, 5) K-T Fault Ridge, 6) Cayes/Barrier Reef, 7) Yalbac Hills, and 8) Tertiary Rocks, although only five are intensely karsted and thus likely to form caves. These cover extensive areas with

varied geomorphology with some containing haphazardly distributed depressions, also known as cockpits, while others are characterized by allogenic streams running along dry valleys, disappearing underground or in some instances, coalescing into free-flowing rivers (Miller, 1996).

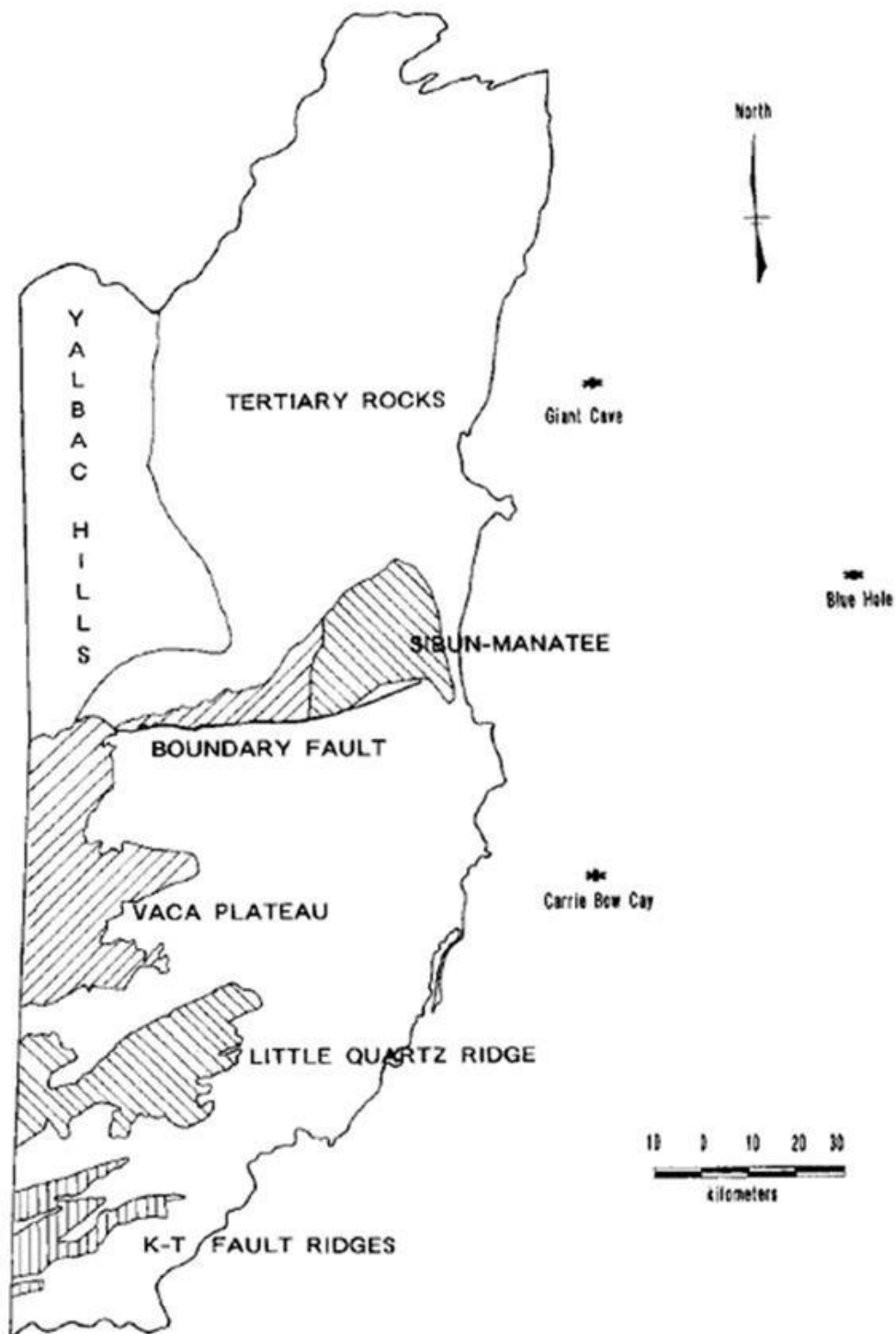


Figure 4. Karst regions of Belize: 1) Boundary Fault, 2) Vaca Plateau, 3) SibunManatee, 4) Little Quartz Ridge, 5) K-T Fault Ridge, 6) Cayes/Barrier Reef, 7) Yalbac Hills, and 8) Tertiary Rocks (from Miller, 1996).

3.3. Study Area Geology and Karst Landscape

The study area comprises the following karst regions as outlined by Miller (1996): 1) Tertiary Rocks of the Northern Belize Region, 2) the Yalbac Hills, 3) the Boundary Fault and 4) the Sibun-Manatee karsts.

The underlying geology of the study area consists primarily of the Barton Creek Formation, however, most of the karst surficial deposits consist of varying deposits of Cenozoic age representative of various depositional environments such as near-shore, lagoon, evaporites and shallow marine deposits. Depending on the proximity to adjacent orogenies, volcanic and metamorphic detritus from the Maya Mountains and the Santa Rosa Formation can be expected in samples from the Sibun River Basin, while those towards the east may incorporate detritus from the Yalbac Formation. In general, the uppermost cover consists of Pleistocene and Holocene detrital deposits forming in a relatively thin layer of clastic soils from parent carbonates, marls, bentonitic clays, poorly consolidated sands and basement rock. However, as noted above, the composition of the speleothems within these areas is not only the result of the geology, but also of the hydrology and hydrogeology of the terrain, as the solutes are carried downstream and thus reflective of upstream composition.

3.4 Expectations and Implications

With the above and given the complexity of the underlying terrain, we can hypothesize the possible compositional determinants and expected results for our samples. The main samples analyzed by INAA are from the Cayo District in west central Belize, and encompassed six cave areas or groups (i.e., Barton Creek, Cave's Branch, Macal, Pine Ridge, Roaring Creek and San Antonio) and should have a very similar elemental composition in general given their proximity and topography. However, samples from the easternmost areas (San Antonio, Macal and Pine Ridge), should have some similarities among them, probably

influenced by the Yalbac Formation and should be slightly different from those in the western portion of the study area (i.e. Roaring Creek and Caves' Branch). The samples in the middle (from Barton Creek and portions of Pine Ridge) should exhibit a blended composition with some compositional characteristics intrinsic to the Barton Creek Formation and the underlying rock of Pine Ridge.

The comparative samples from the Sibun River Basin analyzed by ICPMS, while generally similar being carbonates, may exhibit distinguishable composition given their proximity to the Maya Mountains and outcroppings of the Santa Rosa Formation towards their south. Metamorphic and igneous detritus and elements characteristic of these sources would be expected to be present in slightly greater quantity than in samples from the first group. Enriched Rare Earth Elements (REE) are characteristic of intrusive felsic rock and their derivatives (Balashov and Khitrov, 1967). Moreover, enrichment in the heavy Rare Earth Elements (HREE) with respect to the lighter Rare Earth Elements (LREE) would be expected in samples from farther downstream (i.e.: Cedar Banks, and Oshon) as these are preferentially leached from the stable carbonate and fluoride complexes (Balashov and Khitrov, 1982). Lastly, samples from the northern Barton Creek, Roaring Creek and Cave's Branch while may be enriched in halide elements given their ancient evaporative depositional environments, only those collected from locales farther downstream would be preferentially enriched given halide solubility.

In summary, speleothem formation is a complex process in which the composition of the redeposited lithic material is controlled by multiple factors at several spatial and temporal scales. Spatial determinants include large geographical areas defined by their geology. These are divided regionally by topographical characteristics such as watersheds or drainage basins, and sub-regionally by hydrological (surface) and hydrogeological (subsurface) drainage. At the area and regional level, the composition of limestone parent material and

surface soils affect availability of trace elements, while at the sub-regional level precipitation and drainage affect leaching and movement of these elements in the substrate. Local spatial determinants include microenvironmental factors such as humidity, percolation rate, and wind currents within each cave that can affect the rate of formation.

Temporal determinants affecting speleothem formation, in order of chronology and time scales, include: deposition, faulting and uplift of geological substrate over millions of years, and erosion of substrate and formation of cave systems coterminally with the dissolution, transport, and redeposition of speleothems over thousands to hundreds of thousands of years. Finally, longer term trends in climate (specifically precipitation) can create chemical and age differences among speleothems in the same cave based on the rate of leaching and redeposition particular to each specimen. Given the complexity of this situation, the ability to distinguish speleothems from different caves or regions needs to be empirically demonstrated.

Chapter 4. Materials and Methods

4.1 Sample Materials

This study examines the chemistry of speleothems from two different regions of Belize and using two different analytical methods. A total of one hundred and four (104) speleothem samples were analyzed via instrumental neutron activation analysis (INAA) for this study. The samples were provided by Dr. Holly Moyes of UC Merced and procured during the Belize Valley Speleothem Project (BVSP) 2006 field season. These samples are derived from the Cayo District in Central Belize and encompass a variety of caves from different geological regions. The samples used in this study originate from six (6) locales: Barton Creek (n= 17), Caves Branch (n = 16), Macal (n = 22), Pine Ridge (n = 14), Roaring Creek (n = 20) and San Antonio (n = 15).

In addition, the study draws on prior analyses of 10 samples from the Sibun River Basin, and 8 from the Poptun Region of Guatemala, recovered by the Xibun Archaeological Research Project (XARP) and provided by Polly Peterson and Patricia McAnany. The XARP sample analyses were conducted using LA-TOF-ICP-MS and the results (published in Nation *et al.*, 2012) will be used for comparison with those from the Cayo District. The approximate areas of each set of samples are shown in Figure 5. Photographs of the Cayo District samples can be found in Appendix A.

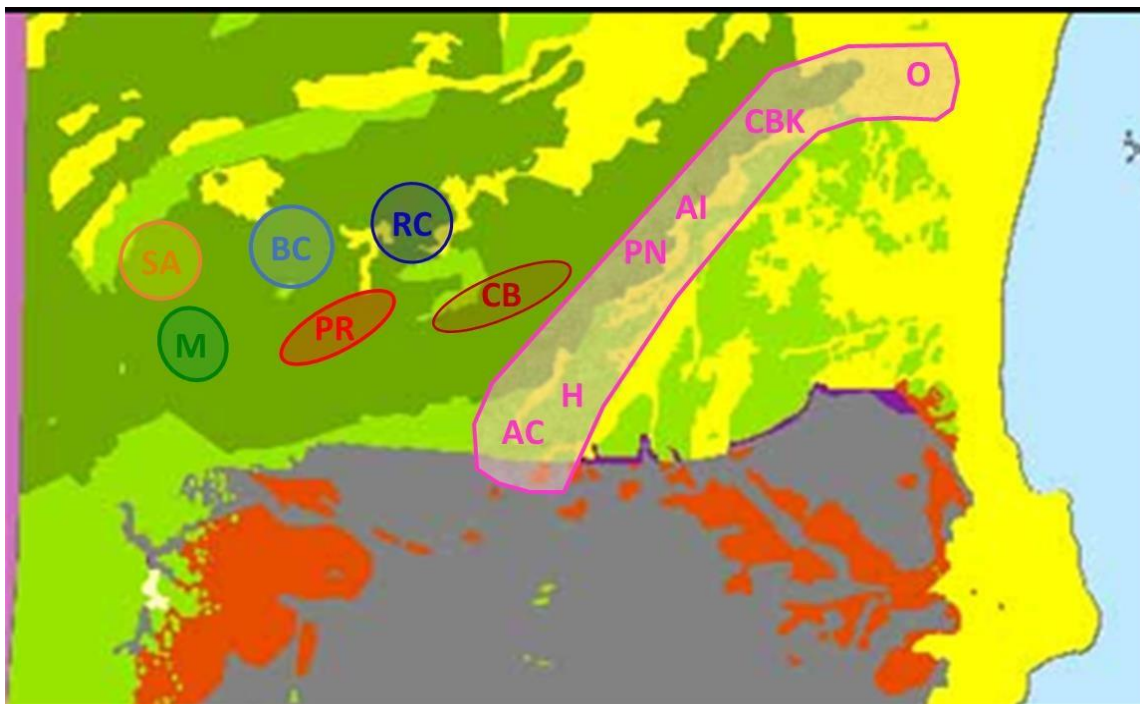


Figure 5. Cayo District group samples: Barton Creek (BC), Cave's ranch (CB), Macal (M), Pine Ridge (PR), Roaring Creek (RC), and San Antonio (SA). XARP samples as follows: Actun Chanona (AC), Hershey (H), Pakal Na (PN), Actun Ik (AI), Cedars Bank (CBK) and Oshon (O). Group color selected for identification purposes. Geological Color Legend: Yellow = Quaternary Alluvium, Red = Granite; Lt. Green = Limestone; Dk. Green = Dolomitic/Bentonitic Limestone; Purple = Shales and Sandstones and Gy = Santa Rosa Formation.

4.2 INAA

Instrumental Neutron Activation Analysis is an analytical technique that consists of exposing (irradiating) small amounts of sample material to a neutron flux generated by a nuclear reactor. These neutrons result from the fission of the heavy U-235 nuclei in the reactor fuel. About 2.5 extra neutrons are generated with every fission, with one neutron needed to perpetuate the fission chain reaction. The activated nucleus of the compound almost instantaneously decays into a more stable configuration through the emission of one or more *prompt* gamma rays, with a half-life of 10^{-13} to 10^{-3} sec. This new configuration is sometimes stable. However, typically, the resulting configuration is also a

radioactive nucleus which further decays, with the emission of a beta particle and a characteristic *delayed* gamma rays, in accordance to the exclusive half-life of the radioactive nucleus. Half-lives can range from a second to many years. The energy released in each decay is carried off by the gamma particle and is characteristic of the isotope undergoing decay. Detection and measurement of gamma ray intensities permits identification and precise quantification of radioisotopes present.

4.2.1 Speleothem Analysis by INAA

One way to validate the interpretations and theories that surround the movement of speleothem materials to and from caves as discussed in section 2.5, is to chemically source them to its geographical origin. Identifying the origin of these materials will provide a solid physical basis from which more sound theories and interpretations can be formulated to elucidate the extent, meaning, and significance of these practices by the Maya.

The geochemical analysis of geological samples by Instrumental Neutron Activation Analyses (INAA) is a very common and reliable practice as mentioned above. Moreover, its sensitivity and simultaneous wide spectra collection makes it ideal when analyzing “homogeneous” lithic materials such as basalt, obsidian, and calcite, where small inclusions of trace and REE elements in the matrix became significant, especially for differentiating apparently similar materials and for sourcing them.

However, to be effective, it is necessary to first demonstrate the existence of sufficient chemical variability between caves to distinguish caves individually, and thus be able to apply a chemical analysis as a basis of determining provenance of cave material found at surface sites and in other caves. The first check to validate the proposed goals of this study, is to test the applicability of the Provenance Postulate to our samples. The Provenance Postulate (Weigand

et al., 1977) states that the between-source differences must exceed within-source variation for sourcing determination to be possible. If it is found that there exists a noticeable level of elemental variation between caves, and low variation within caves, chemical characterization by INAA would be an appropriate method for sourcing these samples.

Except for a few pilot studies utilizing various analytical methods including INAA (Brady *et al.*, 1997; Nation *et al.*, 2012; Brennan *et al.*, 2013), no substantial effort has been made in developing a methodology and database that would help establish the provenance of speleothem materials. This project will characterize the chemical composition of various speleothems derived from caves with heavy cultural alterations by means of Instrumental Neutron Activation Analysis.

4.2.2 Sample Preparation for INAA

Each of the (104) speleothem fragments selected for this study was carefully catalogued and photographed; for documentation, see tables and sample photographs in appendix A. A small piece (ca. 1 cm cube or less) of each speleothem was then removed for analysis with the remainder, if any left archived for future use. Surface contamination was removed with a tungsten carbide burr; the piece was then rinsed with deionized water and dried at 80°C over a 48-hour period. Each small piece was then crushed to a consistency of fine granular powder in an agate mortar and pestle. To reduce cross contamination, between crushing each sample the mortar and pestle were rinsed with deionized water, patted dry with a kimwipe, and rinsed two more times with deionized water, followed by one last rinse with methanol before drying with compressed air. The crushed powder was stored in clean glass vials and dried again at 80°C for a 24-hour period, allowed to cool and quickly closed with new screw cap vials and sealed with parafilm to prevent moisture contamination.

From these vials, approximately 400 mg of dry powder was weighed and encapsulated in high purity polyethylene vials for irradiation. Each batch consisted of 24 samples and along with the following standard reference materials (SRM): NIST 1c (limestone; three replicates of ca. 400 mg), NIST 1633a (Coal fly ash; 1 replicate of ca. 100 mg) and NIST 88b (dolomite limestone; two replicates of ca. 400 mg).

4.2.3 Analysis Protocol

All samples were analyzed at the Oregon State University TRIGA Reactor (OSTR), a water-cooled, Mark III research reactor with graphite-shielded core, designed to provide intense radiation fluxes for research and isotope production. This reactor is licensed by the U.S. Nuclear Regulatory Commission to operate at maximum steady state power of 1.1 MW, generating a peak in-core thermal neutron flux of $10^{13} \text{ n} \cdot \text{cm}^{-2} \cdot \text{s}^{-1}$ and a peak fast neutron flux $5.0 \times 10^{12} \text{ n} \cdot \text{cm}^{-2} \cdot \text{s}^{-1}$ ($E > 1 \text{ MeV}$).

All samples were characterized for a suite of 30 major, minor and trace elements, through a protocol of two neutron irradiations and multiple counts of gamma activity. To quantify elements with short half-life isotopes (major elements Al, Mg, Ca, K, and Na; trace elements Mn, Ti, V, Ba, and Dy), samples were delivered via pneumatic tube to an in-core location with a nominal thermal neutron flux of $10^{13} \text{ n} \cdot \text{cm}^{-2} \cdot \text{s}^{-1}$ for a 30-s irradiation. After a 22-minute decay, a single count of gamma activity (540 s real-time) was collected using a 25-30% relative efficiency HPGe detector. Concentrations of this suite of elements were determined via the direct comparison method, based on activity generated in the standard reference material NIST1633a (coal fly ash); Mg values were corrected for interferences from the fast-neutron reaction on Al. Replicates of NIST1c (limestone) and NIST88b (dolomite limestone) were utilized as check-standards on accuracy and precision (see Table 11 in Appendix B).

To quantify elements with intermediate and long half-live isotopes, sample materials were subjected to a 14-hr irradiation in the rotating rack of the reactor, a location which experiences a nominal thermal neutron flux of $2.3 \times 10^{12} \text{ n} \cdot \text{cm}^{-2} \cdot \text{s}^{-1}$. In this case, two separate counts of gamma activity were acquired, the first count of 5000 s (live-time) began 6 days after the end of irradiation, while the second count for 10000 s followed a 4-week decay. These two counts provided data on As, Br, La, Lu, K, Na, Sm, U, W, and Yb; and Ba, Ce, Co, Cr, Cs, Eu, Fe, Hf, Nd, Ni, Rb, Sb, Sc, Sr, Ta, Tb, Th, Zn, and Zr, respectively. Element concentrations were determined via the direct comparison method; in this case, three replicates of the standard reference material NIST1c (limestone), and one of NIST1633a (coal fly ash) were utilized as standards, while NIST88b (dolomite limestone) was utilized as a check-standard.

Element concentrations are reported in ppm in Appendix B, but were converted to log (10) values for analysis. Elemental concentrations below detection limits are shown as negative values in the appendix; the values represent minimum detectable concentrations (MDCs) given the sample mass and all other analytical parameters and should be interpreted as “less than” the value indicated. The MDCs were substituted for missing values in quantitative analyses, as they indicate extreme low values that can be converted to a log scale, unlike zero. Of the elements listed above, the following were consistently below detection limits in the speleothems and therefore removed from quantitative analyses: Dy, K, Nd, Ni, Rb, Ta, Tb, W, and Zr.

4.3 Analysis by LA- TOF- ICP-MS

Inductively Coupled Plasma Mass Spectrometry (ICP-MS) is one of the most common spectroscopic methods now in use. Its importance derives from its low detection limits for most elements, allowing for very accurate qualitative and quantitative characterization of *trace* (parts per million to parts per billion) and *ultra-trace* (parts per trillion to parts per quadrillion) elements.

Most samples analyzed by ICP-MS are introduced as liquids. Solid samples are “digested” using acids and heat treatment. The liquid is introduced via a peristaltic pump into a line with argon gas as a carrier and transported into a nebulizer. In the nebulizer, the liquid samples are transformed into a fine aerosol with a stream of argon gas. These droplets are carried through the spray chamber and injected into a plasma torch. At the torch, a plasma is formed and ignited by a radio frequency emission “spark” from a tesla coil. The ignition of the plasma causes and propagates collisions between electrons and argon atoms resulting in the creation of more argon ions and electrons and so the process becomes self-sustaining. The plasma ionizes the argon and other element atoms in the sample. The temperatures within this plasma range between 9500 and 11000 K. The nebulized sample is introduced into this plasma at which point its elemental components are ionized. The resulting ions are then passed into a high vacuum mass spectrometer through an interface ion lens where they are focused. The focused ion stream is then passed through the quadrupole which separates the ions by their mass-to-charge ratio (m/z) before reaching the detector. The detector measures the spectral intensity of the ions signal; where the intensity of a specific peak in the mass spectrum is proportional to the concentration of that isotope (element) in the original sample. Finally, a graphic and tabular report of the results is generated.

Alternatively, some solid matrices can be analyzed using laser ablation (LA) to vaporize the sample. In this case, the vaporized sample is introduced directly into the instrument for measurement. The advantages of laser ablation (LA) lies in the ability for transient signals from any solid material to be analyzed, with analysis of solid samples by requiring little preparation. Lastly, the introduction of a dry sample into the plasma results in a lack of polyatomic interference species produced by the interaction of water and acid species with the argon plasma.

The suite of elements detected with ICP-MS are as follows: Li, Na, Mg, Ca, Br, Al, Si, V, Ti, Mn, Sc, Cr, Fe, Co, Zn, Ni, Cu, Mo, Cd, Sn, Sb, Ba, Rb, W, Tl, Pb, La, Ce, Pr, Nd, Sm, Eu, Tb, Gd, Dy, Ho, Er, Tm, Ta, Lu, Hf, Th and U. From these, there were clear differences between the Sibun River Basin and those from the Petén Basin. For the Sibun River Basin samples, the following were consistently near detection limits of 0.01 ppm (Li, Na, Mg, Al, Si, V, Ti, Pb, Pr W, and Lu) or below detection limits 0.001 ppm (Al, Si, Mn, Mo, Cd, Sn, Sb, Tl, Nd, Tb, Ho, Er, Tm, and Ta). For the Petén Basin samples the following elements were near detection limits of 0.01 ppm: Na, Mg, Ca, Br, Rb, Pr, Nd, Sm, and U; and the following were below detection limits of 0.001 ppm or absent: Al, Si, Mo, Cd, W, Tl, Pb, Eu, Tb, Gd, Dy, Ho, Er, Tm, Ta, Lu, Hf, and Th. However, for the comparative analysis, we utilized only those that mirror the ones from the INAA analysis, these are: Al, Na, Mg, Ca, Br, Ti, Mn, Sc, Cr, Fe, Co, Zn, Sr, Cs, Ba, La, Sm, Eu, Yb, Lu, Hf, Th and U.

Chapter 5. Results for the Cayo District

5.1 Analytical Approaches

To test the provenance postulate, we first examined variability among speleothems within each cave, followed by an assessment of variation among caves. The data were examined using exploratory data analysis approaches using JMP 14 statistical software, with an emphasis on univariate and bivariate plots, as well as descriptive statistics.

All the samples from the Belize Valley Speleothem Project were characterized for a suite of 30 major and trace elements, of which 22 were examined in quantitative analyses. The results are presented as follows: major and trace elements, Tables 3, 5 and 7; rare earth elements, Tables 4, 6 and 8. Combined results for the XARP samples are presented in Tables 9a and 9b; see appendix B. The absolute ppm values obtained for the REE for the BVSP were normalized against Chondrite, using values suggested by Korotev (1996).

5.2. Variability among Speleothems within a Cave

The BVSP and XARP samples accounted for 121 total combined speleothem samples representing 53 caves. Of these 53 caves, only 18 caves have three or more replicates, with ten caves having exactly 3 replicates. Given the limited number of caves with three or more sample replicates, statistical tests of intra-cave homogeneity relative to inter-cave differences were not conducted. However, several visual trends were noted.

Overall, concentration values for all elements among samples from the same cave are variable. However, variation among the caves and among groups is discernable with the best differentiation given by Mg, Br, Sc, Co, and Sr; see Figures 6-12. Caves with three or more replicates better exhibit this variability within and between caves. These caves are: Barton Creek, Migdalia, and Arnulfo

from the Barton Creek Group (1); St Hermans and Jaguar Paw from the Cave's Branch Group (7); Actun Isabella, Flour Camp, and House of Pain from the Macal Group (3); Las Cuevas and Rio Frio from the Pine Ridge Group (4); Hand Print, Nakbe and ATM from the Roaring Creek Group (5); Bols Museum and Crystal Palace from the San Antonio Group (6); Actun Chanona and Hershey from the Sibun Group (7); and Poptun from the Petén Group (8).

Although samples sizes are too small to permit statistical tests, it is visually apparent that speleothems from some caves are highly variable in composition, while those from other caves are more homogenous. Further, the degree of within-cave variability differs by element. For example, caves from Barton Creek, Pine Ridge, Roaring Creek, and San Antonio (Groups 1, 3, 4, and 5) are highly variable in Mg content, whereas Groups 7 and 8 are highly variable on Sc and Co.

This is also apparent when considering Br and Sr. Caves from Barton Creek, Cave's Branch, Pine Ridge, Roaring Creek, and San Antonio (Groups 1, 2, 4, 5 and 6) show more variability in Br than caves from the Macal, Sibun, and Petén (Groups 3, 7 and 8). This variability is less pronounced for Sr where the greatest variability occurs in the Barton Creek, Chapat, Las Cuevas, Rio Frio, and Handprint caves from Groups 1, 3, 4 and 5; with virtually no variability in the rest of the caves or groups.

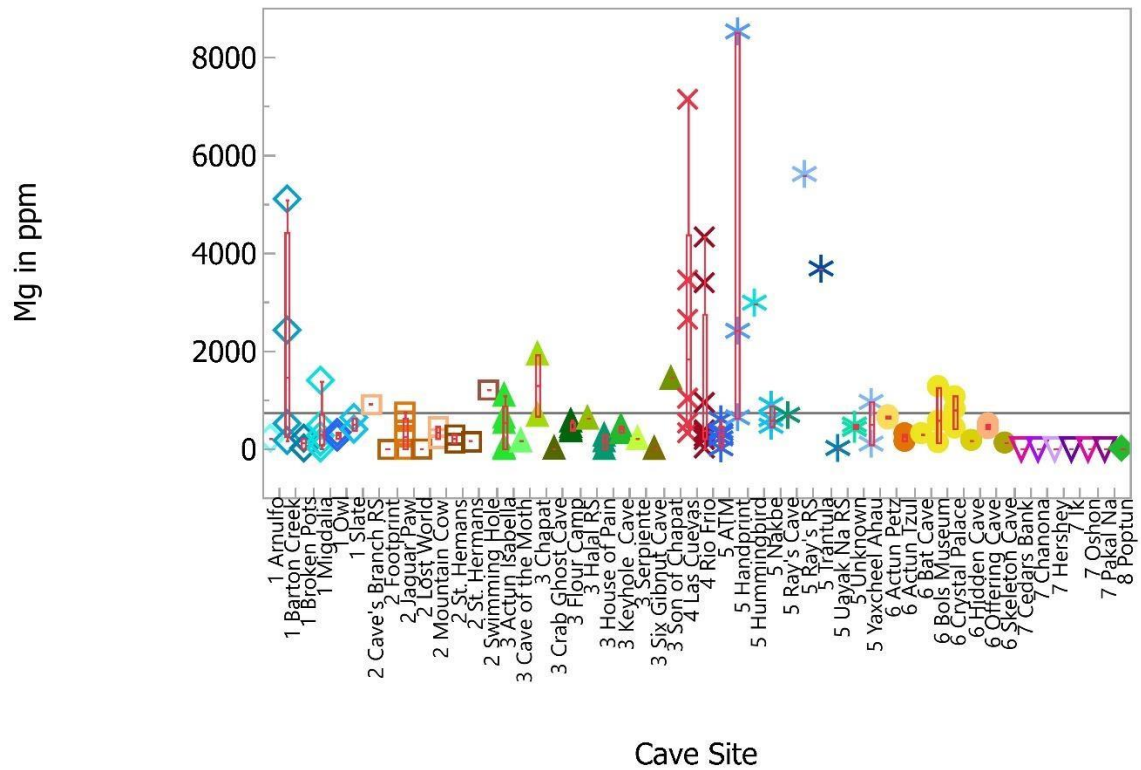


Figure 6. Magnesium concentrations by cave, coded by color and symbol to distinguish their respective geographic groups. Note some variability in caves from BSVP samples (Groups 1, 3, 4 and 5) and almost no variability in XARP samples (Group 7 and 8).

The relative high Mg concentrations are reflective of the dolomitic limestone underlying the region of Groups 1 thru 6. Lower concentrations in the Sibun and Petén, Groups 7 and 8, may be attributed to a non-dolomitic limestone substrate in the Sibun River Valley and the Poptun region of Petén.

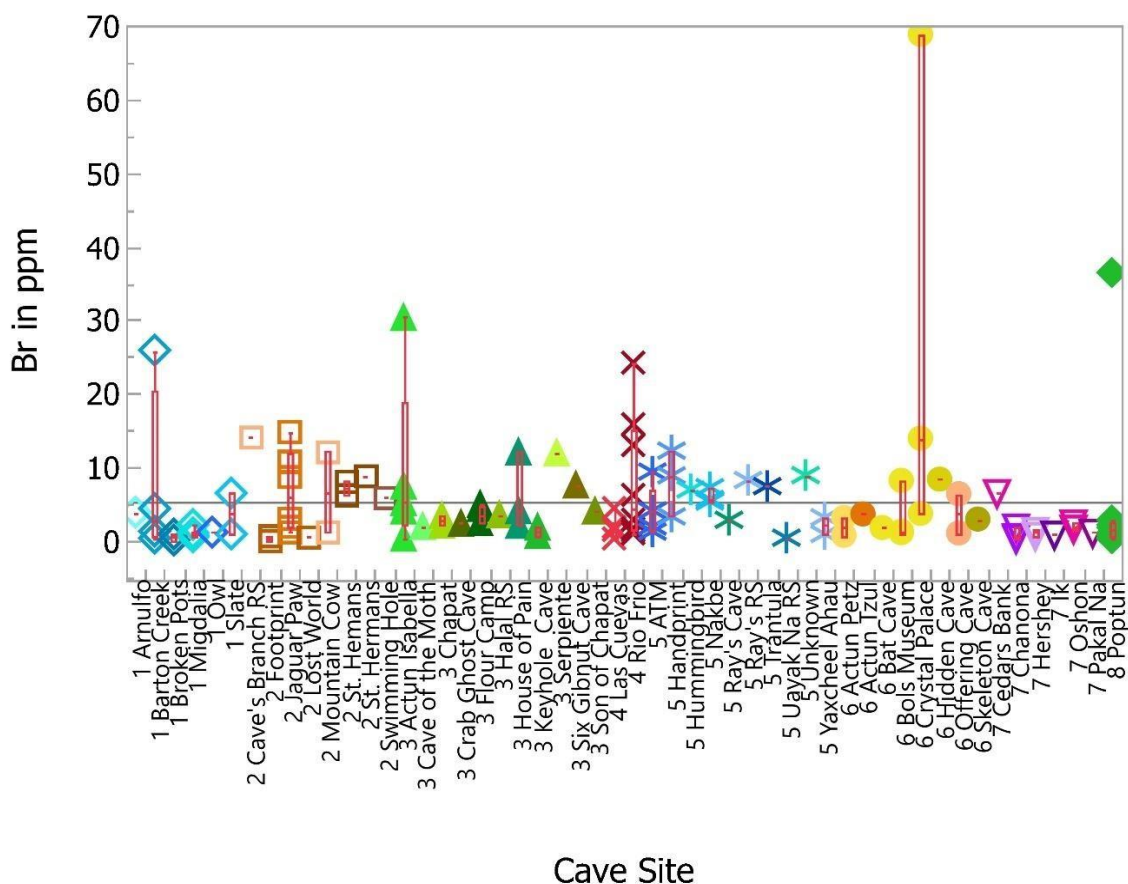


Figure 7. Bromine concentrations by caves within their respective groups. Note more variability in caves from BSVP samples and minor variability in XARP samples.

Variability in Br (Figure 7) is more pronounced in caves from the Cave's Branch, Pine Ridge, Roaring Creek, and San Antonio (Groups 2, 4, 5, and 6) and to lesser extent in caves from the Barton Creek, Macal, Sibun, and Petén (Groups 1,3, 7, and 8). With the exception of four outliers from Barton Creek, Actun Isabella, Crystal Place, and Poptun caves, the overall Br concentrations are in accordance with crustal rocks, between 10 and 20 ppm (Kendrick, 2016) and likely derive from tertiary evaporative lagoons that concentrate halides.

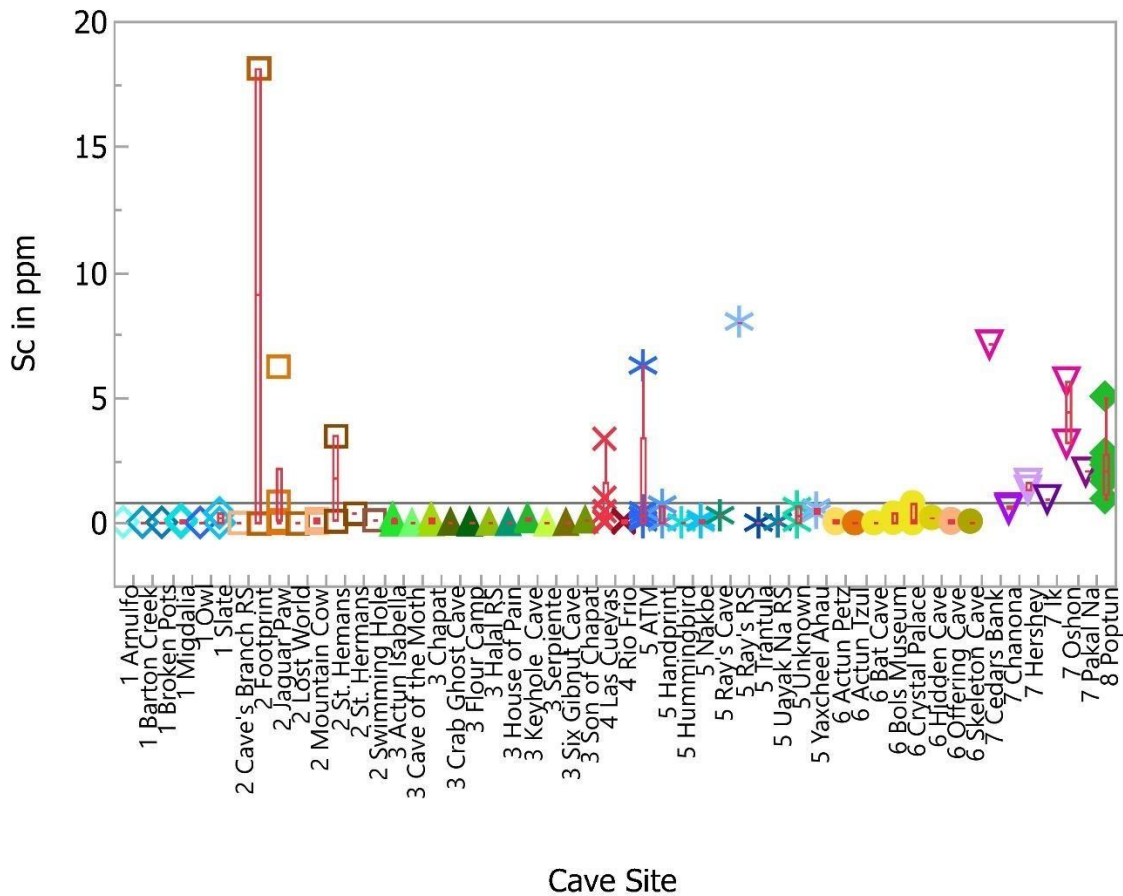


Figure 8. Scandium concentrations by caves within their respective groups. Note more variability in caves from Sibun and Petén (XARP), with minor variability in samples from BVSP.

With the exception of three outliers from Footprint, ATM, and Ray's RS from Groups 2 and 5, the caves from the Sibun and Petén (Groups 7 and 8) show greater intra- and inter-group variability in Sc concentrations as compared with those from Groups 1 through 6 (Figure 8). Notice that for the BVSP samples, the average Sc concentration remains below the grand mean for all samples, with only samples from Groups 7 and 8 at or above the mean.

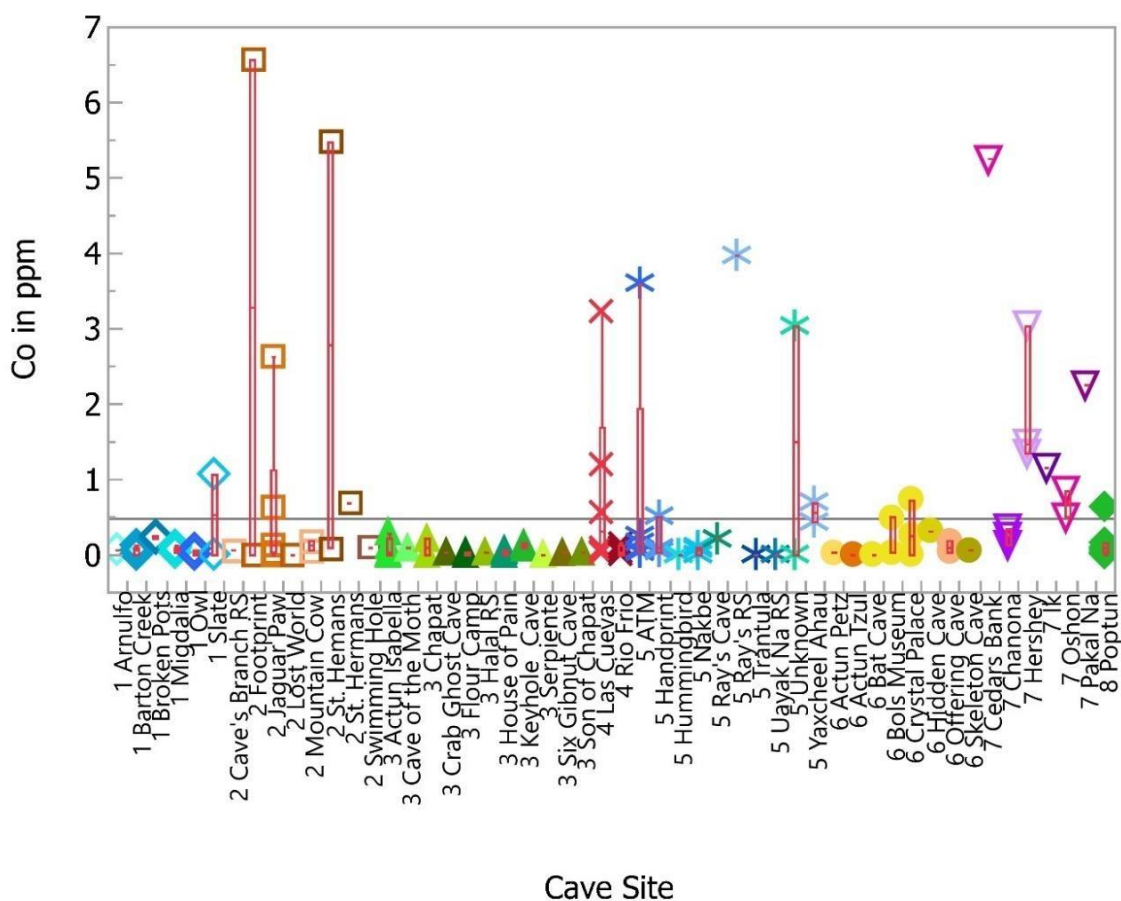


Figure 9. Cobalt concentrations by caves within their respective groups. Note more variability in caves from Sibun and Petén (XARP), with minor variability in samples from BVSP.

The behavior of Co (Figure 9) is similar to that of Sr (Figure 10) but with more variability in caves from Groups 2, 4, 5, and 7. Here, the greatest intra- and inter-group variability is seen from Jaguar Paw, Las Cuevas, ATM, and Crystal Palace (Groups 2, 4, 5, and 6, respectively), all caves from Sibun (Group 7), and to a lesser extent Petén (Group 8). The greater variability in Co may be due to detrital material originating from granitic outcroppings to the south of the Sibun River Basin. The inter-cave variability shown here could contribute to provenance determination. Although it doesn't help us source specimens with low concentrations, high concentrations of specific elements could identify likely sources, e.g., a sample high in Co is more likely to come from Groups 2, 4, 5, or 7.

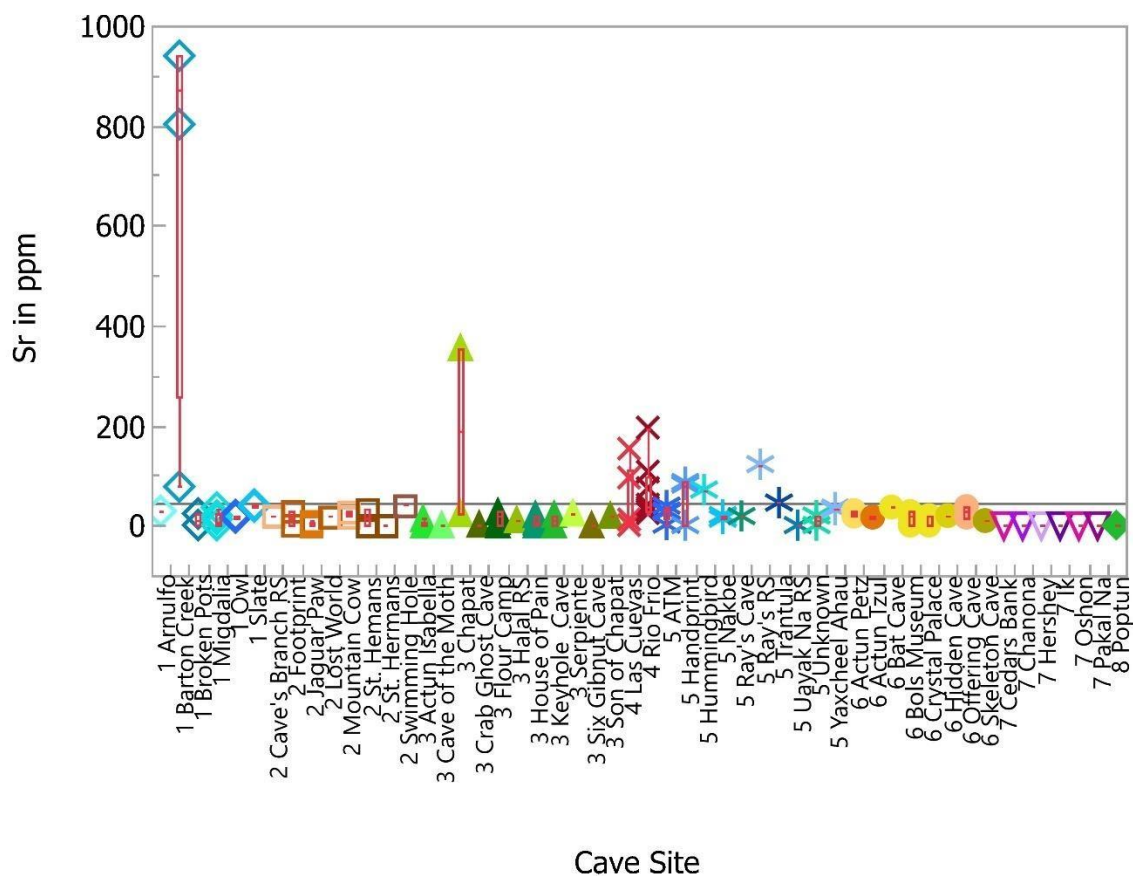


Figure 10. Strontium concentrations by caves within their respective groups. Note more variability in caves from Sibun and Petén (XARP), with minor variability in samples from BVSP.

Moreover, the LREE such as Eu (Figure 11) and HREE represented by U (Figure 12) have very low concentrations throughout all the samples with some below the limits of detection for the INAA analyzed samples. However, this does not mean that these species are not there; rather they are present in very small quantities. To use these data comparatively with the data from the XARP samples, we used the minimum detectable concentrations or MDCs, as described above.

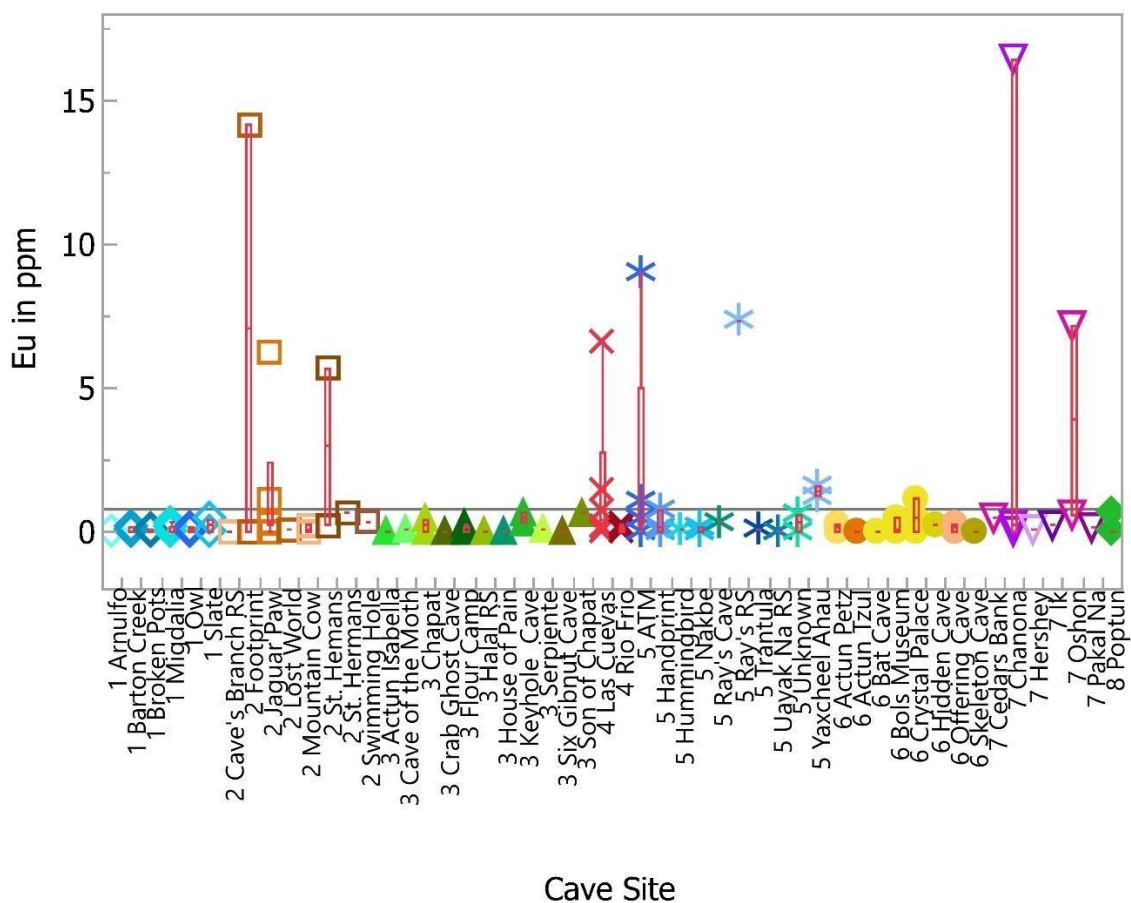


Figure 11. Europium concentrations by caves within their respective groups. Note variability in caves from Sibun and Petén (XARP), are closer to the overall mean with minor variability in samples from BVSP.

As seen in Figure 11, the variability in Eu content within and among caves from all groups is similar throughout with the exceptions of the following caves: Footprint, Jaguar Paw, and St Herman's (Group 2); Las Cuevas (Group 4); ATM, Ray's RS, and Yaxcheel (Group 5); Crystal Palace (Group 6); and Chanona and Oshon (Group 7). Higher concentrations are expected in dry or dead (not actively forming) samples deposited and collected farther downstream due to preferential leaching of LREE from halide complexes in the limestone substrate.

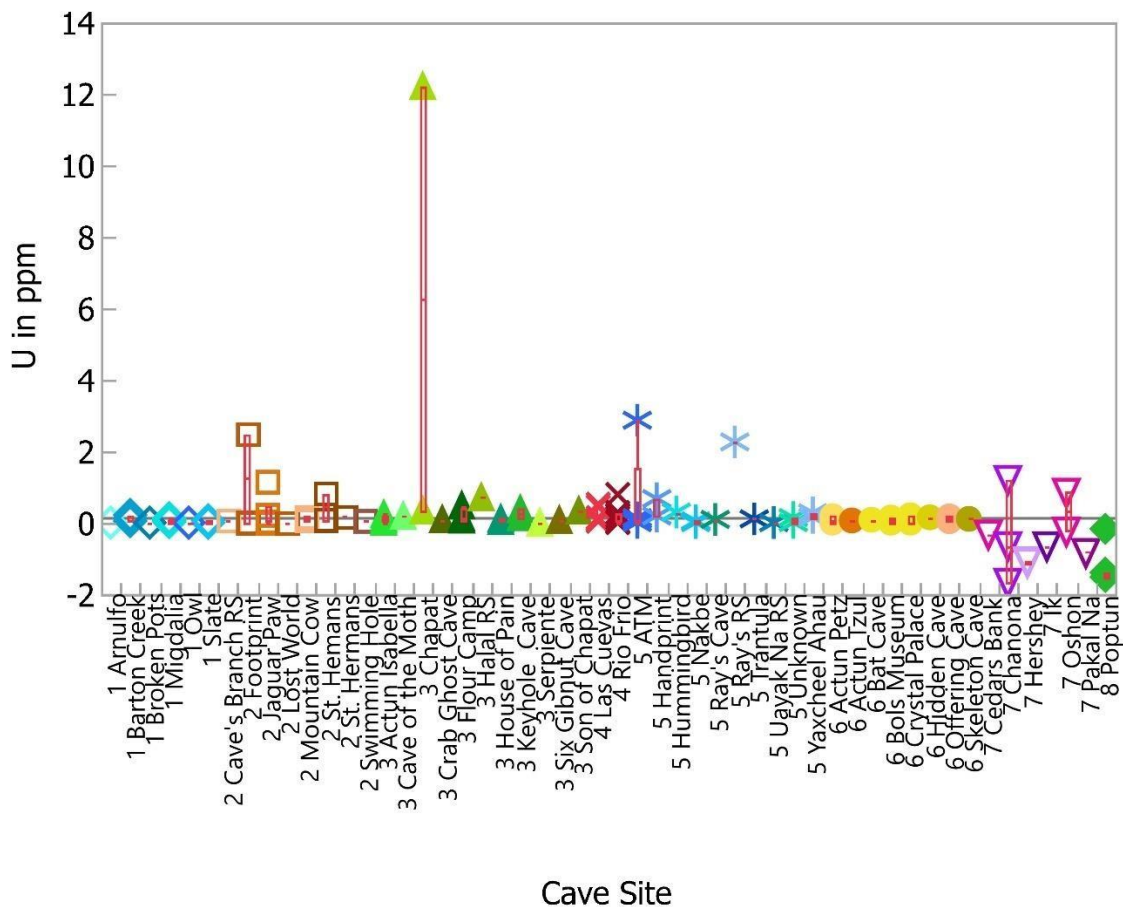


Figure 12. Uranium concentrations by caves within their respective groups. Note more variability in caves from Sibun and Petén (XARP), with minor variability in samples from BVSP.

There are several factors that might contribute to this variability such as different deposition rates within caves and between them. However, given the relative geographical proximity and assuming relatively similar pluvial inputs, except for the Petén group; different deposition rates would likely result from changes in the percolation and hydrogeological movement solutes in the conduits feeding the growth of speleothems. In such events, deposition rates may slow, stop and restart over periods of years to millennia with present day speleothems not only with varying elemental compositions but ages.

5.3 Variability among Cave Groups

The average element concentrations across all samples for speleothems from each of the six BVSP cave groups are shown in Figure 13; element abundances are as expected for calcareous material, as evident by the high Ca concentrations. Major elements Al, Na, Mg, Mn, Cr, Fe and Zn, denote significant terrigenous inputs occur with slight variations between groups except for Ti, in which a slight differentiation between groups is more evident. Concentrations of aluminum (Al) and iron (Fe), associated with terrigenous inputs, were relatively significant with a grand mean of 3192 and 1428 ppm, and maximum values of 9751 and 4550 ppm, respectively. Trace elements Sc, Sr, and Cs also show slight variability between groups. A wider spread between groups is given by the rare earth elements (REE), with three groups, Barton Creek, Cave's Branch and Pine Ridge, relatively enriched in both Light Rare Earth Elements (LREE) and Heavy Rare Earth Elements (HREE) with respect to Macal, Roaring Creek and San Antonio. Lastly, Macal group shows an inverse U to Th concentration profile with respect to all other groups.

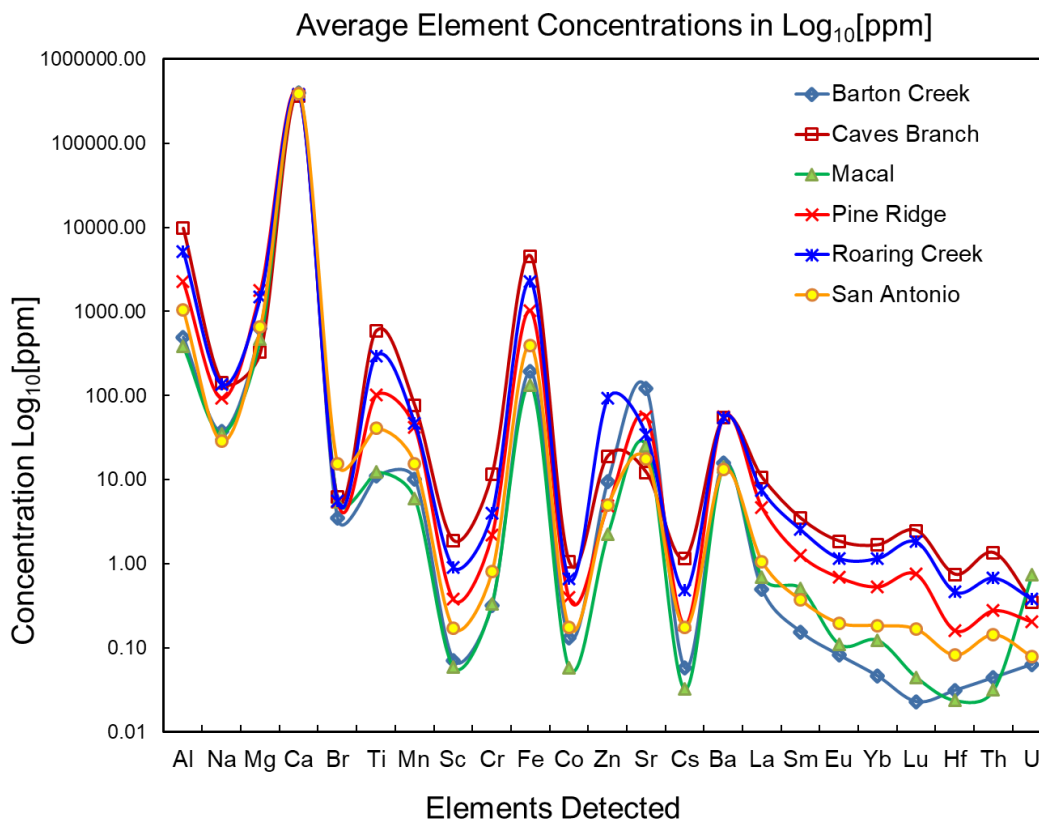


Figure 13. Average elemental concentrations in log base 10 in speleothems from the Barton Creek (BC), Caves Branch (CB), Macal (M), Pine ridge (PR), Roaring Creek (RC), and San Antonio (SA) cave sites. Note the significant presence of Al, Fe, and Mg.

In general, the REE were largely depleted with many below detection limits. From the Lanthanide series, the analyses only consistently obtained concentration values for La, Sm, Eu, Yb, Lu, and Hf, as shown in Figure 14. Similarly, from the Actinide series, only Th and U were measurable. The extremely low concentrations of most lanthanide series elements in all samples can, by itself, be used as a tool in the provenance determination of these lithic materials as their very low concentrations may be part of the geochemical signature of the limestone in this area of central Belize. A thorough discussion on this anomaly and other finding follows in the next chapter.

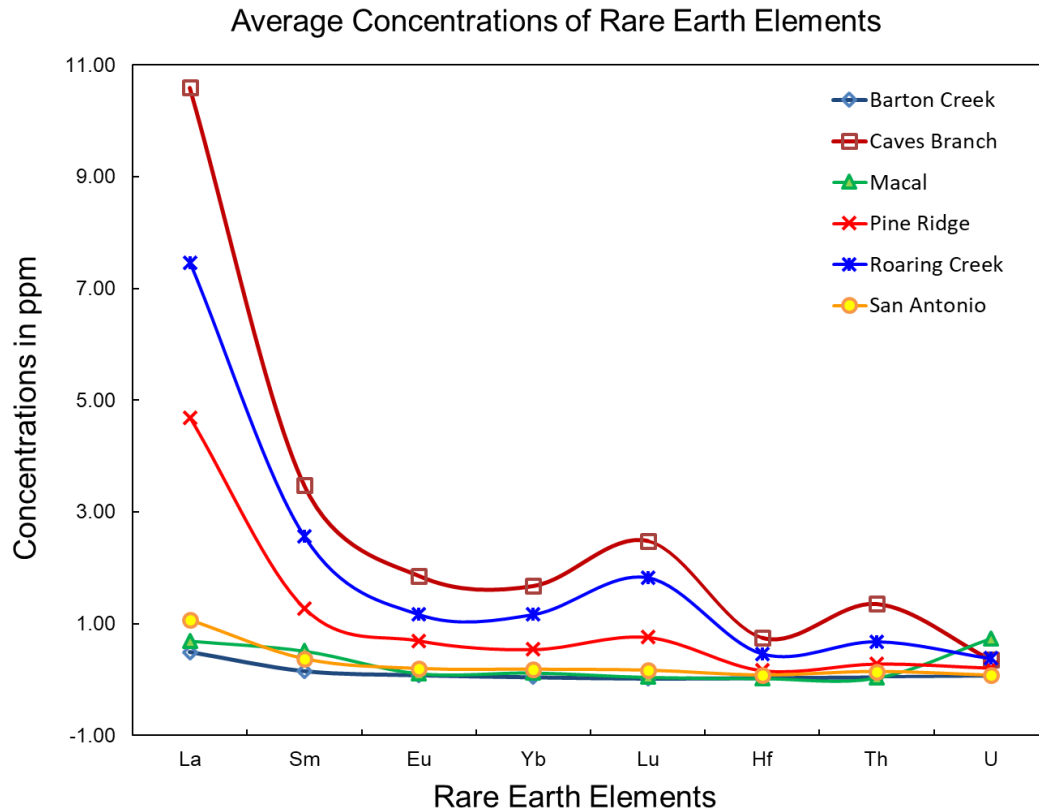


Figure 14. Average absolute elemental concentrations for Rare Earth Elements (REE) from the Barton Creek (BC), Caves Branch (CB), Macal (M), Pine ridge (PR), Roaring Creek (RC), and San Antonio (SA). Notice the inverse relationship of Th and U for Cave's Branch, Macal, and Roaring Creek.

The relationship between Al and Fe, both indicative of terrigenous inputs, is shown in Figure 15, below. The linear trend is common for these elements; however, note the increasing concentration for all groups, but most notably with Cave's Branch group with the highest values for both elements (19557 ppm Al and 8970 ppm Fe). Most data points fall within 139 - 5000 ppm for Al and 21 - 2937 ppm for Fe, respectively. All groups have a representation in the bottom cluster with extremely low values ranging between 89 - 280 ppm Al and Fe undetected.

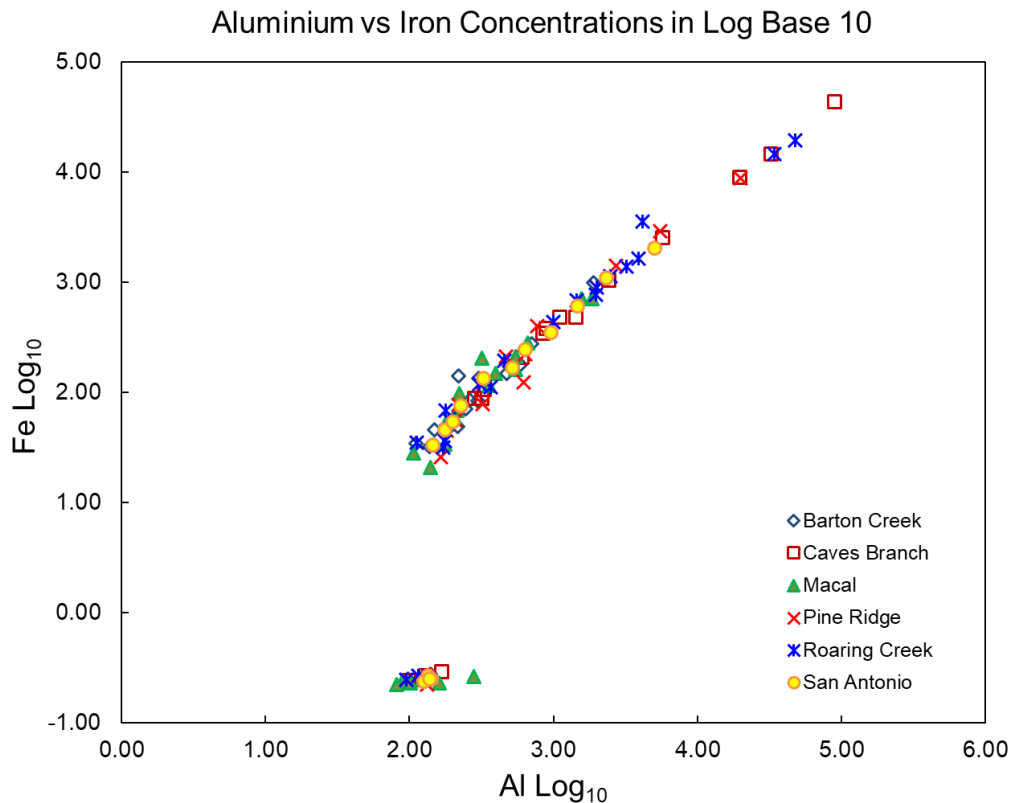


Figure 15. Concentrations in log base 10 of Al vs Fe. Main distribution for both Al and Fe is found in central cluster, with the highest concentrations found in the Cave's Branch, Roaring Creek, and Pine Ridge groups.

Using the alkali elements Cs and Sr (Figure 16), we begin to see a separation into three main clusters with a fourth one very small and tightly cluster in the negative log values, effectively concentrations of less than 1.0 ppm for both Sr and Cs. We must note that all groups except for Cave's Branch and San Antonio had one or more replicates in this tiny cluster. This is of interest as these two groups are found along the East and West sides of the BVSP study area, respectively. Again, the Cave's Branch and Pine Ridge groups seem to have the greatest Cs concentrations ranging from 0.23 to 10.62 ppm. The Sr values range from < 1 to 939 ppm.

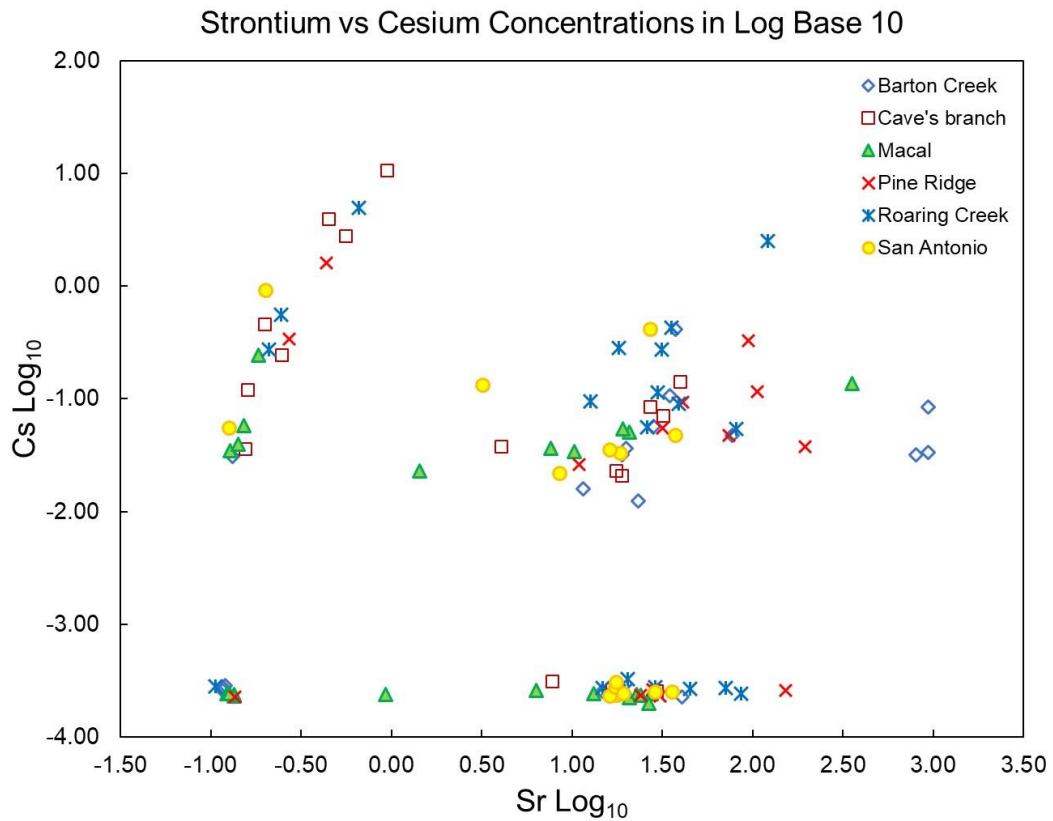


Figure 16. Bivariate plot of Sr vs. Cs, differentiating three clusters of samples. The upper left shows Cave's Branch, Roaring Creek and Pine Ridge with the highest Cs concentrations. The center right cluster shows Barton Creek, Macal, and Pine Ridge with the most Sr.

In working with the light Rare Earth Elements (LREE), we see that most samples from all six cave groups align well in the La vs. Sm plot (Figure 17), with extreme low values for one or both elements creating some scattering. The alignment is likely due to their shared 3⁺ valance charge and highly similar ionic radius. Again, the values for the REE in general were very low or below detection limits. However, the geochemistry of the LREE favors their retention.

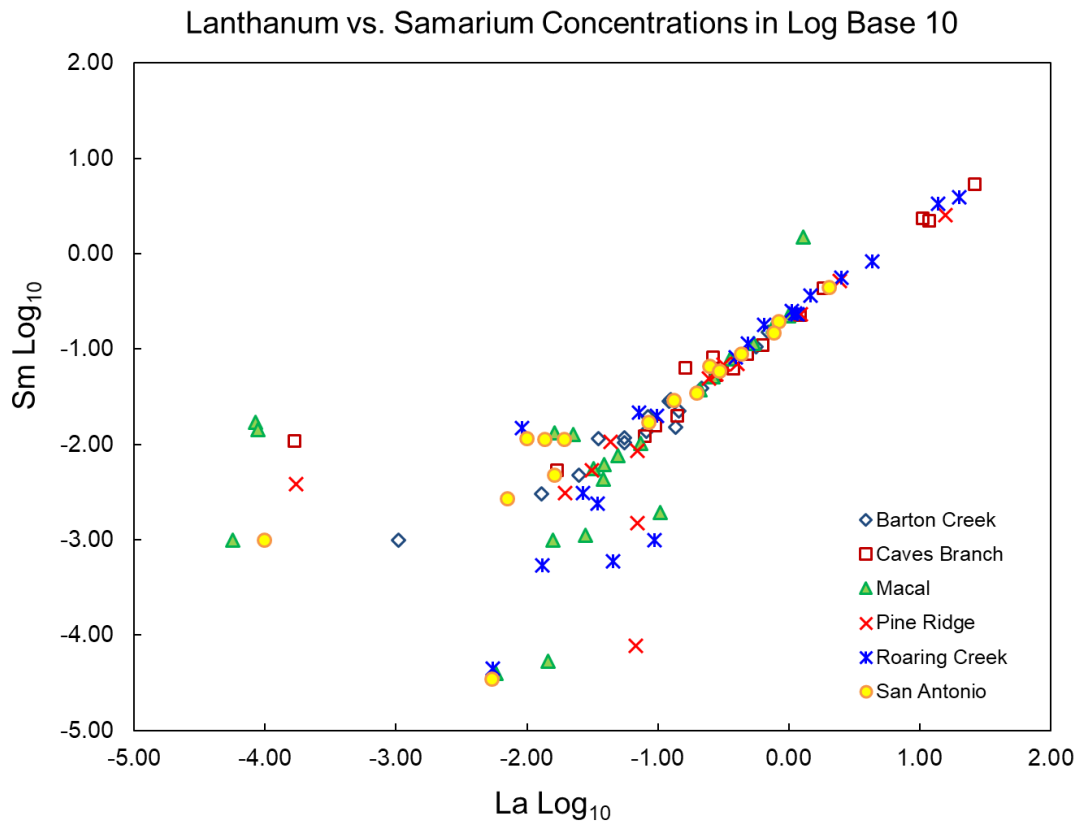


Figure 17. Concentrations in log base 10 of Lanthanum vs Samarium. Most aligned with some minor scattering for the negative values.

In a plot of the heavier REE (Figure 18), we observe again a clustering pattern but independent of prior groupings. Again, a cluster of extreme low values is present. The two main clusters occur between the log values -2.0 and 0.0 for U and -4.5 to 0.0 for Lu. Herein, the Macal and Cave's Branch groups have the highest values for U and Lu. Also, the San Antonio and Roaring Creek groups seem split between both main clusters while the Macal concentrates most in the left cluster. Finally, the Barton Creek samples seem to link both clusters while the Cave's Branch samples occur continuously from left to right.

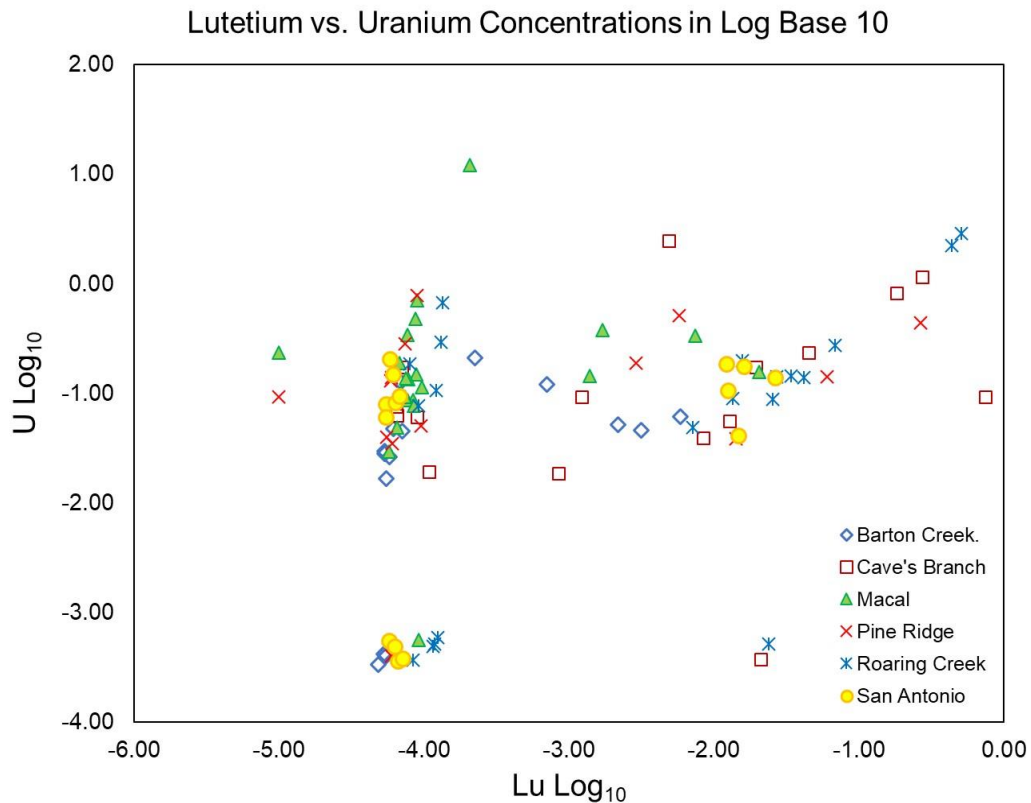


Figure 18. Concentrations in log base 10 of Lutetium vs Uranium. Note the splitting of San Antonio and the continuance of Barton Creek and Cave's Branch groups.

Lastly, Figure 19 shows the relationship between Th and U. Again, four clusters are differentiated. One tightly formed cluster has extremely low values of both elements with Th and U log values ranging between -3.74 and -3.23, and 3.23 and -3.43, respectively. Another cluster in the negative range made up of only four data points from three series (Barton Creek, Roaring Creek and San Antonio), has detectable thorium values and extremely low uranium values between (-3.476 to -3.265). Next, a nearly linear vertical cluster with very consistent thorium log values between -3.76 and -3.75 and a wider uranium log values between -0.032 and -1.526. Lastly, there is the largely unconsolidated cluster with U log base 10 values ranging between -1.730 and 1.087 (0.0186 to 12.215 ppm) and Th log base 10 values between -1.961 and 1.089 corresponding to (0.011 to 12.275 ppm).

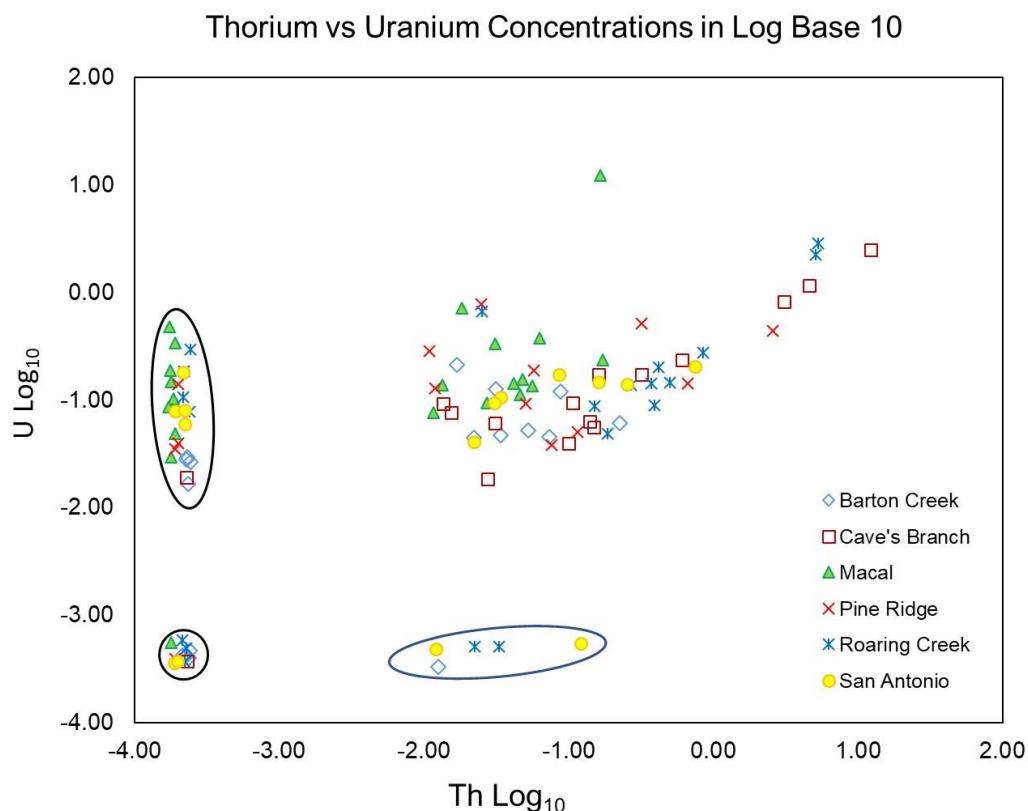


Figure 19. Concentrations in log base 10 of Th vs. U showing four distinct clusters.

Unfortunately, these relationships as exemplified in Figure 19 cannot readily help us discern between different caves. However, the relationship between Th and U is helpful as it is the preferred method of dating carbonate materials such as speleothems. The age is measured from the degree to which secular equilibrium has been established between the parent U-234 and the daughter Th-230 isotopes. We must point out that while we have the capability for isotopic analysis, in this case we measured elemental concentrations, in parts per million, not isotopic concentrations. Notwithstanding, this information is valuable due to the chemistry of Th and U discussed in next chapter.

In summary, intra-variability within each cave is such that individual differentiation is extremely difficult, although the speleothems from some caves are more variable than others. Also, inter-variability among the cave groups is

limited to specific elements, namely Mg, Br, Co, Sc, and Sr; but still not sufficient by itself to clearly differentiate between them. However, high concentrations on some of these elements could help identify probable source areas.

Chapter 6. Results for Inter-Regional Comparisons

The BVSP samples analyzed by INAA derive from the Cayo District in Central Belize and encompass a variety of caves from different regions. From the six groups identified, none had substantial number of samples (i.e., more than 15), from one individual cave that would allow us to explore the provenance postulate meaningfully. The samples do, however, represent a general geographical and topographical area and so these can be utilized to explore the variability on a larger spatial scale. Here we compared the BVSP samples to the XARP data set from Honduras to explore inter-basin variability.

6.1. Drainage Systems

Given the relative homogeneity of the sample materials, our analytical results were organized to approach the data from a macro-scale. To explore the inter-basin variability, we identified four (4) drainage systems based of the topography and drainage of the river systems within. Thus, samples from the BVSP yielded two drainage systems, one designated the Cayo District Drainage and composed by samples from groups Barton Creek, Macal, Pine Ridge, Roaring Creek, and San Antonio as all these areas drain in the Cayo District into the Belize River to the North. The second drainage system was designated as the Cave's Branch group, as this sample set represents an area that straddles the Cayo District but drains into the Sibun River to the East. From the XARP data set two other drainage systems were designated, the Sibun and Petén.

As noted above, each group is composed of samples from multiple caves within their specific geographical coordinates. The allocation of the drainage systems and the groups caves site composition are shown in Table 8.

Table 8. Showing cave site composition for each group and divided by drainage systems. Notice, Cave's Branch makes its own system as it's a tributary of the Sibun River and straddles the Cayo District and Sibun Basins.

Caves Site Composition By Group

Draniage	Group	Cave Sites	# per Cave
Cayo District	Barton Creek (n= 17)	Barton Creek	4
		Migdalia	6
		Amulfo	3
		Slate	2
		Owl	2
	Macal (n = 22)	Actun Isabella	5
		Flour Camp	4
		Keyhole	2
		Cave of the Moth	1
		Crab Ghost	1
		Son of Chapat	1
		Hala RS	1
		Chapat	2
		Serpiente	1
		Six Gibnut	1
		House of Pain	3
	Pine Ridge (n=17)	Las Cuevas	5
		Rio Frio A	2
		Rio Frio B	2
		Rio Frio	1
		Rio Frio E	3
	Roaring Creek	Yaxcheel Ahau	2
		Handprint	3
		Nakbe	3
		Uyak Na RS	1
		Hummingbird	1
		Taratula	1
		Ray's cave	1
		Unknown Cave	2
		Ray's RS	1
	ATM	5	
	San Antonio (n = 15)	Bols Museum	3
Actun Petz		2	
Crystal Palace		3	
Bat Cave		1	
Skeleton Cave		1	
Hidden Cave		1	
Actun Tzul		2	
Offering Cave	2		

Caves Site Composition by Group

Caves Site Composition By Group (Cont.)

Drainage	Group	Cave Sites	# per Cave
Cave's Branch	Caves's Branch (n= 16)	St Hermans	3
		Jaguar Paw	5
		Caves Branch RS	1
		Swimming Hole	1
		Mountain Cow	2
		Lost World	1
		FootPrint	2
Sibun	Actun Chanona (n = 3)	Chanona 200	1
		Chanona 201	1
		Chanona 202	1
	Hershey (n = 3)	Hershey 68	1
		Hershey 97	1
		Hershey 96	1
	Actun lk (n = 1)	lk	1
Pakal Na (n = 1)	Pakal Na	1	
Oshon (n = 2)	Oshon 5	1	
	Oshon 6	1	
Cedars Bank (n = 1)	Cedars Bank	1	
Peten	Poptun (n = 8)	Poptun 1	1
		Poptun 2	1
		Poptun 3	1
		Poptun 4	1
		Poptun 5	1
		Poptun 6	1
		Poptun 7	1
		Poptun 8	1

6.2 Geochemistry of Drainage Systems

As seen in Figure 20, there is a differentiation among samples from different drainages based on magnesium content, with higher concentrations of Mg in the Cayo System than any other. Box plots indicate that the median concentrations differ by drainage; the Kruskal-Wallis test (a non-parametric ANOVA based on rank sums) is significant ($p < 0.0001$). The likely source of Mg is the dolomitic Barton Creek and Yalbac Formations that underlie the area.

Moreover, the concentrations of Mg in the Sibun and Petén systems are very low. From Figures 4 and 5 in Chapter 3, we can see that the drainages of Sibun are underlain by the Sibun-Manatee Karst and are bordered to the south by the Border Fault and the Vaca Plateau, and to the north by tertiary limestone deposits.

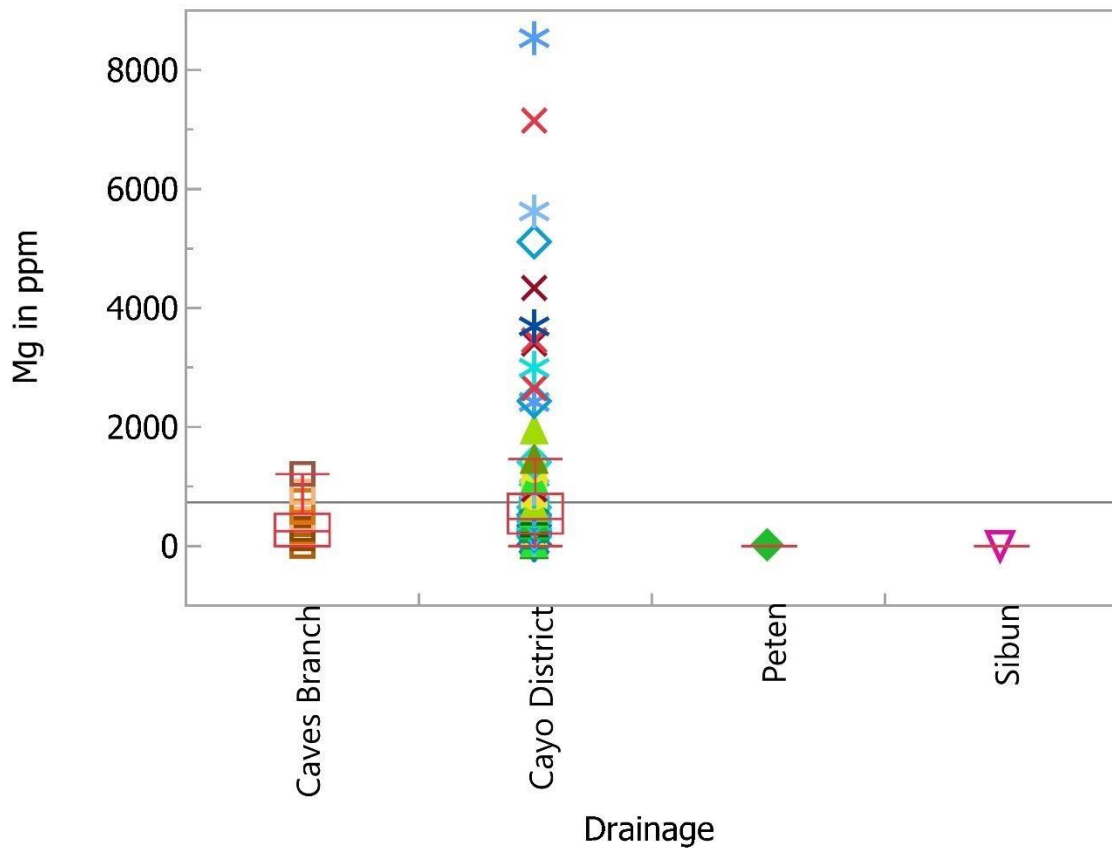


Figure 20. Magnesium concentrations by drainage systems. Showing the depletion of Mg in the Sibun and Petén, and limited range of the Cave's Branch with respect to the Cayo District system.

Previous studies (Peterson *et al.*, 2006; and Nation *et al.*, 2012) found the samples from the Sibun and Petén to be depleted in Mg, Na, Si, and Ni. Furthermore, towards the southernmost area of the Sibun River Basin, there is a transition between two karstic terrains, the Sibun-Manatee in the east, and the Hummingbird karst to the west. This transition occurs in the proximity of the

Boundary Fault and Vaca Plateau from which the Sibun River and all its watershed receive most water and soluble elements. Further downstream, the Cave's Branch River joins the Sibun, but the recharge is mainly from the elevated Boundary Fault and Vaca Plateau Formations.

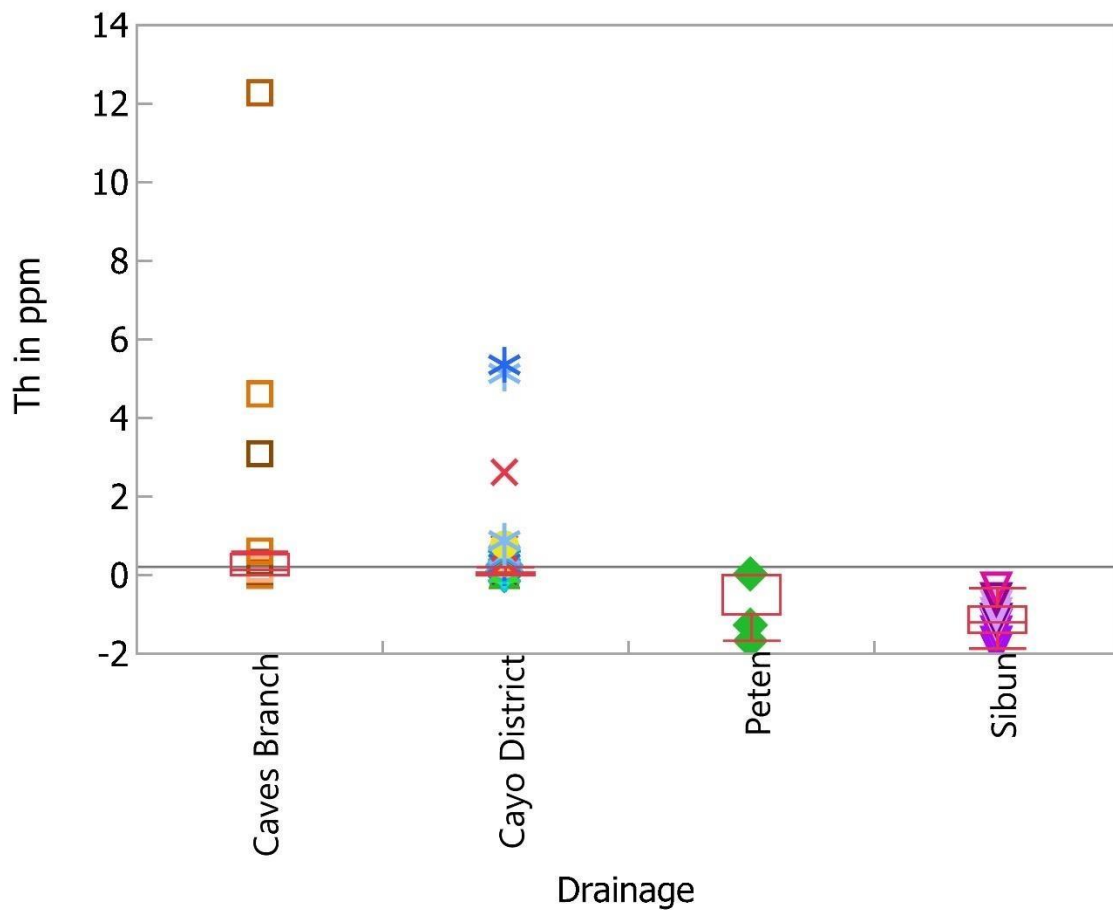


Figure 21. Thorium concentrations by drainage systems, showing the depletion of Th in the Sibun and Petén with respect to the BVSP samples.

Similarly, the XARP samples, with few exceptions, are depleted in actinides. As shown previously in Figure 19, in Chapter 5, the Th vs. U plot indicated that most BVSP samples except for Macal in the Cayo Drainage and Cave's Branch were depleted in U. Box plots confirm that the median concentrations of Th also differ by drainage (Figure 21), and the Kruskal-Wallis test is significant ($p < 0.0001$).

The Uranium-Thorium relationship is one we must address as it elucidates the sources of these elements not only in the speleothems but in other culturally important materials such as clays. Uranium is a naturally occurring element commonly found in all types of rock (i.e. igneous, sedimentary and metamorphic). However, it is most commonly found in light-colored igneous rocks such as granite and andesite, sedimentary rocks rich in phosphates (carbonates) and dark shales, and metamorphic rock derived from these.

Thorium is a natural occurring element also found in many rocks like those for uranium; however, thorium is insoluble under natural surface or near surface conditions, and thus is not present prior or during the deposition of carbonates. In contrast, uranium is soluble in water, and despite occurring in the parts per billion range, it is carried and accumulated in the carbonate material. Over time, the radioactive U-234 decays into Th-230. Thus, the presence of thorium in our samples cannot only be used to date them but also to differentiate between them based on the Th/U content. The uranium and thorium concentrations are mostly depleted except for in a few samples. Moreover, some samples from the Macal group and the Sibun drainage in general have higher than average uranium concentrations with respect to the other groups, while the Cave's Branch and most of the Cayo System groups show higher concentrations of thorium relative to uranium. There are three possibilities to account for this disparity:

- 1) samples with higher uranium and lower thorium may have formed so recently so that U-Th decay has not affected the ratios; 2) the samples with relative higher uranium or thorium represent deposition from substrate material enriched with these elements, and thus are representative of the geochemistry of the basin; or 3) the depletion is due to scavenging of heavy rare earth elements (HREE) with respect to the lighter ones. While all are possible, we believe that the last factor is more plausible given the geochemistry of HREE as previously discussed (Balashov and Khitrov, 1982).

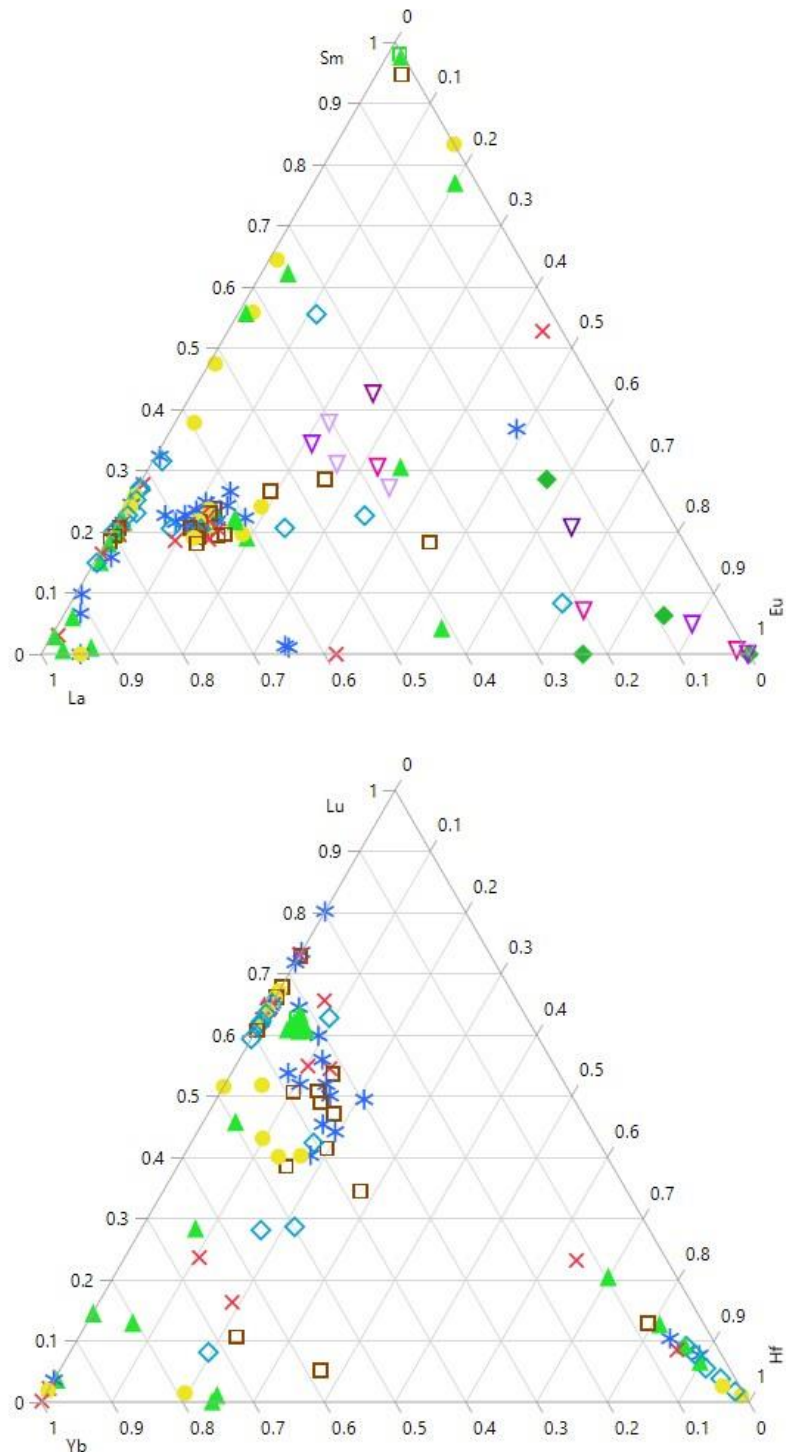


Figure 22. Ternary plots of the rare earth elements. Top: La, Sm, and Eu (LREE); and Bottom: Yb, Lu, and Hf (HREE). Note the depletion of HREE in Sibun and Petén samples. Group colors: Blue diamond (1), Brown Square (2), Green Triangle (3), Red X' (4), Blue Asterisk (5), Yellow Dot (6), Inverted Triangle (7) and Green Diamond (8).

Figure 22 shows the relative concentrations of LREE (top) and HREE (bottom) in samples from the BVSP and XARP, with upside down magenta triangles representing Sibun, and solid green diamonds indicating the Petén. In karstic systems, the HREE are preferentially leached because of the greater stability of the fluoride and carbonate complexes with which they are generally associated. This means that the further downstream the samples are located, the more depleted they would be in HREE with respect to the LREE. As evidenced in the above-mentioned graph, the XARP samples do not appear in the bottom plot as their concentration values for the HREE are zero, only retaining the LREE as seen on the top plot.

Curiously, we must note that the concentration of La seems low with respect to Sm and Eu, while all samples seem to be enriched in all HREE. For this, possible explanations are that the samples from the Cayo District Drainage, are either: 1) too young, geologically speaking; or 2) formed near the source of the soluble material and have not been leached of the HREE as those for the Sibun River Basin.

Chapter 7. Discussion and Conclusions

As introduced in Chapter 3, when interpreting speleothem data, we must consider the various factors that contribute to the formation of a speleothem. In addition to geology, geochemistry, solubility, hydrology and geomorphology of the area of study, we must also consider the ever-changing nature of karstic environments. As rainwater becomes acidified by contact with the soils and calcite, it further dissolves the underlying strata. Thus, the hydrogeology of the system also changes in response to bigger conduits. The volume and movement of groundwater feeding the formation of speleothems can increase or be interrupted, thereby affecting the growth and deposition of solutes in the speleothems. In other words, the chemical composition of speleothems is dynamic, both in their formative stages and post deposition. This is not to say that chemical characterization of speleothems and most importantly, provenance, cannot be determined. Rather, we suggest that these processes must be accounted for in the research design, selection of sampling sites, and sample collection.

7.1 Analytical Considerations

A very important aspect of chemical characterization is the instrumentation and methods of analysis. For archaeological or culturally derived samples, nondestructive methods are the preferred choice. However, of the few methods in existence today, the ones that offer the lowest limits of detection for trace element species are neutron activation analysis (INAA) and Laser Ablation ICPMS. While both are destructive in nature, they require very small amounts of material, or an inconspicuous surface to be ablated.

In this study, we compared the results obtained from both methods. As with any spectral instrumentation, both have specific limitations. For example, accurate characterization of high energy species by NAA is difficult. Moreover,

the neutron flux required for irradiation and the resulting radioactive samples, necessitate a reactor and specialized disposal protocols. In contrast, laser ablation ICP-MS represents a more compact analytical instrument with wider range of detectable elements; however, its limits of detection are higher, especially for the REE. Additionally, one must also consider the availability of appropriate standard reference material (SRM) for either method given the matrix to be analyzed.

Given the above, analyses by both INAA and LA-ICP-MS, if budget and samples permit, will certainly complement each other and ensure an expanded and robust data set.

The pilot study presented herein, is the first systematic attempt to explore the possibility of speleothem sourcing utilizing two instrumental methodologies and a significant larger sample size. As our results suggest, sourcing speleothems by INAA and ICP-MS is potentially viable but not a straight forward process. Our negative results to obtain a cave's "chemical fingerprint" from its speleothems in order to differentiate between caves, are nonetheless an integral part of the scientific discovery process. Moreover, as our research suggests, there are numerous temporal and spatial factors to consider when examining speleothems. This evidence highlights the need for a systematic study focusing on the full range of speleothem variability.

7.2 Conclusions

From our findings, we draw several conclusions as follows:

First, Instrumental Neutron Activation Analysis is an adequate methodological tool for elemental characterization of speleothems to a high degree of precision. Sensitivity is sufficient to detect a suite of 71 elements, even

using relatively small masses and relatively low neutron fluences. However, due to a series of factors (isotopic abundance, activation cross-section, decay constant) its capabilities can be limited for some elements. Notwithstanding previous success in using INAA in sourcing speleothems (Brady, 1997), the homogeneity of the geological substrates in Belize do represent a greater challenge for sourcing by one method alone.

Second, the analysis and results are as good as the samples examined. In this case, the samples from both surveys discussed herein were collected with other research designs in mind. Both the Belize Valley Speleothem Project (BVSP) and the Xibun Archaeological Research Project (XARP) aims were not to evaluate empirically the provenance postulate, but rather to characterize cave modification by the Maya and identify settlements in the Sibun Valley, respectively. Nonetheless, our study demonstrates that these still yield valuable information regarding calcareous substrates and speleothems, albeit at a regional level.

Third, the absence or strong presence of elements in any given sample by itself is a discriminating measure that can help label and classify the speleothem to a discrete group. The depletion in HREE, especially in the Sibun and Petén drainages, while miniscule, clearly differentiates these systems from those in the Cayo District. However, we must emphasize that very rarely does only one element make the difference; rather, a combination of patterns, distributions, and relative concentrations help differentiate source areas among such complex and homogeneous materials.

Fourth, and perhaps the most important, especially when dealing with potentially homogeneous lithic materials such as speleothems, is our understanding of biochemical and physico-chemical processes that first deposited the source material (limestone) and then contributed to the diagenesis and deposition of the speleothems themselves. This helps us make sense of otherwise cryptic data.

7.3 Recommendations for Future Work

Herein, we made several recommendations that aim to validate: 1) The technical and theoretical applicability of analytical techniques to the sourcing of speleothems from homogeneous substrates; and 2) The religious significance of caves to the ancient Maya, the anthropological and archaeological imperative.

As our study demonstrates, sourcing speleothems or any other lithic material by INAA or ICP-MS is possible; however, we must know the intrinsic limitations of these methods.

First, given the homogeneity of the material in question, a research designed should include the collection of a sufficient number of samples per cave to verify homogeneity, from at least three cave systems within a given drainage or watershed system. The more samples from a cave that can be analyzed, the more likely we are to determine if there exists compositional variability within a cave. Moreover, the sampling of a minimum of three proximal caves within a watershed will allow us to determine if there is variation among caves from the same watershed or drainage system. This is important, as it fulfills the first tenant of the provenance postulate (to paraphrase) that the “variability within the cave is less than the variability between the caves” in a given area.

Second, replicate samples from as many caves from at least three different regions, watersheds or drainages systems must be collected and analyzed to verify the second postulate of the provenance postulate, that “the variation between caves (or regions) is greater than the variation between them.”

Third, if and once individual caves are individually identified based chemically composition, then and only then, analysis of culturally derived speleothem fragments from surface sites can be analyzed to identify the cave or caves of origin (provenance) that account for the greatest contribution, and hence its importance to the ancient Maya.

Fourth, we must utilize a synergistic combination of instrumental methods that will allow us a wider range and precision in the chemical characterization of samples with the minimal destructive effects of other analytical techniques. Thus, laser ablation ICP-MS in combination with INAA is likely to complement and give the greatest elemental characterization range with minimal destruction of sample material.

Fifth, to conclusively address the anthropological and archaeological questions such as cave use, preference, and visitation, we must sample and analyze other types of anthropogenic material found within such caves sites (e.g., ceramics) and attempt to source them to adjacent surface sites or clay sites.

A conscientious study that utilizes complementary methodology, instrumentation and combined analysis of ceramics, speleothems, clays, and perhaps human remains found within the caves of Belize, would certainly yield a deeper understanding on the religious importance and ritualistic use of caves by the ancient Maya.

Referenced Cited

Alden, J. R., Minc, L. D. and Lynch, T. F. 2005. Identifying the sources of Inka period ceramics from northern Chile: results of a neutron activation study. *Journal of Archaeological Science* 33(4):575-594.

Andrews, E. W. 1971. Balankanche. Throne of the Tiger Priest. *Explorers Journal*. 49 (4). Pp.254-262.

Andrews, A. P. 1984. The Political Geography of the Sixteenth Century Yucatan Maya: Comments and Revisions. *Journal of Anthropological Research* 40 (4): 589–96.

Andrews, E., & Hammond, N. 1990. Redefinition of the Swasey Phase at Cuello, Belize. *American Antiquity*, 55(3), 570-584. doi:10.2307/281287

Aitken, J. A., and Stewart, R., R. 2002. A geological / geoscience overview of the hydrocarbon exploration potential of Belize, Central America. CREWES Research Report Volume 14.

Balashov, A. and Khitrov, L. M. 1967. *Geochem. Int.*, 1967, 14,404. Edited by: V. V. Burkov and Y. K. Podporina, Dokl. Acad. Sci. USSR, Earth Sci. Sect., 1967, 177, 214. Reprinted in Environmental Chemistry Volume 2, 1982. Royal Society of Chemistry.

Bassie, K. 2002. The Jolja' Cave Project. Report submitted to the Foundation for the Advancement of Mesoamerican Archaeology, Inc.

Bishop, R. L. 1987. Ceramic Paste Compositional Chemistry: Initial Observations of Variation in the Tucson Basin. In *The Archaeology of the San Xavier Bridge Site (AZ BB:13-14) Tucson Basin, Southern Arizona*. Appendix E, pages 395-408, edited by J.E. Ravesloot. Arizona State Museum, University of Arizona, Tucson.

Bishop, R., L. and Neff, H. 1989. Compositional Data Analysis in Archaeology. In *Archaeological Chemistry, Volume IV*, edited by R.O. Allen, pp. 57-86. American Chemical Society, Washington, D.C.

Brady, J. E. 1989. An Investigation of Maya Ritual Cave Use with Special Reference to Naj Tunich, Petén, Guatemala. Ph.D. dissertation, University of California, Los Angeles.

Brady, J. E. 1991 The Petexbatun Regional Cave Survey: Ritual and Sacred Geography. Paper presented at the 47th Inter-national Congress of Americanists, New Orleans.

- Brady, J. E. 1996. *Sources for the Study of Mesoamerican Ritual Cave Use*. Studies in Mesoamerican Cave Use, Publication 1. George Washington University, Washington, DC.
- Brady, J. E., Scott, A., Neff, H. and Glascock, M. D. 1997. Speleothem Breakage, Movement, Removal, and Caching: An Aspect of Ancient Maya Cave Modification. *Geoarchaeology: An International Journal*, Vol. 12, No. 6, 725–750.
- Brady, J. E., Ware, G. E., Luke, B. Cobb, A. Fogarty, J. and Shade, B. 1997. Preclassic Cave Utilization near Cobanerita, San Benito, Petén. *Mexicon*, Vol 19, No. 5 pp. 19-96.
- Brady, J. E. 2009. *Exploring Highland Maya Ritual Cave Use: Archaeology & Ethnography in Huehuetenango, Guatemala*, edited by James E. Brady. Association for Mexican Cave Studies Bulletin 20, Austin.
- Brady, J. E., and Ashmore, W. 1999. Mountains, Caves, Water: Ideational Landscapes of the Ancient Maya. In *Archaeologies of Landscapes: Contemporary Perspectives*, edited by Wendy Ashmore and A. Bernard Knapp, pp. 124-145. Blackwell Publishers, Oxford.
- Brady, J. E. and Colas. P. R. 2005. Nikte Mo' Scattered Fire in the Cave of K'abChante: Epigraphic and Archaeological Evidence for Cave Desecration in Ancient Maya Warfare. In *Stone Houses and Earth Lords: Maya Religion in the Cave Context*, edited by Keith M. Prufer and James E. Brady, pp. 149-166. University Press of Colorado, Boulder.
- Brady, J. E. and Delgado, A. 2009. The Chicomoztoc and Modern Jalkatek Ethnography. In *Exploring Highland Maya Ritual Cave Use: Archaeology & Ethnography in Huehuetenango, Guatemala*, edited by James E. Brady, pp. 6771. Association for Mexican Cave Studies Bulletin 20, Austin.
- Brady, J. E. and Peterson., P. A. 2008. Re-envisioning Ancient Maya Ritual Assemblages. In *Religion, Archaeology, and the Material World*, edited by Lars Fogelin, pp. 78-96. Center for Archaeological Investigations, Occasional Paper No.36, Southern Illinois University, Carbondale.
- Brady, J. E. and Prufer K., M. 1999. Caves and Crystalmancy: Evidence for the Use of Crystals in Ancient Maya Religion. *Journal of Anthropological Research* 55:129-144. 2005a In *the Maw of the Earth Monster: Mesoamerican-can Ritual Cave Use*. University of Texas Press, Austin.
- Brady, J. E. 2005b. Introduction: A History of Mesoamerican Cave Interpretation. In *In the Maw of the Earth Monster: Mesoamerican Ritual Cave Use*, edited by James E. Brady and Keith M. Prufer, pp. 1-17. University of Texas Press, Austin.

- Brady, J. E. 2005c. Maya Cave Archaeology: A New Look at Religion and Cosmology. In *Stone Houses and Earth Lords: Maya Religion in the Cave Context*, edited by Keith M. Prufer and James E. Brady, pp. 365-379. University Press of Colorado, Boulder.
- Brady, J. E. 1997a. A History of Mesoamerican Cave Archaeology. Paper presented at the 62nd Annual Meeting of the Society for American Archaeology, Nashville.
- Brady, J. E. 1997b. Settlement Configuration and Cosmology: The Role of Caves at Dos Pilas. *American Anthropologist* 99(3): 602-618.
- Brady, J. E. and Prufer, K. M. 2002. A History of Mesoamerican Cave Interpretation. In *In the Maw of the Earth Monster. Studies of Mesoamerican Ritual Cave Use*, edited by James E. Brady and Keith M. Prufer. University of Texas Press, Austin.
- Brennan, M. L., M. King, E. M., Shaw, L. C., Walling, S. L. and Valdez Jr. F. 2013. Preliminary geochemical assessment of limestone resources and stone use at Maya sites in the Three Rivers Region, Belize. *Journal of Archaeological Science* 40, 3178 - 3192
- Byrne, R.H., Kim, K.-H., 1990. Rare earth element scavenging in seawater. *Geochim. Cosmochim. Acta* 54, 2645 – 2656.
- Cherry, J. F., Faro, E. Z. and Minc, L. D. 2007. Field Exploration and Instrumental Neutron Activation Analysis of the Obsidian Sources in Southern Armenia. *Bulletin of the International Association for Obsidian Studies Bulletin* 39: 3-6.
- Chatters, J. C., Kennett, D. J., Asmerom, Y., Kemp, B. M., Polyak, V., Nava-Blank, A., Beddows, P. A., Reinhardt, E., Arroyo-Cabrales, J., Bolnick, D. A., Malhi, R. S., Culleton, B. J., Luna- Erreguerena, P., Rissolo, D., Morell-Hart, S., and Stafford Jr. T. W. 2014. Late Pleistocene Human Skeleton and mtDNA Link Paleoamericans and Modern Native Americans. *Science* 344, 750 (2014)
- Coe, M. D. 1999. *The Maya*. Ancient peoples and places series (6th edition, fully revised and expanded ed.). London and New York.
- Dao-Hui Pi, Cong-Qiang Liu, Graham A. Shields-Zhou, Shao-Yong Jiang. 2013 Trace and rare earth element geochemistry of black shale and kerogen in the early Cambrian Niutitang Formation in Guizhou province, South China: Constraints for redox environments and origin of metal enrichments. *Precambrian Research*, Volume 225, pp. 218-229

del Águila Flores, P.2007. "Zaculeu: Ciudad Postclásica en las Tierras Altas Mayas de Guatemala" Guatemala City, Guatemala: Ministerio de Cultura y Deportes.

Demarest, A. 2004. *Ancient Maya: The Rise and Fall of a Rainforest Civilization*. Cambridge University Press, Cambridge

Drever J.I. 1994. The effect of land plants on weathering rates of silicate minerals, *Geochimica et Cosmochimica Acta*, Volume 58, Issue 10, Pages 2325-2332,

Drever J.I., Vance G.F. 1994. Role of Soil Organic Acids in Mineral Weathering Processes. In: Pittman E.D., Lewan M.D. (eds) *Organic Acids in Geological Processes*. Springer, Berlin, Heidelberg

Fairchild, I. J.; Treble, P. C. 2009. Trace elements in speleothems as recorders of environmental change. *Quaternary Science Reviews* 28, 449–468

Fernandez-Cortes, A., Cuezva, S., Garcia-Anton, E., Garcia-Guinea, J., and Sanchez-Moral, S. 2011. Rare Earth Elements in a Speleothem Analyzed by ICP-MS, EDS, and Spectra Cathodoluminescence, *Spectroscopy Letters: An International Journal for Rapid Communication*, 44:7-8, 474-479

Foster, L.2002. *Handbook to Life in the Ancient Maya World*. New York: Oxford University Press

Gill, K. K., King Jr., D., T., and Smith, F., G.2016. Stratigraphy and Depositional Environments of the Hillbank and Yalbac Formations, Corozal Basin, Northern Belize. *Geological Society of America Abstracts with Programs*. Vol. 48, No. 7

Glascok, M. D. 1986. Characterization of Mesoamerican Obsidian by NAA for Provenance Studies. In *Transactions of the American Nuclear Society*. January 1986

Glascok, M. D. 1992. Characterization of Archaeological Ceramics at MURR by Neutron Activation Analysis and Multivariate Statistics. In *Chemical Characterization of Ceramic Pastes in Archaeology*. edited by Hector Neff. Prehistory Press.

Glascok, M., D. and Neff, H. 2003. Neutron Activations Analysis an Provenance Research in Archaeology. *Measurements Science and Technology* (14), pg. 1561 – 1526. Institute of Physics Publishing.

Glascoek, M., D.; Speakma, R. J. and Popelka-Filcoff, R. S. 2007. Archaeological Chemistry. Analytical techniques and Archaeological Interpretation. ACS Symposium Series 968. Sponsored by the ACS Divisions of Nuclear Chemistry and Technology and the History of Chemistry. American Chemical Society, Washington D.C.

Gonzalez, A.H., Rojas Sandoval, C., Terrazas Mata, A., Benavente Sanvicente, M., Stinnesbeck, W., Aviles O., J., de los Rios, M., and Acevez, E. 2008. The Arrival of Humans on the Yucatan Peninsula: Evidence from Submerged Caves in the State of Quintana Roo, Mexico. Special Report. Current Research in the Pleistocene. Vol. 25.

Grigor'ev, D. P., 1961, Ontogeny of minerals: Lvov, Izdatel'stvo L'vovskogo Univ. In Russian. English translation 1965, Israel Program for Scientific Translations, 250 p.

Hammond, N., Pring, D. Berger, R., Switsur, V. R., Ward, A. P. 1976. Radiocarbon chronology for early Maya occupation at Cuello, Belize. *Nature* 260, 579-581.

Hammond, N., Harbottle, G. and Gazard, T. (1976). Neutron Activation and Statistical Analysis of Maya Ceramics and Clays from Lubaantun, Belize. *Archaeometry* 18, 2, 147 -168

Hansen, R. 2014 The Origins & Collapse of the Preclassic Maya in the Mirador Basin. The Library of Congress.

Helmke, Christophe G. B. 1999 Exploration and Investigations of the Sinkhole Tunnels, Actun Tunichil Muknal, Belize. In *The Western Belize Regional Cave Project: A Report of the 1998 Field Season*, edited by Jaime J. Awe, pp. 146–165, Department of Anthropology Occasional Paper No. 2. University of New Hampshire, Durham

Hill, C. A., & Forti, P., 1997, *Cave minerals of the world* (2nd ed.): National Speleological Society, Huntsville, Alabama, 463 p.

Hodell, D. A., Quinn, R. L., Brennera, M., and Kamenova G. (2004). Spatial variation of strontium isotopes ($^{87}\text{Sr}/^{86}\text{Sr}$) in the Maya region: a tool for tracking ancient human migration. *Journal of Archaeological Science* 31, 585–601.

Holland, W. R. 1961. Relaciones Entre la Religión Tzotzil Contemporánea y la Maya Antigua. Instituto Nacional de Antropología e Historia, Anales, 13 pp 113131, Mexico.

Holmes, L. L., Little, C. T. and Sayre, E. V. 1986. "Elemental Characterization of Medieval Limestone Sculpture from Parisian and Burgundian Sources." *Journal of Field Archaeology* 13: 419-438.

Holmes, L. L. and Harbottle, G. 1994a "Analysis of Medieval Limestone Sculpture from Southwestern France and the Paris Basin by NAA." *Transactions, The American Nuclear Society* 71: 15.

Hubbard, H., A., and Ericksen, G., E. 1949. Limestone and Dolomite U.S. Geological Survey Professional Paper, Issue 820 Government Printing Office, 1949

Ilyin, A.V., 1998a. Rare-earth geochemistry of "old" phosphorites and probability of syngenetic precipitation and accumulation of phosphate. *Chem. Geol.* 144, 243 – 256.

Ilyin, A.V., 1998b. Rare-earth element geochemistry of the Mesozoic phosphorites of the East European Platform, with applications to some problems of phosphogenesis. *Geochem. Int.* 36, 489 – 495.

Jones, G. D. 1998. *The Conquest of the Last Maya Kingdom*. Stanford, California: Stanford University Press

Kelly, J. 1996. *An Archaeological Guide to Northern Central America: Belize, Guatemala, Honduras, and El Salvador*. Norman. University of Oklahoma Press.

Kendrick, M. A. 2016. *Encyclopedia of Geochemistry: A Comprehensive Reference Source on the Chemistry of the Earth*. Editors: White, W. Springer Publishing.

Kieffer, C.L. 2010. Determining Status of Ancient Maya from Looted and Sacrificial Context. *The University of New Mexico Best Student Essays*. Vol. 22, No. 2 pp. 33-41

Kieffer, C. L. 2015. Sacrifice of the Social Outcasts: Two Cases of Klippel–Feil Syndrome at Midnight Terror Cave, Belize. *International Journal of Osteoarchaeology*. Special Issue Paper.

Kilikoglou, V., Bassiakos, Y., Doonan, R.C., & Stratis, J. 1997. NAA and ICP analysis of obsidian from Central Europe and the Aegean Source characterization and provenance determination. *Journal of Radioanalytical and Nuclear Chemistry*, 216(1), 87-93.

King, D. T., Jr., and Petruny, L. W. 2003. Stratigraphy and sedimentology of Cretaceous-Tertiary boundary breccia deposits at Albion Island, Belize, in Koeberl, C., and F. Martinez-Ruiz, eds., *Impact markers in the stratigraphic record (Impact Studies)*: Berlin, Springer-Verlag, p. 203-228.

King, D.T., Jr., Pope, K. O., Petruny, L.W., Ocampo, A. C. and Fischer, A.G. 2002. Cretaceous-Tertiary boundary stratigraphy in Belize and adjacent México: Geological Society of America, Annual Meeting Abstracts with Programs, v. 34, no. 6, p. 545.

King, D.T., Jr., Petruny, L.W. and Pope, K.O. 2003. Shallow-marine facies of the Orange Walk group, Miocene-Pliocene, northern Belize (Central America): Gulf Coast Association of Geological Societies Transactions, v. 53, p. 384-397.

King Jr., D., T., Pope, K. O., and Petruny, L. W. 2004. Stratigraphy of Belize, North of the 17th Parallel. Gulf Coast Association of Geological Societies Transactions, Volume 54. 289-304.

Korotev, R., L. 1996. A Self-Consistent Compilation of Elemental Concentration Data for 93 Geochemical Reference Samples. *Geostandards Newsletter* 20, 217-245.

Landa, D. de. *Relacion de las Cosas de Yucatán*. Translated and annotated by Alfred M. Tozzer. (1941). Papers of the Peabody Museum of American Archaeology and Ethnology, Harvard University, v. 18.

Leeming, D. A., and Page, J. 2000. *The Mythology of Native North America*. University of Oklahoma Press.

Lev, S.M., McLennan, S.M., Hanson, G.N., 1999. Mineralogic controls on REE mobility during black-shale diagenesis. *J. Sediment. Res.* 69, 1071 – 1082.

Little, C. T. 1994. "Searching for the Provenances of Medieval Stone Sculpture: Possibilities and Limitations." *Gesta* 33 (1): 29-37.

Lopez Austin, A. 1997. *Monografías del Jardín Botánico de Córdoba*, 1997. Instituto de Investigaciones Antropológicas de la Universidad Nacional Autónoma de México.

López Varela, S. and Dore, C. 2005. The Construction of Social Space and Production in the Sibun River Valley. *Research Reports in Belizean Archaeology*, Vol. 2, 2005, pp. 329-338. Institute of Archaeology, NICH, Belize.

MacLeod, B. and Puleston, D. 1978. Pathways into darkness: The search for the road to Xibalba. *Tercera Mesa Redonda de Palenque*, 4, 71-77.

Maltsev, V. A. 1997a. A model of structure and genesis for the gypsum “nest” found in the Geophysicheskaya Cave (Kugitangtou Mountains, Turkmenistan): *Journal of Cave and Karst Studies*, v. 59, n. 2, p. 87-90.

Maltsev, V. A. 1997b. Overview of cave minerals ontogeny: Proceedings of the 12th International Congress of Speleology, La Chaux-de-Fonds, Switzerland, v. 1, p. 219-222.

Maltsev, V. A. 1997c. Stalactites, cryslactites, corlactites, tuflactites – 4 types of “stalactite-like” formations, generated from crystallization environments with different physical properties: Proceedings of the 12th International Congress of Speleology, La Chaux-de-Fonds, Switzerland, v. 1, p. 267-270.

Maltsev, V. A. 1998. Stalactites with “internal” and “external” feeding: Proceedings of the University of Bristol Spelaeological Society, v. 21, n. 2, p.149158.

Marcus, J.; Flannery, K. V. 1996. *Zapotec Civilization: How Urban Society Evolved in Mexico's Oaxaca Valley*. New aspects of antiquity series. New York.

Masson, M. A. 2012. "Maya collapse cycles". *Proceedings of the National Academy of Sciences of the United States of America*. 109 (45): 18237–38

Masson, M. A.; Peraza-Lope, C. 2014. "Militarism, Misery and Collapse". In Marilyn A. Masson; Carlos Peraza Lope. *Kukulcan's Realm: Urban Life at Ancient Mayapán*. Boulder, Colorado, US: University Press of Colorado.

Martin, S., and Grube, N. 2000. *Chronicle of the Maya Kings and Queens: Deciphering the Dynasties of the Ancient Maya*. London and New York.

McAnany, P. A., Harrison-Buck, E. and Murata, S. 2005. Desire and Political Influence, The Archaeology of the Sibun River Valley. Research Reports in Belizean Archaeology, Vol. 2, 2005, pp. 329-338. Institute of Archaeology, NICH, Belize.

McArthur, J. M., Walsh, J. N. 1984. Rare-earth geochemistry of phosphorites. *Chem. Geol.* 47, 191 – 220.

Miller, T. E. 1983. Hydrology and Hydrochemistry of the Caves Branch Karst, Belize. *Journal of Hydrology* 61: 83-88.

Miller, T. E. 1984. *The Karst Hydrology and Associated Archeology of the Chiquibul, Belize*. Report of Grant #2742-83 to the National Geographic Society, 48 pp

- Miller, T. E. 1996. Geologic and Hydrologic Controls on Karst and Cave Development in Belize. *Journal of Cave and Karst Studies* 58(2):100-120
- Minc, L. D. 2008. Neutron Activation Analysis (NAA). In *Encyclopedia of Archaeology*, Vol 3 edited by D. M. Pearsall. Academic Press, NY, pg. 1669 – 1683.
- Minc, L. D. and Sherman, R. J. 2011. Assessing natural clay composition in the Valley of Oaxaca as a basis for ceramic provenance studies. *Archaeometry* 53:285-328.
- Minc L. D. and Pink, J. 2014. Trace-Element Analysis of Oaxacan Ceramics: Insights into the Regional Organization of Ceramic Production and Exchange in the Valley of Oaxaca during the Late Classic (AD 550-850). Final technical report circulated to collaborators for analyses supported by NSF award 1005945: Support of Coordinated, Regional Trace-Element Studies at the OSU-RC. OSU Archaeometry Lab, Corvallis, OR.
- Moore, G. W. 1962. The growth of stalactites: *National Speleological Society Bulletin*, v. 24, n. 2, p. 95-106.
- Moyes, H., and Brady, J. E. 2005. The Heart of Creation, The Heart of Darkness: Ritual Cave Use in Mesoamerica. *Expedition* 47, no. 3: 30-36.
- Neff, H. and Glascock, M. D. 1995. The state of nuclear archaeology in North America. *Journal of Radioanalytical and Nuclear Chemistry* 196: 275–285.
- Nothdurft, L. D. 2001. Rare earth element geochemistry of Late Devonian reefal carbonates, Canning Basin, Western Australia: a proxy for ancient seawater chemistry. Unpubl. Honours thesis, Queensland Univ. Tech. 103 pp., Brisbane
- Ochoa, L., and Martel, P. 2002. *Lengua y cultura mayas*. UNAM. Universidad Nacional Autónoma de México, Instituto de Investigaciones Antropológicas,
- Petersen, H., Holland, B., Nytoft, H., Cho, A., Piasecki, S., de la Cruz, J. and Cornec, J. 2012. Geochemistry of Crude Oils, Seepage Oils and Source Rocks from Belize and Guatemala: Indications of Carbonate-Source Petroleum Systems. *Journal of Petroleum Geology*, 35: 127-163.
- Phillips, L. H., Moyes, H., Issavi, J., and Bourgeois, N. 2014. Mapping the Underworld: Innovations in Cave Mapping Using GIS. The Light and Dark Side of Las Cuevas: 3rd Report the Las Cuevas Archaeological Reconnaissance Project: The 2013 Field Season. Belmopan, Belize: Institute of Archaeology, NICH.

Picard, S., Le´cuyer, C., Barrat, J.-A., Garcia, J.-P., Dromart, G., Sheppard, S. M. F. 2002. Rare-earth element contents of Jurassic fish and reptile teeth and their potential relation to seawater composition (Anglo-Paris Basin, France and England). *Chem. Geol.* 186, 1 – 16

Price, T. D., Manzanilla, L., and Middleton, W. D. 2000. Immigration and the Ancient City of Teotihuacan in Mexico: a Study Using Strontium Isotope Ratios in Human Bone and Teeth *Journal of Archaeological Science* 27, 903–913.

Prufer, K. M. and Brady, J. E. 2004. Introduction: Religion and Role of Caves in Lowland Maya Archaeology. In *Reconstructing Maya Ritual and Cosmology in the Cave Context*. University Press of Colorado.

Prufer, K., and Brady, J. E. 2005. Stone Houses and Earth Lords: Maya Religion in the Cave Context. University Press of Colorado.

Pusey, W. C. III. 1975. Holocene Carbonate Sedimentation on Northern Belize Shelf. In *American Association of Petroleum Geologists Bulletin Studies in Geology No.2*: 131-234.

Recinos, A. 1950 *Popol Vuh: The Sacred Book of the Ancient Maya*. University of Oklahoma Press, Norman.

Reeder, P. P. 1993. Cave Exploration and Mapping on the Northern Vaca Plateau. *National Speleological Society News* 51(11): 296-300.

Reynard, B., Le´cuyer, C., and Grandjean, P. 1999. Crystal-chemical controls on rare-earth element concentrations in fossil biogenic apatites and implications for paleoenvironmental reconstructions. *Chem. Geol.* 155, 233 – 241

Seibold, E. and Berger, W.H. 1993. *The Sea Floor, An introduction to Marine Geology*. 1st Ed. Springer-Verlag, Berlin Heidelberg GmbH. 2nd Ed. Springer Science & Business Media, 2013

Self, C. A., and Hill, C. A. 2003. How speleothems grow: An introduction to the ontogeny of cave minerals: *Journal of Cave and Karst Studies*, v. 65, n. 2, p. 130-151.

Self, C. A. 2004. The internal organization of speleothems. *Acta Carsologica*, 33/1

Sharer, R. J. and Loa, P. T. 2006. *The Ancient Maya* (6th, fully revised ed.). Stanford, CA: Stanford University Press

Shields, G. A., and Webb, G. E. 2004. Has the REE composition of seawater changed over geological time? *Chemical Geology* 204, 103–107.

Sholle, P.A., Bebout, D. G., and Moore, C. H. 1983. *Carbonate Depositional Environments*. American Association of Petroleum Geologists.

Slyotov (Sletov), V. A. 1985. Concerning the ontogeny of crystallite and helictite aggregates of calcite and aragonite from the karst caves of southern Fergana: *Novye Dannye o Mineralakh CCCP (New Data on Minerals)*, "Nauka", Moscow, v. 32, p. 119-127. In Russian. English translation 1999, *Cave Geology*, v. 2, no. 4, p. 196-208.

Stepanov, V. I. 1971. Crystallization processes periodicity in karst caves: *Trudy Mineralogicheskogo Muzeya imini A.E. Fersmana*, Moscow, n. 20, p. 198-206. In Russian. English translation, 1999, *Cave Geology*, v. 2, no. 4, p. 209-220.

Stinnesbeck, W., Becker, J., Hering, F., Frey E, González, A. G., and Fohlmeister, J. 2017. The earliest settlers of Mesoamerica date back to the late Pleistocene. *PLoS ONE* 12(8).

Stone, A. J. 1995. *Images from the Underworld: Naj Tunich and the Tradition of Maya Cave Painting*. Austin: University of Texas Press.

Stross, F., Sheets, P., Asaro, F. and Michel, H. 1983. Precise Characterization of Guatemalan Obsidian Sources and Source Determination of artifacts from Quiriguá. *American Antiquity*, 48(2), 323-346.

Stuart, D. 2000. The Arrival of Strangers. Teotihuacan and Tollan in Classic Maya History in *Mesoamerica's Classic Heritage, From Teotihuacan to the Aztecs*, edited by David Carrasco, Lindsay Jones and Scott Sessions. University Press of Colorado. 465-513.

Thompson, J. E. S. 1970. *Maya History and Religion*. *University of Oklahoma Press, Norman*.

Thompson, J. E. S. 1975. Introduction to the 1896 Reprint Edition. In *The HillCaves of Yucatan. A Search for Evidence of Man's Antiquity in the Caverns of Central America*. By Henry C Mercer University of Oklahoma Press. Norman.

Tucker, M.E., Wright, V. P., and Dickson, J. A. D. 1990. *Carbonate Sedimentology*. Blackwell Science Ltd.

Viveros de Castro, E. 1998. Cosmological Deixis and Amerindian Perspectivism. *The Journal of the Royal Anthropological Institute*. Vol. 4, No. 3, pp. 469-488.

Vogt, E. Z. 1981. Some Aspects of the Sacred Geography of Highland Chiapas. In *Mesoamerican Sites and World Views.*, edited by Elizabeth P. Benson. Pp. 119-142. Dumbarton Oaks, Washington D.C.

Vogt, E. Z. and Stuart, S. 2002. Some Notes on Ritual Caves among the Ancient and Modern Maya. In: J. E. Brady and K. M. Prufer, eds. *In the Maw of the Earth Monster: Mesoamerican Ritual Cave Use*, Linda Schele Series in Maya and PreColumbian Studies, Pp. 155–185. Austin: University of Texas Press.

Webb, G. E. and, Kamber, B. S. 2000. Rare earth elements in Holocene reefal microbialites: a new shallow seawater proxy. *Geochim. Cosmochim. Acta* 64, 1557 – 1565.

Weber, B., Schaaf, P., Valencia, V. A., Iriondo, A., and Ortega-Gutiérrez, F. 2006. Provenance ages of late Paleozoic sandstones (Santa Rosa Formation) from the Maya block, SE Mexico. Implications on the tectonic evolution of western Pangea. *Revista Mexicana de Ciencias Geológicas*, v. 23, núm. 3, 2006, p. 262-276

Webster, D. L. 2002. *The Fall of the Ancient Maya: Solving the Mystery of the Maya Collapse*. London

Weigand, P., C. Harbottle, G. and Sayre, E., V. 1977. Turquoise Sources and Source Analysis: Mesoamerica and the Southwestern U.S.A. In T.K. Earle and J.E. Ericson, Eds. *Exchange Systems in Prehistory*, pp. 15–34. New York: Academic Press

Wolfgang, D. 2004. Dissolution: Carbonate rocks. *Encyclopedia of caves and karst science* 608b to 621b

Wollast, R. 1990. Rate and mechanism of dissolution of carbonates in the system $\text{CaCO}_3\text{-MgCO}_3$. In: Stumm W (ed) *Aquatic chemical kinetics*. WileyInterscience, New York, pp 431–445.

Wright, L. E., Valdes, J. A., Burton, J. H., Price, T. D., and Schwarcz, H. P. 2010. The children of Kaminaljuyu: Isotopic insight into diet and long distance interaction in Mesoamerica. *Journal of Anthropological Archaeology* 29, 155 – 178.

Wright, L. E. 2012. Immigration to Tikal, Guatemala: Evidence from stable strontium and oxygen isotopes. *Journal of Anthropological Archaeology* 31, 334–352.

Wrobel, G. D., Andres, C. R., Morton, S. G., Shelton, R., Michael, A. and Helmke C. 2012. Ritual Landscapes of the Caves Branch River Valley. *Research Reports in Belizean Archaeology*, Vol. 9, 2012, pp. 233-244. Institute of Archaeology, NICH, Belize.

Wrobel, G. D., Shelton, R., Morton, S., Lynch, J. and Andres, C. 2013. The view of Maya cave ritual from the Overlook Rockshelter, Caves Branch River Valley, Central Belize. *Journal of Cave and Karst Studies*, v. 75, no. 2, p. 126–135

Wrobel, G. D., Freiwald, M. A., Helmke C., Awe, J., Kennett, D. J., Gibbs, S., Ferguson, J. M., and Griffith, C. 2017. Social identity and geographic origin of Maya burials at Actun Uayazba Kab, Roaring Creek Valley, Belize. *Journal of Anthropological Archaeology* 45, 98–114.

Appendix A

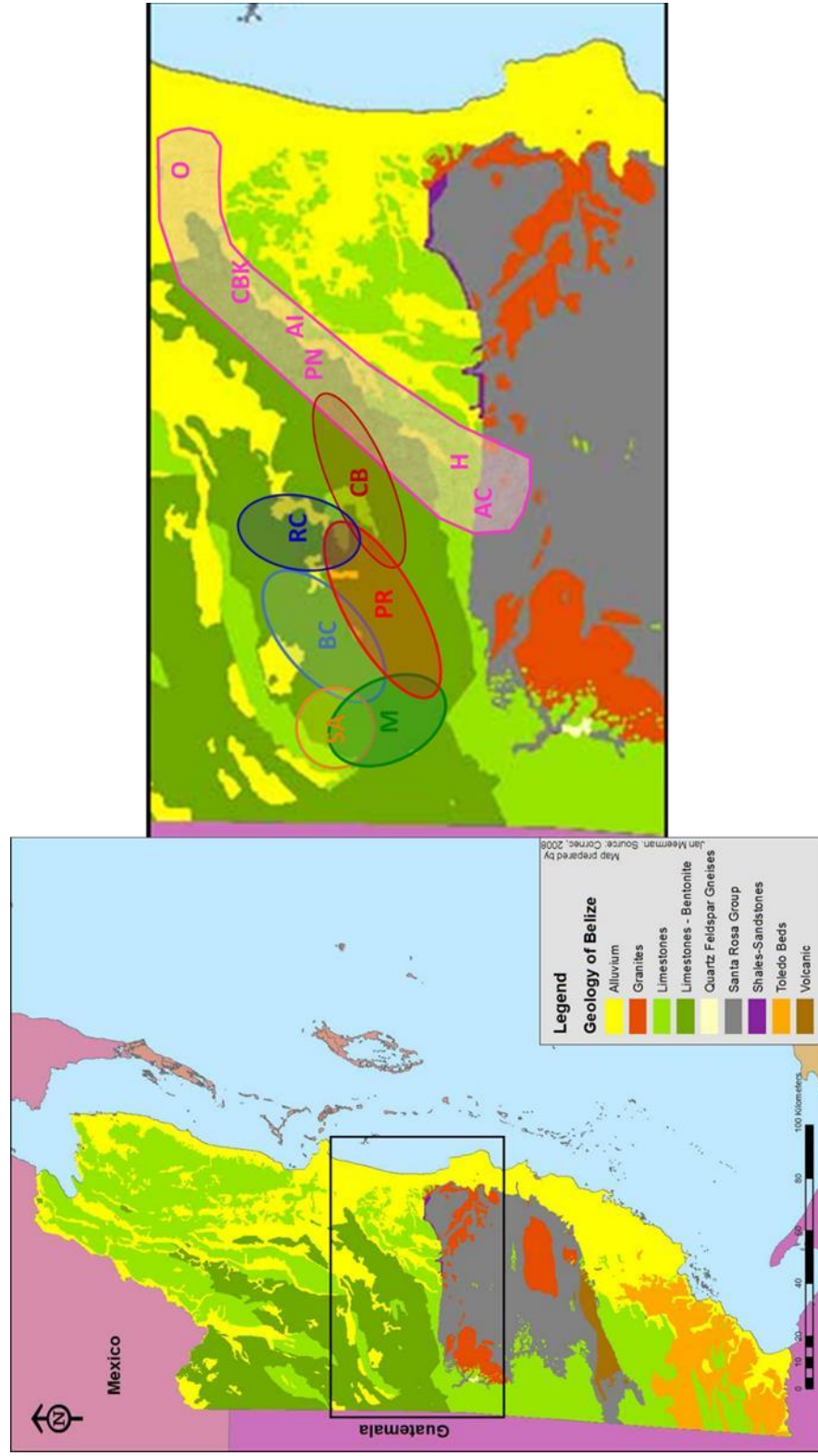


Figure 2. Geological Map of Belize. As adapted from Jan Meeman (2008), and showing the study area inset) and the approximate range from the Cayo District group samples as follows: Barton Creek (BC), Cave's Branch (CB), Macal (M), Pine Ridge (PR), Roaring Creek (RC), and San Antonio (SA). XARP samples as follows: Actun Chanona (AC), Hershey (H), Pakal na (PN), Actun Ik (AI), Cedars Bank (CBK) and Oshon (O).

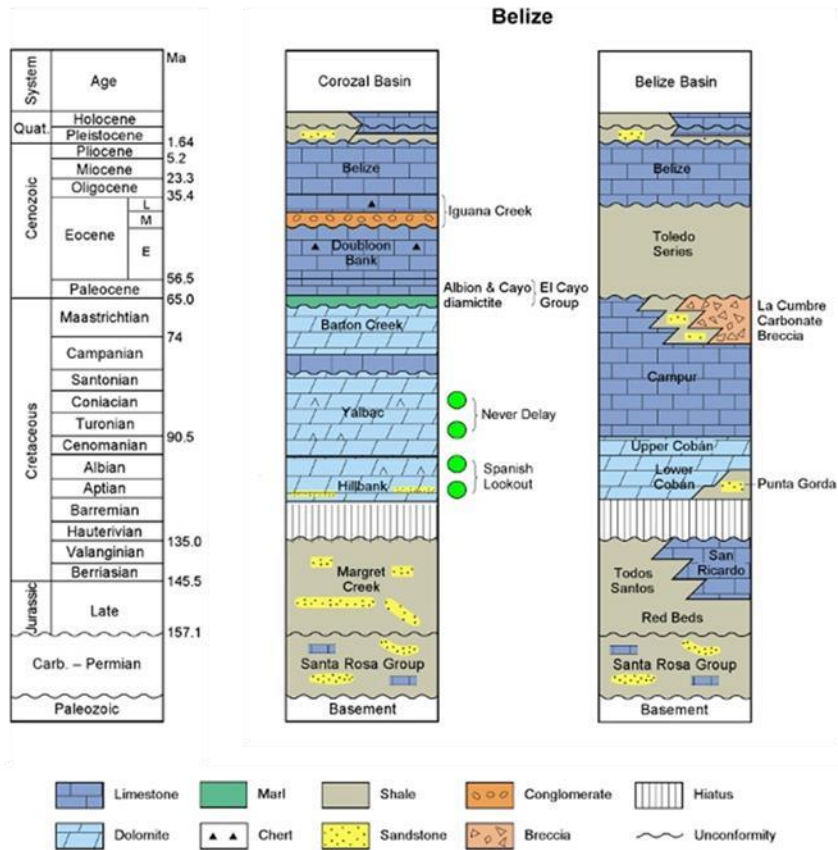


Figure 3. Stratigraphic Columns for the Corozal and Belize Basins in correspondence to chronostratigraphic column. Most of the calcareous horizons are unconformably deposited and date to the middle Cretaceous

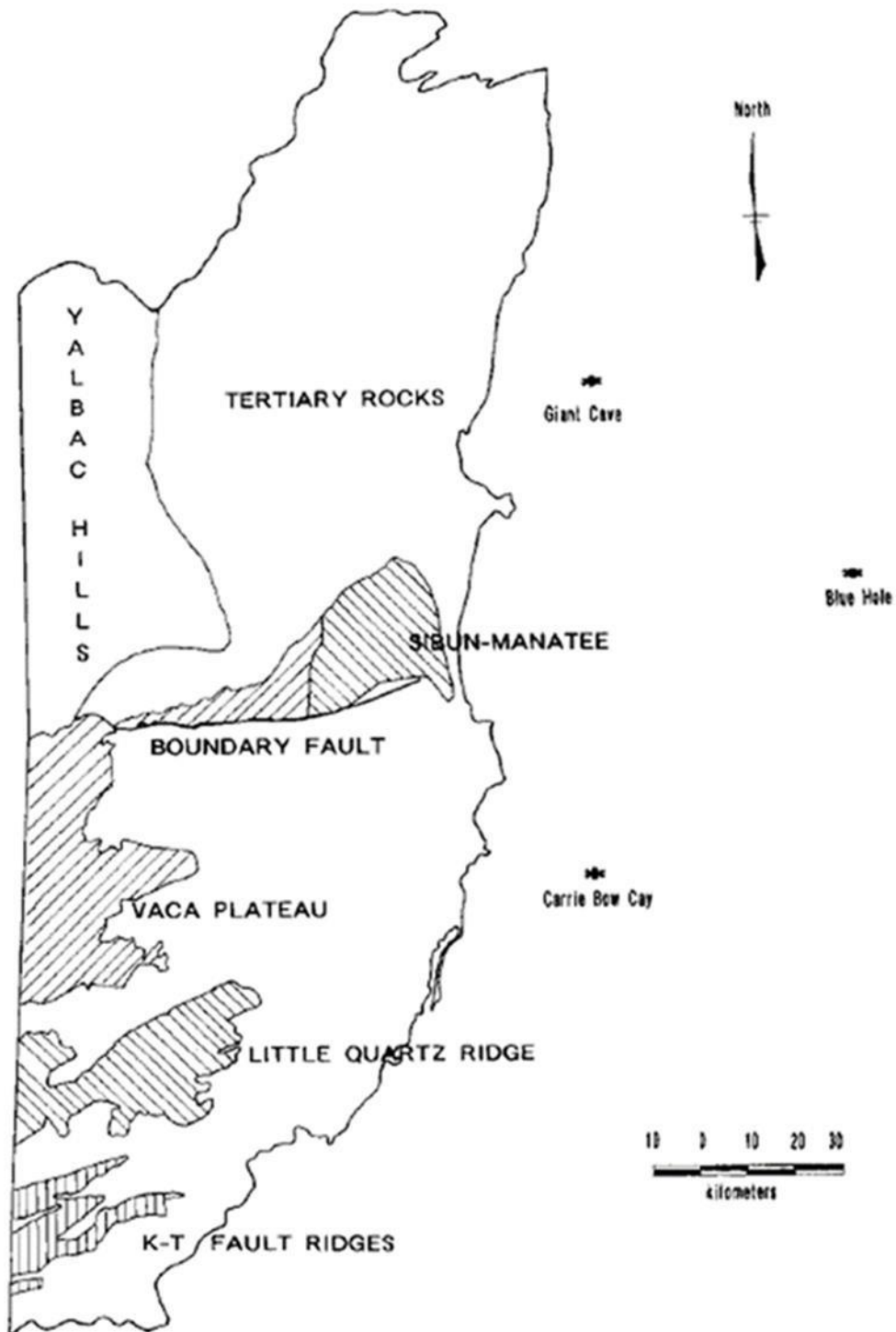


Figure 4. Karst regions of Belize, 1) Boundary Fault, 2) Vaca Plateau, 3) Sibun-Manatee, 4) Little Quartz Ridge, 5) K-T Fault Ridge, 6) Cayes/Barrier Reef, 7) Yalbac Hills, and 8) Tertiary Rocks

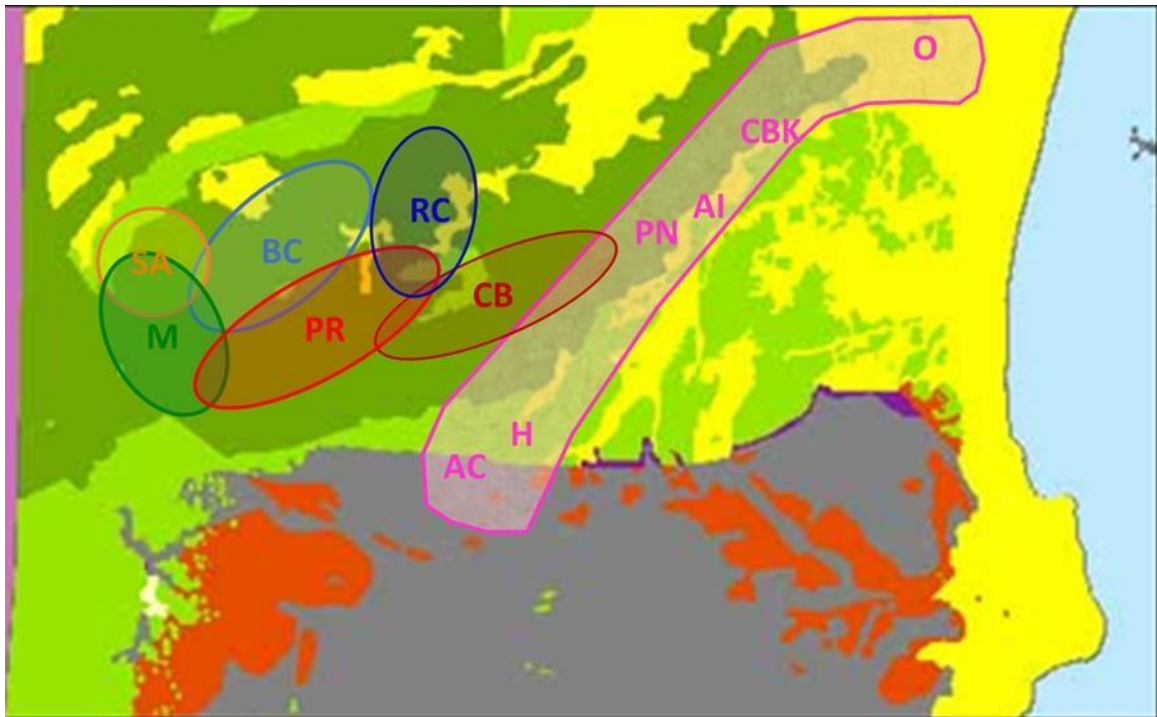


Figure 5. Cayo District group samples: Barton Creek (BC), Cave's Branch (CB), Macal (M), Pine Ridge (PR), Roaring Creek (RC), and San Antonio (SA). XARP samples as follows: Actun Chanona (AC), Hershey (H), Pakal Na (PN), Actun Ik (AI), Cedars Bank (CBK) and Oshon (O).

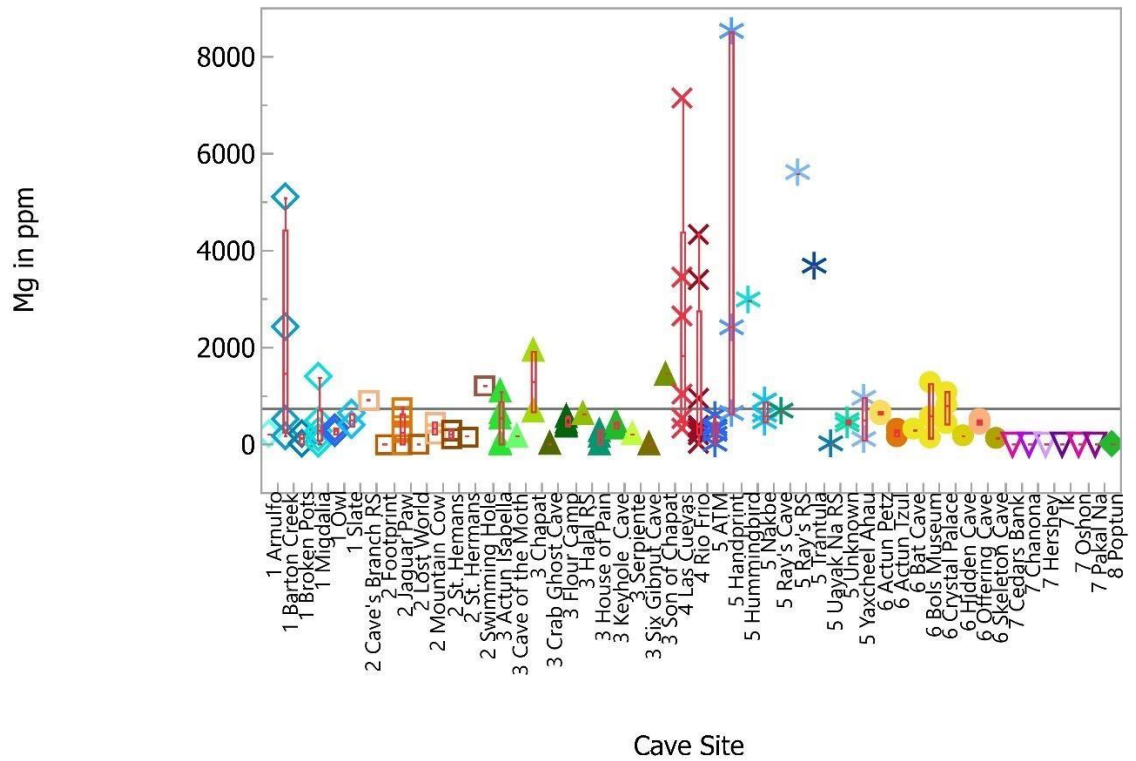


Figure 6. Magnesium concentrations by cave, coded by color and symbol to distinguish their respective geographic groups. Note some variability in caves from BSVP samples (Groups 1 through 6) and almost no variability in XARP samples (Group 7).

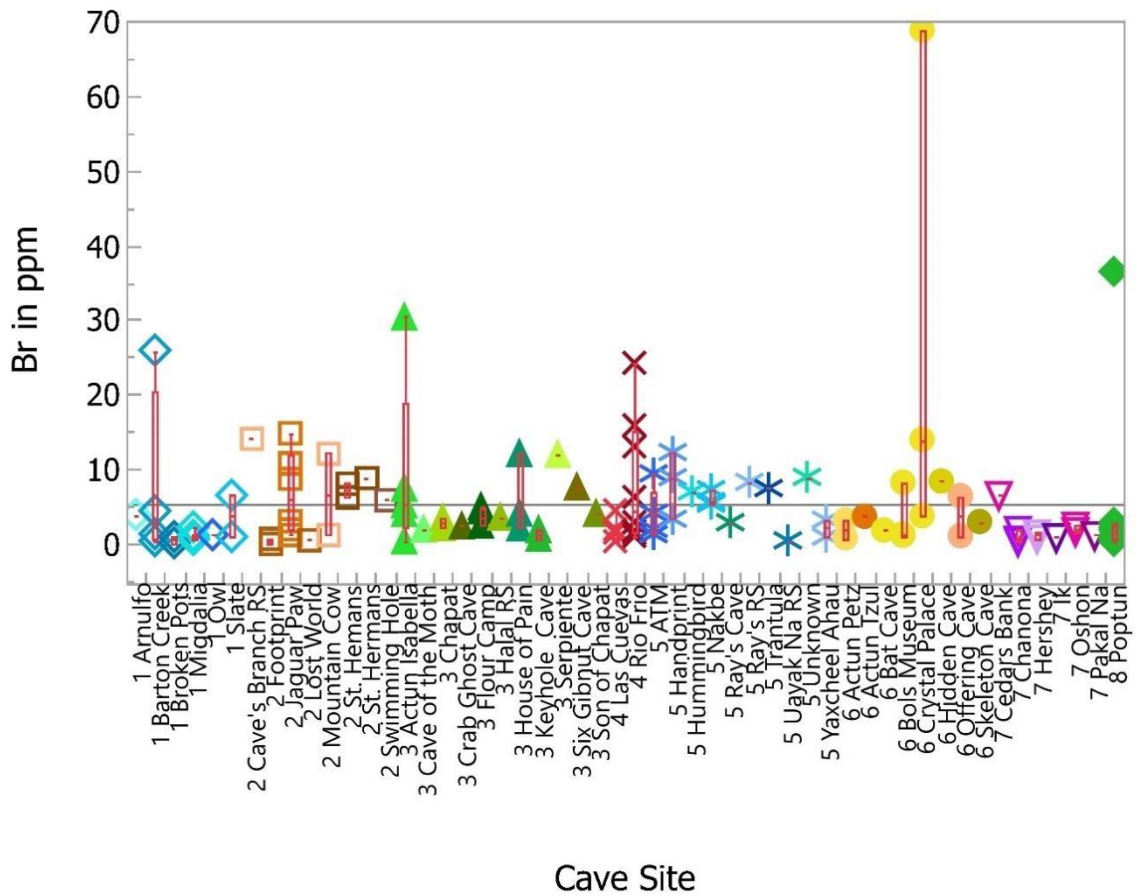


Figure 7. Bromine concentrations by caves within their respective groups. Note more variability in caves from BSVP samples and minor variability in XARP samples.

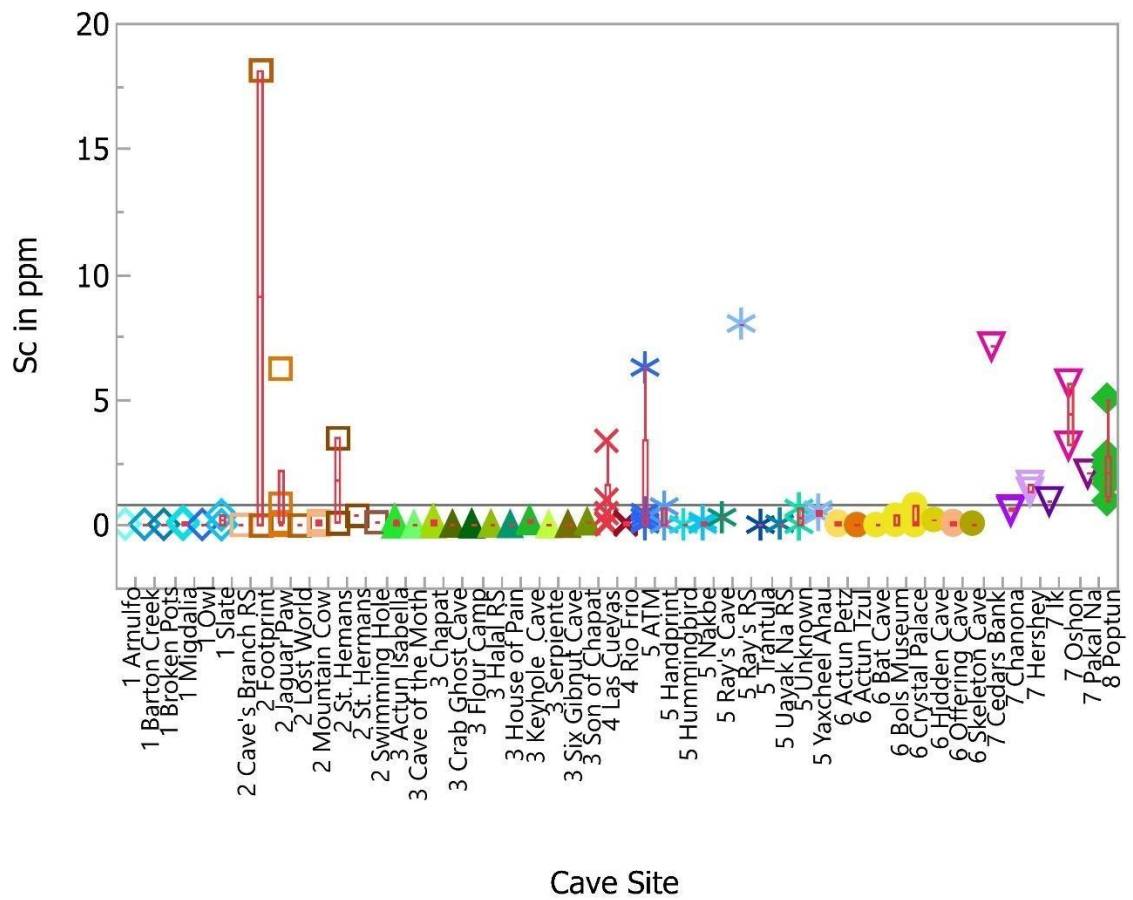


Figure 8. Scandium concentrations by caves within their respective groups. Note more variability in caves from Sibun and Petén (XARP), with minor variability in samples from BVSP.

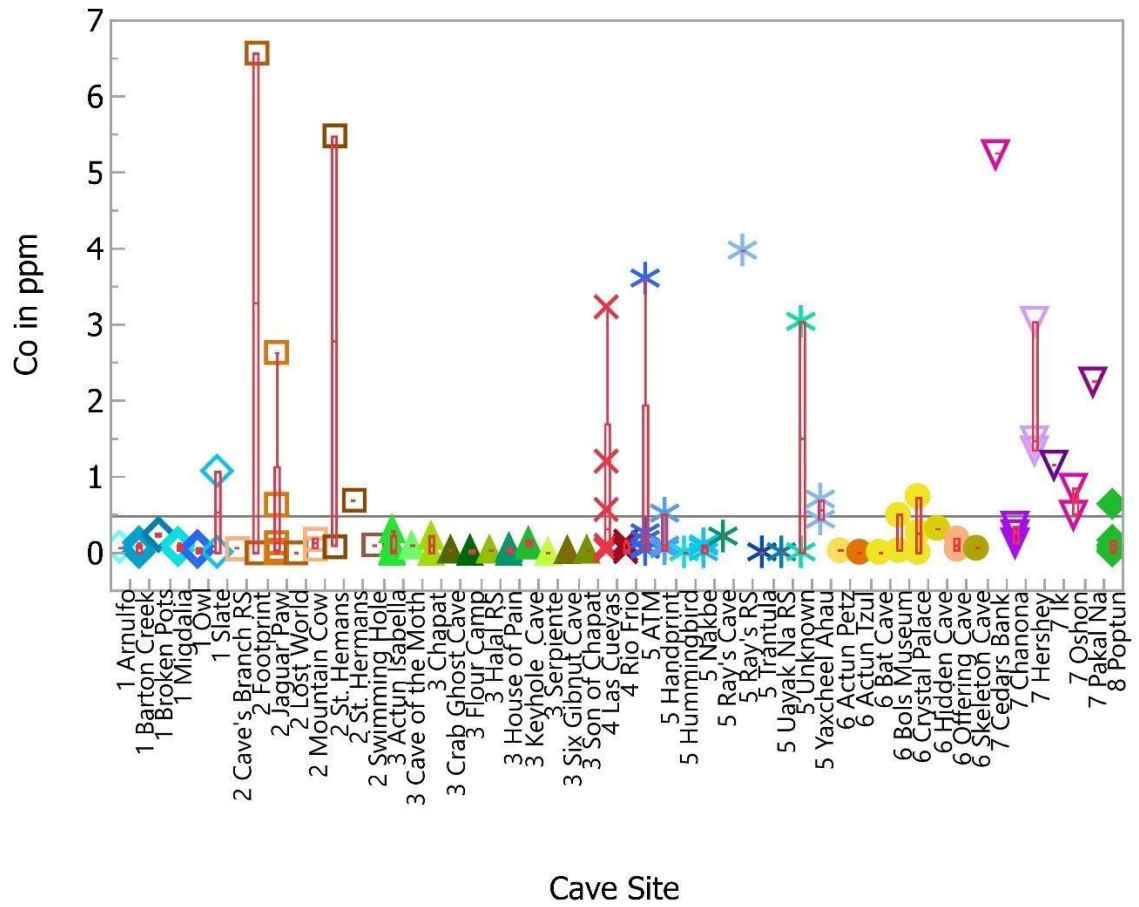


Figure 9. Cobalt concentrations by caves within their respective groups. Note more variability in caves from Sibun and Petén (XARP), with minor variability in samples from BVSP.

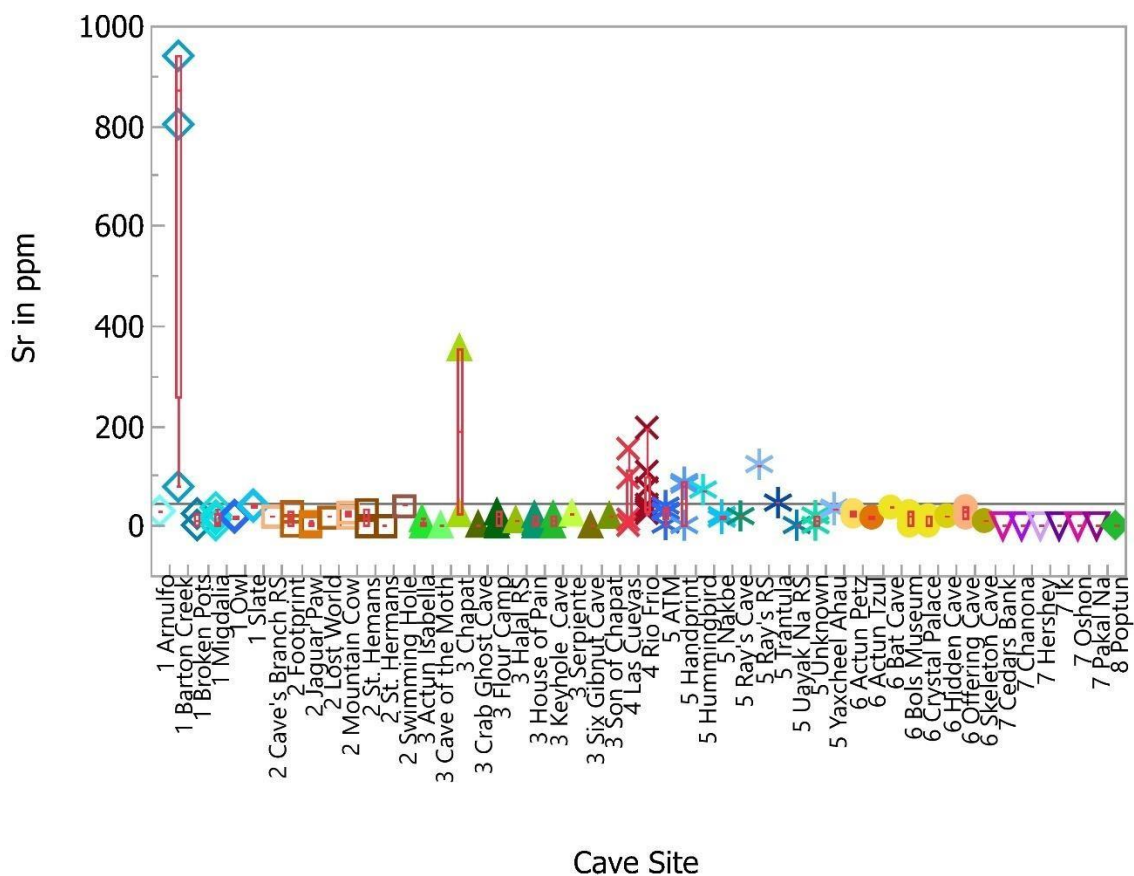


Figure 10. Strontium concentrations by caves within their respective groups. Note more variability in caves from Sibun and Petén (XARP), with minor variability in samples from BVSP.

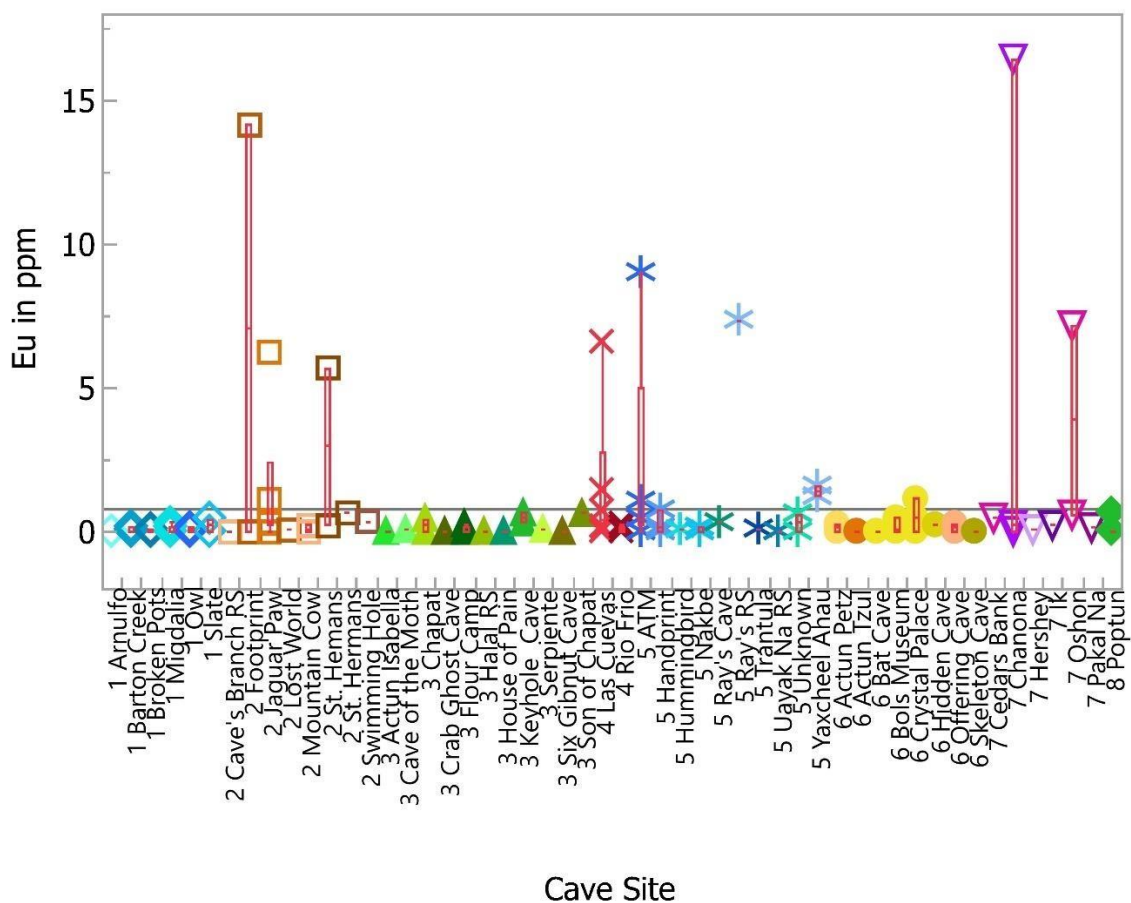


Figure 11. Europium concentrations by caves within their respective groups. Note more variability in caves from Sibun and Petén (XARP), with minor variability in samples from BVSP.

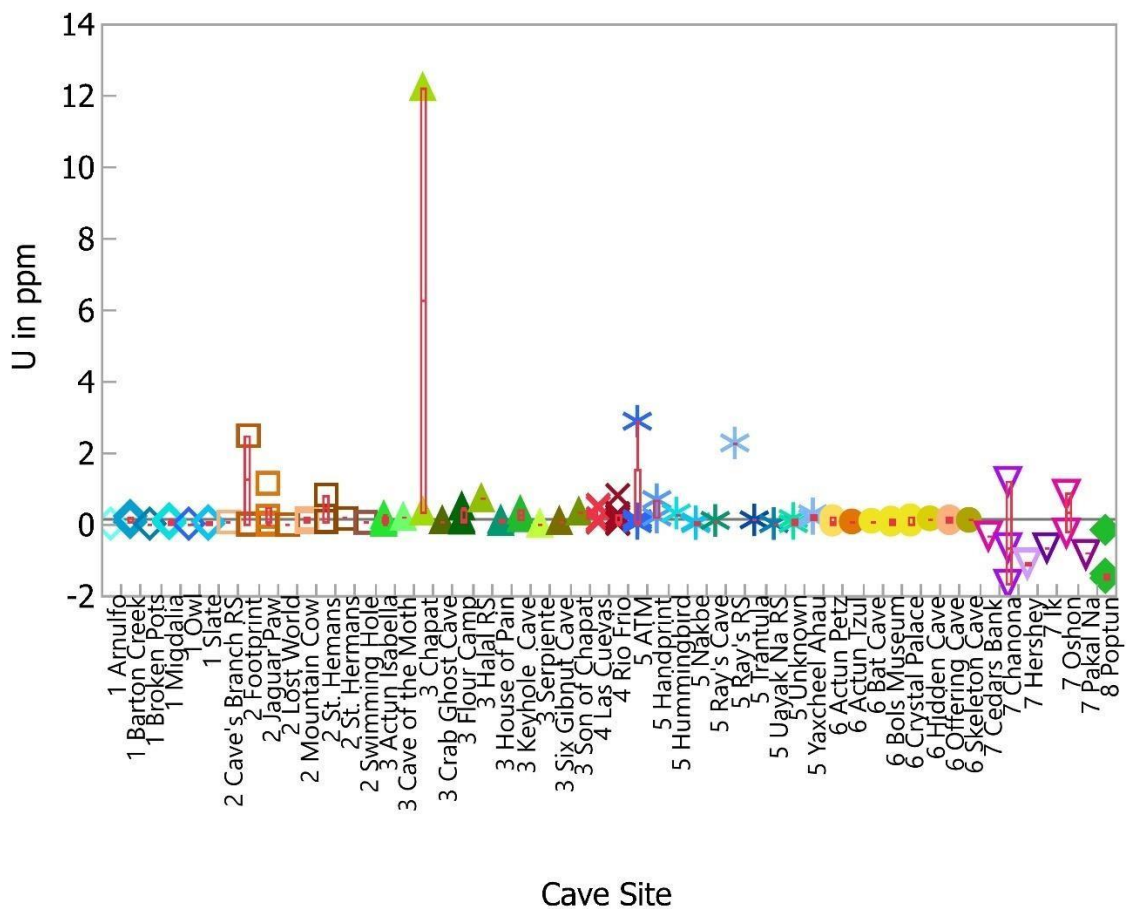


Figure 12. Uranium concentrations by caves within their respective groups. Note more variability in caves from Sibun and Petén (XARP), with minor variability in samples from BVSP.

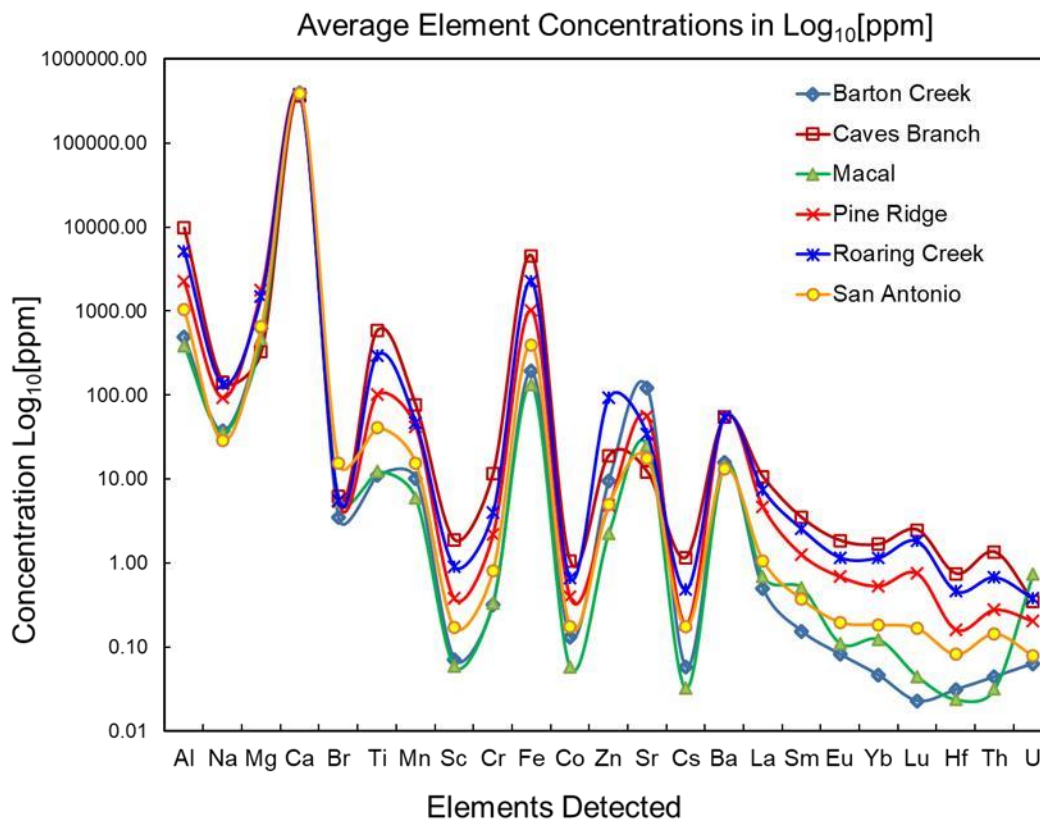


Figure 13. Average absolute elemental concentrations in log base 10 from the Barton Creek (BC), Caves Branch (CB), Macal (M), Pine ridge (PR), Roaring Creek (RC) and San Antonio (SA). Notice a significant Al, Fe and low Mg.

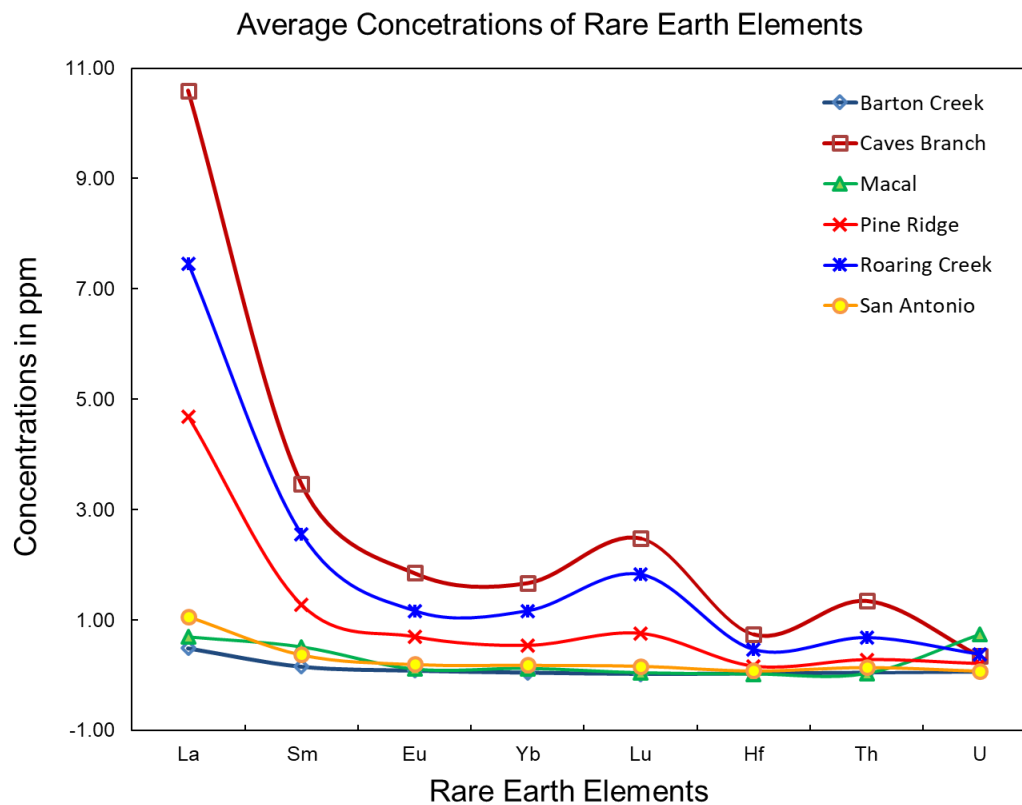


Figure 14. Average absolute elemental concentrations for Rare Earth Elements (REE) from the Barton Creek (BC), Caves Branch (CB), Macal (M), Pine ridge (PR), Roaring Creek (RC) and San Antonio (SA). Notice the inverse relationship of Thorium and Uranium for Cave's Branch, Macal and Roaring Creek.

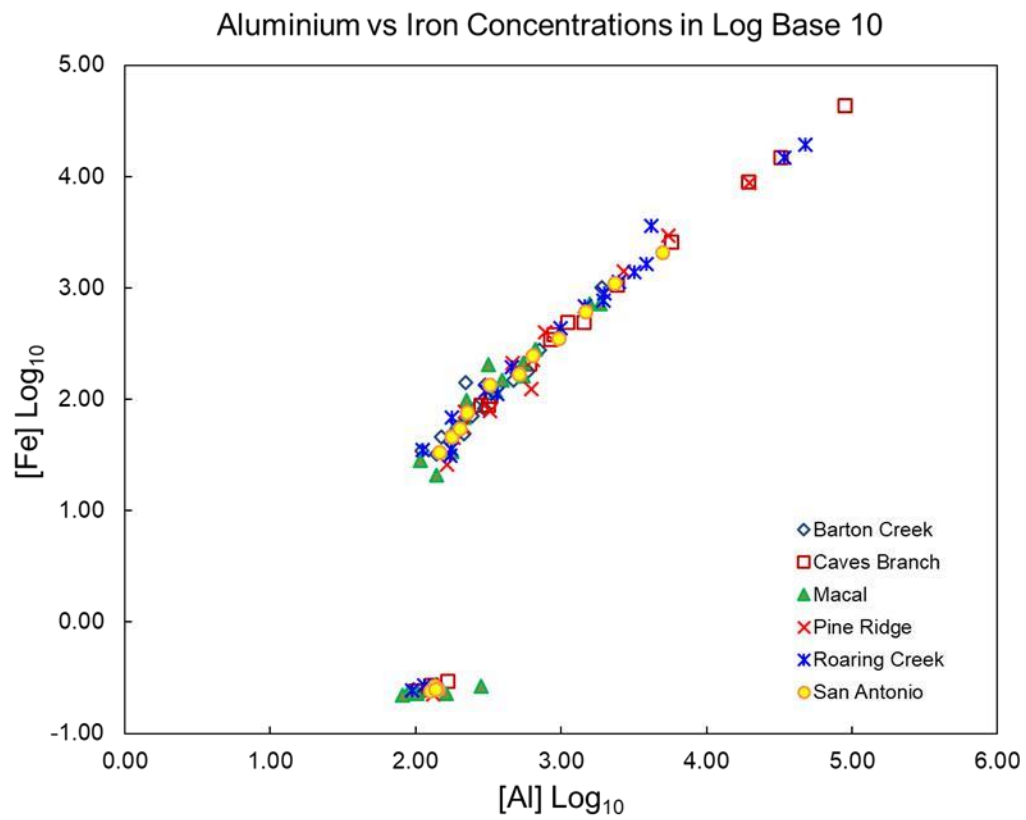


Figure 15. Concentrations in log base 10 of Aluminum vs Iron. Main distribution for both Al and Fe is found in central cluster, with the highest concentrations found in the Cave's Branch, Roaring Creek and Pine Ridge groups.

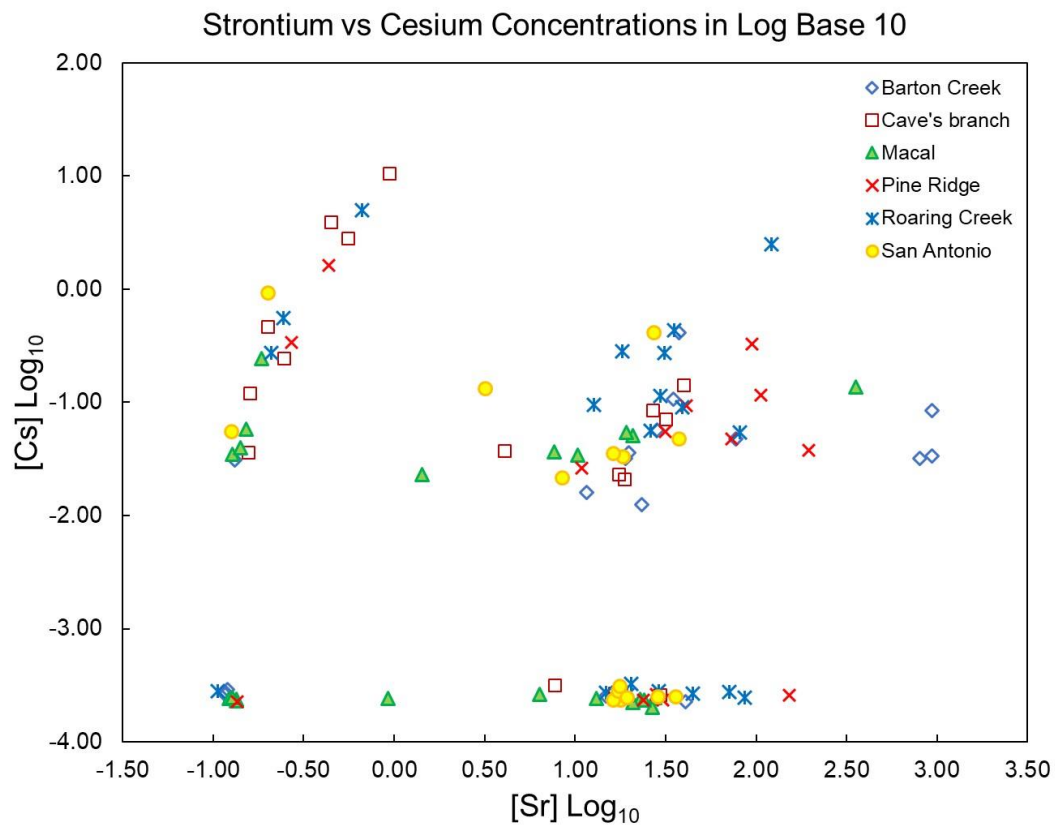


Figure 16. Three clusters differentiate. The upper left show Cave's Branch, Roaring Creek and Pine Ridge with the highest Cs concentrations. The center right cluster shows Barton Creek, Macal and Pine Ridge with the most Strontium. A gap in the negative values and between cluster begins to become common.

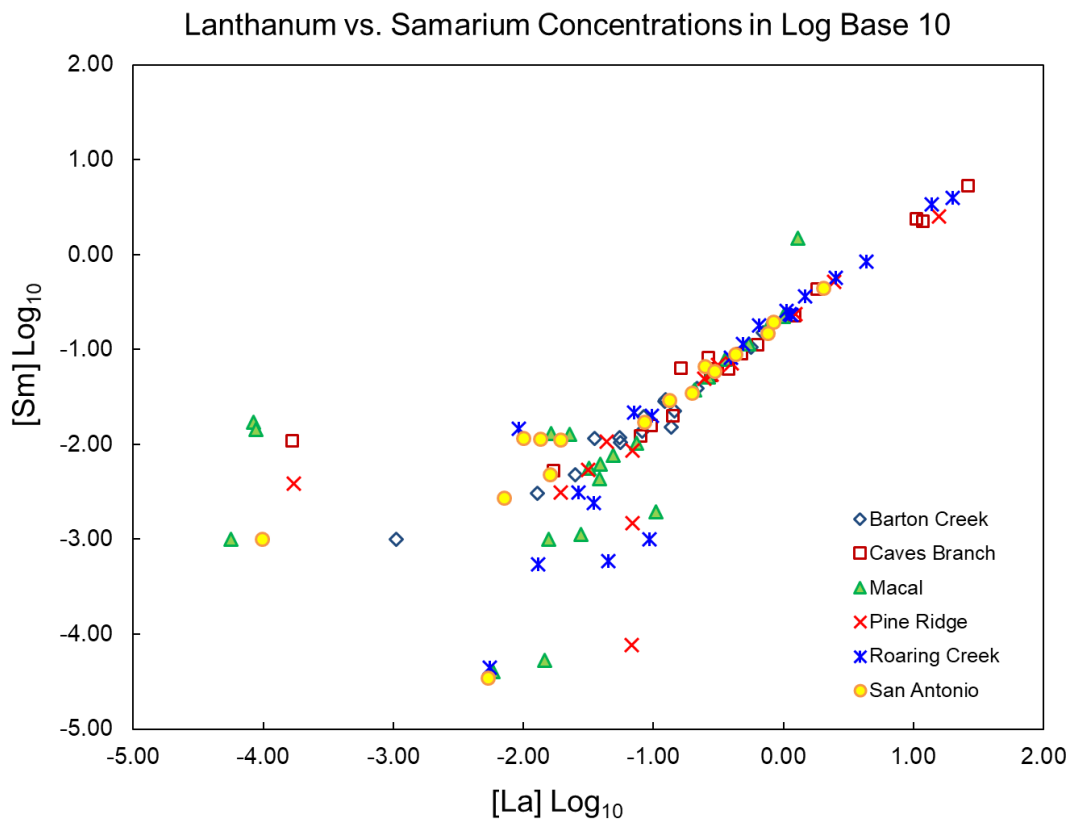


Figure 17. Concentrations in log base 10 of Lanthanum vs Samarium. Most aligned with some minor scattering for the negative values.

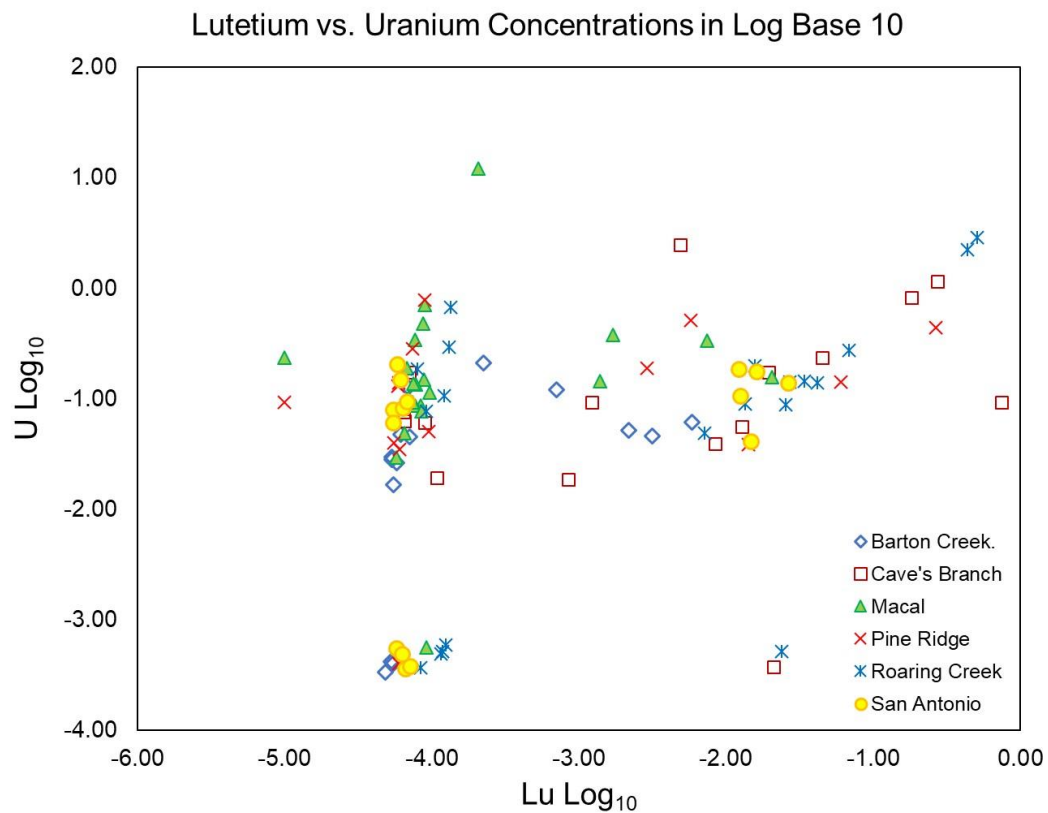


Figure 18. Concentrations in log base 10 of Lutetium vs Uranium. Note the splitting of San Antonio and the continuance of Barton Creek and Cave's Branch groups.

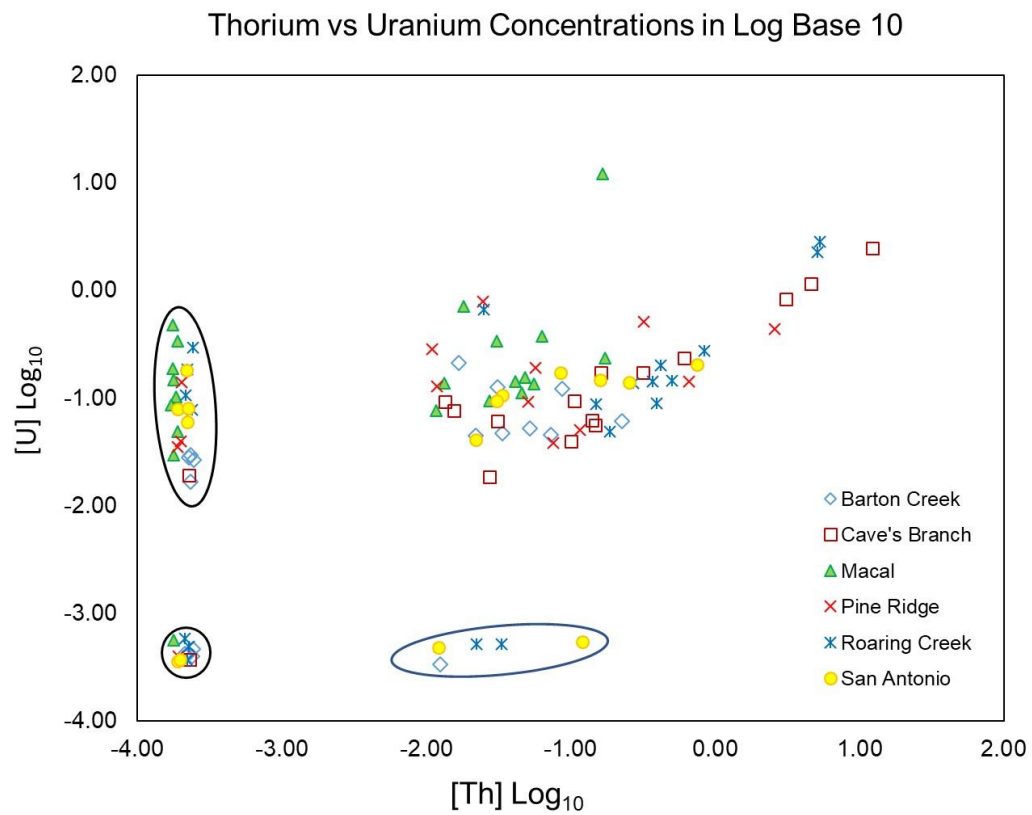


Figure 19. Concentrations in log base 10 of Thorium vs Uranium showing four distinct clusters.

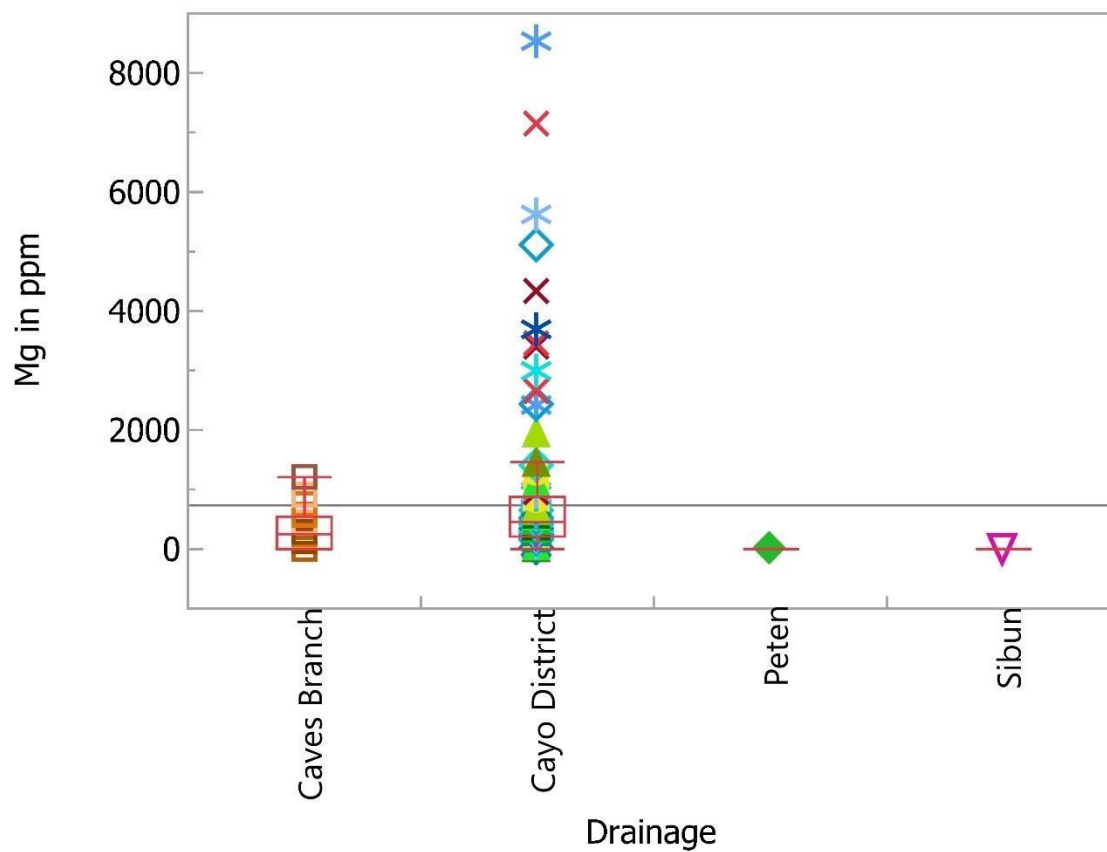


Figure 20. Magnesium concentrations by drainage systems. Showing the depletion of Mg in the Sibun and Petén, and limited range of the Cave's Branch with respect to the Cayo District system.

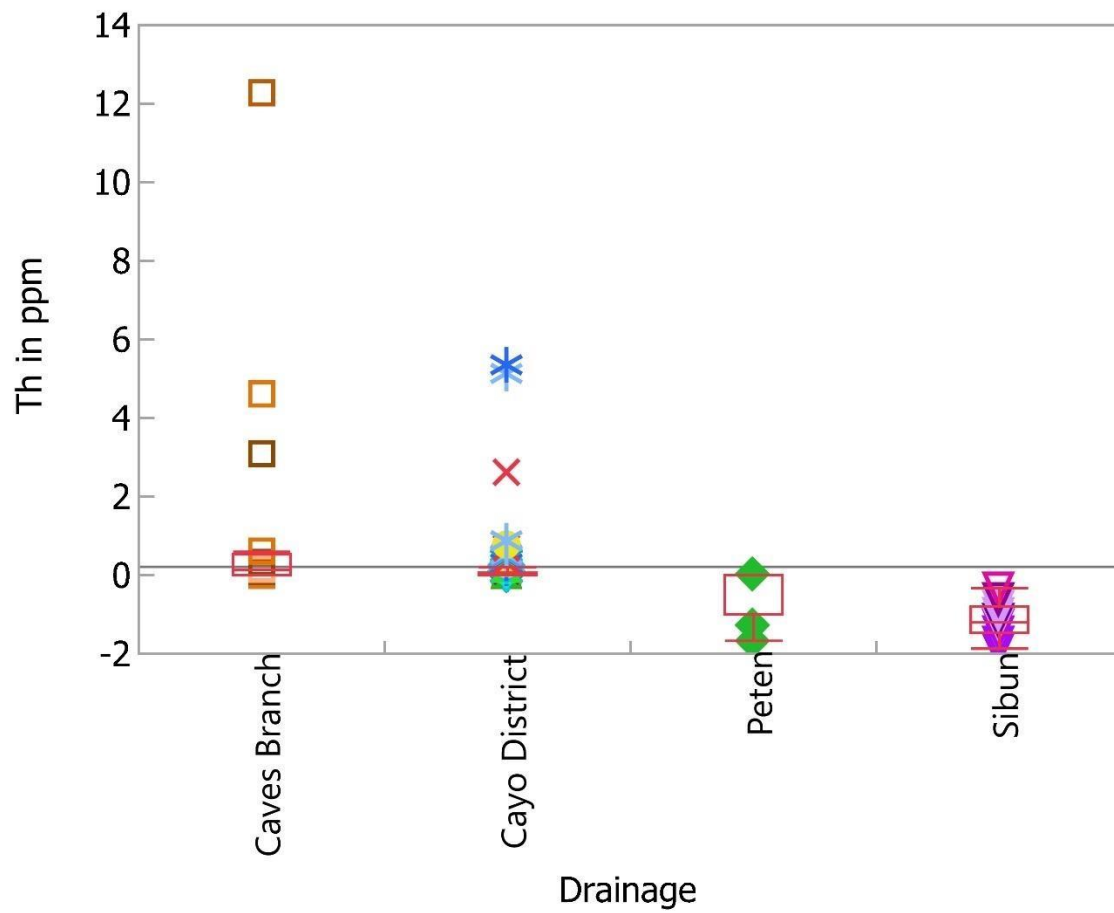


Figure 21. Thorium concentrations by drainage systems. Showing the depletion of Th in the Sibun and Petén with respect to the BVSP samples.

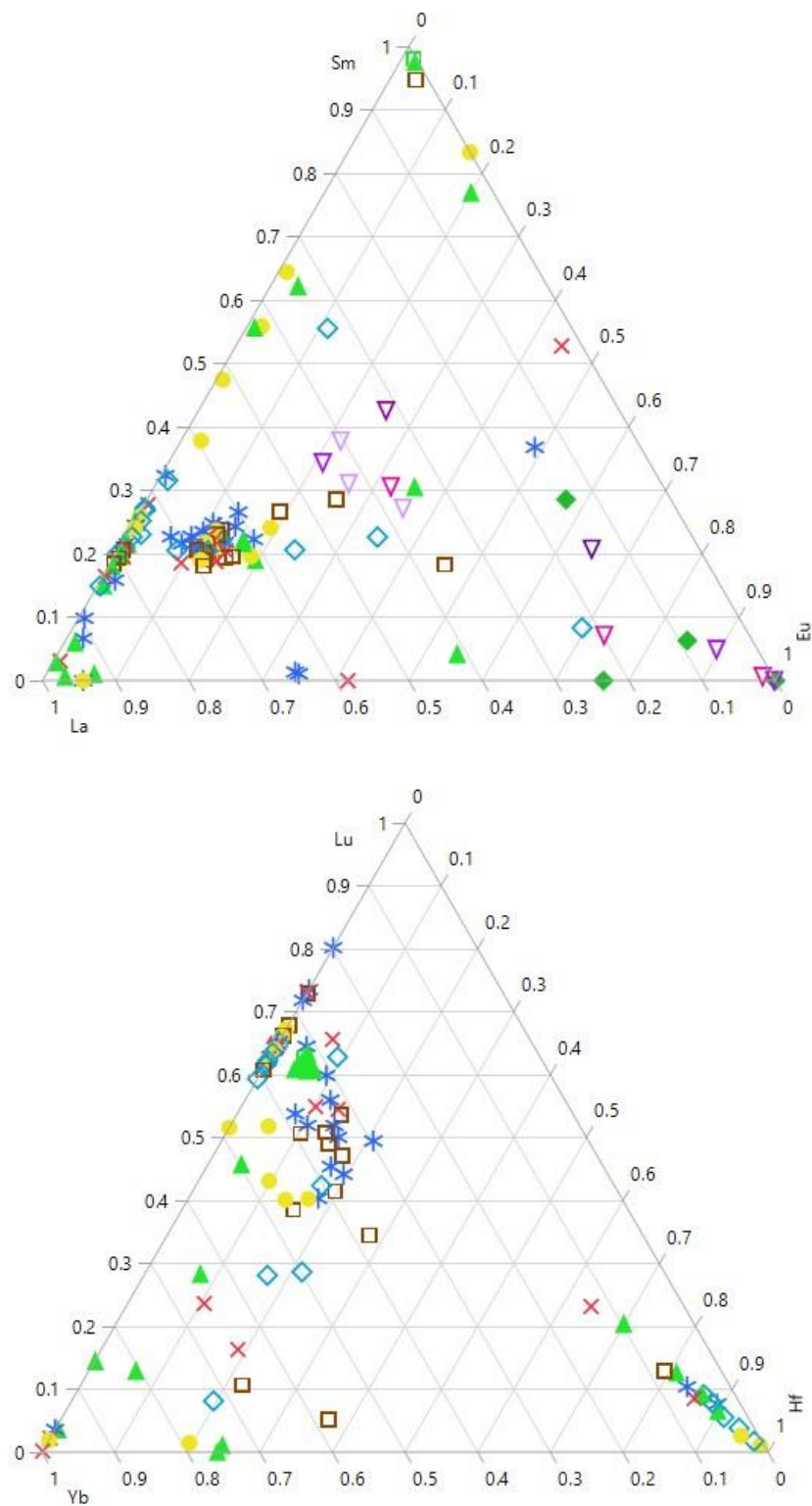


Figure 22. Ternary plots of: Top: La, Sm, and Eu (LREE) and; Bottom: Yb, Lu, and Hf (HREE). Note the depletion in HREE in Sibun and Petén Samples.



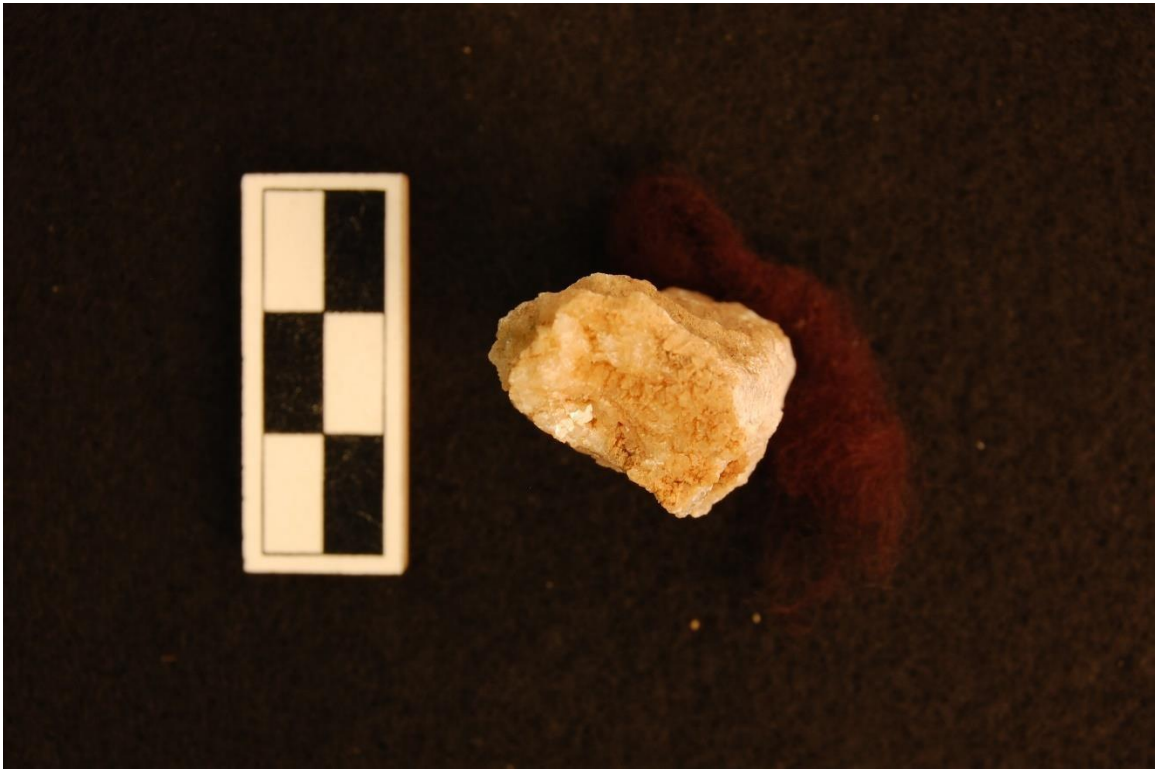
BC 0034 1 (above) and 2 (below)



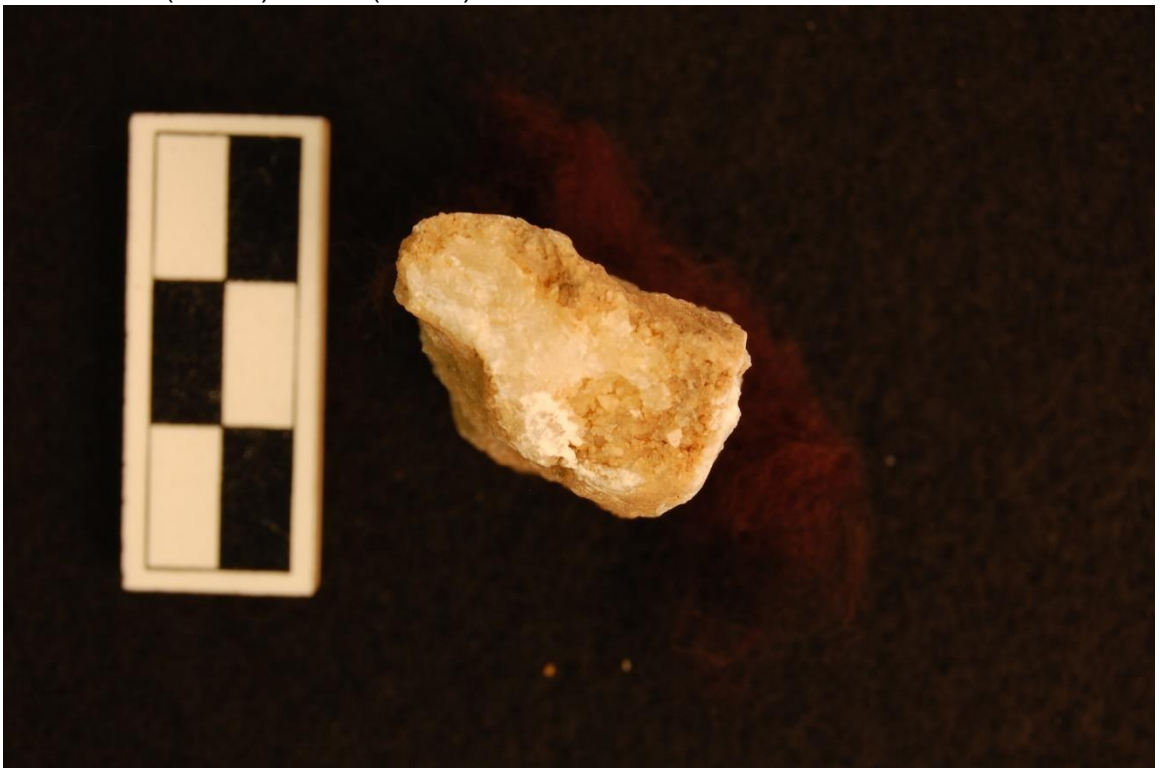


BC 0034 3 (above) and 4 (below)



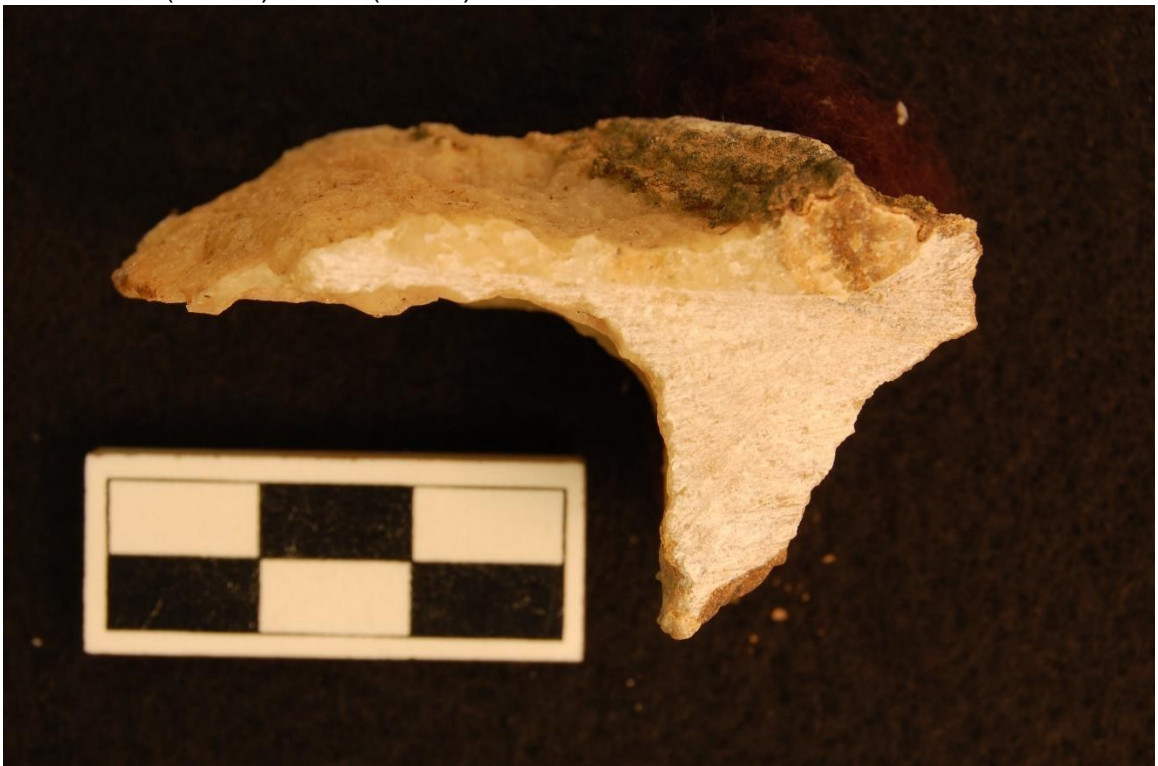


BC 0034 5 (above) and 6 (below)





BC 0035 1 (above) and 2 (below)





BC 0035 3 (above) and 4 (below)





BC 0036 1 (above) and 2 (below)





BC 0036 3



BC 0037 1 (above) and 2 (below)





BC 0037 3 (above) and 4 (below)





BC 0037 5 (above) and 6 (below)





BC 0039 1 (above) and 2 (below)





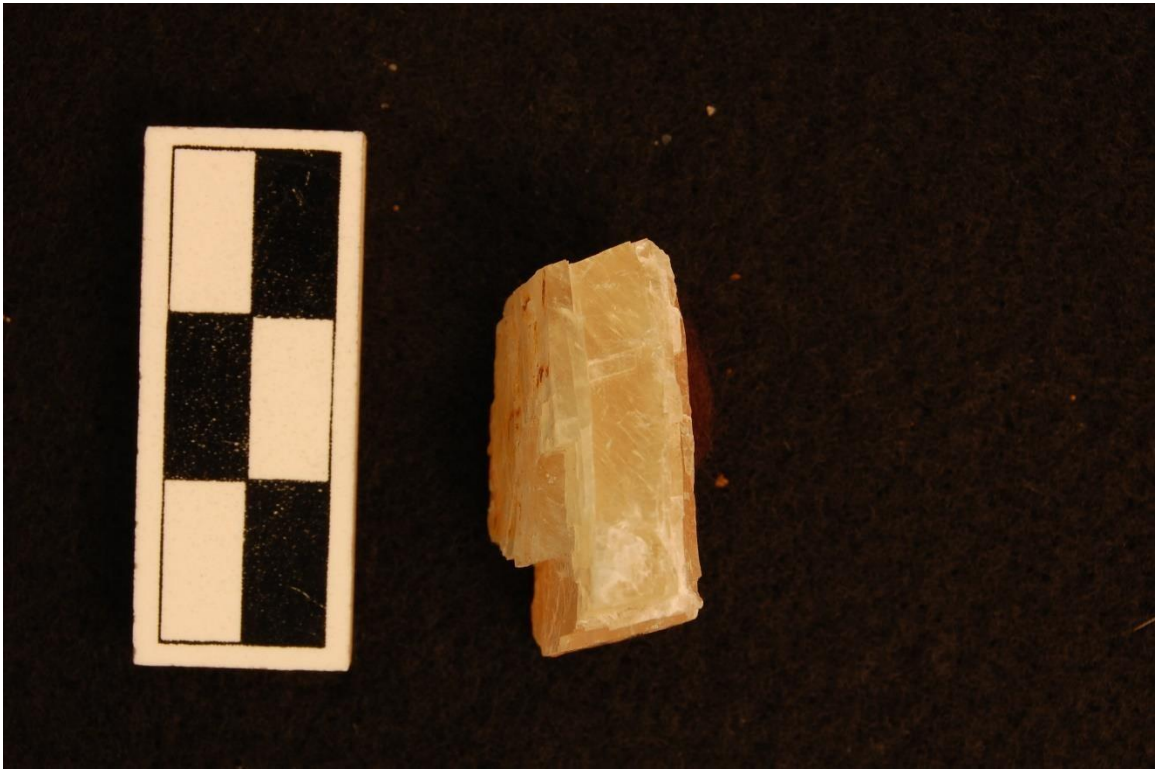
BC 0039 3 (above) and 4 (below)





BC 0040 1 (above) and 2 (below)





BC 0040, 3 (above) and 4 (below)





BC 0040 5 (above) and 6 (below)





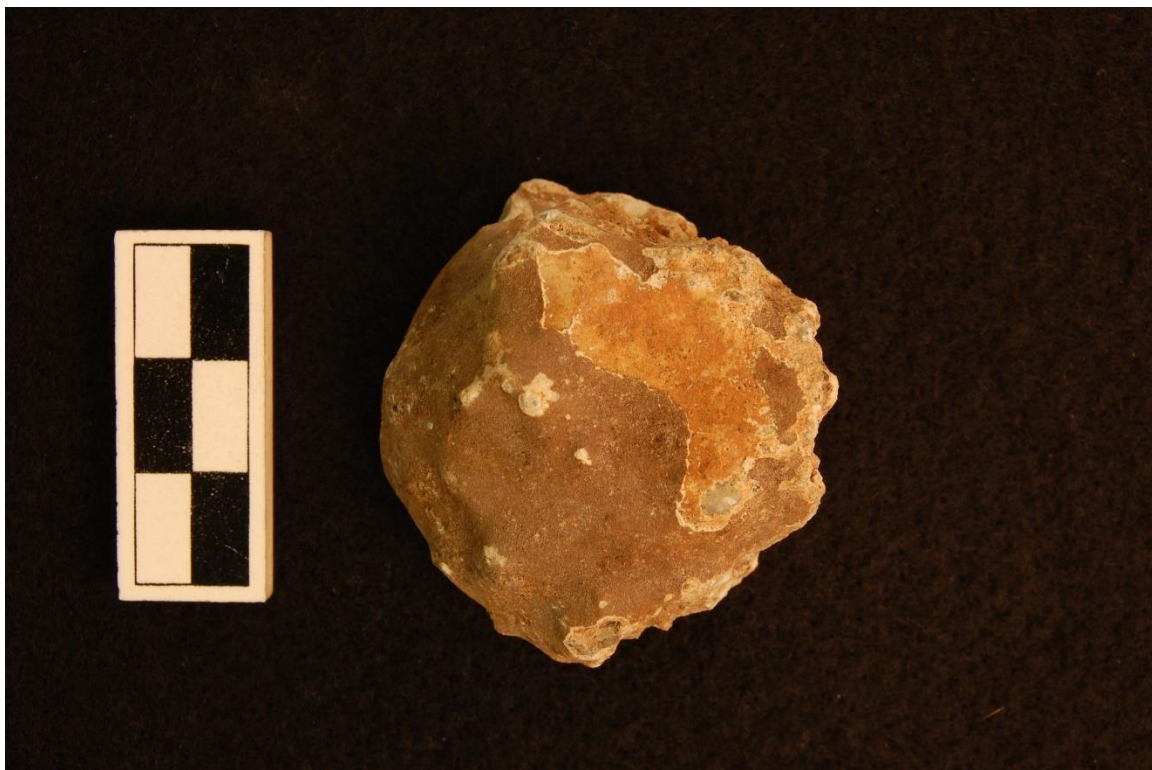
BC 0041, 1 (above) and 2 (below)





BC 0041, 3 (above) and 4 (below)





BC 0042, 1 (above) and 2 (below)





BC 0042, 3 (above) and 4 (below)





BC 0085, 1 (above) and 2 (below)





BC 0085 3 (above) and 4 (below)





CB0118, 1



CB 0120, 1 (above) and 2 (below)





CB 0120, 3 (above) and 4 (below)





CB 0121, 1 (above) and 2 (below)





CB 0121, 3



CB 0122, 1 (above) and 2 (below)





CB 0122, 3 (above) and 4 (below)





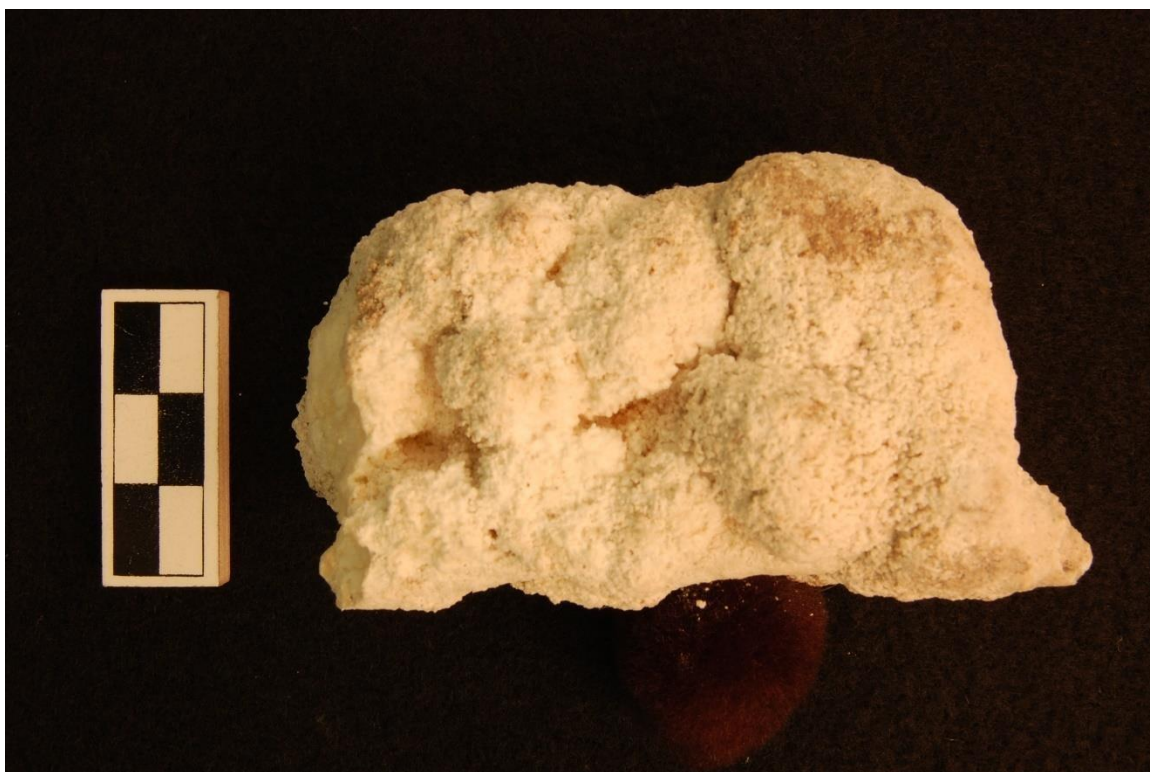
CB 0123, 1 (above) and 2 (below)





CB 0123, 3 (above) and 4 (below)





Ma 0009, 1 (above) and 2 (below)





Ma 0009, 4 (above) and 5 (below)





Ma 0009, 5



Ma 0011, 1 (above) and 2 (below)





Ma 0011, 3

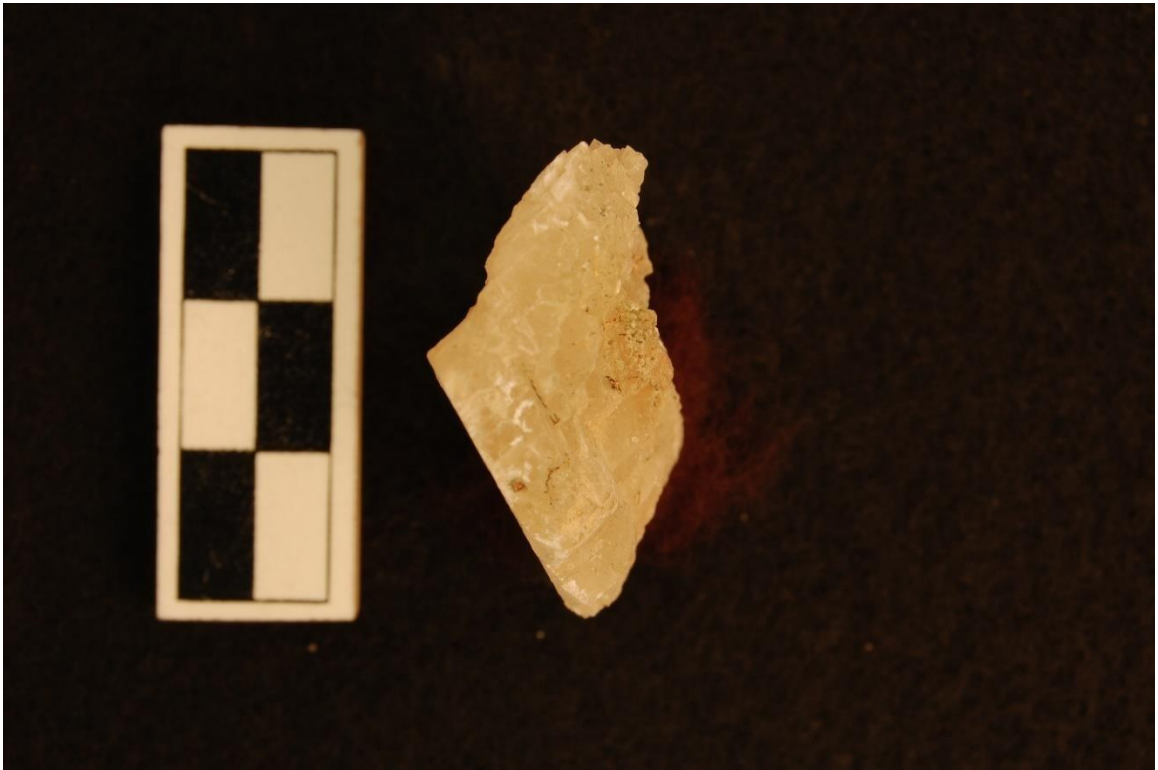


Ma 0013, 1



Ma 0014, 1 (above) and 2 (below)





Ma 0014, 3 (above) and 4 (below)





Ma 0015, 1 (above) and 2 (below)





Ma 0015, 3



Ma 0016, 1 (above) and 2 (below)





Ma 0016, 3



Ma 0017, 1 (above) and 2 (below)





Ma 0017, 3 (above) and 4 (below)



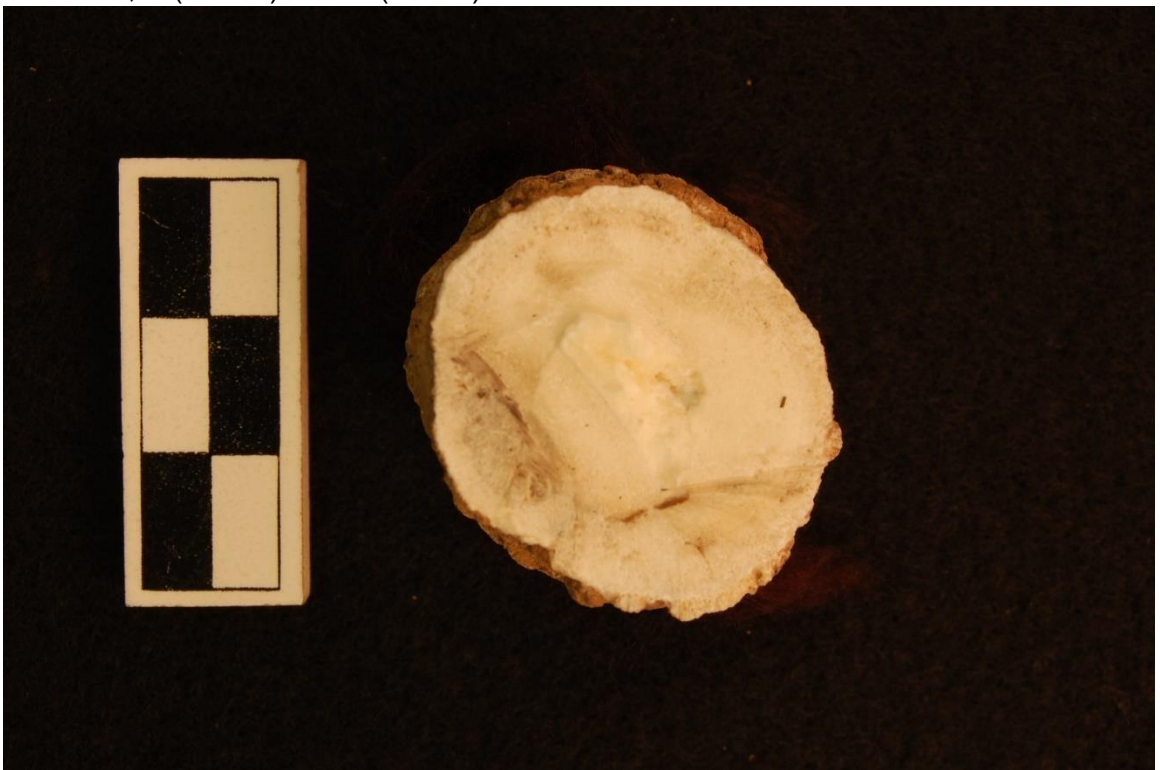


Ma 0017, 5 (above) and 6 (below)





Ma 0018, 1 (above) and 2 (below)





Ma 0018, 3 (above) and 4 (below)





Ma 0019, 1 (above) and 2 (below)





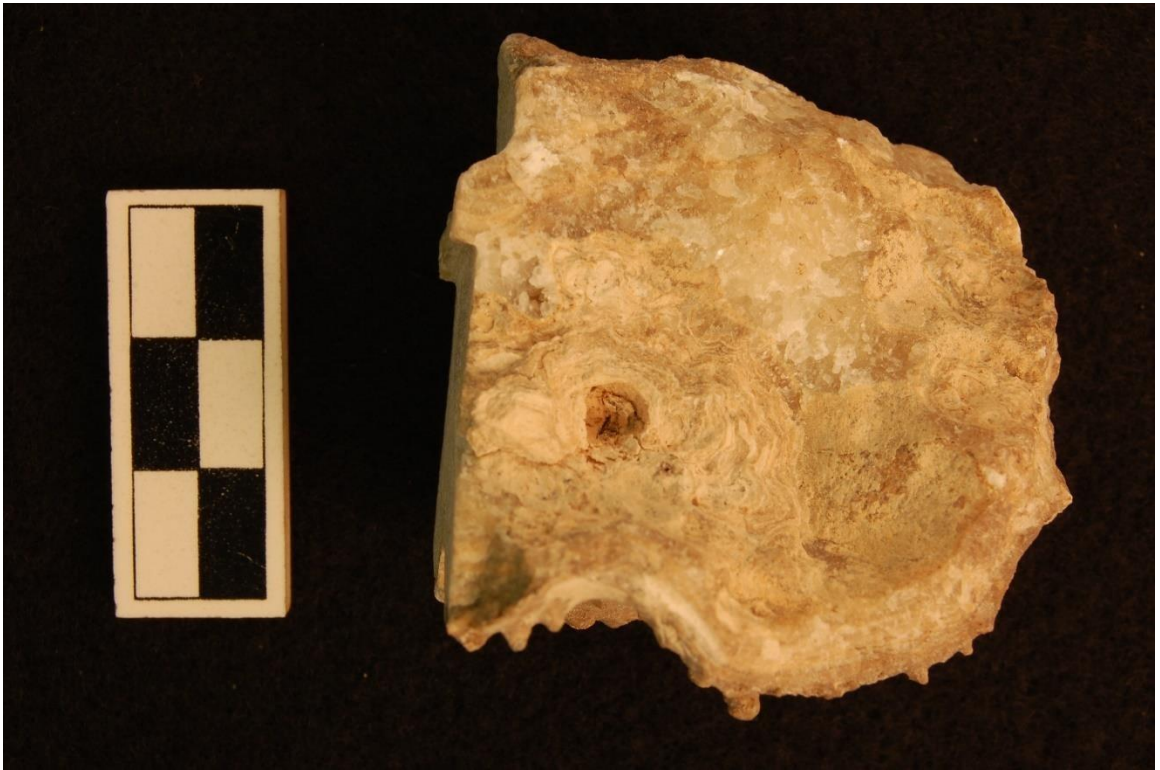
Ma 0019, 3 (above) and 4 (below)





Ma 0019, 5 (above) and 6 (below)



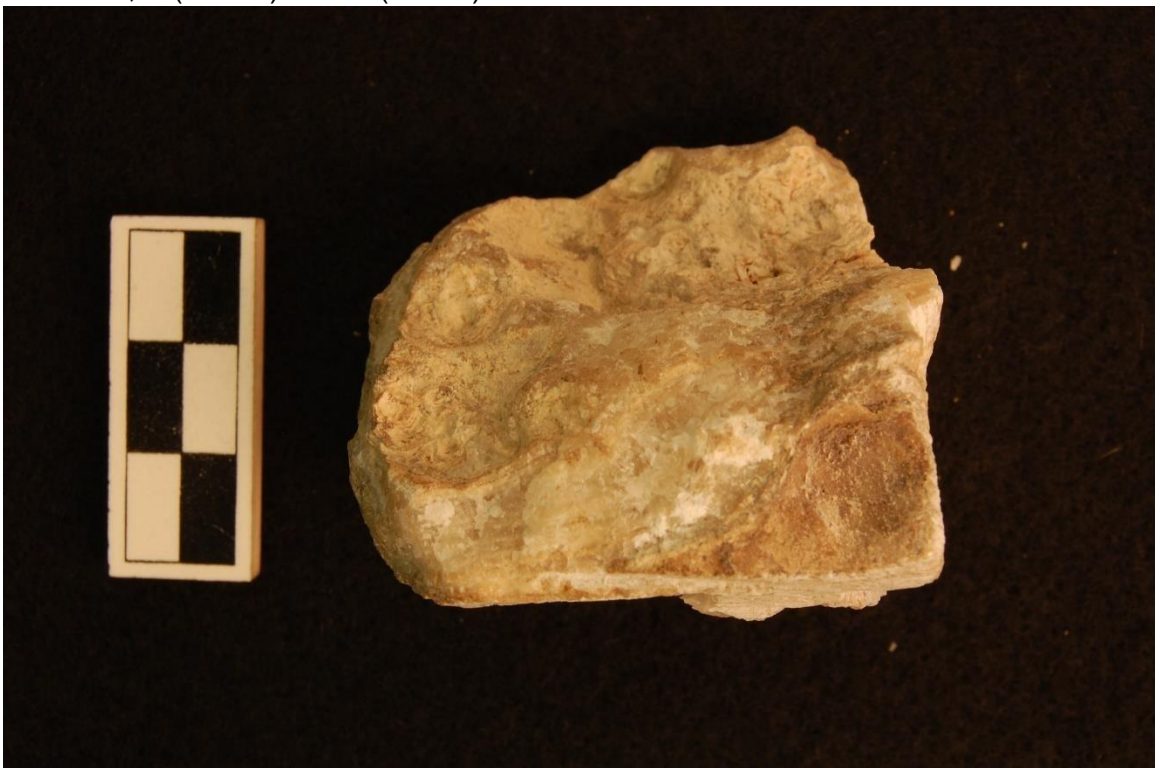


PR 0078, 1 (above) and 2 (below)





PR 0078, 3 (above) and 4 (below)





PR 0078, 5 (above) and 6 (below)





PR 0080, 1 (above) and 2 (below)



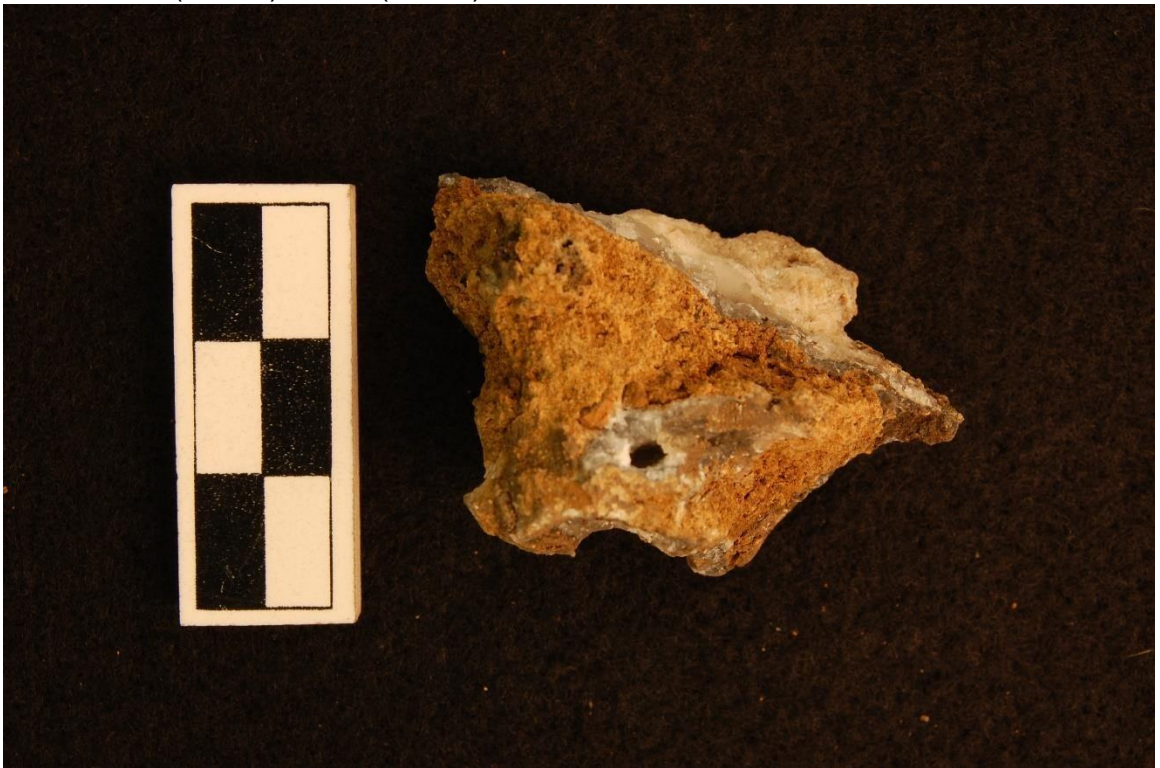


PR 0080, 3 (above) and 4 (below)





PR 0081, 1 (above) and 2 (below)





PR 0081, 3



PR 0082, 1 (above) and 2 (below)





PR 0082, 3 (above) and 4 (below)





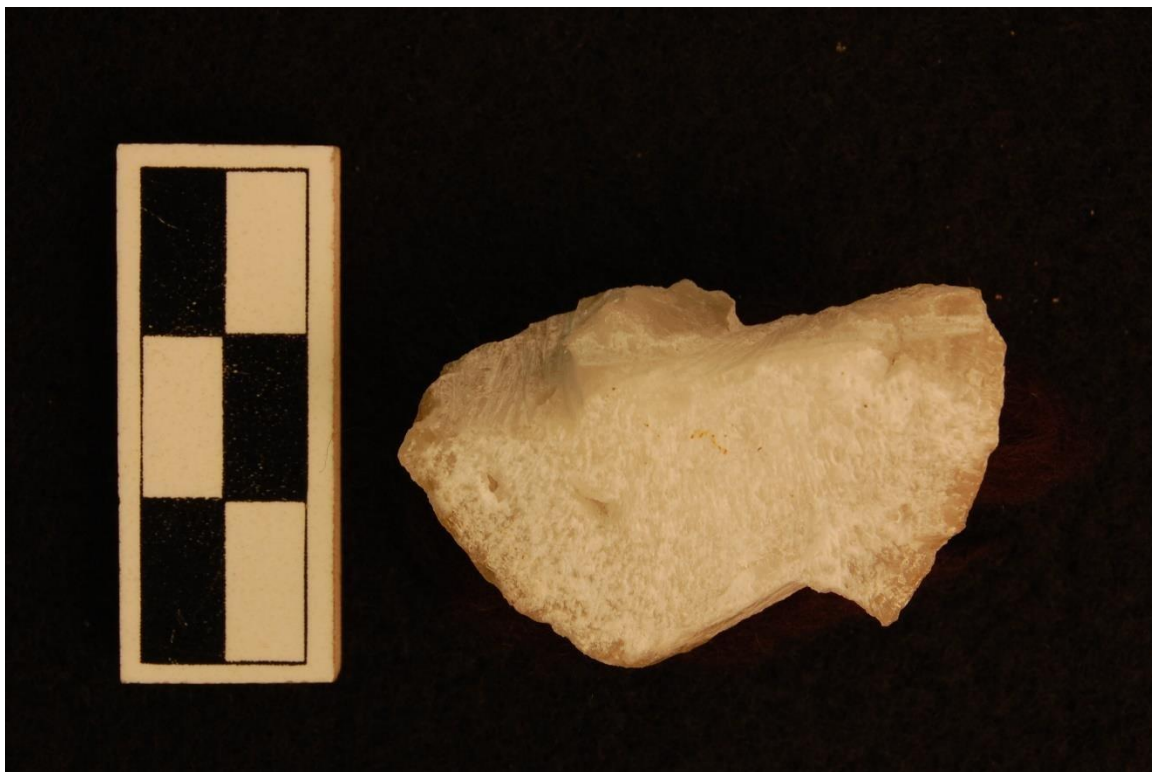
PR 0082, 5 (above) and 6 (below)



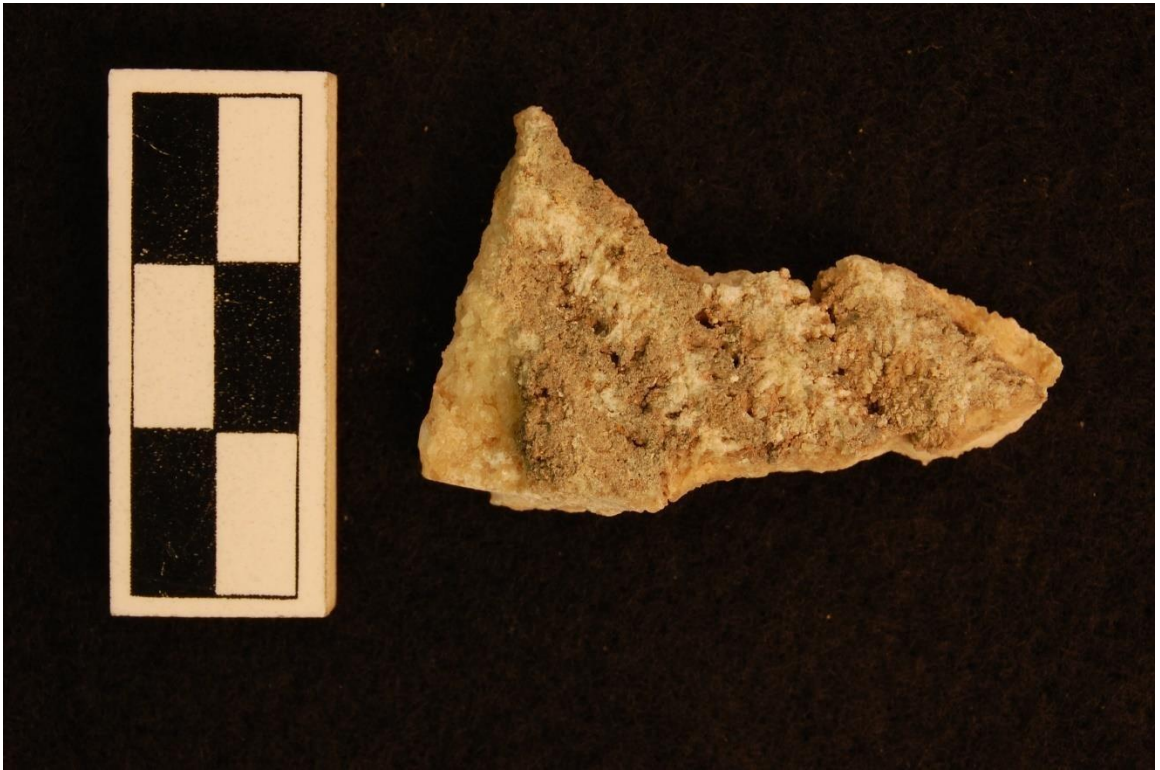


PR 0083, 1 (above) and 2 (below)





PR 0083, 3



PR 0132, 1 (above) and 2 (below)





PR 0132, 3



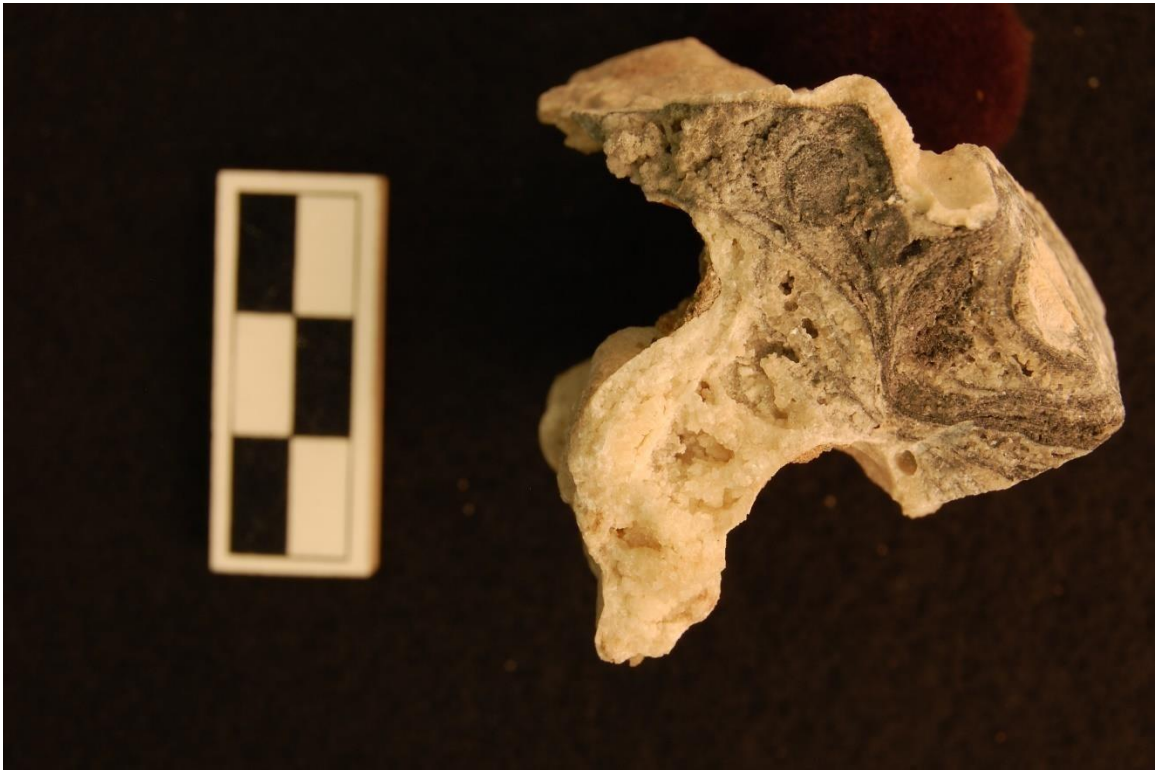
PR 0133, 1 (above) and 2 (below)





PR 0133, 3 (above) and 4 (below)





PR 0133, 5



PR 0133A, 1 (above) and 2 (below)



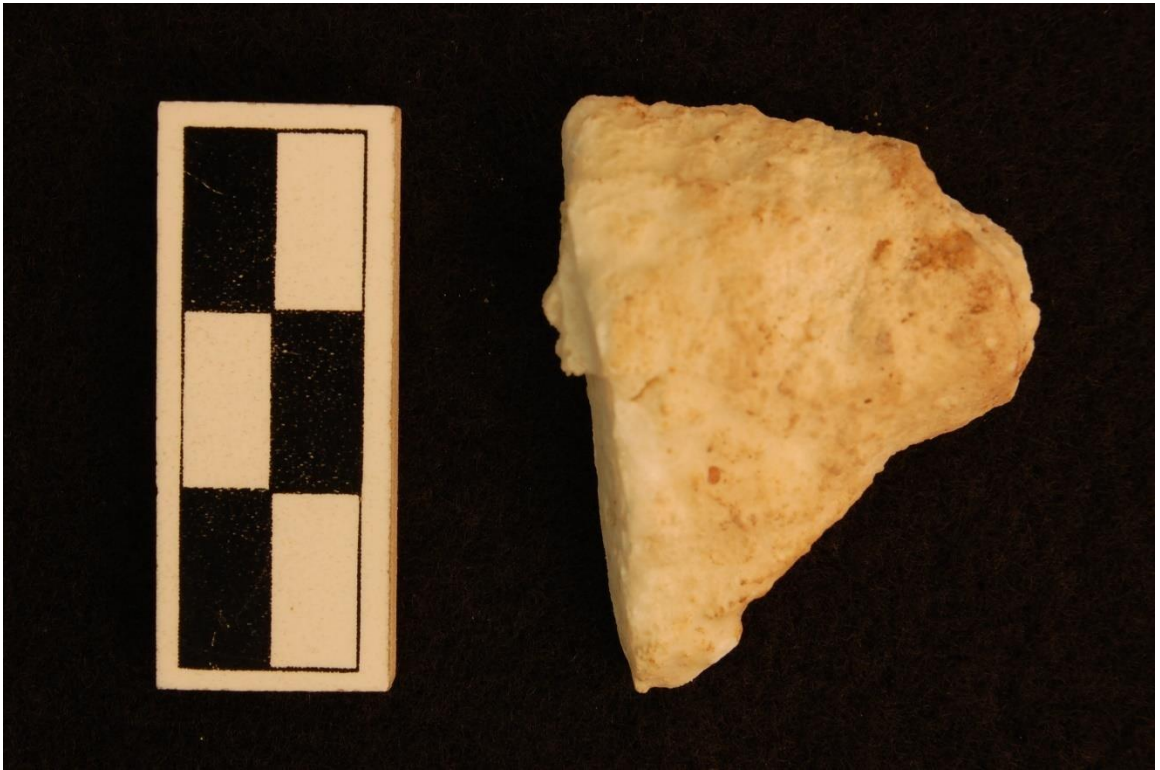


PR 0134, 1(above) and 2 (below)

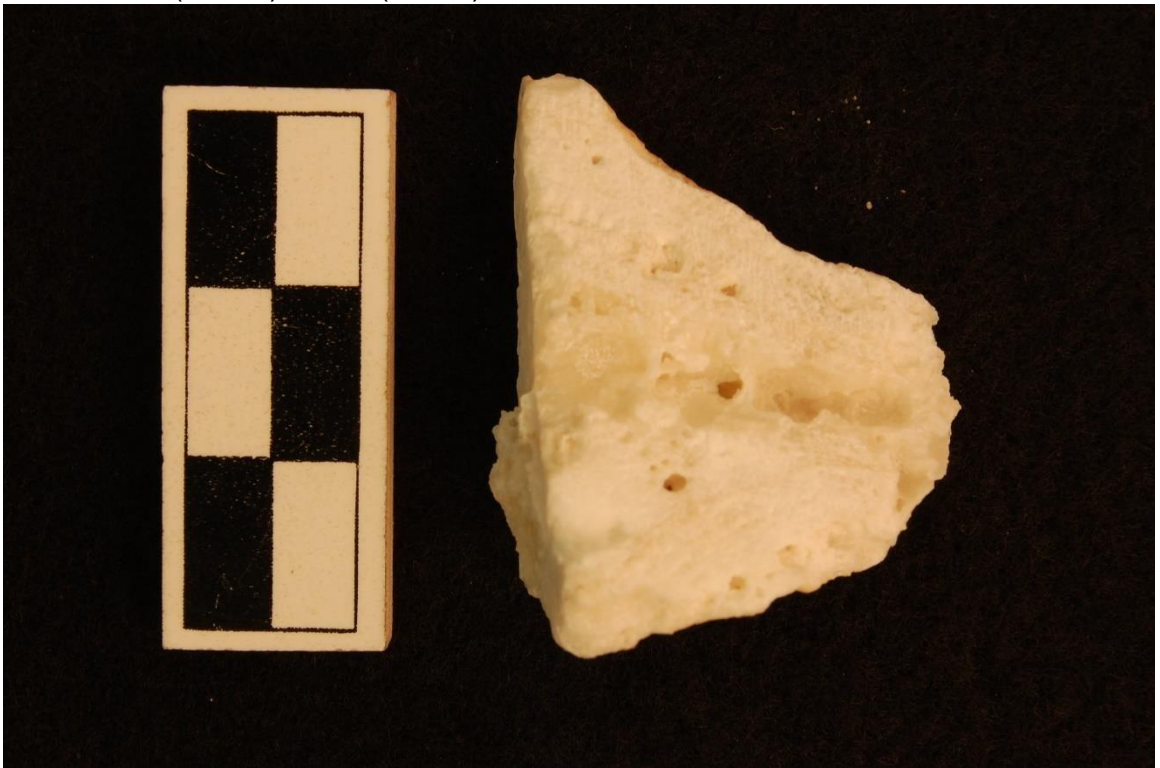




PR 0134, 3



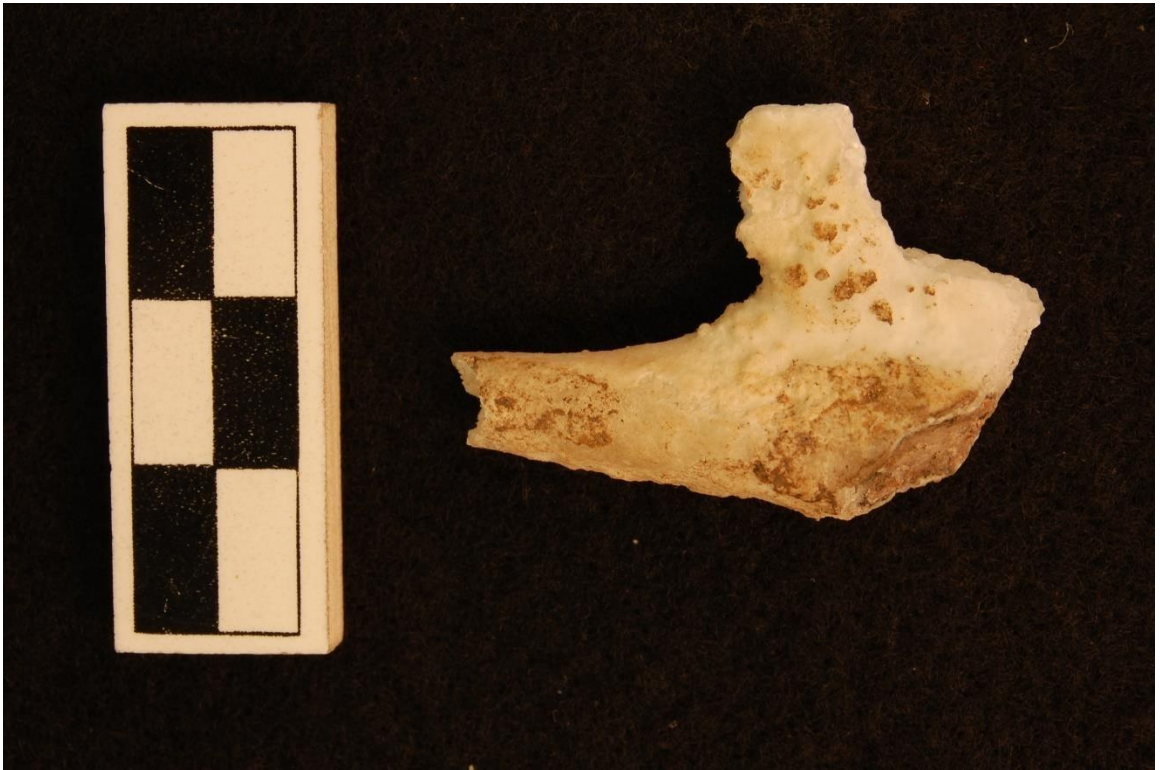
PR 0135, 1 (above) and 2 (below)





PR 0135, 3 (above) and 4 (below)





PR 0140, 1 (above) and 2 (below)





PR 0140, 3 (above) and 4 (below)





PR 0141, 1



PR 0142, 1 (above) and 2 (below)





PR 0142, 3 (above) and 4 (below)





PR 0142, 5



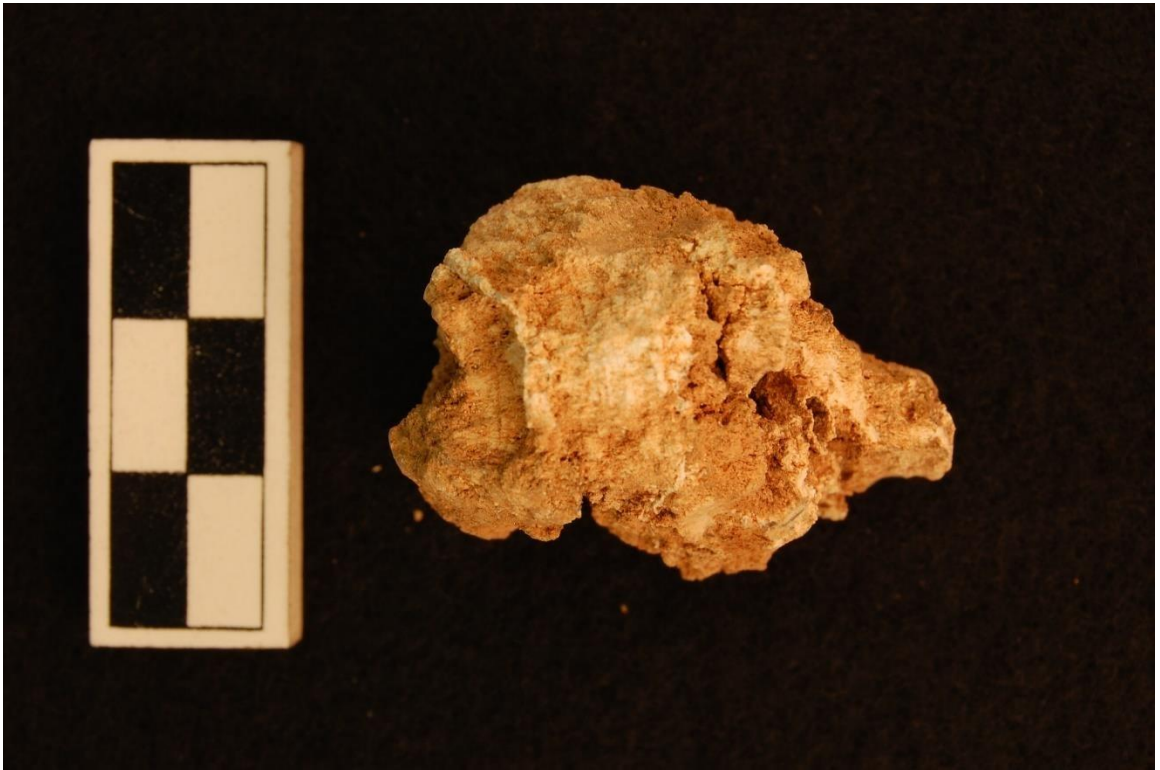
RC 0175, 1 (above) and 2 (below)



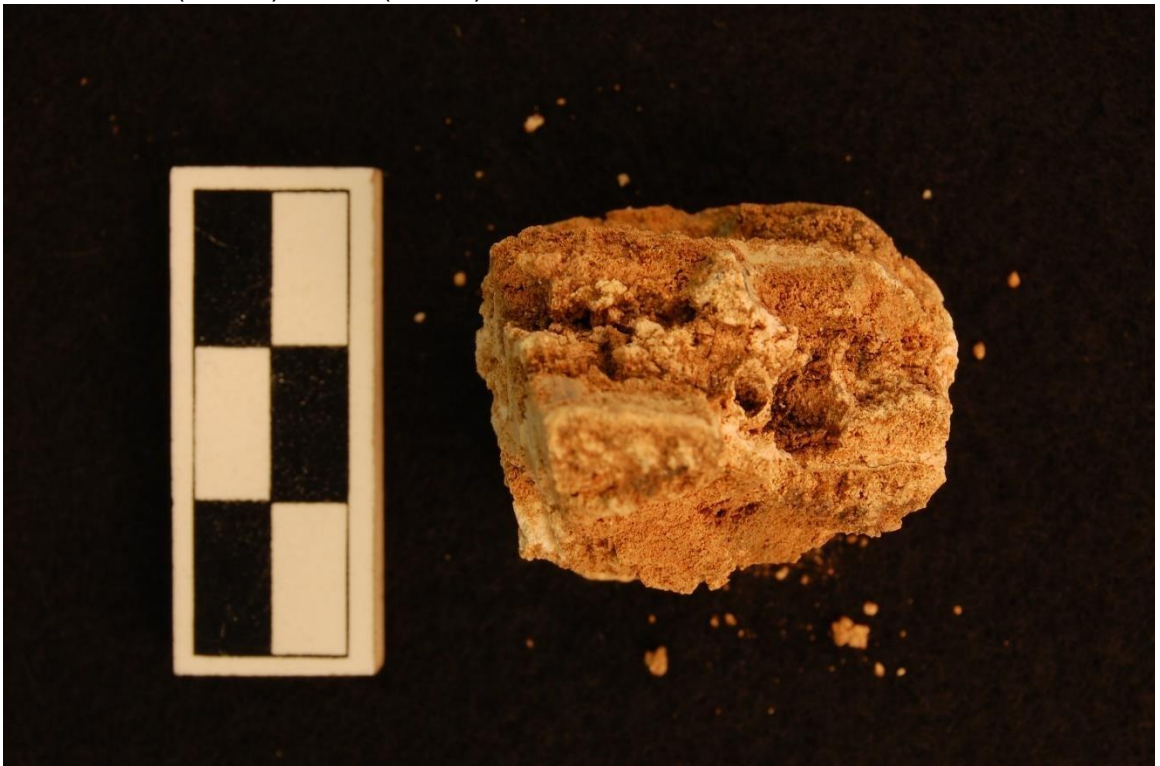


RC 0175, 3 (above) and 4 (below)





RC 0176, 1 (above) and 2 (below)





RC 0177, 1 (above) and 2 (below)



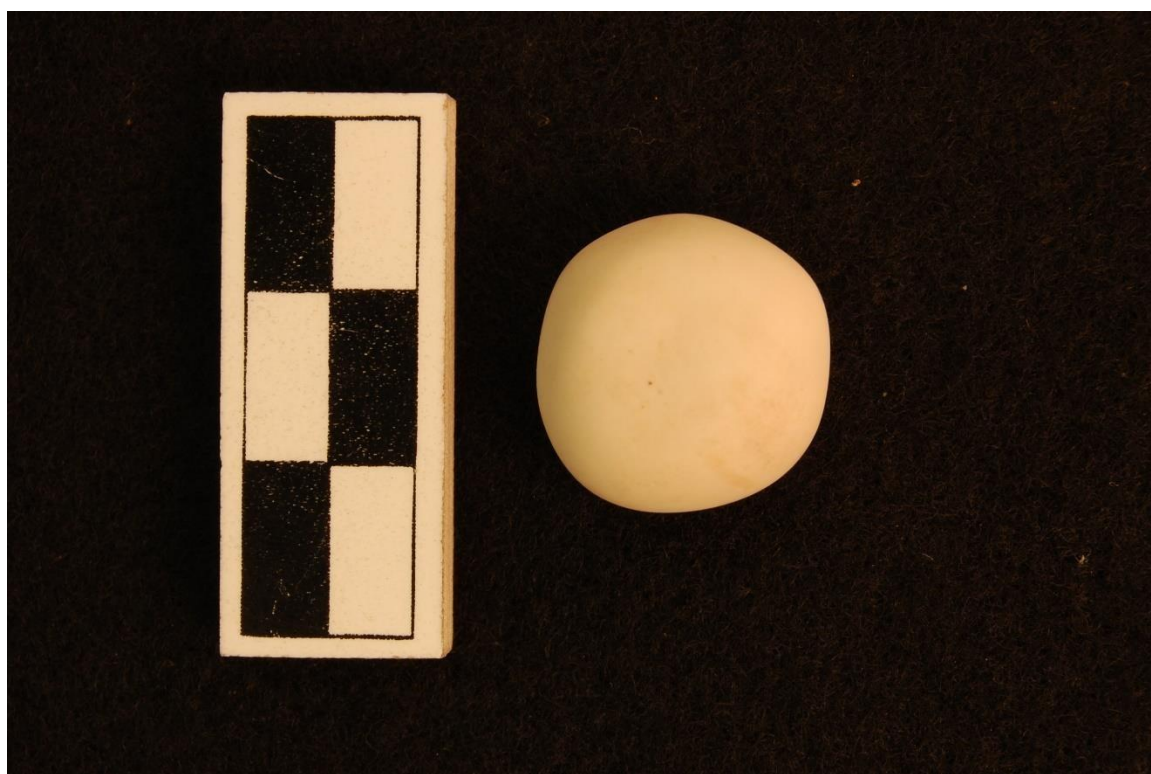


RC 0177, 3 (above) and 4 (below)





RC 0177, 5



RC 0180, 1



RC 0181, 1 (above) and 2 (below)



Appendix B

PERIOD	DIVISION	DATES	
Archaic		8000 - 2000 BCE	
Preclassic	Early Preclassic	2000 - 1000 BCE	
	Middle Preclassic	Early Middle Preclassic	1000-600 BCE
		Late Middle Preclassic	600 – 350 BCE
	Late Preclassic	Early Late Preclassic	350 – 1BCE
		Late Preclassic	1 BCE – 159 CE
		Terminal Preclassic	159 – 250 CE
Classic	Early Classic	250 – 550 CE	
	Late Classic	550 – 830 CE	
	Terminal Classic	830 – 950 CE	
Postclassic	Early Postclassic	950 BC – 1200 CE	
	Late Postclassic	1200 – 1539 CE	
Contact		1511 – 1697 CE	

Table 1. Maya Chronology, (Estrada-Belli, 2011)**Samples from 2006 Belize Valley Speleothem Project (BVSP)**

Barton Creek (n = 17)										
Sample #	ID Sample	Group	Ref #	Cave Site	Area	Unit	Type	Date Col.	Notes	
1	BC0034	7	23	Barton Creek	Darkzone, beneath Ledge2	harvested	Stalac	May-26-06	white crystalline eroded stalac	
2	BC0035		24	Barton Creek	Darkzone, beneath Ledge4	harvested	Stalac	May-26-06	dark brown stalac cut near river	
3	BC0036		25	Barton Creek	Twilight area, Ledge 1	surface	Travertine	May-26-06	fragments of dark travertine from base of Ledge 1	
4	BC0037		6	Barton Creek	Darkzone, Ledge 8, top	harvested	Stalac	May-26-06	small stalac near datum 2-24, top Ledge 8	
5	BC0039	8	27	Migdalia	Darkzone, West Wall	harvested	Stalac	May-28-07	150 m into dark zone west wall	
6	BC0040		28	Migdalia	Darkzone, center cave	Surface	spar	May-28-07		
7	BC0041		29	Migdalia	Darkzone, alcove	Surface	Stalag	May-28-07	Stalactite framents from looting activity	
8	BC0042		30	Migdalia	Darkzone	harvested	Stalag	May-29-07	Stalagmite harvested from Chamber 5	
9	BC0084		31	Migdalia	Darkzone, back tunnels,450m	surface	Stalag	June-25-06	back tunnel, 400-450m from ent	
10	BC0085	11	32	Migdalia	Darkzone, back tunnels,450m	surface	Stalag	June-26-06	back tunnel, 400-450m from ent	
11	BC0087	12	33	Broken Pots (Arnulfo)	Darkzone, 30m from ent	surface	Stalag	June-26-06	from looters pit-white crystalline	
12	BC0088		34	Broken Pots (Arnulfo)	Darkzone, 30m from ent	surface	Stalac	June-26-06	from looters pit	
13	BC0089	13	35	Arnulfo 1	Vertical Drop	surface	Stalac	June-26-06		
14	BC0090	14	36	Slate(BoxTunich)	Darkzone,100mfrom ent	harvested	Stalac	June-28-06	ent to east wall alcove, rear of cave	
15	BC0091		37	Slate(BoxTunich)	Twilight, 5m from ent	surface	Stalac	June-28-06	south wall	
16	BC0093	15	38	Owl(Tecolote)	Entrance, light	harvested	Spar	June-28-06	spar from entrance area	
17	BC0095		4	Owl(Tecolote)	Darkzone,60-90m from ent	harvested	Stalac	June-28-06	back wall crawl space	
Caves Branch (n = 16)										
18	CB0026	4	87	St.Hermans	Dark zone near river	harvested	Stalac	May-22-06	stalac harvested from near river @100m into dark zone	
19	CB0027		88	St.Hermans	Dark zone Maya chamber	surface	Stalac	May-22-06	broken stalac from beneath drapery in Maya chamber	
20	CB0028		89	St.Hermans	Dark zone Maya chamber	surface	Stalac	May-22-06	broken stalac from beneath draperie in Maya chamber	
21	CB0118	23	90	Jaguar Paw	50m from ent	surface	Pearls	July-16-06	two venues adjacent to each other	
22	CB0120		91	Jaguar Paw	Darkzone, 250-300m from ent	surface	Stalactite	July-16-06	from Crystal room	
23	CB0121		92	Jaguar Paw	Darkzone, 250-300m from ent	harvested	Travertine	July-16-06	contains charcoal from hearth	
24	CB0121a		93	Jaguar Paw	Darkzone, 250-300m from ent	harvested	Travertine	July-16-06	contains charcoal from hearth	
25	CB0122		93	Jaguar Paw	Darkzone, 250-300m from ent	harvested	Stalag	July-16-06	adjacent to hearth, previous breakage	
26	CB0123		94	Jaguar Paw	50m from ent	harvested	Stalactite	July-16-06	above pottery cache	
27	CB00193	43	95	Cave's Branch RS	Light	harvested	Stalactite	Aug 3-06	old stalac, few choices, none on ceiling above excavations	
28	CB0196	44	96	Swimming Hole	Entrance, light	harvested	Stalactite	Aug 3-06	part of huge Blue Hole system that runs to Jaguar Paw Cave	
29	CB0197	45	97	Mountain Cow	Twilight	harvested	Stalactite	Aug 3-06	cut from stalactite formation fallen from ceiling	
30	CB0200		98	Mountain Cow	Twilight	surface	Pearls	Aug 3-06	8, one is covered sherd	
31	CB0205	46	99	Lost World	Darkzone, N.Wall breakdown	surface	Stalactite	Aug 4_06	3 collected in breakdown	
32	CB0207	47	100	Footprint	Darkzone, 100m from ent	harvested	Spar	Aug 4_06	2 pieces	
33	CB0208		101	Footprint	Darkzone, 200m from ent	surface	Pearls	Aug 4_06	5	

Table 2a. Sample inventory of the Belize Valley Speleothem Project. Barton Creek and Cave's Branch groups shown.

Macal (n = 22)										
Sample #	ID Sample	Group	Ref #	Cave Site	Area	Unit	Type	Date Col.	Notes	
34	M 0009	1	1	Actun Isabella	West Wall	harvested	Stalac	May-17-06	outside layer is friable and disintegrating, white, popcorn	
35	M 0011		2	Actun Isabella	West Wall	surface	Stalag	May-17-06	popcorn appearance	
36	M 0013		3	Actun Isabella	East side	surface	Pearls	May-17-06	1cm-4mm	
37	M 0014		4	Actun Isabella	East side	surface	Spar	May-17-06	yellow crystalline fragment	
38	M 0015		5	Actun Isabella	East side	surface	Stalag	May-17-06	spar growth on side	
39	M 0016	2	6	Flour Camp	West Wall,WestChamber	harvested	Stalag	May-18-06	had regrowth, collected soda straw and base	
40	M 0017		7	Flour Camp	West Wall,WestChamber	harvested	Stalac	May-18-06		
41	M 0018		8	Flour Camp	West Wall,WestChamber	surface	Stalac	May-18-06	found near 0016,0017	
42	M 0019		9	Flour Camp	Crawl Space,WestChamber	surface	Stalac	May-18-06	crawl space boundary wall of offering group	
43	M 0022	3	10	Keyhole Cave	Dark zone in rear	harvested	Stalac	May-21-06	this was from an unused dark zone area, broken previously	
44	M 0023		11	Keyhole Cave	Dark zone in rear	surface	Stalac	May-21-06	this was from an unused dark zone area,on floor	
45	M 0111	21	12	Cave of the Moth	20m from entrance	surface	Stalac	July-15-06	recent break	
46	M 0113	22	13	Crab Ghost Cave	Ch2	harvested	Stalctite	July-15-06	above pottery scatter	
47	M 0124	24	14	Son of Chapat	Darkzone, 50-80m from ent	harvested	Stalactite	July-17-06	previous breakage, no regrowth	
48	M 0125	25	15	Halal RS	Light, s wall alcove	harvested	Stalactite	July-17-06		
49	M 0126	26	16	Chapat	Darkzone,150-200m from ent2	surface	Stalactite	July-17-06	area of heavy breakage	
50	M 0128		17	Chapat	Darkzone, 100m from ent	surface	Stalactite	July-17-06	Ledge 4, pottery cache	
51	M 0139	31	18	Serpiente(Waterfall)	Entrance, light	harvested	Stalactite	July-21-06	few speleos in this cave ent	
52	M 0153	38	19	Six Gibnut Cave	Darkzone, 20m from ent	surface	Stalactite	July-27-06	south alcove, clearly from area	
53	M 0170	40	20	House of Pain	Darkzone, 20m from ent	surface	Stalactite	July 29-06	cave is only about 20-25m in length, possibly from looters trenc	
54	M 0171		21	House of Pain	Darkzone, 10m from ent	surface	Stalactite	July 29-06	accompanied pottery cache	
55	M 0172		22	House of Pain	Darkzone, 10m from ent	harvested	Stalactite	July 29-06	located above 0171 cache	
Pine Ridge (n = 14)										
56	PR 0078	10	55	Las Cuevas	Darkzone,200m from ent	harvested	Stalag	June-24-06	cut with Dr. Drimmel	
57	PR 0080		56	Las Cuevas	Darkzone,225m from ent	surface	Stalac	June-24-08	collected from wall construction sealing alcove	
58	PR 0081		57	Las Cuevas	Darkzone,225m from ent	surface	Stalag	June-24-09	Ch 2 west area near pottery	
59	PR 0082		58	Las Cuevas	Darkzone,225m from ent	surface	Stalac	June-24-10	Ch 2 east area near pottery	
60	PR 0083		59	Las Cuevas	Darkzone,250m from ent	surface	Stalag	June-24-11	Ch 3 - charcoal in based	
61	PR0083a			Las Cuevas	Darkzone,250m from ent		Stalac	June-24-11		
62	PR 0132	29	60	Rio Frio Twin A (1)	Darkzone, rear alcove	surface	Stalactite	July-19-06		
63	PR 0133		61	Rio Frio Twin B	Twilight near entrance	harvested	Stalactite	July-19-06	color differentiation in stalac	
64	PR0133a		62	Rio Frio Twin B	Twilight near entrance	harvested	Stalactite	July-19-06	very hard and couldn't break	
65	PR 0134		63	Rio Frio Cave	Twilight, 30m from ent	harvested	Stalactite	July-19-06	few formations in cave, most very high	
66	PR 0135		64	Rio Frio Twin A (1)	Twilight, 15m from ent	harvested	Stalactite	July-19-06		
67	PR 0140	32	65	Rio Frio E	Darkzone	surface	Stalactite	July-21-06	rear wall alcove, clearly originated in area	
68	PR 0141		66	Rio Frio E	Twilight, 20m from ent	surface	Peals	July-22-06	one is calcified jute 68	
69	PR 0142		67	Rio Frio E	Twilight, 150m from ent	harvested	Stalactite	July-22-06	5 frags	

Table 2b. (cont.) Sample inventory of the Belize Valley Speleothem Project. Macal and Pine Ridge groups shown.

Roaring Creek (n = 20)										
Sample #	ID Sample	Group	Ref #	Cave Site	Area	Unit	Type	Date Col.	Notes	
70	RC 0029	5	68	Yaxcheel Ahau	Darkzone, 100m from ent	harvested	Stalac	May-24-06	stalac harvested from near river @100m into dark zone	
71	RC 0030		69	Yaxcheel Ahau	Darkzone, 400m from ent	harvested	Stalag	May-24-06	stalagmite harvested from shelf at river edge @400m dk zone	
72	RC 0031	6	70	Handprint	Darkzone, int chamber	harvested	Stalac	May-24-06	stalac under crawl, broken w/regrowth	
73	RC 0032		71	Handprint	Darkzone, int chamber	surface	Pearls	May-24-06	pearls located under overhang	
74	RC 0033		72	Handprint	Darkzone, int chamber	harvested	Stalac	May-24-06	small fragment from under crawl	
75	RC 0043	9	73	Nakbe	Darkzone lower alcove	harvested	Stalac	May-29-08		
76	RC 0044		74	Nakbe	Darkzone lower alcove	surface	Stalac	May-29-09		
77	RC 0045		75	Nakbe		surface	Stalac			
78	RC 0146	33	76	Uayak Na RS	Twilight	surface	Spar	July-24-06	from wall construction	
79	RC 0147	34	77	Hummingbird	Twilight, 7m from entrance	harvested	Stalactite	July-25-06		
80	RC 0148	35	78	Tarantula	Darkzone, Stela Chamber	harvested				
81	RC 0149	36	79	Ray's Cave	Twilight, 15m from ent	harvested				
82	RC 0150	37	80	Unknown Cave	Darkzone, 8m from ent	harvested	Stalactite	July-26-06	small cave, 18m long	
83	RC0151			Unknown Cave	Darkzone, 8m from ent	surface	Stalactite	July-26-06	small cave, 18m long	
84	RC 0164	39	81	Ray's Rockshelter	Lightzone	surface	Stalactite	July-25-06		
85	RC 0175	41	82	ATM	Darkzone, Upper Tunnels	surface	Stalactite	July 30-06	Cam collected from far back/architecture?	
86	RC 0176		83	ATM	Darkzone, Upper Tunnels	harvested	Stalactite	July 30-06	old and disintegrating- like Cahal Pech example	
87	RC 0177		84	ATM	Darkzone, Upper Tunnels	surface	Stalactite	July 30-06	old and disintegrating- like Cahal Pech example	
89	RC 0180		85	ATM	Darkzone, Upper Tunnels	surface	Pearls	July 30-06		
90	RC 0181		86	ATM	Darkzone, Upper Tunnels	surface	Pearls	July 30-06		
San Antonio (n = 15)										
91	SA 0096	16	40	Bols Museum	Darkzone,alcove,40m from ent	harvested	Stalac	June 29-06	harvested from crawl space	
92	SA 0097		41	Bols Museum	Main Chamber,50m from ent	surface	Stalac	June 29-06		
93	SA 0098		42	Bols Museum	Twilight	surface	Stalac	June 29-06	broken from stalac 30m from ent	
94	SA 0100	17	43	Actun Petz(Tzul)	Darkzone,30m from ent	surface	Stalac	July-2-06	collected antechamber skeleton room	
95	SA 0101		44	Actun Petz(Tzul)	Twilight,10m from ent	surface	Stalac	July-2-06	from alcove	
96	SA 0102	18	45	Crystal Palace(Tzul)	Darkzone, 60-70m from ent	harvested	Stalac	July-2-06		
97	SA 0103		46	Crystal Palace(Tzul)	Darkzone,60-70m from ent	surface	Stalac	July-2-06		
98	SA 0104		47	Crystal Palace(Tzul)	Dark Zone Crawl Pit	surface	Stalac	July-2-06	probable artifact	
99	SA 0106	19	48	Bat Cave(Bols)	Twilight, 5m from ent	surface	Stalac	June 29-06	near pottery cache	
100	SA 0108	20	49	Skeleton Cave(Bols)	Vert,30m from drop	surface	Stalac			
101	SA 0129	27	50	Hidden Cave	Darkzone, 25m from ent	harvested	Stalactite	July-18-06		
102	SA 0130	28	51	Actun Tzul	Darkzone, Chamber 1	surface	Stalactite	July-18-06	looks like old breakage	
103	SA 0131		52	Actun Tzul	Darkzone, Chamber 1	surface	Travertine	July-18-06	LC usage	
104	SA 0190	42	53	Offering Cave (Ka'am)	Twilight, 30m from ent	harvested	Stalactite	Aug 1-06		
105	SA 0192		54	Offering Cave (Ka'am)	Darkzone, 200m from ent	harvested	Stalactite	Aug 1-06	break and regrowth, rear wall above pottery cache	

Table 2c. (cont.) Sample inventory of the Belize Valley Speleothem Project. Roaring Creek and San Antonio groups shown.

Major and Trace Element Raw Data for Speleothem Samples. All values in ppm.

Group	INAA ID	Batch	Vial ID	Al	Na	Mg	Ca	Br	Ti	Mn	Sc	Cr	Fe	Co	Zn	Sr	Cs	Ba	
B a r t o n C r e e k	SAMPLE_028	RC2080-Pt	BC0034	473	11.403	507	392540	0.375	-1.435	2.158	0.067	-0.004	147.530	0.059	0.789	939.470	0.085	38.628	
	SAMPLE_029	RC2080-Pt	BC0035	220	36.392	2416	396370	1.316	-1.458	4.072	0.022	-0.004	142.080	0.000	-0.029	939.180	0.034	73.629	
	SAMPLE_032	RC2080-Pt	BC0036	592	303.340	160	366080	25.905	48.736	56.484	0.045	-0.013	178.900	0.122	144.170	77.100	0.048	31.375	
	SAMPLE_033	RC2080-Pt	BC0037	262	44.922	5094	394360	4.402	-1.535	8.007	0.032	-0.004	84.726	0.054	11.115	801.680	0.032	72.814	
	SAMPLE_034	RC2080-Pt	BC0039	150	18.438	129	399570	1.105	-1.439	1.545	0.016	-0.004	46.080	0.033	-0.045	-0.117	0.000	8.771	
	SAMPLE_035	RC2080-Pt	BC0040	709	24.685	1391	389320	0.555	-1.538	6.936	0.128	0.661	275.880	0.114	-0.050	34.983	0.107	24.903	
	SAMPLE_036	RC2080-Pt	BC0041	138	19.325	-7	391970	0.896	-1.441	1.259	0.037	-0.004	32.117	0.025	1.855	11.589	0.016	-0.067	
	SAMPLE_038	RC2080-Pt	BC0042	297	32.576	280	396920	2.222	-1.481	3.587	0.040	0.081	83.180	0.086	2.051	18.948	0.032	-0.066	
	SAMPLE_039	RC2080-Pt	BC0084	496	25.571	470	400060	0.763	-1.517	6.892	0.070	0.387	172.910	0.089	9.089	-0.132	0.031	-0.071	
	SAMPLE_040	RC2080-Pt	BC0085	181	27.384	263	400770	1.093	-1.471	1.431	0.018	-0.004	45.101	0.040	3.151	-0.121	0.000	-0.068	
	SAMPLE_041	RC2080-Pt	BC0087	216	9.622	-7	398110	0.107	-1.475	16.614	0.017	-0.004	48.660	0.209	-0.044	-0.116	0.000	5.928	
	SAMPLE_043	RC2080-Pt	BC0088	246	19.595	207	399760	0.944	-1.499	15.165	0.040	0.247	71.365	0.247	1.501	23.383	0.012	6.218	
	SAMPLE_044	RC2080-Pt	BC0089	301	37.654	208	402420	3.914	-1.515	12.080	0.030	-0.004	133.430	0.065	4.742	28.381	0.057	-0.071	
	SAMPLE_045	RC2080-Pt	BC0090	98	60.212	632	397650	0.940	-1.455	-0.010	0.001	-0.004	-0.249	0.000	-0.038	40.813	0.000	8.712	
	SAMPLE_046	RC2080-Pt	BC0091	1910	42.322	391	388260	6.500	110.010	49.037	0.385	2.384	998.230	1.064	20.516	37.342	0.412	5.962	
	SAMPLE_047	RC2080-Pt	BC0093	140	15.974	227	390560	1.229	-1.404	1.145	0.008	-0.004	-0.276	0.000	1.281	14.844	0.000	4.063	
	SAMPLE_049	RC2080-Pt	BC0095	111	14.955	326	385160	1.191	-1.358	0.997	0.022	-0.004	34.370	0.073	2.122	19.878	0.036	-0.065	
	C a v e s B r a n c h	SAMPLE_114	RC2080-Pt	CB0026	19557	285.140	126	334660	8.181	1103.300	678.140	3.492	17.280	8970.400	5.480	26.352	-0.450	3.926	147.270
		SAMPLE_115	RC2080-Pt	CB0027	2427	64.396	154	384910	8.934	140.400	101.720	0.400	2.090	1051.100	0.692	4.040	-0.200	0.464	48.161
SAMPLE_116		RC2080-Pt	CB0028	607	37.279	289	388420	6.353	-1.504	4.408	0.101	0.654	207.930	0.081	-0.048	31.718	0.071	19.267	
SAMPLE_118		RC2080-Pt	CB0118	891	27.174	0	396530	8.831	62.902	6.414	0.168	1.958	380.460	0.134	7.224	-0.160	0.120	-0.081	
SAMPLE_119		RC2080-Pt	CB0120	1113	15.788	756	383750	3.142	58.657	8.544	0.163	2.570	485.040	0.139	-0.052	-0.156	0.036	-0.080	
SAMPLE_120		RC2080-Pt	CB0121	32406	339.880	575	296060	14.921	2313.700	106.070	6.263	46.954	14681.0	2.634	60.199	-0.557	2.810	90.540	
SAMPLE_122		RC2080-Pt	CB0121a	5744	40.687	285	384610	10.900	248.040	61.277	0.873	7.819	2564.100	0.635	24.589	-0.247	0.245	-0.138	
SAMPLE_123		RC2080-Pt	CV0122	329	19.540	250	398020	1.290	-1.467	3.307	0.034	0.912	106.560	0.032	1.853	7.720	0.000	-0.071	
SAMPLE_124		RC2080-Pt	CV0123	167	18.677	-7	402740	2.058	7.506	0.668	0.128	-0.004	-0.291	0.000	-0.048	4.063	0.038	-0.079	
SAMPLE_126		RC2080-Pt	CV0193	317	40.735	911	384340	14.174	-1.482	4.028	0.034	0.651	88.569	0.055	-0.044	18.758	0.021	-0.072	
SAMPLE_127		RC2080-Pt	CV0196	846	62.381	1210	398780	5.970	49.625	20.007	0.136	0.922	344.300	0.104	-0.052	39.615	0.141	22.509	
SAMPLE_128		RC2080-Pt	CV0197	283	32.688	217	402530	1.300	-1.483	9.731	0.031	0.219	87.677	0.051	3.729	17.440	0.023	-0.078	
SAMPLE_130		RC2080-Pt	CB0200	1432	21.737	455	395930	12.193	87.443	13.484	0.193	1.374	485.080	0.178	10.285	26.933	0.085	-0.095	
SAMPLE_131		RC2080-Pt	CB0205	130	13.940	-7	393980	0.609	-1.441	1.019	0.012	-0.004	-0.268	0.000	0.925	16.614	0.000	4.634	
SAMPLE_132		RC2080-Pt	CB0207	99	7.445	-7	399320	0.093	-1.441	0.267	0.008	-0.004	-0.241	0.000	1.737	29.437	0.000	-0.071	
SAMPLE_133	RC2080-Pt	CB0208	89675	1264.300	0	29190	0.768	5238.900	192.320	18.151	101.500	43405.000	6.571	163.450	-0.944	10.632	536.490		

Elemental concentrations below detection limits are shown as negative values in the appendix; the values represent minimum detectable concentrations (MDCs) given the sample mass and all other analytical parameters and should be interpreted as "less than" the value indicated. The MDCs were substituted for missing values in quantitative analyses, as they indicate extreme low values that can be converted to a log scale, unlike zero.

Table 3a. Raw Data for Major and Trace element concentration in ppm, per group. Baton Creek and Cave's Branch groups shown.

Major and Trace Element Raw Data for Speleothem Samples. All values in ppm

Group	INAA ID	Batch	Vial ID	Al	Na	Mg	Ca	Br	Ti	Mn	Sc	Cr	Fe	Co	Zn	Sr	Cs	Ba	
M a c a i	SAMPLE_002	RC2080-Pt	M0009	89	23.884	-7	402710	7.457	-1.423	0.538	0.003	-0.003	-0.236	0.117	-0.034	0.927	0.000	-0.056	
	SAMPLE_003	RC2080-Pt	M0011	124	43.655	34	401180	5.241	-1.429	0.499	0.005	-0.003	-0.244	0.000	3.777	13.124	0.000	-0.058	
	SAMPLE_004	RC2080-Pt	M0013	1856	43.607	539	390900	30.354	88.538	37.044	0.265	1.419	713.460	0.296	13.522	-0.184	0.242	10.388	
	SAMPLE_005	RC2080-Pt	M0014	89	7.838	1093	401710	0.379	-1.411	-0.010	0.004	-0.003	-0.228	0.000	-0.031	-0.123	0.000	-0.061	
	SAMPLE_006	RC2080-Pt	M0015	280	17.350	645	400400	4.071	-1.413	0.873	0.026	-0.003	-0.264	0.024	1.640	-0.128	0.035	-0.060	
	SAMPLE_007	RC2080-Pt	M0016	548	27.453	460	398310	2.490	-1.439	5.253	0.071	0.577	161.320	0.040	2.770	7.629	0.036	-0.069	
	SAMPLE_009	RC2080-Pt	M0017	102	74.921	571	403760	4.974	-1.439	0.222	0.000	-0.003	-0.227	0.036	-0.032	27.515	0.000	13.352	
	SAMPLE_010	RC2080-Pt	M0018	107	30.142	371	391820	2.535	25.633	0.502	0.007	-0.003	28.009	0.012	-0.032	-0.134	0.000	-0.058	
	SAMPLE_011	RC2080-Pt	M0019	81	31.624	405	399570	4.425	36.674	-0.010	0.000	0.123	-0.220	0.000	1.976	26.582	0.000	12.798	
	SAMPLE_012	RC2080-Pt	M0022	549	15.708	465	397240	0.730	-1.461	6.438	0.225	0.325	212.030	0.084	1.358	-0.152	0.058	-0.081	
	SAMPLE_013	RC2080-Pt	M0023	662	31.637	333	397480	1.873	-1.503	11.340	0.125	0.610	282.770	0.142	2.754	20.876	0.051	11.400	
	SAMPLE_014	RC2080-Pt	M0111	139	17.426	164	404600	1.980	-1.427	3.776	0.005	0.115	20.814	0.084	2.132	-0.134	0.000	-0.062	
	SAMPLE_016	RC2080-Pt	M0113	223	12.757	14	398670	2.379	-1.407	3.714	0.033	0.466	98.176	0.030	2.161	1.430	0.023	-0.059	
	SAMPLE_017	RC2080-Pt	M0124	318	35.083	1439	396110	4.071	-1.450	4.322	0.122	0.509	204.340	0.029	4.382	19.168	0.054	9.387	
	SAMPLE_018	RC2080-Pt	M0125	356	135.860	627	388910	3.544	-1.451	7.401	0.037	0.212	116.440	0.029	1.960	10.343	0.034	12.022	
	SAMPLE_019	RC2080-Pt	M0126	1566	62.761	684	393360	2.163	66.934	22.925	0.256	2.046	715.020	0.210	-0.046	354.810	0.136	164.590	
	SAMPLE_020	RC2080-Pt	M0128	177	42.084	1935	398560	3.420	28.159	1.171	0.008	-0.003	33.844	0.000	1.762	22.892	0.000	-0.068	
	SAMPLE_021	RC2080-Pt	M0139	162	29.443	215	385860	11.975	-1.390	1.488	0.010	0.144	-0.229	0.000	1.240	23.998	0.000	14.067	
	SAMPLE_023	RC2080-Pt	M0153	215	24.487	-7	393570	7.607	-1.446	3.690	0.018	0.552	68.736	0.023	1.313	-0.127	0.000	51.314	
	SAMPLE_024	RC2080-Pt	M0170	396	43.674	277	391820	12.105	-1.491	14.409	0.048	-0.003	147.510	0.063	3.187	-0.142	0.040	3.289	
	SAMPLE_025	RC2080-Pt	M0171	182	17.312	-7	394500	4.106	-1.429	3.036	0.017	-0.003	53.849	0.000	1.608	20.771	0.000	1.869	
	SAMPLE_027	RC2080-Pt	M0172	205	12.171	166	398780	2.126	-1.413	2.265	0.018	0.290	59.716	0.045	1.284	6.338	0.000	4.400	
	P i n e R i d g e	SAMPLE_069	RC2080-Pt	PR0078	2715	154.080	7130	371540	4.461	166.940	57.903	0.461	3.888	1408.700	0.556	16.880	94.678	0.326	43.100
		SAMPLE_070	RC2080-Pt	PR0080	466	19.925	318	393050	1.485	-1.493	8.467	0.086	0.485	211.340	0.085	1.614	10.907	0.026	19.162
		SAMPLE_071	RC2080-Pt	PR0081	5500	49.081	517	370660	1.550	305.040	98.262	0.995	6.394	2936.900	1.191	4.217	-0.272	0.337	10.018
		SAMPLE_073	RC2080-Pt	PR0082	181	22.213	1023	394080	0.342	-1.459	1.965	0.017	-0.003	45.372	0.019	1.148	-0.136	0.000	7.203
		SAMPLE_074	RC2080-Pt	PR0083	218	63.722	3437	385980	0.331	-1.518	2.585	0.023	-0.003	76.635	0.037	-0.035	152.990	0.000	29.335
SAMPLE_075		RC2080-Pt	PR0083A	19798	92.405	2634	328650	1.905	912.230	337.320	3.344	17.087	8788.700	3.220	25.463	-0.437	1.615	35.283	
SAMPLE_076		RC2080-Pt	PR0132	624	56.998	182	380560	13.007	-1.525	24.277	0.058	0.287	124.110	0.145	2.408	31.655	0.055	12.890	
SAMPLE_077		RC2080-Pt	PR0133	129	14.364	-7	401790	2.885	-1.444	1.235	0.008	-0.003	-0.244	0.000	-0.034	23.914	0.000	-0.062	
SAMPLE_079		RC2080-Pt	PR0133A	775	33.907	333	386690	15.859	-1.501	3.102	0.125	1.001	399.360	0.140	-0.040	41.030	0.094	-0.079	
SAMPLE_080		RC2080-Pt	PR0134	209	165.190	4317	381900	6.248	-1.534	4.998	0.018	0.434	55.729	0.036	5.025	195.030	0.037	103.180	
SAMPLE_081		RC2080-Pt	PR0135	165	20.469	935	401990	1.008	-1.470	1.486	0.013	-0.003	25.814	0.000	1.067	27.980	0.000	9.192	
SAMPLE_082		RC2080-Pt	PR0140	324	59.297	3382	376160	1.375	-1.512	6.705	0.026	0.539	78.202	0.000	2.368	73.677	0.048	365.780	
SAMPLE_083		RC2080-Pt	PR0141	638	537.270	242	385620	24.208	21.962	40.398	0.119	0.563	224.240	0.093	6.096	106.510	0.115	63.470	
SAMPLE_085		RC2080-Pt	PR0142	132	21.589	376	399850	1.709	-1.469	1.120	0.008	-0.003	-0.222	0.000	1.472	30.676	0.000	87.482	

Elemental concentrations below detection limits are shown as negative values in the appendix; the values represent minimum detectable concentrations (MDCs) given the sample mass and all other analytical parameters and should be interpreted as "less than" the value indicated. The MDCs were substituted for missing values in quantitative analyses, as they indicate extreme low values that can be converted to a log scale, unlike zero.

Table 3b. (cont.) Raw Data for Major and Trace element concentration in ppm, per group. Macal and Pine Ridge groups shown.

Major and Trace Element Raw Data for Speleothem Samples. All values in ppm

Group	INAA ID	Batch	Vial ID	Al	Na	Mg	Ca	Br	Ti	Mn	Sc	Cr	Fe	Co	Zn	Sr	Cs	Ba	
R o a r i n g	SAMPLE_086	RC2080-Pt	RC0029	3197	67.394	946	383910	3.208	148.890	94.127	0.606	2.576	1385.600	0.694	7.042	35.412	0.431	19.947	
	SAMPLE_087	RC2080-Pt	RC0030	1992	48.733	95	394850	0.941	180.860	46.417	0.386	1.903	900.450	0.430	1.905	31.324	0.273	14.879	
	SAMPLE_088	RC2080-Pt	RC0031	179	91.234	2401	389950	8.899	-1.481	3.357	0.015	-0.003	68.792	0.039	3.294	86.264	0.000	54.671	
	SAMPLE_089	RC2080-Pt	RC0032	3880	40.060	633	384280	12.264	171.360	28.779	0.721	2.927	1643.300	0.508	46.287	-0.244	0.555	12.774	
	SAMPLE_092	RC2080-Pt	RC0033	366	53.469	8515	376510	3.318	-1.584	6.023	0.030	-0.004	111.450	0.087	17.397	81.492	0.054	311.350	
	SAMPLE_093	RC2080-Pt	RC0043	115	27.639	890	398650	5.701	-1.432	0.355	0.006	-0.003	-0.268	0.000	0.482	14.777	0.000	22.976	
	SAMPLE_094	RC2080-Pt	RC0044	305	17.958	460	399850	5.360	41.536	3.230	0.041	-0.004	119.290	0.072	2.391	20.347	0.000	22.298	
	SAMPLE_096	RC2080-Pt	RC0045	993	31.498	599	394430	7.289	67.337	5.574	0.147	0.900	437.600	0.104	5.645	12.688	0.095	28.486	
	SAMPLE_097	RC2080-Pt	RC0146	175	17.526	-7	406040	0.442	-1.481	0.963	0.042	-0.004	35.892	0.000	-0.039	-0.106	0.000	-0.065	
	SAMPLE_098	RC2080-Pt	RC0147	172	54.999	2975	396710	6.988	-1.518	0.950	0.013	-0.004	31.414	0.000	-0.043	71.108	0.000	25.792	
	SAMPLE_100	RC2080-Pt	RC0148	95	46.359	3673	396450	7.435	-1.479	-0.012	0.003	-0.004	-0.245	0.000	0.249	44.868	0.000	20.812	
C r e e k	SAMPLE_101	RC2080-Pt	RC0149	1962	51.297	682	396140	2.870	99.702	17.890	0.297	1.098	767.170	0.206	4.070	18.180	0.284	12.105	
	SAMPLE_102	RC2080-Pt	RC0150	112	14.039	398	397450	8.938	-1.435	0.868	0.000	-0.003	35.195	0.000	-0.040	19.473	0.000	12.737	
	SAMPLE_104	RC2080-Pt	RC0151	4166	30.205	484	385670	8.960	265.630	111.540	0.659	2.859	3576.800	3.029	9.451	-0.210	0.274	32.972	
	SAMPLE_105	RC2080-Pt	RC0164	47591	1141.600	5603	216660	8.281	2374.400	214.010	8.019	34.948	19388.000	3.965	69.090	121.950	2.505	156.420	
	SAMPLE_106	RC2080-Pt	RC0175	187	21.767	355	399110	1.270	-1.456	1.169	0.013	-0.004	57.336	0.030	1.974	28.884	0.000	16.889	
	SAMPLE_108	RC2080-Pt	RC0176	34177	910.780	0	257050	9.407	2404.100	373.440	6.270	29.549	14787.000	3.598	1651.500	-0.664	4.981	280.960	
	SAMPLE_109	RC2080-Pt	RC0177	458	19.700	301	393240	1.967	-1.485	5.306	0.120	-0.004	195.390	0.057	8.171	26.176	0.056	-0.089	
	SAMPLE_110	RC2080-Pt	RC0180	1451	25.386	203	389420	4.128	76.236	10.534	0.309	1.089	683.330	0.162	7.885	39.046	0.090	20.800	
	SAMPLE_111	RC2080-Pt	RC0181	2491	19.233	593	388790	4.278	111.070	16.312	0.497	1.598	1135.600	0.251	17.469	29.713	0.115	28.829	
	S a n A n t h o n i o	SAMPLE_050	RC2080-Pt	SA0096	516	13.319	119	401440	2.973	-1.523	8.552	0.064	-0.004	167.020	0.053	13.693	8.513	0.022	-0.084
		SAMPLE_051	RC2080-Pt	SA0097	1472	37.230	172	394230	8.390	-1.609	15.984	0.209	1.263	611.100	0.316	4.579	18.506	0.033	-0.089
SAMPLE_052		RC2080-Pt	SA0098	127	20.089	308	395190	3.668	-1.441	0.288	0.003	-0.004	-0.238	0.000	-0.036	17.873	0.000	-0.064	
SAMPLE_053		RC2080-Pt	SA0100	137	22.748	153	399220	3.812	-1.468	2.226	0.006	-0.004	-0.248	0.000	-0.038	16.287	0.000	-0.069	
SAMPLE_055		RC2080-Pt	SA0101	962	30.047	414	386480	6.411	27.851	10.346	0.125	0.636	349.920	0.174	2.606	16.212	0.035	-0.082	
SAMPLE_056		RC2080-Pt	SA0102	228	22.876	511	394610	1.082	-1.450	2.428	0.025	0.104	76.425	0.040	0.704	37.494	0.047	48.018	
SAMPLE_057		RC2080-Pt	SA0103	2332	34.029	1269	384770	8.228	66.912	29.380	0.377	2.042	1096.700	0.486	14.408	27.239	0.411	71.667	
SAMPLE_058		RC2080-Pt	SA0104	325	23.112	564	398690	1.119	-1.447	3.603	0.047	0.504	133.800	0.039	7.677	-0.127	0.055	8.274	
SAMPLE_059		RC2080-Pt	SA0106	201	26.508	127	394890	1.308	-1.481	3.194	0.022	-0.004	53.961	0.024	1.120	17.356	0.000	-0.070	
SAMPLE_062		RC2080-Pt	SA0108	146	19.178	609	390260	3.181	-1.449	1.085	0.007	-0.003	33.053	0.036	0.818	28.845	0.000	13.046	
SAMPLE_063		RC2080-Pt	SA0129	177	12.291	676	405830	0.771	-1.465	1.074	0.107	-0.004	45.476	0.021	7.821	17.638	0.000	10.491	
SAMPLE_064	RC2080-Pt	SA0130	639	27.538	426	388810	13.962	-1.518	14.593	0.117	0.641	245.490	0.258	1.194	3.192	0.132	12.810		
SAMPLE_065	RC2080-Pt	SA0131	5010	54.752	1063	368210	68.805	237.390	67.765	0.795	4.167	2061.000	0.733	10.002	-0.201	0.923	26.074		
SAMPLE_066	RC2080-Pt	SA0190	135	28.621	809	393900	3.736	-1.452	8.615	0.006	-0.003	-0.264	0.000	9.926	19.326	0.000	-0.059		
SAMPLE_068	RC2080-Pt	SA0192	143	29.523	311	402830	1.818	-1.429	0.488	0.004	-0.003	-0.249	0.000	-0.034	35.852	0.000	16.681		

Elemental concentrations below detection limits are shown as negative values in the appendix; the values represent minimum detectable concentrations (MDCs) given the sample mass and all other analytical parameters and should be interpreted as "less than" the value indicated. The MDCs were substituted for missing values in quantitative analyses, as they indicate extreme low values that can be converted to a log scale, unlike zero.

Table 3c. (cont.) Raw Data for Major and Trace element concentration in ppm, per group. Roaring Creek and San Antonio groups shown.

Rare Earth Element Raw Data for Speleothem Samples. All values in Log₁₀[ppm].											
Group	INAA ID	Batch	Vial ID	La	Sm	Eu	Yb	Lu	Hf	Th	U
B a r t o n C r e e k	SAMPLE_028	RC2080-Pt	BC0034	0.297	0.057	0.013	0.037	0.003	0.072	0.073	0.046
	SAMPLE_029	RC2080-Pt	BC0035	0.144	0.023	0.000	0.000	0.000	0.020	0.022	0.045
	SAMPLE_032	RC2080-Pt	BC0036	0.137	0.015	0.000	-0.001	0.000	-0.001	0.017	0.213
	SAMPLE_033	RC2080-Pt	BC0037	0.217	0.039	0.006	0.000	0.000	0.024	0.031	0.127
	SAMPLE_034	RC2080-Pt	BC0039	0.056	0.010	0.000	0.000	0.000	0.000	0.000	0.017
	SAMPLE_035	RC2080-Pt	BC0040	0.563	0.105	0.023	0.042	0.001	0.051	0.088	0.121
	SAMPLE_036	RC2080-Pt	BC0041	0.055	0.012	0.000	0.000	0.000	0.090	0.000	0.028
	SAMPLE_038	RC2080-Pt	BC0042	0.082	0.014	0.000	0.000	0.000	0.045	0.034	0.047
	SAMPLE_039	RC2080-Pt	BC0084	0.122	0.029	0.013	0.014	0.002	0.027	0.052	0.052
	SAMPLE_040	RC2080-Pt	BC0085	0.025	0.005	0.000	0.000	0.000	0.000	0.000	0.027
	SAMPLE_041	RC2080-Pt	BC0087	0.035	0.012	0.007	0.000	0.000	0.000	0.013	0.000
	SAMPLE_043	RC2080-Pt	BC0088	0.125	0.029	0.000	0.000	0.000	0.027	0.000	0.000
	SAMPLE_044	RC2080-Pt	BC0089	0.084	0.020	0.000	0.000	0.000	0.000	0.000	0.000
	SAMPLE_045	RC2080-Pt	BC0090	0.001	0.000	0.000	0.000	0.000	0.000	0.000	0.000
	SAMPLE_046	RC2080-Pt	BC0091	0.699	0.150	0.035	0.077	0.006	0.108	0.227	0.061
	SAMPLE_047	RC2080-Pt	BC0093	0.013	0.003	0.009	0.000	0.000	0.000	0.000	0.000
SAMPLE_049	RC2080-Pt	BC0095	0.016	0.005	0.000	0.000	0.000	0.000	0.000	0.030	
C a v e s B r a n c h	SAMPLE_114	RC2080-Pt	CB0026	11.764	2.222	0.434	0.900	0.183	1.673	3.091	0.830
	SAMPLE_115	RC2080-Pt	CB0027	1.222	0.228	0.050	0.100	0.019	0.117	0.318	0.174
	SAMPLE_116	RC2080-Pt	CB0028	0.275	0.053	0.016	0.051	0.001	0.076	0.106	0.094
	SAMPLE_118	RC2080-Pt	CB0118	0.478	0.089	0.026	0.093	0.013	0.311	0.148	0.056
	SAMPLE_119	RC2080-Pt	CB0120	0.264	0.081	0.022	0.067	0.008	0.100	0.101	0.040
	SAMPLE_120	RC2080-Pt	CB0121	10.509	2.360	0.476	1.357	0.272	3.079	4.617	1.161
	SAMPLE_122	RC2080-Pt	CB0121a	1.830	0.431	0.086	0.211	0.045	0.361	0.610	0.236
	SAMPLE_123	RC2080-Pt	CV0122	0.080	0.012	0.000	0.000	0.000	0.000	0.031	0.061
	SAMPLE_124	RC2080-Pt	CV0123	0.162	0.064	0.022	0.090	0.021	0.000	0.028	0.019
	SAMPLE_126	RC2080-Pt	CV0193	0.096	0.016	0.000	0.000	0.000	0.020	0.015	0.076
	SAMPLE_127	RC2080-Pt	CV0196	0.633	0.111	0.028	0.030	0.005	0.069	0.140	0.063
	SAMPLE_128	RC2080-Pt	CV0197	0.141	0.020	0.000	0.000	0.000	0.000	0.014	0.093
	SAMPLE_130	RC2080-Pt	CB0200	0.378	0.062	0.017	0.063	0.001	0.180	0.161	0.174
	SAMPLE_131	RC2080-Pt	CB0205	0.017	0.005	0.005	0.000	0.000	0.000	0.000	0.000
SAMPLE_132	RC2080-Pt	CB0207	0.000	0.011	0.000	0.000	0.000	0.000	0.000	0.019	
SAMPLE_133	RC2080-Pt	CB0208	26.212	5.351	1.077	2.962	0.742	5.972	12.275	2.496	

Elemental concentrations below detection limits are shown as negative values in the appendix; the values represent minimum detectable concentrations (MDCs) given the sample mass and all other analytical parameters and should be interpreted as “less than” the value indicated. The MDCs were substituted for missing values in quantitative analyses, as they indicate extreme low values that can be converted to a log scale, unlike zero.

Table 4a. Raw Data for Rare Earth Element concentration in Log Base 10, per group. Barton Creek and Cave's Branch groups shown.

Rare Earth Element Raw Data for Speleothem Samples. All values in Log₁₀[ppm].

Group	INAA ID	Batch	Vial ID	La	Sm	Eu	Yb	Lu	Hf	Th	U	
M a c a l	SAMPLE_002	RC2080-Pt	M0009	0.000	0.017	0.000	0.000	0.000	0.000	0.000	0.149	
	SAMPLE_003	RC2080-Pt	M0011	0.000	0.014	0.000	0.000	0.000	0.000	0.000	0.087	
	SAMPLE_004	RC2080-Pt	M0013	0.541	0.114	0.000	0.100	0.000	0.145	0.173	0.236	
	SAMPLE_005	RC2080-Pt	M0014	0.000	0.000	0.000	0.000	0.000	0.000	0.000	0.029	
	SAMPLE_006	RC2080-Pt	M0015	0.032	0.006	0.000	0.014	0.000	0.000	0.056	0.135	
	SAMPLE_007	RC2080-Pt	M0016	0.264	0.051	0.020	0.055	0.001	0.000	0.042	0.144	
	SAMPLE_009	RC2080-Pt	M0017	0.015	0.000	0.000	0.000	0.000	0.000	0.000	0.482	
	SAMPLE_010	RC2080-Pt	M0018	0.016	0.013	0.000	0.000	0.000	0.000	0.000	0.102	
	SAMPLE_011	RC2080-Pt	M0019	0.006	0.000	0.000	0.000	0.000	0.000	0.000	0.087	
	SAMPLE_012	RC2080-Pt	M0022	0.996	0.224	0.049	0.149	0.020	0.062	0.048	0.157	
	SAMPLE_013	RC2080-Pt	M0023	0.358	0.079	0.023	0.071	0.002	0.026	0.063	0.376	
	SAMPLE_014	RC2080-Pt	M0111	0.016	0.000	0.005	0.000	0.000	0.007	0.000	0.189	
	SAMPLE_016	RC2080-Pt	M0113	0.074	0.010	0.000	0.000	0.000	0.014	0.027	0.094	
	SAMPLE_017	RC2080-Pt	M0124	0.758	0.172	0.048	0.112	0.007	0.061	0.031	0.338	
	SAMPLE_018	RC2080-Pt	M0125	0.105	0.002	0.000	0.000	0.000	0.025	0.018	0.713	
	SAMPLE_019	RC2080-Pt	M0126	1.296	1.485	0.034	0.096	0.000	0.141	0.166	12.215	
	SAMPLE_020	RC2080-Pt	M0128	0.028	0.001	0.000	0.000	0.000	0.000	0.000	0.342	
	SAMPLE_021	RC2080-Pt	M0139	0.023	0.013	0.006	0.000	0.000	0.000	0.000	0.001	
	SAMPLE_023	RC2080-Pt	M0153	0.049	0.008	0.000	0.000	0.000	0.000	0.012	0.077	
	SAMPLE_024	RC2080-Pt	M0170	0.209	0.037	0.000	0.000	0.000	0.039	0.046	0.113	
	SAMPLE_025	RC2080-Pt	M0171	0.038	0.004	0.000	0.000	0.000	0.000	0.013	0.138	
	SAMPLE_027	RC2080-Pt	M0172	0.039	0.006	0.000	0.000	0.000	0.000	0.000	0.049	
	P i n e R i d g e	SAMPLE_069	RC2080-Pt	PR0078	1.239	0.234	0.055	0.152	0.006	0.200	0.321	0.517
		SAMPLE_070	RC2080-Pt	PR0080	0.247	0.049	0.013	0.032	0.000	0.000	0.051	0.092
		SAMPLE_071	RC2080-Pt	PR0081	2.449	0.514	0.109	0.237	0.060	0.453	0.663	0.143
		SAMPLE_073	RC2080-Pt	PR0082	0.044	0.011	0.000	0.000	0.000	0.000	0.000	0.040
		SAMPLE_074	RC2080-Pt	PR0083	0.070	0.009	0.000	0.000	0.000	0.000	0.000	0.140
SAMPLE_075		RC2080-Pt	PR0083A	15.659	2.541	0.502	1.127	0.265	1.497	2.589	0.440	
SAMPLE_076		RC2080-Pt	PR0132	0.316	0.069	0.013	0.054	0.003	0.039	0.057	0.190	
SAMPLE_077		RC2080-Pt	PR0133	0.019	0.003	0.000	0.000	0.000	0.005	0.000	0.000	
SAMPLE_079		RC2080-Pt	PR0133A	0.281	0.054	0.012	0.000	0.000	0.029	0.115	0.051	
SAMPLE_080		RC2080-Pt	PR0134	0.068	0.000	0.012	0.000	0.000	0.000	0.025	0.787	
SAMPLE_081		RC2080-Pt	PR0135	0.032	0.005	0.000	0.000	0.000	0.000	0.012	0.130	
SAMPLE_082		RC2080-Pt	PR0140	0.070	0.001	0.000	0.021	0.000	0.000	0.011	0.285	
SAMPLE_083		RC2080-Pt	PR0141	0.403	0.071	0.021	0.039	0.014	0.047	0.076	0.039	
SAMPLE_085		RC2080-Pt	PR0142	0.000	0.004	0.001	0.000	0.000	0.000	0.000	0.035	

Elemental concentrations below detection limits are shown as negative values in the appendix; the values represent minimum detectable concentrations (MDCs) given the sample mass and all other analytical parameters and should be interpreted as "less than" the value indicated. The MDCs were substituted for missing values in quantitative analyses, as they indicate extreme low values that can be converted to a log scale, unlike zero.

Table 4b. (Cont.) Raw Data for Rare Earth Element concentration in Log Base 10, per group. Macal and Pine Ridge groups shown.

Rare Earth Element Raw Data for Speleothem Samples. All values in Log₁₀[ppm].

Group	INAA ID	Batch	Vial ID	La	Sm	Eu	Yb	Lu	Hf	Th	U
R o a r i n g C r e e k	SAMPLE_086	RC2080-Pt	RC0029	2.539	0.565	0.093	0.164	0.034	0.210	0.502	0.145
	SAMPLE_087	RC2080-Pt	RC0030	4.324	0.833	0.121	0.377	0.068	0.912	0.845	0.276
	SAMPLE_088	RC2080-Pt	RC0031	0.035	0.002	0.000	0.000	0.000	0.028	0.000	0.187
	SAMPLE_089	RC2080-Pt	RC0032	1.114	0.237	0.058	0.109	0.016	0.210	0.421	0.201
	SAMPLE_092	RC2080-Pt	RC0033	0.094	0.000	0.012	0.000	0.000	0.000	0.025	0.672
	SAMPLE_093	RC2080-Pt	RC0043	0.013	0.001	0.000	0.000	0.000	0.028	0.000	0.000
	SAMPLE_094	RC2080-Pt	RC0044	0.098	0.020	0.000	0.000	0.000	0.000	0.033	0.001
	SAMPLE_096	RC2080-Pt	RC0045	0.395	0.083	0.012	0.028	0.007	0.091	0.186	0.049
	SAMPLE_097	RC2080-Pt	RC0146	0.071	0.022	0.000	0.000	0.000	0.000	0.000	0.000
	SAMPLE_098	RC2080-Pt	RC0147	0.045	0.001	0.006	0.023	0.000	0.000	0.000	0.295
	SAMPLE_100	RC2080-Pt	RC0148	0.009	0.015	0.007	0.000	0.000	0.000	0.000	0.106
SAMPLE_101	RC2080-Pt	RC0149	1.159	0.232	0.024	0.075	0.014	0.154	0.392	0.090	
SAMPLE_102	RC2080-Pt	RC0150	0.005	0.000	0.000	0.000	0.000	0.000	0.000	0.001	
SAMPLE_104	RC2080-Pt	RC0151	1.062	0.253	0.047	0.124	0.027	0.258	0.371	0.142	
SAMPLE_105	RC2080-Pt	RC0164	13.889	3.368	0.560	1.698	0.440	2.789	5.102	2.258	
SAMPLE_106	RC2080-Pt	RC0175	0.027	0.003	0.000	0.000	0.000	0.000	0.000	0.077	
SAMPLE_108	RC2080-Pt	RC0176	20.078	3.946	0.686	2.212	0.509	4.252	5.321	2.865	
SAMPLE_109	RC2080-Pt	RC0177	0.490	0.114	0.034	0.078	0.024	0.047	0.022	0.001	
SAMPLE_110	RC2080-Pt	RC0180	0.648	0.180	0.035	0.122	0.026	0.115	0.150	0.088	
SAMPLE_111	RC2080-Pt	RC0181	1.476	0.365	0.081	0.144	0.042	0.194	0.271	0.139	
S a n A n t o n i o	SAMPLE_050	RC2080-Pt	SA0096	0.133	0.029	0.000	0.023	0.000	0.026	0.034	0.106
	SAMPLE_051	RC2080-Pt	SA0097	0.432	0.088	0.017	0.090	0.012	0.084	0.160	0.149
	SAMPLE_052	RC2080-Pt	SA0098	0.000	0.000	0.000	0.000	0.000	0.000	0.000	0.060
	SAMPLE_053	RC2080-Pt	SA0100	0.014	0.011	0.000	0.000	0.000	0.000	0.000	0.081
	SAMPLE_055	RC2080-Pt	SA0101	0.295	0.059	0.021	0.000	0.000	0.078	0.085	0.174
	SAMPLE_056	RC2080-Pt	SA0102	0.019	0.011	0.000	0.000	0.000	0.000	0.022	0.041
	SAMPLE_057	RC2080-Pt	SA0103	0.765	0.147	0.035	0.090	0.013	0.156	0.254	0.140
	SAMPLE_058	RC2080-Pt	SA0104	0.199	0.034	0.008	0.000	0.000	0.000	0.031	0.095
	SAMPLE_059	RC2080-Pt	SA0106	0.086	0.017	0.000	0.019	0.000	0.000	0.012	0.000
	SAMPLE_062	RC2080-Pt	SA0108	0.007	0.003	0.000	0.000	0.000	0.000	0.000	0.000
	SAMPLE_063	RC2080-Pt	SA0129	0.250	0.067	0.020	0.102	0.016	0.000	0.000	0.184
SAMPLE_064	RC2080-Pt	SA0130	0.843	0.194	0.037	0.083	0.015	0.046	0.121	0.001	
SAMPLE_065	RC2080-Pt	SA0131	2.042	0.443	0.086	0.207	0.027	0.271	0.747	0.206	
SAMPLE_066	RC2080-Pt	SA0190	0.005	0.000	0.000	0.000	0.000	0.000	0.000	0.000	
SAMPLE_068	RC2080-Pt	SA0192	0.010	0.012	0.000	0.000	0.000	0.176	0.000	0.080	

Elemental concentrations below detection limits are shown as negative values in the appendix; the values represent minimum detectable concentrations (MDCs) given the sample mass and all other analytical parameters and should be interpreted as “less than” the value indicated. The MDCs were substituted for missing values in quantitative analyses, as they indicate extreme low values that can be converted to a log scale, unlike zero.

Table 4c. (Cont.) Raw Data for Rare Earth Element concentration in Log Base 10, per group. Roaring Creek and San Antonio groups shown.

Major and Trace Element Data for Speleothem Samples. All values in ppm.

Group	INAA ID	Batch	Vial ID	Al	Na	Mg	Ca	Ti	Mn	Sc	Cr	Fe	Co	Zn	Sr	Cs	Ba
B a t o n C r e e k	SAMPLE_028	RC2080-Pt	BC0034	473	11	507	392540	1.44	2.16	0.067	0.004	148	0.059	0.79	939	0.085	38.63
	SAMPLE_029	RC2080-Pt	BC0035	220	36	2416	396370	1.46	4.07	0.022	0.004	142	0.000	0.03	939	0.034	73.63
	SAMPLE_032	RC2080-Pt	BC0036	592	303	160	366080	48.74	56.48	0.045	0.013	179	0.122	144.17	77	0.048	31.38
	SAMPLE_033	RC2080-Pt	BC0037	262	45	5094	394360	1.54	8.01	0.032	0.004	85	0.054	11.12	802	0.032	72.81
	SAMPLE_034	RC2080-Pt	BC0039	150	18	129	399570	1.44	1.55	0.016	0.004	46	0.033	0.04	0	0.000	8.77
	SAMPLE_035	RC2080-Pt	BC0040	709	25	1391	389320	1.54	6.94	0.128	0.661	276	0.114	0.05	35	0.107	24.90
	SAMPLE_036	RC2080-Pt	BC0041	138	19	7	391970	1.44	1.26	0.037	0.004	32	0.025	1.85	12	0.016	0.07
	SAMPLE_038	RC2080-Pt	BC0042	297	33	280	396920	1.48	3.59	0.040	0.081	83	0.086	2.05	19	0.032	0.07
	SAMPLE_039	RC2080-Pt	BC0084	496	26	470	400060	1.52	6.89	0.070	0.387	173	0.089	9.09	0	0.031	0.07
	SAMPLE_040	RC2080-Pt	BC0085	181	27	263	400770	1.47	1.43	0.018	0.004	45	0.040	3.15	0	0.000	0.07
	SAMPLE_041	RC2080-Pt	BC0087	216	10	7	398110	1.48	16.61	0.017	0.004	49	0.209	0.04	0	0.000	5.93
	SAMPLE_043	RC2080-Pt	BC0088	246	20	207	399760	1.50	15.17	0.040	0.247	71	0.247	1.50	23	0.012	6.22
	SAMPLE_044	RC2080-Pt	BC0089	301	38	208	402420	1.51	12.08	0.030	0.004	133	0.065	4.74	28	0.057	0.07
	SAMPLE_045	RC2080-Pt	BC0090	98	60	632	397650	1.45	0.01	0.001	0.004	0	0.000	0.04	41	0.000	8.71
	SAMPLE_046	RC2080-Pt	BC0091	1910	42	391	388260	110.01	49.04	0.385	2.384	998	1.064	20.52	37	0.412	5.96
SAMPLE_047	RC2080-Pt	BC0093	140	16	227	390560	1.40	1.15	0.008	0.004	0	0.000	1.28	15	0.000	4.06	
SAMPLE_049	RC2080-Pt	BC0095	111	15	326	385160	1.36	1.00	0.022	0.004	34	0.073	2.12	20	0.036	0.07	
C a v e . s B r a n c h	SAMPLE_114	RC2080-Pt	CB0026	19557	285	126	334660	1103.30	678.14	3.492	17.280	8970	5.480	26.35	0	3.926	147.27
	SAMPLE_115	RC2080-Pt	CB0027	2427	64	154	384910	140.40	101.72	0.400	2.090	1051	0.692	4.04	0	0.464	48.16
	SAMPLE_116	RC2080-Pt	CB0028	607	37	289	388420	1.50	4.41	0.101	0.654	208	0.081	0.05	32	0.071	19.27
	SAMPLE_118	RC2080-Pt	CB0118	891	27	0	396530	62.90	6.41	0.168	1.958	380	0.134	7.22	0	0.120	0.08
	SAMPLE_119	RC2080-Pt	CB0120	1113	16	756	383750	58.66	8.54	0.163	2.570	485	0.139	0.05	0	0.036	0.08
	SAMPLE_120	RC2080-Pt	CB0121	32406	340	575	296060	2313.70	106.07	6.263	46.954	14681	2.634	60.20	1	2.810	90.54
	SAMPLE_122	RC2080-Pt	CB0121e	5744	41	285	384610	248.04	61.28	0.873	7.819	2564	0.635	24.59	0	0.245	0.14
	SAMPLE_123	RC2080-Pt	CB0122	329	20	250	398020	1.47	3.31	0.034	0.912	107	0.032	1.85	8	0.000	0.07
	SAMPLE_124	RC2080-Pt	CB0123	167	19	7	402740	7.51	0.67	0.128	0.004	0	0.000	0.05	4	0.038	0.08
	SAMPLE_126	RC2080-Pt	CB0193	317	41	911	384340	1.48	4.03	0.034	0.651	89	0.055	0.04	19	0.021	0.07
	SAMPLE_127	RC2080-Pt	CB0196	846	62	1210	398780	49.63	20.01	0.136	0.922	344	0.104	0.05	40	0.141	22.51
	SAMPLE_128	RC2080-Pt	CB0197	283	33	217	402530	1.48	9.73	0.031	0.219	88	0.051	3.73	17	0.023	0.08
	SAMPLE_130	RC2080-Pt	CB0200	1432	22	455	395930	87.44	13.48	0.193	1.374	485	0.178	10.29	27	0.085	0.10
	SAMPLE_131	RC2080-Pt	CB0205	130	14	7	393980	1.44	1.02	0.012	0.004	0	0.000	0.93	17	0.000	4.63
	SAMPLE_132	RC2080-Pt	CB0207	99	7	7	399320	1.44	0.27	0.008	0.004	0	0.000	1.74	29	0.000	0.07
SAMPLE_133	RC2080-Pt	CB0208	89675	1264	0	29190	5238.90	192.32	18.151	101.500	43405	6.571	163.45	1	10.632	536.49	

Elemental concentrations below detection limits are shown as negative values in the appendix; the values represent minimum detectable concentrations (MDCs) given the sample mass and all other analytical parameters and should be interpreted as "less than" the value indicated. The MDCs were substituted for missing values in quantitative analyses, as they indicate extreme low values that can be converted to a log scale, unlike zero.

Table 5a. Absolute Values for Major and Trace element concentration in ppm, per group. Baton Creek and Cave's Branch groups shown.

Major and Trace Element Data for Speleothem Samples. All values in ppm.

Group	INAA ID	Batch	Vial ID	Al	Na	Mg	Ca	Ti	Mn	Sc	Cr	Fe	Co	Zn	Sr	Cs	Ba	
M a c a l	SAMPLE_002	RC2080-Pt	M0009	89	24	7	402710	1.42	0.54	0.003	0.003	0	0.117	0.03	1	0.000	0.06	
	SAMPLE_003	RC2080-Pt	M0011	124	44	34	401180	1.43	0.50	0.005	0.003	0	0.000	3.78	13	0.000	0.06	
	SAMPLE_004	RC2080-Pt	M0013	1856	44	539	390900	88.54	37.04	0.265	1.419	713	0.296	13.52	0	0.242	10.39	
	SAMPLE_005	RC2080-Pt	M0014	89	8	1093	401710	1.41	0.01	0.004	0.003	0	0.000	0.03	0	0.000	0.06	
	SAMPLE_006	RC2080-Pt	M0015	280	17	645	400400	1.41	0.87	0.026	0.003	0	0.024	1.64	0	0.035	0.06	
	SAMPLE_007	RC2080-Pt	M0016	548	27	460	398310	1.44	5.25	0.071	0.577	161	0.040	2.77	8	0.036	0.07	
	SAMPLE_009	RC2080-Pt	M0017	102	75	571	403760	1.44	0.22	0.000	0.003	0	0.036	0.03	28	0.000	13.35	
	SAMPLE_010	RC2080-Pt	M0018	107	30	371	391820	25.63	0.50	0.007	0.003	28	0.012	0.03	0	0.000	0.06	
	SAMPLE_011	RC2080-Pt	M0019	81	32	405	399570	36.67	0.01	0.000	0.123	0	0.000	1.98	27	0.000	12.80	
	SAMPLE_012	RC2080-Pt	M0022	549	16	465	397240	1.46	6.44	0.225	0.325	212	0.084	1.36	0	0.058	0.08	
	SAMPLE_013	RC2080-Pt	M0023	662	32	333	397480	1.50	11.34	0.125	0.610	283	0.142	2.75	21	0.051	11.40	
	SAMPLE_014	RC2080-Pt	M0111	139	17	164	404600	1.43	3.78	0.005	0.115	21	0.084	2.13	0	0.000	0.06	
	SAMPLE_016	RC2080-Pt	M0113	223	13	14	398670	1.41	3.71	0.033	0.466	98	0.030	2.16	1	0.023	0.06	
	SAMPLE_017	RC2080-Pt	M0124	318	35	1439	396110	1.45	4.32	0.122	0.509	204	0.029	4.38	19	0.054	9.39	
	SAMPLE_018	RC2080-Pt	M0125	356	136	627	388910	1.45	7.40	0.037	0.212	116	0.029	1.96	10	0.034	12.02	
	SAMPLE_019	RC2080-Pt	M0126	1566	63	684	393360	66.93	22.93	0.256	2.046	715	0.210	0.05	355	0.136	164.59	
	SAMPLE_020	RC2080-Pt	M0128	177	42	1935	398560	28.16	1.17	0.008	0.003	34	0.000	1.76	23	0.000	0.07	
	SAMPLE_021	RC2080-Pt	M0139	162	29	215	385860	1.39	1.49	0.010	0.144	0	0.000	1.24	24	0.000	14.07	
	SAMPLE_023	RC2080-Pt	M0153	215	24	7	393570	1.45	3.69	0.018	0.552	69	0.023	1.31	0	0.000	51.31	
	SAMPLE_024	RC2080-Pt	M0170	396	44	277	391820	1.49	14.41	0.048	0.003	148	0.063	3.19	0	0.040	3.29	
	SAMPLE_025	RC2080-Pt	M0171	182	17	7	394500	1.43	3.04	0.017	0.003	54	0.000	1.61	21	0.000	1.87	
	SAMPLE_027	RC2080-Pt	M0172	205	12	166	398780	1.41	2.27	0.018	0.290	60	0.045	1.28	6	0.000	4.40	
	P i n e R i d g e	SAMPLE_069	RC2080-Pt	PR0078	2715	154	7130	371540	166.94	57.90	0.461	3.888	1409	0.556	16.88	95	0.326	43.10
		SAMPLE_070	RC2080-Pt	PR0080	466	20	318	393050	1.49	8.47	0.086	0.485	211	0.085	1.61	11	0.026	19.16
		SAMPLE_071	RC2080-Pt	PR0081	5500	49	517	370660	305.04	98.26	0.995	6.394	2937	1.191	4.22	0	0.337	10.02
		SAMPLE_073	RC2080-Pt	PR0082	181	22	1023	394080	1.46	1.97	0.017	0.003	45	0.019	1.15	0	0.000	7.20
		SAMPLE_074	RC2080-Pt	PR0083	218	64	3437	385980	1.52	2.59	0.023	0.003	77	0.037	0.03	153	0.000	29.34
SAMPLE_075		RC2080-Pt	PR0083A	19798	92	2634	328650	912.23	337.32	3.344	17.087	8789	3.220	25.46	0	1.615	35.28	
SAMPLE_076		RC2080-Pt	PR0132	624	57	182	380560	1.53	24.28	0.058	0.287	124	0.145	2.41	32	0.055	12.89	
SAMPLE_077		RC2080-Pt	PR0133	129	14	7	401790	1.44	1.23	0.008	0.003	0	0.000	0.03	24	0.000	0.06	
SAMPLE_079		RC2080-Pt	PR0133A	775	34	333	386690	1.50	3.10	0.125	1.001	399	0.140	0.04	41	0.094	0.08	
SAMPLE_080		RC2080-Pt	PR0134	209	165	4317	381900	1.53	5.00	0.018	0.434	56	0.036	5.02	195	0.037	103.18	
SAMPLE_081		RC2080-Pt	PR0135	165	20	935	401990	1.47	1.49	0.013	0.003	26	0.000	1.07	28	0.000	9.19	
SAMPLE_082		RC2080-Pt	PR0140	324	59	3382	376160	1.51	6.70	0.026	0.539	78	0.000	2.37	74	0.048	365.78	
SAMPLE_083		RC2080-Pt	PR0141	638	537	242	385620	21.96	40.40	0.119	0.563	224	0.093	6.10	107	0.115	63.47	
SAMPLE_085		RC2080-Pt	PR0142	132	22	376	399850	1.47	1.12	0.008	0.003	0	0.000	1.47	31	0.000	87.48	

Elemental concentrations below detection limits are shown as negative values in the appendix; the values represent minimum detectable concentrations (MDCs) given the sample mass and all other analytical parameters and should be interpreted as "less than" the value indicated. The MDCs were substituted for missing values in quantitative analyses, as they indicate extreme low values that can be converted to a log scale, unlike zero.

Table 5b. Absolute Values for Major and Trace element concentration in ppm, per group. Macal and Pine Ridge groups shown.

Major and Trace Element Data for Speleothem Samples. All values in ppm.

Group	INAA ID	Batch	Vial ID	Al	Na	Mg	Ca	Ti	Mn	Sc	Cr	Fe	Co	Zn	Sr	Cs	Ba	
R o a r i n g	SAMPLE_086	RC2080-Pt	RC0029	3197	67	946	383910	148.89	94.13	0.606	2.576	1386	0.694	7.04	35	0.431	19.95	
	SAMPLE_087	RC2080-Pt	RC0030	1992	49	95	394850	180.86	46.42	0.386	1.903	900	0.430	1.91	31	0.273	14.88	
	SAMPLE_088	RC2080-Pt	RC0031	179	91	2401	389950	1.48	3.36	0.015	0.003	69	0.039	3.29	86	0.000	54.67	
	SAMPLE_089	RC2080-Pt	RC0032	3880	40	633	384280	171.36	28.78	0.721	2.927	1643	0.508	46.29	0	0.555	12.77	
	SAMPLE_092	RC2080-Pt	RC0033	366	53	8515	376510	1.58	6.02	0.030	0.004	111	0.087	17.40	81	0.054	311.35	
	SAMPLE_093	RC2080-Pt	RC0043	115	28	890	398650	1.43	0.36	0.006	0.003	0	0.000	0.48	15	0.000	22.98	
	SAMPLE_094	RC2080-Pt	RC0044	305	18	460	399850	41.54	3.23	0.041	0.004	119	0.072	2.39	20	0.000	22.30	
	SAMPLE_096	RC2080-Pt	RC0045	993	31	599	394430	67.34	5.57	0.147	0.900	438	0.104	5.65	13	0.095	28.49	
	SAMPLE_097	RC2080-Pt	RC0146	175	18	7	406040	1.48	0.96	0.042	0.004	36	0.000	0.04	0	0.000	0.06	
	SAMPLE_098	RC2080-Pt	RC0147	172	55	2975	396710	1.52	0.95	0.013	0.004	31	0.000	0.04	71	0.000	25.79	
	SAMPLE_100	RC2080-Pt	RC0148	95	46	3673	396450	1.48	0.01	0.003	0.004	0	0.000	0.25	45	0.000	20.81	
C r e e k	SAMPLE_101	RC2080-Pt	RC0149	1962	51	682	396140	99.70	17.89	0.297	1.098	767	0.206	4.07	18	0.284	12.11	
	SAMPLE_102	RC2080-Pt	RC0150	112	14	398	397450	1.44	0.87	0.000	0.003	35	0.000	0.04	19	0.000	12.74	
	SAMPLE_104	RC2080-Pt	RC0151	4166	30	484	385670	265.63	111.54	0.659	2.859	3577	3.029	9.45	0	0.274	32.97	
	SAMPLE_105	RC2080-Pt	RC0164	47591	1142	5603	216660	2374.40	214.01	8.019	34.948	19388	3.965	69.09	122	2.505	156.42	
	SAMPLE_106	RC2080-Pt	RC0175	187	22	355	399110	1.46	1.17	0.013	0.004	57	0.030	1.97	29	0.000	16.89	
	SAMPLE_108	RC2080-Pt	RC0176	34177	911	0	257050	2404.10	373.44	6.270	29.549	14787	3.598	1651.50	1	4.981	280.96	
	SAMPLE_109	RC2080-Pt	RC0177	458	20	301	393240	1.49	5.31	0.120	0.004	195	0.057	8.17	26	0.056	0.09	
	SAMPLE_110	RC2080-Pt	RC0180	1451	25	203	389420	76.24	10.53	0.309	1.089	683	0.162	7.89	39	0.090	20.80	
	SAMPLE_111	RC2080-Pt	RC0181	2491	19	593	388790	111.07	16.31	0.497	1.598	1136	0.251	17.47	30	0.115	28.83	
	S a n A n t o n i o	SAMPLE_050	RC2080-Pt	SA0096	516	13	119	401440	1.52	8.55	0.064	0.004	167	0.053	13.69	9	0.022	0.08
		SAMPLE_051	RC2080-Pt	SA0097	1472	37	172	394230	1.61	15.98	0.209	1.263	611	0.316	4.58	19	0.033	0.09
SAMPLE_052		RC2080-Pt	SA0098	127	20	308	395190	1.44	0.29	0.003	0.004	0	0.000	0.04	18	0.000	0.06	
SAMPLE_053		RC2080-Pt	SA0100	137	23	153	399220	1.47	2.23	0.006	0.004	0	0.000	0.04	16	0.000	0.07	
SAMPLE_055		RC2080-Pt	SA0101	962	30	414	386480	27.85	10.35	0.125	0.636	350	0.174	2.61	16	0.035	0.08	
SAMPLE_056		RC2080-Pt	SA0102	228	23	511	394610	1.45	2.43	0.025	0.104	76	0.040	0.70	37	0.047	48.02	
SAMPLE_057		RC2080-Pt	SA0103	2332	34	1269	384770	66.91	29.38	0.377	2.042	1097	0.486	14.41	27	0.411	71.67	
SAMPLE_058		RC2080-Pt	SA0104	325	23	564	398690	1.45	3.60	0.047	0.504	134	0.039	7.68	0	0.055	8.27	
SAMPLE_059		RC2080-Pt	SA0106	201	27	127	394890	1.48	3.19	0.022	0.004	54	0.024	1.12	17	0.000	0.07	
SAMPLE_062		RC2080-Pt	SA0108	146	19	609	390260	1.45	1.09	0.007	0.003	33	0.036	0.82	29	0.000	13.05	
SAMPLE_063		RC2080-Pt	SA0129	177	12	676	405830	1.47	1.07	0.107	0.004	45	0.021	7.82	18	0.000	10.49	
SAMPLE_064	RC2080-Pt	SA0130	639	28	426	388810	1.52	14.59	0.117	0.641	245	0.258	1.19	3	0.132	12.81		
SAMPLE_065	RC2080-Pt	SA0131	5010	55	1063	368210	237.39	67.77	0.795	4.167	2061	0.733	10.00	0	0.923	26.07		
SAMPLE_066	RC2080-Pt	SA0190	135	29	809	393900	1.45	8.61	0.006	0.003	0	0.000	9.93	19	0.000	0.06		
SAMPLE_068	RC2080-Pt	SA0192	143	30	311	402830	1.43	0.49	0.004	0.003	0	0.000	0.03	36	0.000	16.68		

Elemental concentrations below detection limits are shown as negative values in the appendix; the values represent minimum detectable concentrations (MDCs) given the sample mass and all other analytical parameters and should be interpreted as "less than" the value indicated. The MDCs were substituted for missing values in quantitative analyses, as they indicate extreme low values that can be converted to a log scale, unlike zero.

Table 5c. Absolute Values for Major and Trace element concentration in ppm. Roaring Creek and San Antonio groups shown.

Rare Earth Element Data for Speleothem Samples. All values in ppm.

Group	INAA ID	Batch	Vial ID	La	Sm	Eu	Yb	Lu	Hf	Th	U
B a r t o n C r e e k	SAMPLE_028	RC2080-Pt	BC0034	0.297	0.057	0.013	0.037	0.00317	0.072	0.073	0.046
	SAMPLE_029	RC2080-Pt	BC0035	0.144	0.023	0.000	0.000	0.00007	0.020	0.022	0.045
	SAMPLE_032	RC2080-Pt	BC0036	0.137	0.015	0.000	0.001	0.00022	0.001	0.017	0.213
	SAMPLE_033	RC2080-Pt	BC0037	0.217	0.039	0.006	0.000	0.00007	0.024	0.031	0.127
	SAMPLE_034	RC2080-Pt	BC0039	0.056	0.010	0.000	0.000	0.00005	0.000	0.000	0.017
	SAMPLE_035	RC2080-Pt	BC0040	0.563	0.105	0.023	0.042	0.00071	0.051	0.088	0.121
	SAMPLE_036	RC2080-Pt	BC0041	0.055	0.012	0.000	0.000	0.00005	0.090	0.000	0.028
	SAMPLE_038	RC2080-Pt	BC0042	0.082	0.014	0.000	0.000	0.00006	0.045	0.034	0.047
	SAMPLE_039	RC2080-Pt	BC0084	0.122	0.029	0.013	0.014	0.00219	0.027	0.052	0.052
	SAMPLE_040	RC2080-Pt	BC0085	0.025	0.005	0.000	0.000	0.00006	0.000	0.000	0.027
	SAMPLE_041	RC2080-Pt	BC0087	0.035	0.012	0.007	0.000	0.00005	0.000	0.013	0.000
	SAMPLE_043	RC2080-Pt	BC0088	0.125	0.029	0.000	0.000	0.00005	0.027	0.000	0.000
	SAMPLE_044	RC2080-Pt	BC0089	0.084	0.020	0.000	0.000	0.00006	0.000	0.000	0.000
	SAMPLE_045	RC2080-Pt	BC0090	0.001	0.001	0.000	0.000	0.00005	0.000	0.000	0.000
	SAMPLE_046	RC2080-Pt	BC0091	0.699	0.150	0.035	0.077	0.00588	0.108	0.227	0.061
	SAMPLE_047	RC2080-Pt	BC0093	0.013	0.003	0.009	0.000	0.00005	0.000	0.000	0.000
SAMPLE_049	RC2080-Pt	BC0095	0.016	0.005	0.000	0.000	0.00005	0.000	0.000	0.030	
C a v e s B r a n c h	SAMPLE_114	RC2080-Pt	CB0026	11.764	2.222	0.434	0.900	0.18277	1.673	3.091	0.830
	SAMPLE_115	RC2080-Pt	CB0027	1.222	0.228	0.050	0.100	0.01936	0.117	0.318	0.174
	SAMPLE_116	RC2080-Pt	CB0028	0.275	0.053	0.016	0.051	0.00122	0.076	0.106	0.094
	SAMPLE_118	RC2080-Pt	CB0118	0.478	0.089	0.026	0.093	0.01281	0.311	0.148	0.056
	SAMPLE_119	RC2080-Pt	CB0120	0.264	0.081	0.022	0.067	0.00839	0.100	0.101	0.040
	SAMPLE_120	RC2080-Pt	CB0121	10.509	2.360	0.476	1.357	0.27227	3.079	4.617	1.161
	SAMPLE_122	RC2080-Pt	CB0121e	1.830	0.431	0.086	0.211	0.04500	0.361	0.610	0.236
	SAMPLE_123	RC2080-Pt	CB0122	0.080	0.012	0.000	0.000	0.00007	0.000	0.031	0.061
	SAMPLE_124	RC2080-Pt	CB0123	0.162	0.064	0.022	0.090	0.02094	0.000	0.028	0.019
	SAMPLE_126	RC2080-Pt	CB0193	0.096	0.016	0.000	0.000	0.00011	0.020	0.015	0.076
	SAMPLE_127	RC2080-Pt	CB0196	0.633	0.111	0.028	0.030	0.00486	0.069	0.140	0.063
	SAMPLE_128	RC2080-Pt	CB0197	0.141	0.020	0.000	0.000	0.00009	0.000	0.014	0.093
	SAMPLE_130	RC2080-Pt	CB0200	0.378	0.062	0.017	0.063	0.00085	0.180	0.161	0.174
	SAMPLE_131	RC2080-Pt	CB0205	0.017	0.005	0.005	0.000	0.00006	0.000	0.000	0.000
	SAMPLE_132	RC2080-Pt	CB0207	0.000	0.011	0.000	0.000	0.00006	0.000	0.000	0.019
SAMPLE_133	RC2080-Pt	CB0208	26.212	5.351	1.077	2.962	0.74211	5.972	12.275	2.496	

Elemental concentrations below detection limits are shown as negative values in the appendix; the values represent minimum detectable concentrations (MDCs) given the sample mass and all other analytical parameters and should be interpreted as “less than” the value indicated. The MDCs were substituted for missing values in quantitative analyses, as they indicate extreme low values that can be converted to a log scale, unlike zero.

Table 6a. Absolute Values for Rare Earth Element concentration in ppm. Baton Creek and Cave’s Branch groups shown.

Rare Earth Element Data for Speleothem Samples. All values in ppm.

Group	INAA ID	Batch	Vial ID	La	Sm	Eu	Yb	Lu	Hf	Th	U	
M a c a l	SAMPLE_002	RC2080-Pt	M0009	0.000	0.017	0.000	0.000	0.00009	0.000	0.000	0.149	
	SAMPLE_003	RC2080-Pt	M0011	0.000	0.014	0.000	0.000	0.00008	0.000	0.000	0.087	
	SAMPLE_004	RC2080-Pt	M0013	0.541	0.114	0.000	0.100	0.00001	0.145	0.173	0.236	
	SAMPLE_005	RC2080-Pt	M0014	0.000	0.001	0.000	0.000	0.00006	0.000	0.000	0.029	
	SAMPLE_006	RC2080-Pt	M0015	0.032	0.006	0.000	0.014	0.00008	0.000	0.056	0.135	
	SAMPLE_007	RC2080-Pt	M0016	0.264	0.051	0.020	0.055	0.00139	0.000	0.042	0.144	
	SAMPLE_009	RC2080-Pt	M0017	0.015	0.000	0.000	0.000	0.00009	0.000	0.000	0.482	
	SAMPLE_010	RC2080-Pt	M0018	0.016	0.013	0.000	0.000	0.00007	0.000	0.000	0.102	
	SAMPLE_011	RC2080-Pt	M0019	0.006	0.000	0.000	0.000	0.00008	0.000	0.000	0.087	
	SAMPLE_012	RC2080-Pt	M0022	0.996	0.224	0.049	0.149	0.02050	0.062	0.048	0.157	
	SAMPLE_013	RC2080-Pt	M0023	0.358	0.079	0.023	0.071	0.00170	0.026	0.063	0.376	
	SAMPLE_014	RC2080-Pt	M0111	0.016	0.001	0.005	0.000	0.00007	0.007	0.000	0.189	
	SAMPLE_016	RC2080-Pt	M0113	0.074	0.010	0.000	0.000	0.00007	0.014	0.027	0.094	
	SAMPLE_017	RC2080-Pt	M0124	0.758	0.172	0.048	0.112	0.00743	0.061	0.031	0.338	
	SAMPLE_018	RC2080-Pt	M0125	0.105	0.002	0.000	0.000	0.00009	0.025	0.018	0.713	
	SAMPLE_019	RC2080-Pt	M0126	1.296	1.485	0.034	0.096	0.00021	0.141	0.166	12.215	
	SAMPLE_020	RC2080-Pt	M0128	0.028	0.001	0.000	0.000	0.00008	0.000	0.000	0.342	
	SAMPLE_021	RC2080-Pt	M0139	0.023	0.013	0.006	0.000	0.00009	0.000	0.000	0.001	
	SAMPLE_023	RC2080-Pt	M0153	0.049	0.008	0.000	0.000	0.00008	0.000	0.012	0.077	
	SAMPLE_024	RC2080-Pt	M0170	0.209	0.037	0.000	0.000	0.00010	0.039	0.046	0.113	
	SAMPLE_025	RC2080-Pt	M0171	0.038	0.004	0.000	0.000	0.00007	0.000	0.013	0.138	
	SAMPLE_027	RC2080-Pt	M0172	0.039	0.006	0.000	0.000	0.00007	0.000	0.000	0.049	
	P i n e R i d g e	SAMPLE_069	RC2080-Pt	PR0078	1.239	0.234	0.055	0.152	0.00573	0.200	0.321	0.517
		SAMPLE_070	RC2080-Pt	PR0080	0.247	0.049	0.013	0.032	0.00001	0.000	0.051	0.092
		SAMPLE_071	RC2080-Pt	PR0081	2.449	0.514	0.109	0.237	0.06024	0.453	0.663	0.143
		SAMPLE_073	RC2080-Pt	PR0082	0.044	0.011	0.000	0.000	0.00006	0.000	0.000	0.040
		SAMPLE_074	RC2080-Pt	PR0083	0.070	0.009	0.000	0.000	0.00006	0.000	0.000	0.140
SAMPLE_075		RC2080-Pt	PR0083A	15.659	2.541	0.502	1.127	0.26545	1.497	2.589	0.440	
SAMPLE_076		RC2080-Pt	PR0132	0.316	0.069	0.013	0.054	0.00289	0.039	0.057	0.190	
SAMPLE_077		RC2080-Pt	PR0133	0.019	0.003	0.000	0.000	0.00006	0.005	0.000	0.000	
SAMPLE_079		RC2080-Pt	PR0133A	0.281	0.054	0.012	0.000	0.00010	0.029	0.115	0.051	
SAMPLE_080		RC2080-Pt	PR0134	0.068	0.000	0.012	0.000	0.00009	0.000	0.025	0.787	
SAMPLE_081		RC2080-Pt	PR0135	0.032	0.005	0.000	0.000	0.00006	0.000	0.012	0.130	
SAMPLE_082		RC2080-Pt	PR0140	0.070	0.001	0.000	0.021	0.00007	0.000	0.011	0.285	
SAMPLE_083		RC2080-Pt	PR0141	0.403	0.071	0.021	0.039	0.01412	0.047	0.076	0.039	
SAMPLE_085		RC2080-Pt	PR0142	0.000	0.004	0.001	0.000	0.00006	0.000	0.000	0.035	

Elemental concentrations below detection limits are shown as negative values in the appendix; the values represent minimum detectable concentrations (MDCs) given the sample mass and all other analytical parameters and should be interpreted as "less than" the value indicated. The MDCs were substituted for missing values in quantitative analyses, as they indicate extreme low values that can be converted to a log scale, unlike zero.

Table 6b. (cont.) Absolute Values Rare Earth Element concentration in ppm. Macal and Pine Ridge groups shown.

Rare Earth Element Data for Speleothem Samples. All values in ppm.

Group	INAA ID	Batch	Vial ID	La	Sm	Eu	Yb	Lu	Hf	Th	U
R o a r i n g C r e e k	SAMPLE_086	RC2080-Pt	RC0029	2.539	0.565	0.093	0.164	0.03396	0.210	0.502	0.145
	SAMPLE_087	RC2080-Pt	RC0030	4.324	0.833	0.121	0.377	0.06833	0.912	0.845	0.276
	SAMPLE_088	RC2080-Pt	RC0031	0.035	0.002	0.000	0.000	0.00008	0.028	0.000	0.187
	SAMPLE_089	RC2080-Pt	RC0032	1.114	0.237	0.058	0.109	0.01564	0.210	0.421	0.201
	SAMPLE_092	RC2080-Pt	RC0033	0.094	0.001	0.012	0.000	0.00013	0.000	0.025	0.672
	SAMPLE_093	RC2080-Pt	RC0043	0.013	0.001	0.000	0.000	0.00012	0.028	0.000	0.000
	SAMPLE_094	RC2080-Pt	RC0044	0.098	0.020	0.000	0.000	0.00012	0.000	0.033	0.001
	SAMPLE_096	RC2080-Pt	RC0045	0.395	0.083	0.012	0.028	0.00711	0.091	0.186	0.049
	SAMPLE_097	RC2080-Pt	RC0146	0.071	0.022	0.000	0.000	0.00008	0.000	0.000	0.000
	SAMPLE_098	RC2080-Pt	RC0147	0.045	0.001	0.006	0.023	0.00013	0.000	0.000	0.295
	SAMPLE_100	RC2080-Pt	RC0148	0.009	0.015	0.007	0.000	0.00012	0.000	0.000	0.106
	SAMPLE_101	RC2080-Pt	RC0149	1.159	0.232	0.024	0.075	0.01351	0.154	0.392	0.090
	SAMPLE_102	RC2080-Pt	RC0150	0.005	0.000	0.000	0.000	0.00012	0.000	0.000	0.001
	SAMPLE_104	RC2080-Pt	RC0151	1.062	0.253	0.047	0.124	0.02703	0.258	0.371	0.142
	SAMPLE_105	RC2080-Pt	RC0164	13.889	3.368	0.560	1.698	0.43961	2.789	5.102	2.258
	SAMPLE_106	RC2080-Pt	RC0175	0.027	0.003	0.000	0.000	0.00009	0.000	0.000	0.077
	SAMPLE_108	RC2080-Pt	RC0176	20.078	3.946	0.686	2.212	0.50850	4.252	5.321	2.865
SAMPLE_109	RC2080-Pt	RC0177	0.490	0.114	0.034	0.078	0.02401	0.047	0.022	0.001	
SAMPLE_110	RC2080-Pt	RC0180	0.648	0.180	0.035	0.122	0.02554	0.115	0.150	0.088	
SAMPLE_111	RC2080-Pt	RC0181	1.476	0.365	0.081	0.144	0.04158	0.194	0.271	0.139	
S a n A n t o n i o	SAMPLE_050	RC2080-Pt	SA0096	0.133	0.029	0.000	0.023	0.00007	0.026	0.034	0.106
	SAMPLE_051	RC2080-Pt	SA0097	0.432	0.088	0.017	0.090	0.01228	0.084	0.160	0.149
	SAMPLE_052	RC2080-Pt	SA0098	0.000	0.001	0.000	0.000	0.00006	0.000	0.000	0.060
	SAMPLE_053	RC2080-Pt	SA0100	0.014	0.011	0.000	0.000	0.00006	0.000	0.000	0.081
	SAMPLE_055	RC2080-Pt	SA0101	0.295	0.059	0.021	0.000	0.00007	0.078	0.085	0.174
	SAMPLE_056	RC2080-Pt	SA0102	0.019	0.011	0.000	0.000	0.00005	0.000	0.022	0.041
	SAMPLE_057	RC2080-Pt	SA0103	0.765	0.147	0.035	0.090	0.01253	0.156	0.254	0.140
	SAMPLE_058	RC2080-Pt	SA0104	0.199	0.034	0.008	0.000	0.00006	0.000	0.031	0.095
	SAMPLE_059	RC2080-Pt	SA0106	0.086	0.017	0.000	0.019	0.00005	0.000	0.012	0.000
	SAMPLE_062	RC2080-Pt	SA0108	0.007	0.003	0.000	0.000	0.00006	0.000	0.000	0.000
	SAMPLE_063	RC2080-Pt	SA0129	0.250	0.067	0.020	0.102	0.01613	0.000	0.000	0.184
	SAMPLE_064	RC2080-Pt	SA0130	0.843	0.194	0.037	0.083	0.01491	0.046	0.121	0.001
	SAMPLE_065	RC2080-Pt	SA0131	2.042	0.443	0.086	0.207	0.02667	0.271	0.747	0.206
	SAMPLE_066	RC2080-Pt	SA0190	0.005	0.000	0.000	0.000	0.00007	0.000	0.000	0.000
	SAMPLE_068	RC2080-Pt	SA0192	0.010	0.012	0.000	0.000	0.00006	0.176	0.000	0.080

Elemental concentrations below detection limits are shown as negative values in the appendix; the values represent minimum detectable concentrations (MDCs) given the sample mass and all other analytical parameters and should be interpreted as "less than" the value indicated. The MDCs were substituted for missing values in quantitative analyses, as they indicate extreme low values that can be converted to a log scale, unlike zero.

Table 6c. Absolute Values for Rare Earth Element concentration in Log Base 10. Barton Creek and Cave's Branch groups shown.

Major and Trace Element Data for Speleothem Samples. All values in Log₁₀[ppm].

Group	INAA ID	Batch	Vial ID	Al	Na	Mg	Ca	Ti	Mn	Sc	Cr	Fe	Co	Zn	Sr	Cs	Ba
B a r t o n	SAMPLE_028	RC2080-Pt	BC0034	2.675	1.057	2.705	5.594	0.157	0.334	-1.173	-2.405	2.169	-1.226	-0.103	2.973	-1.072	1.587
	SAMPLE_029	RC2080-Pt	BC0035	2.341	1.561	3.383	5.598	0.164	0.610	-1.651	-2.427	2.153	-3.501	-1.537	2.973	-1.473	1.867
	SAMPLE_032	RC2080-Pt	BC0036	2.773	2.482	2.204	5.564	1.688	1.752	-1.346	-1.896	2.253	-0.913	2.159	1.887	-1.320	1.497
	SAMPLE_033	RC2080-Pt	BC0037	2.418	1.652	3.707	5.596	0.186	0.903	-1.498	-2.354	1.928	-1.264	1.046	2.904	-1.497	1.862
	SAMPLE_034	RC2080-Pt	BC0039	2.175	1.266	2.111	5.602	0.158	0.189	-1.785	-2.424	1.664	-1.478	-1.348	-0.932	-3.556	0.943
	SAMPLE_035	RC2080-Pt	BC0040	2.851	1.392	3.143	5.590	0.187	0.841	-0.892	-0.180	2.441	-0.944	-1.299	1.544	-0.969	1.396
	SAMPLE_036	RC2080-Pt	BC0041	2.141	1.286	0.859	5.593	0.159	0.100	-1.434	-2.421	1.507	-1.597	0.268	1.064	-1.796	-1.176
	SAMPLE_038	RC2080-Pt	BC0042	2.473	1.513	2.447	5.599	0.171	0.555	-1.403	-1.090	1.920	-1.067	0.312	1.278	-1.498	-1.181
	SAMPLE_039	RC2080-Pt	BC0084	2.695	1.408	2.672	5.602	0.181	0.838	-1.156	-0.412	2.238	-1.052	0.958	-0.880	-1.508	-1.147
C r e e k	SAMPLE_040	RC2080-Pt	BC0085	2.257	1.437	2.420	5.603	0.168	0.156	-1.749	-2.395	1.654	-1.400	0.498	-0.918	-3.540	-1.169
	SAMPLE_041	RC2080-Pt	BC0087	2.334	0.983	0.856	5.600	0.169	1.220	-1.765	-2.446	1.687	-0.680	-1.356	-0.935	-3.583	0.773
	SAMPLE_043	RC2080-Pt	BC0088	2.391	1.292	2.317	5.602	0.176	1.181	-1.400	-0.608	1.853	-0.607	0.176	1.369	-1.906	0.794
	SAMPLE_044	RC2080-Pt	BC0089	2.478	1.576	2.317	5.605	0.180	1.082	-1.523	-2.395	2.125	-1.187	0.676	1.453	-1.243	-1.150
	SAMPLE_045	RC2080-Pt	BC0090	1.989	1.780	2.801	5.600	0.163	-1.983	-2.903	-2.436	-0.603	-3.511	-1.419	1.611	-3.642	0.940
	SAMPLE_046	RC2080-Pt	BC0091	3.281	1.627	2.593	5.589	2.041	1.691	-0.414	0.377	2.999	0.027	1.312	1.572	-0.385	0.775
	SAMPLE_047	RC2080-Pt	BC0093	2.145	1.203	2.356	5.592	0.147	0.059	-2.082	-2.430	-0.560	-3.533	0.108	1.172	-3.594	0.609
	SAMPLE_049	RC2080-Pt	BC0095	2.045	1.175	2.513	5.586	0.133	-0.001	-1.667	-2.416	1.536	-1.137	0.327	1.298	-1.441	-1.184
	C a v e ' s B r a n c h	SAMPLE_114	RC2080-Pt	CB0026	4.291	2.455	2.102	5.525	3.043	2.831	0.543	1.238	3.953	0.739	1.421	-0.347	0.594
SAMPLE_115		RC2080-Pt	CB0027	3.385	1.809	2.186	5.585	2.147	2.007	-0.397	0.320	3.022	-0.160	0.606	-0.700	-0.333	1.683
SAMPLE_116		RC2080-Pt	CB0028	2.783	1.571	2.461	5.589	0.177	0.644	-0.996	-0.184	2.318	-1.092	-1.316	1.501	-1.149	1.285
SAMPLE_118		RC2080-Pt	CB0118	2.950	1.434	-1.000	5.598	1.799	0.807	-0.775	0.292	2.580	-0.874	0.859	-0.795	-0.919	-1.093
SAMPLE_119		RC2080-Pt	CB0120	3.046	1.198	2.879	5.584	1.768	0.932	-0.787	0.410	2.686	-0.856	-1.280	-0.808	-1.441	-1.100
SAMPLE_120		RC2080-Pt	CB0121	4.511	2.531	2.760	5.471	3.364	2.026	0.797	1.672	4.167	0.421	1.780	-0.255	0.449	1.957
SAMPLE_122		RC2080-Pt	CB0121a	3.759	1.609	2.454	5.585	2.395	1.787	-0.059	0.893	3.409	-0.197	1.391	-0.607	-0.611	-0.859
SAMPLE_123		RC2080-Pt	CB0122	2.517	1.291	2.398	5.600	0.166	0.519	-1.471	-0.040	2.028	-1.494	0.268	0.888	-3.500	-1.152
SAMPLE_124		RC2080-Pt	CB0123	2.223	1.271	0.861	5.605	0.875	-0.175	-0.891	-2.404	-0.536	-3.539	-1.321	0.609	-1.424	-1.102
SAMPLE_126		RC2080-Pt	CB0193	2.501	1.610	2.960	5.585	0.171	0.605	-1.470	-0.187	1.947	-1.260	-1.359	1.273	-1.679	-1.141
SAMPLE_127		RC2080-Pt	CB0196	2.928	1.795	3.083	5.601	1.696	1.301	-0.865	-0.035	2.537	-0.982	-1.283	1.598	-0.849	1.352
SAMPLE_128		RC2080-Pt	CB0197	2.452	1.514	2.337	5.605	0.171	0.988	-1.506	-0.660	1.943	-1.294	0.572	1.242	-1.633	-1.110
SAMPLE_130		RC2080-Pt	CB0200	3.156	1.337	2.658	5.598	1.942	1.130	-0.715	0.138	2.686	-0.749	1.012	1.430	-1.069	-1.022
SAMPLE_131		RC2080-Pt	CB0205	2.112	1.144	0.852	5.595	0.159	0.008	-1.932	-2.415	-0.573	-3.541	-0.034	1.220	-3.571	0.666
SAMPLE_132	RC2080-Pt	CB0207	1.996	0.872	0.862	5.601	0.159	-0.573	-2.076	-2.414	-0.619	-3.563	0.240	1.469	-3.587	-1.152	
SAMPLE_133	RC2080-Pt	CB0208	4.953	3.102	-1.000	4.465	3.719	2.284	1.259	2.006	4.638	0.818	2.213	-0.025	1.027	2.730	

Elemental concentrations below detection limits are shown as negative values in the appendix; the values represent minimum detectable concentrations (MDCs) given the sample mass and all other analytical parameters and should be interpreted as "less than" the value indicated. The MDCs were substituted for missing values in quantitative analyses, as they indicate extreme low values that can be converted to a log scale, unlike zero.

Table 7a. Major and Trace element concentration in Log Base 10. Baton Creek and Cave's Branch Groups shown.

Major and Trace Element Data for Speleothem Samples. All values in Log₁₀[ppm].

Group	INAA ID	Batch	Vial ID	Al	Na	Mg	Ca	Ti	Mn	Sc	Cr	Fe	Co	Zn	Sr	Cs	Ba	
M a c a l	SAMPLE_002	RC2080-Pt	M0009	1.949	1.378	0.860	5.605	0.153	-0.269	-2.485	-2.505	-0.627	-0.933	-1.464	-0.033	-3.617	-1.250	
	SAMPLE_003	RC2080-Pt	M0011	2.092	1.640	1.536	5.603	0.155	-0.302	-2.269	-2.523	-0.612	-3.619	0.577	1.118	-3.617	-1.233	
	SAMPLE_004	RC2080-Pt	M0013	3.269	1.640	2.731	5.592	1.947	1.569	-0.577	0.152	2.853	-0.528	1.131	-0.734	-0.616	1.017	
	SAMPLE_005	RC2080-Pt	M0014	1.948	0.894	3.038	5.604	0.150	-2.003	-2.455	-2.521	-0.641	-3.565	-1.509	-0.910	-3.617	-1.217	
	SAMPLE_006	RC2080-Pt	M0015	2.447	1.239	2.810	5.602	0.150	-0.059	-1.593	-2.508	-0.579	-1.617	0.215	-0.894	-1.461	-1.219	
	SAMPLE_007	RC2080-Pt	M0016	2.739	1.439	2.662	5.600	0.158	0.720	-1.149	-0.239	2.208	-1.398	0.442	0.882	-1.440	-1.160	
	SAMPLE_009	RC2080-Pt	M0017	2.007	1.875	2.757	5.606	0.158	-0.653	-4.666	-2.527	-0.644	-1.439	-1.492	1.440	-3.611	1.126	
	SAMPLE_010	RC2080-Pt	M0018	2.031	1.479	2.570	5.593	1.409	-0.299	-2.133	-2.525	1.447	-1.934	-1.501	-0.872	-3.624	-1.234	
	SAMPLE_011	RC2080-Pt	M0019	1.909	1.500	2.607	5.602	1.564	-2.016	-4.689	-0.911	-0.657	-3.568	0.296	1.425	-3.698	1.107	
	SAMPLE_012	RC2080-Pt	M0022	2.740	1.196	2.668	5.599	0.165	0.809	-0.648	-0.488	2.326	-1.076	0.133	-0.817	-1.236	-1.093	
	SAMPLE_013	RC2080-Pt	M0023	2.821	1.500	2.523	5.599	0.177	1.055	-0.903	-0.215	2.451	-0.849	0.440	1.320	-1.293	1.057	
	SAMPLE_014	RC2080-Pt	M0111	2.143	1.241	2.214	5.607	0.154	0.577	-2.341	-0.939	1.318	-1.076	0.329	-0.871	-3.638	-1.207	
	SAMPLE_016	RC2080-Pt	M0113	2.348	1.106	1.132	5.601	0.148	0.570	-1.488	-0.332	1.992	-1.529	0.335	0.155	-1.636	-1.231	
	SAMPLE_017	RC2080-Pt	M0124	2.502	1.545	3.158	5.598	0.161	0.636	-0.913	-0.293	2.310	-1.533	0.642	1.283	-1.268	0.973	
	SAMPLE_018	RC2080-Pt	M0125	2.552	2.133	2.797	5.590	0.162	0.869	-1.428	-0.673	2.066	-1.534	0.292	1.015	-1.466	1.080	
	SAMPLE_019	RC2080-Pt	M0126	3.195	1.798	2.835	5.595	1.826	1.360	-0.592	0.311	2.854	-0.677	-1.339	2.550	-0.865	2.216	
	SAMPLE_020	RC2080-Pt	M0128	2.249	1.624	3.287	5.600	1.450	0.068	-2.074	-2.521	1.529	-3.584	0.246	1.360	-3.620	-1.169	
	SAMPLE_021	RC2080-Pt	M0139	2.210	1.469	2.332	5.586	0.143	0.173	-1.983	-0.843	-0.640	-3.568	0.093	1.380	-3.627	1.148	
	SAMPLE_023	RC2080-Pt	M0153	2.332	1.389	0.847	5.595	0.160	0.567	-1.735	-0.258	1.837	-1.631	0.118	-0.895	-3.611	1.710	
	SAMPLE_024	RC2080-Pt	M0170	2.598	1.640	2.443	5.593	0.173	1.159	-1.323	-2.461	2.169	-1.202	0.503	-0.848	-1.403	0.517	
	SAMPLE_025	RC2080-Pt	M0171	2.259	1.238	0.863	5.596	0.155	0.482	-1.782	-2.517	1.731	-3.536	0.206	1.317	-3.649	0.272	
	SAMPLE_027	RC2080-Pt	M0172	2.312	1.085	2.219	5.601	0.150	0.355	-1.756	-0.537	1.776	-1.342	0.109	0.802	-3.582	0.643	
	P i n e R i d g e	SAMPLE_069	RC2080-Pt	PR0078	3.434	2.188	3.853	5.570	2.223	1.763	-0.336	0.590	3.149	-0.255	1.227	1.976	-0.487	1.634
		SAMPLE_070	RC2080-Pt	PR0080	2.668	1.299	2.503	5.594	0.174	0.928	-1.064	-0.314	2.325	-1.068	0.208	1.038	-1.579	1.282
		SAMPLE_071	RC2080-Pt	PR0081	3.740	1.691	2.714	5.569	2.484	1.992	-0.002	0.806	3.468	0.076	0.625	-0.565	-0.472	1.001
		SAMPLE_073	RC2080-Pt	PR0082	2.258	1.347	3.010	5.596	0.164	0.293	-1.763	-2.499	1.657	-1.710	0.060	-0.867	-3.644	0.857
		SAMPLE_074	RC2080-Pt	PR0083	2.339	1.804	3.536	5.587	0.181	0.413	-1.636	-2.492	1.884	-1.432	-1.461	2.185	-3.588	1.467
SAMPLE_075		RC2080-Pt	PR0083A	4.297	1.966	3.421	5.517	2.960	2.528	0.524	1.233	3.944	0.508	1.406	-0.359	0.208	1.548	
SAMPLE_076		RC2080-Pt	PR0132	2.795	1.756	2.260	5.580	0.183	1.385	-1.236	-0.543	2.094	-0.838	0.382	1.500	-1.256	1.110	
SAMPLE_077		RC2080-Pt	PR0133	2.109	1.157	0.843	5.604	0.160	0.092	-2.096	-2.524	-0.613	-3.578	-1.471	1.379	-3.627	-1.207	
SAMPLE_079		RC2080-Pt	PR0133A	2.889	1.530	2.522	5.587	0.176	0.492	-0.905	0.001	2.601	-0.854	-1.399	1.613	-1.026	-1.102	
SAMPLE_080		RC2080-Pt	PR0134	2.320	2.218	3.635	5.582	0.186	0.699	-1.742	-0.362	1.746	-1.448	0.701	2.290	-1.426	2.014	
SAMPLE_081		RC2080-Pt	PR0135	2.218	1.311	2.971	5.604	0.167	0.172	-1.875	-2.502	1.412	-3.570	0.028	1.447	-3.578	0.963	
SAMPLE_082		RC2080-Pt	PR0140	2.511	1.773	3.529	5.575	0.180	0.826	-1.585	-0.269	1.893	-3.483	0.374	1.867	-1.322	2.563	
SAMPLE_083		RC2080-Pt	PR0141	2.804	2.730	2.383	5.586	1.342	1.606	-0.923	-0.250	2.351	-1.033	0.785	2.027	-0.939	1.803	
SAMPLE_085		RC2080-Pt	PR0142	2.121	1.334	2.576	5.602	0.167	0.049	-2.077	-2.486	-0.654	-3.595	0.168	1.487	-3.634	1.942	

Elemental concentrations below detection limits are shown as negative values in the appendix; the values represent minimum detectable concentrations (MDCs) given the sample mass and all other analytical parameters and should be interpreted as "less than" the value indicated. The MDCs were substituted for missing values in quantitative analyses, as they indicate extreme low values that can be converted to a log scale, unlike zero.

Table 7b. (Cont.) Major and Trace element concentration in Log Base 10. Macal and Pine Ridge Groups shown.

Major and Trace Element Data for Speleothem Samples. All values in Log₁₀[ppm].

Group	INAA ID	Batch	Vial ID	Al	Na	Mg	Ca	Ti	Mn	Sc	Cr	Fe	Co	Zn	Sr	Cs	Ba	
R o a r i n g	SAMPLE_086	RC2080-Pt	RC0029	3.505	1.829	2.976	5.584	2.173	1.974	-0.217	0.411	3.142	-0.159	0.848	1.549	-0.366	1.300	
	SAMPLE_087	RC2080-Pt	RC0030	3.299	1.688	1.976	5.596	2.257	1.667	-0.414	0.279	2.954	-0.367	0.280	1.496	-0.563	1.173	
	SAMPLE_088	RC2080-Pt	RC0031	2.252	1.960	3.380	5.591	0.171	0.526	-1.831	-2.470	1.838	-1.411	0.518	1.936	-3.611	1.738	
	SAMPLE_089	RC2080-Pt	RC0032	3.589	1.603	2.801	5.585	2.234	1.459	-0.142	0.466	3.216	-0.294	1.665	-0.612	-0.256	1.106	
	SAMPLE_092	RC2080-Pt	RC0033	2.563	1.728	3.930	5.576	0.200	0.780	-1.524	-2.355	2.047	-1.059	1.240	1.911	-1.265	2.493	
	SAMPLE_093	RC2080-Pt	RC0043	2.060	1.442	2.949	5.601	0.156	-0.449	-2.228	-2.468	-0.572	-3.570	-0.317	1.170	-3.566	1.361	
	SAMPLE_094	RC2080-Pt	RC0044	2.484	1.254	2.663	5.602	1.618	0.509	-1.388	-2.398	2.077	-1.145	0.378	1.309	-3.488	1.348	
	SAMPLE_096	RC2080-Pt	RC0045	2.997	1.498	2.778	5.596	1.828	0.746	-0.833	-0.046	2.641	-0.984	0.752	1.103	-1.020	1.455	
	SAMPLE_097	RC2080-Pt	RC0146	2.244	1.244	0.849	5.609	0.170	-0.016	-1.381	-2.435	1.555	-3.471	-1.411	-0.974	-3.550	-1.189	
	SAMPLE_098	RC2080-Pt	RC0147	2.236	1.740	3.473	5.598	0.181	-0.022	-1.886	-2.434	1.497	-3.582	-1.369	1.852	-3.562	1.411	
	SAMPLE_100	RC2080-Pt	RC0148	1.977	1.666	3.565	5.598	0.170	-1.920	-2.490	-2.447	-0.611	-3.580	-0.604	1.652	-3.574	1.318	
C r e e k	SAMPLE_101	RC2080-Pt	RC0149	3.293	1.710	2.834	5.598	1.999	1.253	-0.527	0.041	2.885	-0.687	0.610	1.260	-0.547	1.083	
	SAMPLE_102	RC2080-Pt	RC0150	2.050	1.147	2.600	5.599	0.157	-0.062	-4.611	-2.457	1.546	-3.524	-1.401	1.289	-3.590	1.105	
	SAMPLE_104	RC2080-Pt	RC0151	3.620	1.480	2.685	5.586	2.424	2.047	-0.181	0.456	3.553	0.481	0.975	-0.678	-0.562	1.518	
	SAMPLE_105	RC2080-Pt	RC0164	4.678	3.058	3.748	5.336	3.376	2.330	0.904	1.543	4.288	0.598	1.839	2.086	0.399	2.194	
	SAMPLE_106	RC2080-Pt	RC0175	2.273	1.338	2.550	5.601	0.163	0.068	-1.873	-2.428	1.758	-1.519	0.295	1.461	-3.553	1.228	
	SAMPLE_108	RC2080-Pt	RC0176	4.534	2.959	-1.000	5.410	3.381	2.572	0.797	1.471	4.170	0.556	3.218	-0.178	0.697	2.449	
	SAMPLE_109	RC2080-Pt	RC0177	2.661	1.294	2.478	5.595	0.172	0.725	-0.921	-2.360	2.291	-1.244	0.912	1.418	-1.254	-1.049	
	SAMPLE_110	RC2080-Pt	RC0180	3.162	1.405	2.307	5.590	1.882	1.023	-0.511	0.037	2.835	-0.790	0.897	1.592	-1.045	1.318	
	SAMPLE_111	RC2080-Pt	RC0181	3.396	1.284	2.773	5.590	2.046	1.213	-0.303	0.203	3.055	-0.600	1.242	1.473	-0.941	1.460	
	S a n A n t i o	SAMPLE_050	RC2080-Pt	SA0096	2.713	1.124	2.075	5.604	0.183	0.932	-1.193	-2.353	2.223	-1.280	1.136	0.930	-1.664	-1.078
		SAMPLE_051	RC2080-Pt	SA0097	3.168	1.571	2.235	5.596	0.207	1.204	-0.681	0.101	2.786	-0.501	0.661	1.267	-1.481	-1.052
SAMPLE_052		RC2080-Pt	SA0098	2.104	1.303	2.488	5.597	0.159	-0.541	-2.559	-2.455	-0.623	-3.524	-1.447	1.252	-3.629	-1.194	
SAMPLE_053		RC2080-Pt	SA0100	2.138	1.357	2.185	5.601	0.167	0.348	-2.257	-2.438	-0.605	-3.538	-1.422	1.212	-3.633	-1.162	
SAMPLE_055		RC2080-Pt	SA0101	2.983	1.478	2.617	5.587	1.445	1.015	-0.902	-0.197	2.544	-0.759	0.416	1.210	-1.452	-1.088	
SAMPLE_056		RC2080-Pt	SA0102	2.358	1.359	2.709	5.596	0.161	0.385	-1.596	-0.983	1.883	-1.401	-0.153	1.574	-1.324	1.681	
SAMPLE_057		RC2080-Pt	SA0103	3.368	1.532	3.104	5.585	1.826	1.468	-0.424	0.310	3.040	-0.313	1.159	1.435	-0.386	1.855	
SAMPLE_058		RC2080-Pt	SA0104	2.512	1.364	2.751	5.601	0.160	0.557	-1.325	-0.298	2.126	-1.414	0.885	-0.897	-1.260	0.918	
SAMPLE_059		RC2080-Pt	SA0106	2.304	1.423	2.102	5.596	0.170	0.504	-1.663	-2.420	1.732	-1.618	0.049	1.239	-3.554	-1.152	
SAMPLE_062		RC2080-Pt	SA0108	2.163	1.283	2.785	5.591	0.161	0.035	-2.180	-2.521	1.519	-1.441	-0.087	1.460	-3.602	1.115	
SAMPLE_063		RC2080-Pt	SA0129	2.249	1.090	2.830	5.608	0.166	0.031	-0.969	-2.450	1.658	-1.688	0.893	1.246	-3.511	1.021	
SAMPLE_064	RC2080-Pt	SA0130	2.806	1.440	2.630	5.590	0.181	1.164	-0.930	-0.193	2.390	-0.589	0.077	0.504	-0.880	1.108		
SAMPLE_065	RC2080-Pt	SA0131	3.700	1.738	3.027	5.566	2.375	1.831	-0.100	0.620	3.314	-0.135	1.000	-0.696	-0.035	1.416		
SAMPLE_066	RC2080-Pt	SA0190	2.132	1.457	2.908	5.595	0.162	0.935	-2.219	-2.515	-0.578	-3.465	0.997	1.286	-3.611	-1.231		
SAMPLE_068	RC2080-Pt	SA0192	2.154	1.470	2.492	5.605	0.155	-0.312	-2.392	-2.519	-0.603	-3.643	-1.466	1.555	-3.602	1.222		

Elemental concentrations below detection limits are shown as negative values in the appendix; the values represent minimum detectable concentrations (MDCs) given the sample mass and all other analytical parameters and should be interpreted as "less than" the value indicated. The MDCs were substituted for missing values in quantitative analyses, as they indicate extreme low values that can be converted to a log scale, unlike zero.

Table 7c. (Cont.) Major and Trace element concentration in Log Base 10. Roaring Creek and San Antonio Groups shown.

Major Rare Earth Element Data for Speleothem Samples. All values in Log₁₀[ppm].

Group	INAA ID	Batch	Vial ID	La	Sm	Eu	Yb	Lu	Hf	Th	U
B a r t o n C r e e k	SAMPLE_028	RC2080-Pt	BC0034	-0.031	-0.546	-0.766	-0.777	-1.018	-1.143	-1.136	-1.339
	SAMPLE_029	RC2080-Pt	BC0035	-0.344	-0.946	-2.859	-2.944	-2.669	-1.693	-1.656	-1.346
	SAMPLE_032	RC2080-Pt	BC0036	-0.366	-1.118	-2.799	-2.500	-2.170	-3.170	-1.774	-0.672
	SAMPLE_033	RC2080-Pt	BC0037	-0.167	-0.707	-1.112	-2.871	-2.678	-1.628	-1.505	-0.897
	SAMPLE_034	RC2080-Pt	BC0039	-0.758	-1.285	-2.794	-2.967	-2.782	-3.584	-3.632	-1.774
	SAMPLE_035	RC2080-Pt	BC0040	0.247	-0.279	-0.527	-0.722	-1.669	-1.289	-1.056	-0.916
	SAMPLE_036	RC2080-Pt	BC0041	-0.761	-1.230	-2.770	-2.981	-2.790	-1.046	-3.641	-1.549
	SAMPLE_038	RC2080-Pt	BC0042	-0.591	-1.159	-2.779	-2.920	-2.732	-1.346	-1.470	-1.324
	SAMPLE_039	RC2080-Pt	BC0084	-0.417	-0.845	-0.778	-1.204	-1.179	-1.568	-1.280	-1.282
	SAMPLE_040	RC2080-Pt	BC0085	-1.107	-1.624	-2.806	-2.973	-2.758	-3.566	-3.612	-1.575
	SAMPLE_041	RC2080-Pt	BC0087	-0.958	-1.239	-1.057	-3.030	-2.835	-3.594	-1.902	-3.476
	SAMPLE_043	RC2080-Pt	BC0088	-0.408	-0.832	-2.768	-2.968	-2.778	-1.562	-3.623	-3.394
	SAMPLE_044	RC2080-Pt	BC0089	-0.579	-1.007	-2.778	-2.900	-2.729	-3.561	-3.617	-3.330
SAMPLE_045	RC2080-Pt	BC0090	-2.484	-2.301	-2.845	-2.982	-2.795	-3.618	-3.669	-3.376	
SAMPLE_046	RC2080-Pt	BC0091	0.341	-0.126	-0.342	-0.459	-0.749	-0.968	-0.645	-1.213	
SAMPLE_047	RC2080-Pt	BC0093	-1.394	-1.820	-0.904	-2.987	-2.793	-3.605	-3.649	-3.378	
SAMPLE_049	RC2080-Pt	BC0095	-1.294	-1.621	-2.855	-2.974	-2.790	-3.598	-3.634	-1.529	
C a v e s B r a n c h	SAMPLE_114	RC2080-Pt	CB0026	1.567	1.046	0.756	0.610	0.743	0.224	0.490	-0.081
	SAMPLE_115	RC2080-Pt	CB0027	0.583	0.056	-0.180	-0.345	-0.232	-0.934	-0.498	-0.759
	SAMPLE_116	RC2080-Pt	CB0028	-0.064	-0.578	-0.668	-0.637	-1.431	-1.122	-0.973	-1.028
	SAMPLE_118	RC2080-Pt	CB0118	0.176	-0.350	-0.459	-0.374	-0.411	-0.508	-0.829	-1.248
	SAMPLE_119	RC2080-Pt	CB0120	-0.082	-0.391	-0.541	-0.517	-0.595	-1.000	-0.998	-1.403
	SAMPLE_120	RC2080-Pt	CB0121	1.518	1.072	0.796	0.788	0.916	0.488	0.664	0.065
	SAMPLE_122	RC2080-Pt	CB0121a	0.759	0.333	0.053	-0.021	0.135	-0.443	-0.214	-0.626
	SAMPLE_123	RC2080-Pt	CB0122	-0.601	-1.211	-2.789	-2.984	-2.674	-3.582	-1.508	-1.216
	SAMPLE_124	RC2080-Pt	CB0123	-0.294	-0.495	-0.544	-0.389	-0.198	-3.520	-1.560	-1.730
	SAMPLE_126	RC2080-Pt	CB0193	-0.522	-1.102	-2.789	-2.767	-2.485	-1.700	-1.811	-1.118
	SAMPLE_127	RC2080-Pt	CB0196	0.298	-0.256	-0.439	-0.861	-0.832	-1.161	-0.853	-1.201
	SAMPLE_128	RC2080-Pt	CB0197	-0.355	-0.997	-2.747	-2.963	-2.567	-3.559	-1.870	-1.032
	SAMPLE_130	RC2080-Pt	CB0200	0.073	-0.506	-0.659	-0.546	-1.589	-0.744	-0.793	-0.761
SAMPLE_131	RC2080-Pt	CB0205	-1.272	-1.575	-1.176	-3.032	-2.709	-3.601	-3.635	-3.429	
SAMPLE_132	RC2080-Pt	CB0207	-3.282	-1.263	-2.762	-3.043	-2.707	-3.584	-3.641	-1.714	
SAMPLE_133	RC2080-Pt	CB0208	1.915	1.427	1.151	1.127	1.352	0.776	1.089	0.397	

Elemental concentrations below detection limits are shown as negative values in the appendix; the values represent minimum detectable concentrations (MDCs) given the sample mass and all other analytical parameters and should be interpreted as "less than" the value indicated. The MDCs were substituted for missing values in quantitative analyses, as they indicate extreme low values that can be converted to a log scale, unlike zero.

Table 8a. Rare Earth Element concentration in Log Base 10. Barton Creek and Cave's Branch groups shown.

Major Rare Earth Element Data for Speleothem Samples. All values in Log₁₀[ppm].

Group	INAA ID	Batch	Vial ID	La	Sm	Eu	Yb	Lu	Hf	Th	U	
M a c a l	SAMPLE_002	RC2080-Pt	M0009	-3.576	-1.071	-2.892	-2.849	-2.575	-3.691	-3.747	-0.827	
	SAMPLE_003	RC2080-Pt	M0011	-3.559	-1.144	-2.829	-2.889	-2.597	-3.655	-3.729	-1.062	
	SAMPLE_004	RC2080-Pt	M0013	0.229	-0.245	-2.658	-0.343	-3.519	-0.840	-0.762	-0.627	
	SAMPLE_005	RC2080-Pt	M0014	-3.751	-2.301	-2.887	-3.060	-2.761	-3.648	-3.749	-1.531	
	SAMPLE_006	RC2080-Pt	M0015	-0.997	-1.554	-2.904	-1.194	-2.627	-3.589	-1.252	-0.870	
	SAMPLE_007	RC2080-Pt	M0016	-0.082	-0.592	-0.579	-0.606	-1.377	-3.544	-1.381	-0.842	
	SAMPLE_009	RC2080-Pt	M0017	-1.342	-3.578	-2.901	-2.895	-2.579	-3.656	-3.757	-0.317	
	SAMPLE_010	RC2080-Pt	M0018	-1.293	-1.184	-2.871	-2.972	-2.677	-3.625	-3.732	-0.990	
	SAMPLE_011	RC2080-Pt	M0019	-1.737	-3.700	-2.870	-2.922	-2.635	-3.662	-3.767	-1.059	
	SAMPLE_012	RC2080-Pt	M0022	0.494	0.049	-0.194	-0.171	-0.207	-1.206	-1.318	-0.804	
	SAMPLE_013	RC2080-Pt	M0023	0.051	-0.406	-0.521	-0.494	-1.289	-1.589	-1.199	-0.425	
	SAMPLE_014	RC2080-Pt	M0111	-1.307	-2.301	-1.187	-2.988	-2.687	-2.140	-3.754	-0.724	
	SAMPLE_016	RC2080-Pt	M0113	-0.635	-1.291	-2.807	-2.946	-2.652	-1.852	-1.563	-1.028	
	SAMPLE_017	RC2080-Pt	M0124	0.376	-0.066	-0.201	-0.294	-0.648	-1.217	-1.511	-0.472	
	SAMPLE_018	RC2080-Pt	M0125	-0.483	-2.011	-2.822	-2.901	-2.567	-1.602	-1.739	-0.147	
	SAMPLE_019	RC2080-Pt	M0126	0.609	0.871	-0.348	-0.363	-2.202	-0.850	-0.780	1.087	
	SAMPLE_020	RC2080-Pt	M0128	-1.060	-2.253	-2.842	-2.923	-2.632	-3.676	-3.719	-0.466	
	SAMPLE_021	RC2080-Pt	M0139	-1.150	-1.196	-1.130	-2.791	-2.558	-3.674	-3.748	-3.250	
	SAMPLE_023	RC2080-Pt	M0153	-0.811	-1.418	-2.879	-2.853	-2.591	-3.623	-1.933	-1.114	
	SAMPLE_024	RC2080-Pt	M0170	-0.185	-0.731	-2.751	-2.787	-2.534	-1.404	-1.336	-0.946	
	SAMPLE_025	RC2080-Pt	M0171	-0.920	-1.667	-2.910	-2.917	-2.646	-3.649	-1.875	-0.861	
	SAMPLE_027	RC2080-Pt	M0172	-0.913	-1.514	-2.819	-2.960	-2.703	-3.659	-3.720	-1.313	
	P i n e R i d g e	SAMPLE_069	RC2080-Pt	PR0078	0.589	0.068	-0.138	-0.162	-0.761	-0.698	-0.493	-0.286
		SAMPLE_070	RC2080-Pt	PR0080	-0.111	-0.611	-0.752	-0.840	-3.519	-3.573	-1.294	-1.035
		SAMPLE_071	RC2080-Pt	PR0081	0.885	0.410	0.158	0.030	0.261	-0.344	-0.179	-0.844
		SAMPLE_073	RC2080-Pt	PR0082	-0.862	-1.273	-2.877	-3.020	-2.776	-3.643	-3.700	-1.398
		SAMPLE_074	RC2080-Pt	PR0083	-0.661	-1.370	-2.880	-3.022	-2.741	-3.652	-3.696	-0.855
SAMPLE_075		RC2080-Pt	PR0083A	1.691	1.104	0.819	0.708	0.905	0.175	0.413	-0.357	
SAMPLE_076		RC2080-Pt	PR0132	-0.004	-0.464	-0.769	-0.613	-1.057	-1.413	-1.242	-0.721	
SAMPLE_077		RC2080-Pt	PR0133	-1.215	-1.810	-2.913	-2.960	-2.742	-2.263	-3.718	-3.400	
SAMPLE_079		RC2080-Pt	PR0133A	-0.055	-0.568	-0.785	-2.757	-2.538	-1.542	-0.938	-1.296	
SAMPLE_080		RC2080-Pt	PR0134	-0.670	-3.417	-0.814	-2.851	-2.568	-3.600	-1.605	-0.104	
SAMPLE_081		RC2080-Pt	PR0135	-1.005	-1.569	-2.868	-2.998	-2.748	-3.658	-1.925	-0.887	
SAMPLE_082		RC2080-Pt	PR0140	-0.661	-2.130	-2.824	-1.017	-2.652	-3.583	-1.961	-0.545	
SAMPLE_083		RC2080-Pt	PR0141	0.102	-0.451	-0.568	-0.751	-0.369	-1.329	-1.120	-1.414	
SAMPLE_085		RC2080-Pt	PR0142	-3.268	-1.713	-1.799	-2.981	-2.737	-3.646	-3.722	-1.456	

Elemental concentrations below detection limits are shown as negative values in the appendix; the values represent minimum detectable concentrations (MDCs) given the sample mass and all other analytical parameters and should be interpreted as "less than" the value indicated. The MDCs were substituted for missing values in quantitative analyses, as they indicate extreme low values that can be converted to a log scale, unlike zero.

Table 8b. (Cont.) Rare Earth Element concentration in Log Base 10. Macal and Pine Ridge Groups shown.

Major Rare Earth Element Data for Speleothem Samples. All values in Log₁₀[ppm].

Group	INAA ID	Batch	Vial ID	La	Sm	Eu	Yb	Lu	Hf	Th	U
R o a r i n g C r e e k	SAMPLE_086	RC2080-Pt	RC0029	0.901	0.451	0.087	-0.129	0.012	-0.678	-0.299	-0.838
	SAMPLE_087	RC2080-Pt	RC0030	1.132	0.620	0.202	0.232	0.316	-0.040	-0.073	-0.559
	SAMPLE_088	RC2080-Pt	RC0031	-0.962	-1.917	-2.918	-2.842	-2.617	-1.552	-3.656	-0.729
	SAMPLE_089	RC2080-Pt	RC0032	0.543	0.073	-0.119	-0.309	-0.324	-0.677	-0.376	-0.697
	SAMPLE_092	RC2080-Pt	RC0033	-0.532	-2.301	-0.803	-2.845	-2.393	-3.551	-1.600	-0.173
	SAMPLE_093	RC2080-Pt	RC0043	-1.389	-2.567	-2.835	-2.806	-2.458	-1.546	-3.643	-3.308
	SAMPLE_094	RC2080-Pt	RC0044	-0.514	-0.999	-2.796	-2.802	-2.444	-3.560	-1.481	-3.288
	SAMPLE_096	RC2080-Pt	RC0045	0.093	-0.384	-0.790	-0.890	-0.667	-1.041	-0.731	-1.308
	SAMPLE_097	RC2080-Pt	RC0146	-0.650	-0.967	-2.820	-2.963	-2.594	-3.611	-3.654	-3.434
	SAMPLE_098	RC2080-Pt	RC0147	-0.848	-2.529	-1.132	-0.975	-2.400	-3.602	-3.616	-0.531
	SAMPLE_100	RC2080-Pt	RC0148	-1.541	-1.133	-1.009	-2.778	-2.434	-3.617	-3.664	-0.973
S a n A n t i o	SAMPLE_101	RC2080-Pt	RC0149	0.560	0.064	-0.500	-0.471	-0.388	-0.813	-0.407	-1.047
	SAMPLE_102	RC2080-Pt	RC0150	-1.764	-3.655	-2.827	-2.755	-2.424	-3.636	-3.669	-3.231
	SAMPLE_104	RC2080-Pt	RC0151	0.522	0.101	-0.205	-0.252	-0.087	-0.589	-0.431	-0.847
	SAMPLE_105	RC2080-Pt	RC0164	1.639	1.226	0.867	0.886	1.125	0.445	0.708	0.354
	SAMPLE_106	RC2080-Pt	RC0175	-1.079	-1.808	-2.808	-2.946	-2.556	-3.602	-3.619	-1.111
	SAMPLE_108	RC2080-Pt	RC0176	1.799	1.295	0.955	1.000	1.188	0.629	0.726	0.457
	SAMPLE_109	RC2080-Pt	RC0177	0.186	-0.244	-0.344	-0.452	-0.138	-1.323	-1.649	-3.289
	SAMPLE_110	RC2080-Pt	RC0180	0.308	-0.046	-0.342	-0.259	-0.111	-0.939	-0.823	-1.054
	SAMPLE_111	RC2080-Pt	RC0181	0.665	0.261	0.026	-0.187	0.100	-0.712	-0.567	-0.858
	SAMPLE_050	RC2080-Pt	SA0096	-0.381	-0.836	-2.779	-0.980	-2.698	-1.582	-1.471	-0.974
	SAMPLE_051	RC2080-Pt	SA0097	0.132	-0.355	-0.640	-0.390	-0.429	-1.076	-0.795	-0.826
SAMPLE_052	RC2080-Pt	SA0098	-3.510	-2.301	-2.843	-2.912	-2.758	-3.622	-3.654	-1.221	
SAMPLE_053	RC2080-Pt	SA0100	-1.368	-1.247	-2.802	-2.919	-2.751	-3.605	-3.651	-1.089	
SAMPLE_055	RC2080-Pt	SA0101	-0.034	-0.531	-0.554	-2.819	-2.664	-1.109	-1.069	-0.759	
SAMPLE_056	RC2080-Pt	SA0102	-1.217	-1.252	-2.846	-2.954	-2.779	-3.567	-1.656	-1.389	
SAMPLE_057	RC2080-Pt	SA0103	0.380	-0.133	-0.334	-0.390	-0.421	-0.806	-0.595	-0.855	
SAMPLE_058	RC2080-Pt	SA0104	-0.205	-0.764	-0.962	-2.912	-2.731	-3.539	-1.513	-1.024	
SAMPLE_059	RC2080-Pt	SA0106	-0.570	-1.067	-2.800	-1.074	-2.782	-3.577	-1.915	-3.315	
SAMPLE_062	RC2080-Pt	SA0108	-1.652	-1.869	-2.835	-2.961	-2.711	-3.663	-3.724	-3.443	
SAMPLE_063	RC2080-Pt	SA0129	-0.105	-0.478	-0.581	-0.338	-0.311	-3.585	-3.662	-0.736	
SAMPLE_064	RC2080-Pt	SA0130	0.422	-0.013	-0.315	-0.427	-0.345	-1.337	-0.917	-3.261	
SAMPLE_065	RC2080-Pt	SA0131	0.806	0.346	0.055	-0.029	-0.093	-0.567	-0.127	-0.687	
SAMPLE_066	RC2080-Pt	SA0190	-1.773	-3.763	-2.917	-2.951	-2.688	-3.684	-3.704	-3.426	
SAMPLE_068	RC2080-Pt	SA0192	-1.504	-1.235	-2.893	-2.985	-2.720	-0.755	-3.722	-1.098	

Elemental concentrations below detection limits are shown as negative values in the appendix; the values represent minimum detectable concentrations (MDCs) given the sample mass and all other analytical parameters and should be interpreted as "less than" the value indicated. The MDCs were substituted for missing values in quantitative analyses, as they indicate extreme low values that can be converted to a log scale, unlike zero.

Table 8c. (Cont.) Rare Earth Element concentration in Log Base 10. Roaring Creek and San Antonio Groups shown.

9a

Major, Trace and Rare Earth Element Data for XARP Samples. All values in ppm.

Drainage	Cave	Series	Al	Mg	Br	Ti	Sc	Co	Zn	Sr	Cs	Ba	La	Sm	Eu	Yb	Lu	Hf	Th	U
Sibun	Actun Chanona	Chanona 200	0.354	0.551	3.729	0.354	0.766	0.551	90.851	0.010	225.038	0.132	0.034	0.200	0.009	0.002	0.014	0.013	0.229	
		Chanona 201	0.4	0.341	5.193	0.400	0.773	0.341	41.449	0.027	1.021	0.351	0.132	0.031	0.126	0.019	0.046	0.036	0.022	
		Chanona 202	0.336	1.863	4.368	0.336	0.710	1.863	1529.008	0.017	1199.621	0.241	0.092	1.179	0.015	0.002	0.021	0.019	16.457	
	Hershey	Hershey 68	0.424	0.732	20.513	0.424	0.784	0.732	19.379	0.037	38.216	1.342	0.307	0.102	0.127	0.019	0.082	0.061	0.079	
		Hershey 97	0.516	1.377	27.135	0.516	1.049	1.377	18.153	0.074	39.238	1.476	0.368	0.126	0.348	0.056	0.142	0.104	0.087	
		Hershey 96	0.487	1.444	36.869	0.487	0.930	1.444	20.834	0.103	45.348	3.044	0.611	0.176	0.313	0.047	0.168	0.157	0.090	
	Ik	Ik	0.435	0.871	15.699	0.435	0.779	0.871	37.991	0.047	6.328	1.153	0.300	0.073	0.204	0.032	0.051	0.073	0.227	
	Pakal Na	Pakal Na	0.571	1.145	68.249	0.571	0.949	1.145	22.123	0.182	11.361	2.247	0.526	0.116	0.236	0.034	0.184	0.247	0.148	
	Oshon	Oshon 5	0.33	1.68	26.308	0.325	1.594	1.679	143.955	0.038	2.449	0.496	0.117	0.031	0.078	0.012	0.101	0.053	7.168	
		Oshon 6	0.46	2.40	36.487	0.456	0.862	2.395	18.419	0.072	1.775	0.850	0.209	0.051	0.161	0.023	0.159	0.058	0.588	
	Cedars Bank	Cedars Bank	0.68	6.53	221.837	0.679	1.208	6.527	40.077	0.156	10.442	5.235	1.045	0.221	0.464	0.068	0.559	0.461	0.484	
	Petén	Poptun	Poptun 1	1.47	1.87	0.47	16.785	1.866	0.055	0.466	14.199	0.000	1.533	-0.170	0.014	0.005	0.041	0.008	0.000	0.000
Poptun 2			3.26	1.57	0.29	19.018	1.574	0.058	0.286	32.452	0.003	0.707	0.005	0.000	0.001	0.002	0.000	0.000	0.000	0.040
Poptun 3			129.15	1.50	36.44	44.500	1.496	0.704	36.444	61.639	0.039	8.015	0.630	0.085	0.018	0.085	0.015	0.070	0.050	0.670
Poptun 4			1.00	1.64	1.11	16.647	1.640	0.093	1.114	16.083	0.000	1.664	0.028	0.000	0.000	0.007	0.003	0.000	0.000	0.030
Poptun 5			0.11	1.51	2.18	15.738	1.512	0.103	2.183	15.335	0.000	1.463	0.155	0.010	0.006	0.049	0.007	0.000	0.000	0.030
Poptun 6			2.01	2.75	0.81	16.584	2.754	0.049	0.809	14.077	0.000	1.259	0.090	0.012	0.004	0.026	0.001	0.009	0.000	0.030
Poptun 7			2.75	2.61	1.83	17.538	2.611	0.070	1.826	15.804	0.002	1.564	0.093	0.005	0.000	0.036	0.000	0.000	0.000	0.030
Poptun 8			55.36	2.52	2.85	20.121	2.519	0.121	2.850	33.969	0.018	1.717	0.062	0.006	0.000	0.006	0.000	0.010	0.020	0.040

9b

Major, Trace and Rare Earth Element Data for XARP Samples. All values in Log₁₀[ppm].

Drainage	Cave	Series	Al	Mg	Br	Ti	Sc	Co	Zn	Sr	Cs	Ba	La	Sm	Eu	Yb	Lu	Hf	Th	U
Sibun	Actun Chanona	Chanona 200	-0.451	-0.259	0.572	-0.451	-0.116	-0.259	1.958	-1.982	2.352	-0.880	-1.463	-0.700	-2.026	-2.806	-1.849	-1.890	-0.640	
		Chanona 201	-0.398	-0.467	0.715	-0.398	-0.112	-0.467	1.618	-1.567	0.009	-0.455	-0.881	-1.505	-0.900	-1.712	-1.337	-1.449	-1.663	
		Chanona 202	-0.474	0.2702	0.640	-0.474	-0.148	0.270	3.184	-1.780	3.079	-0.617	-1.037	0.071	-1.815	-2.677	-1.669	-1.713	1.216	
	Hershey	Hershey 68	-0.373	-0.135	1.312	-0.373	-0.106	-0.136	1.287	-1.437	1.582	0.128	-0.513	-0.993	-0.897	-1.729	-1.084	-1.218	-1.103	
		Hershey 97	-0.287	0.1389	1.434	-0.287	0.021	0.139	1.259	-1.129	1.594	0.169	-0.434	-0.898	-0.459	-1.253	-0.848	-0.984	-1.060	
		Hershey 96	-0.312	0.1596	1.567	-0.312	-0.032	0.160	1.319	-0.985	1.657	0.484	-0.214	-0.755	-0.504	-1.330	-0.775	-0.803	-1.044	
	Ik	Ik	-0.362	-0.06	1.196	-0.361	-0.109	-0.060	1.580	-1.331	0.801	0.062	-0.524	-1.138	-0.691	-1.501	-1.288	-1.136	-0.645	
	Pakal Na	Pakal Na	-0.243	0.0588	1.834	-0.243	-0.023	0.059	1.345	-0.740	1.055	0.352	-0.279	-0.934	-0.626	-1.468	-0.735	-0.607	-0.830	
	Oshon	Oshon 5	-0.488	0.2251	1.420	-0.488	0.202	0.225	2.158	-1.419	0.389	-0.304	-0.930	-1.515	-1.107	-1.920	-0.994	-1.274	0.855	
		Oshon 6	-0.341	0.3793	1.562	-0.341	-0.064	0.379	1.265	-1.140	0.249	-0.071	-0.681	-1.295	-0.793	-1.638	-0.798	-1.235	-0.231	
	Cedars Bank	Cedars Bank	-0.168	0.8148	2.346	-0.168	0.082	0.815	1.603	-0.808	1.019	0.719	0.019	-0.655	-0.334	-1.170	-0.253	-0.336	-0.315	
	Petén	Poptun	Poptun 1	0.167	0.2709	-0.332	1.225	0.271	-1.258	-0.331	1.152	-3.485	0.185	-0.770	-1.848	-2.289	-1.382	-2.092	0.000	0.000
Poptun 2			0.514	0.197	-0.544	1.279	0.197	-1.240	-0.544	1.511	-2.505	-0.151	-2.345	0.000	-3.059	-2.749	0.000	0.000	0.000	-1.398
Poptun 3			2.111	0.1749	1.5616	1.648	0.175	-0.152	1.562	1.790	-1.404	0.904	-0.200	-1.071	-1.753	-1.830	-1.155	-1.301	-0.174	
Poptun 4			-0.001	0.2151	0.0469	1.221	0.215	-1.031	0.047	1.206	0.000	0.221	-1.559	0.000	0.000	-2.167	-2.534	0.000	0.000	-1.523
Poptun 5			-0.948	0.1796	0.3391	1.197	0.180	-0.988	0.339	1.186	0.000	0.165	-0.811	-1.995	-2.202	-1.307	-2.158	0.000	0.000	-1.523
Poptun 6			0.304	0.44	-0.092	1.220	0.440	-1.306	-0.092	1.149	0.000	0.100	-1.045	-1.938	-2.367	-1.592	-2.961	-2.038	0.000	-1.523
Poptun 7			0.440	0.4168	0.2615	1.244	0.417	-1.152	0.262	1.199	-2.633	0.194	-1.033	-2.303	0.000	-1.444	0.000	0.000	0.000	-1.523
Poptun 8			1.743	0.4012	0.4548	1.304	0.401	-0.919	0.455	1.531	-1.749	0.235	-1.208	-2.258	0.000	-2.255	0.000	-2.000	-1.699	-1.398

Tables 9a and 9b. Major, Trace and Rare Earth Element Concentration for the XARP samples. Top in ppm; bottom in Log Base 10

Caves Site Composition By Group			
Drainage	Group	Cave Sites # per Cave	
Cayo District	Barton Creek (n= 17)	Barton Creek	4
		Migdalia	6
		Arnulfo	3
		Slate	2
		Owl	2
		Actun Isabella	5
		Flour Camp	4
		Keyhole	2
	Macal (n = 22)	Cave of the Moth	1
		Crab Ghost	1
		Son of Chapat	1
		Hala RS	1
		Chapat	2
		Serpente	1
		Six Gibnut	1
		House of Palm	3
		Las Cuevas	5
Pine Ridge (n=17)	Rio Frio A	2	
	Rio Frio B	2	
	Rio Frio	1	
	Rio Frio E	3	
	Yaxcheel/Ahau	2	
	Handprint	3	
	Nakbe	3	
	Uyak Na RS	1	
	Hummingbird	1	
	Taratula	1	
Cave's Branch	San Antonio (n = 15)	Ray's cave	1
		Unknown Cave	2
		Ray's RS	1
		ATM	5
		Bols Museum	3
		Actun Peiz	2
		Crystal Palace	3
		Bat Cave	1
		Skeleton Cave	1
		Hidden Cave	1
	Actun Tzul	2	
	Offering Cave	2	
	StHermans	3	
	Jaguar Paw	5	
	Cave's Branch (n= 16)	Caves Branch RS	1
Swimming Hole		1	
Mountain Cow		2	
Sibun	Actun Chanona (n = 3)	Lost World	1
		FootPrint	2
		Chanona 200	1
	Hershey (n = 3)	Chanona 201	1
		Chanona 202	1
		Hershey 68	1
		Hershey 97	1
		Hershey 96	1
		Ik	1
		Pakal Na	1
Oshon (n = 2)	Oshon 5	1	
	Oshon 6	1	
	Cedars Bank	1	
Petén	Poplun (n = 8)	Poplun 1	1
		Poplun 2	1
		Poplun 3	1
		Poplun 4	1
		Poplun 5	1
		Poplun 6	1
		Poplun 7	1
		Poplun 8	1

Table 10. Showing cave site composition for each group and divide din drainage systems. Notice, Cave's Branch makes its own system as it's a tributary of the Sibun River and straddles the Cayo District and Sibun Basins.

Standard Reference Materials (SRM) for INAA

NIST-1c								NIST88b							
Element	Certified Values*		Measured Values					Element	Certified Values*		Measured Values				
	ppm	± SD	Mean	StDev	C.V. (%)	Error (%)	Count		ppm	± SD	Mean	StDev	C.V. (%)	%Error	Count
Al	6880	160	6637	92	1.4%	3.5%	Pt	Al	1778	68.8	1764.7	57.3	3.2%	0.8%	Pt
Ca	359600	2100	350463	4388	1.3%	2.5%	Pt	Ca	214050	357	213888	3961	1.9%	0.1%	Pt
K	2320	80	2483	662	26.7%	7.0%	Pt	K	855	19.9	569.1	245.7	43.2%	33.4%	Pt
Mg	2530	240	1806	346	19.2%	28.6%	Pt	Mg	126819	422	112758	1562	1.4%	11.1%	Pt
Mn	190	40	166	2	1.3%	12.9%	Pt	Mn	124	9.3	128.2	2.2	1.7%	3.4%	Pt
Na	150	75	168	10	6.0%	12.0%	Pt	Na	215	5.2	263	4	1.4%	22.0%	W1
Ti	420	60	401	43	10.6%	4.5%	Pt	Ti	96		94.1	29.6	31.5%	1.9%	Pt
As								As			0.90	0.07	8.1%		W1
Ba	84	1	67	16	24.3%	20.4%	Pt	Ba							
Br								Br			25.12	2.53	10.1%		W1
Ce	7.14							Ce	3.83		3.56	0.22	6.2%	7.0%	W4
Co	1.15							Co	1.02		0.96	0.04	3.7%	6.1%	W4
Cr	19							Cr	2.33		2.08	0.30	14.2%	10.4%	W4
Cs	0.59							Cs	0.16		0.16	0.02	12.7%	1.9%	W4
Dy	0.64		0.62	0.11	17.2%	2.8%	Pt	Dy			0.54	0.07	13.3%		Pt
Eu	0.165							Eu			0.11	0.01	10.1%		W4
Fe	3840	210						Fe	1937	14	1940	68	3.5%	0.2%	W4
Hf	0.75							Hf			0.129	0.024	18.3%		W4
La	4.63							La			4.67	0.07	1.5%		W1
Lu	0.06							Lu			0.059	0.013	21.2%		W1
Nd	3.72							Nd			2.489	0.331	13.3%		W4
Rb	12.5							Rb			2.819	0.403	14.3%		W4
Sb								Sb			0.082	0.016	19.5%		W4
Sc	1.3							Sc	0.37		0.345	0.007	1.9%	5.6%	W4
Sm	0.73							Sm			0.55	0.01	2.4%		W1
Sr	250	40						Sr			65.500	10.890	16.6%		W4
Ta	0.09							Ta			0.024	0.006	25.5%		W4
Tb	0.13							Tb			0.103	0.016	15.4%		W4
Th	1.02							Th	0.31		0.268	0.013	4.8%	12.9%	W4
U	1.5							U			0.123	0.021	17.0%		W1
Yb	0.385							Yb			0.300	0.018	6.0%		W1

*Reported values indicated in *italic*, after Gladney *et al.* (1987).

*Noncertified values on certificate are indicated in *italic*.

*Reported values indicated in *italic*, after Gladney *et al.* (1987).

Table 11. Certified values and detected mean deviations for samples base on Standard Reference Materials.